JPL Publication 93-21

Proceedings of the Seventeenth NASA Propagation Experimenters Meeting (NAPEX XVII) and the Advanced Communications Technology Satellite (ACTS) Propagation Studies Miniworkshop

Held in Pasadena, California, June 14–15, 1993

Faramaz Davarian
Editor

August 1, 1993

National Aeronautics and
Space Administration

Jet Propulsion Laboratory
California Institute of Technology
Pasadena, California

JPL Publication 93-21

Proceedings of the Seventeenth NASA Propagation Experimenters Meeting (NAPEX XVII) and the Advanced Communications Technology Satellite (ACTS) Propagation Studies Miniworkshop

Held in Pasadena, California, June 14–15, 1993

Faramaz Davarian
Editor

August 1, 1993

National Aeronautics and
Space Administration

Jet Propulsion Laboratory
California Institute of Technology
Pasadena, California

The research described in this publication was carried out by the Jet Propulsion Laboratory, California Institute of Technology, under a contract with the National Aeronautics and Space Administration.

PREFACE

The NASA Propagation Experimenters (NAPEX) meeting is a forum convened to discuss the studies supported by the NASA Propagation Program. The reports delivered at this meeting by the management and the investigators of the program present our recent activities and future plans. Representatives from domestic and international organizations who have an interest in radio wave propagation studies are invited to NAPEX meetings for discussions and exchange of information. This Proceedings records the content of NAPEX XVII and the ACTS Propagation Studies miniworkshop that preceded it.

NAPEX XVII, which took place at the Pasadena Convention Center, Pasadena, California, June 15, 1993, consisted of "Opening Remarks" and two sessions. Faramaz Davarian and John Kiebler made the opening remarks, which described last year's achievements and the next year's plans. Session 1, entitled "Slant Path Propagation Studies and Measurements," was chaired by Ernie Smith of the University of Colorado. Session 2, entitled "Propagation Studies for Mobile/Personal Communications," was chaired by John Kiebler of Mitre Corporation.

In the opening remarks, I emphasized the importance of industry participation in the program and pointed out that the main focus of the Propagation Program is to enable new satellite communication applications. To underscore the interest in industry participation, Tom Sullivan of ARC discussed the user's needs during the first presentation of Session 1. Regretfully, due to a constrained economy, the NASA Propagation Program is experiencing budget reductions. Therefore, it is ever more important to enjoy industry support and receive funding from industry to partially finance the program's studies.

I would like to thank the participants of both the workshop and NAPEX XVII for their valuable contributions. I would also like to thank Mardy Wilkins and Alan Cha for helping me with the logistics and organization of the meetings. Finally, I would like to express my appreciation to Susan Foster for coordinating publication of this document.

Mos Kharadly of the University of British Columbia has offered to host NAPEX XVIII and the ACTS miniworkshop in Vancouver, June 1994. The exact date of the meeting will be announced later. This date will be selected to conveniently allow for participation in the IEEE APS/URSI meeting in Seattle, June 20-25, 1994. The ACTS Propagation Studies Workshop (APSW-V) will be hosted by Steve Horan of New Mexico State University in White Sands, November 30 - December 1, 1993.

Faramaz Davarian

ABSTRACT

The NASA Propagation Experimenters Meeting (NAPEX), supported by the NASA Propagation Program, is convened annually to discuss studies made on radio wave propagation by investigators from domestic and international organizations. NAPEX XVII was held on June 15, 1993, in Pasadena, California. Participants included representatives from Canada, Japan, Germany, the Netherlands, Portugal, England, Switzerland, Italy, and the United States, including researchers from universities, government agencies, and private industry. The meeting was organized into two technical sessions. The first session was dedicated to slant path propagation studies and experiments. The second session focused on propagation studies for mobile and personal communications. In total, nineteen technical papers and some informal contributions were presented.

Preceding NAPEX XVII, the Advanced Communications Technology Satellite (ACTS) Propagation Studies Miniworkshop was held on June 14, 1993, to review ACTS propagation activities with emphasis on ACTS experiments status and data collection, processing, and exchange. Ten technical papers were presented by contributors from government agencies, private industry, and university research establishments.

CONTENTS
NAPEX-XVII MEETING

SESSION 2. PROPAGATION STUDIES FOR MOBILE/PERSONAL COMMUNICATIONS

J. Kiebler, Chairman

CONTENTS
ACTS MINIWORKSHOP

NAPEX XVII AND ACTS MINIWORKSHOP ATTENDEES

Richard Allnutt
COMSAT Labs.
22300 Comsat Drive
Clarksburg, MD 20871
301-428-4411
301-428-3686 (FAX)

Robert Bauer
NASA Lewis Research Center
21000 Brookpark Rd., MS 54-6
Cleveland, OH 44135
216-433-3431
216-433-6371 (FAX)
E-mail: acbauer@lims01.lerc.nasa.gov

Dennis Bishop
Jet Propulsion Laboratory
MS T-1708
4800 Oak Grove Drive
Pasadena, CA 91109
818-354-9251
818-393-0096 (FAX)

Apolonia Pawlina Bonati
Centro di Studio Sulle Telecomunicazioni
Spaziali CNR
c/o Dipartimento di Elettronica e
Informazione, Politecnico di Milano
Piazza L. de Vinci 32,I
20133 Milano
+39.2399.3581
+39.2.2399.3413 (FAX)

Karen Burcham
FAA Technical Center
Atlantic City Int'l Aiport - ACD 330
NJ 08405
609-485-6993
609-495-5451 (FAX)

Jonathan P. Castro
Ecole Polytechnique Federale
Laboratooire de Telecommunications
Batiment ELD, Rm #341, Ecublens
CH-1015 Lausanne, Switzerland
+41 21 693 4731
+41 21 693 4660 (FAX)
E-mail: castro@sicsun.epfl.ch

Alan Cha
Jet Propulsion Laboratory
MS T-1708
4800 Oak Grove Drive
Pasadena, CA 91109
818-354-0412
818-393-0096 (FAX)
E-mail: cha@java.jpl.nasa.gov

Aimee Chan
University of British Columbia
2356 Main Mall
Vancouver, British Columbia
Canada V6T 1Z4
604-293-6094
604-293-5787 (FAX)
E-mail: achan@mprgate.mpr.ca

Giovanni E. Corazza
University of Rome "Tor Vergata"
Via Della Ricerca Scientifica
Rome 00133
Italy
+39-6 7259-4453
+39-6 2020519 (FAX)

Robert K. Crane
University of Oklahoma
100 East Boyd St., Room 1248
Norman, OK 73019-0628
405-325-4419
405-325-7689 (FAX)
E-mail: bcrane@geohub.gcn.uoknor.edu

Faramaz Davarian
Jet Propulsion Laboratory
MS T-1708
4800 Oak Grove Drive
Pasadena, CA 91109
818-354-4820
818-393-0096 (FAX)
E-mail: davarian@java.jpl.nasa.gov

Mark Dickinson
FAA Technical Center
Atlantic City Int'l Airport - ACD 330
NJ 08405
609-485-6993
609-485-5451 (FAX)

Asoka Dissanayake
COMSAT Labs
22300 Comsat Drive
Clarksburg, MD 20871
301-428-4411
301-428-3638 (FAX)
E-mail: asoka_dissanayake@mr_mail.trans.comsat.com

Barry G. Evans
Centre for Satellite Eng. Research
University of Surrey
Guildford, Surrey
GU2 5XH, U.K.
+44 483 509131
+44 483 34139 (FAX)

Barry Fairbanks
NASA Lewis Research Center
21000 Brookpark Rd., MS 54-6
Cleveland, OH 44135
216-433-3541
216-433-6371 (FAX)
E-mail: acfair@lims01.lerc.nasa.gov

Warren Flock
University of Colorado
ECE Department
Campus Box 425
Boulder, CO 80309-0425
303-492-7012
303-492-2758 (FAX)

Doug Gaff
Virginia Tech
Dept. of Electrical Engineering
Blacksburg, VA 24061-0111
703-231-3355 (FAX)

Julius Goldhirsh
Applied Physics Lab.
Johns Hopkins University
Johns Hopkins Road
Laurel, MD 20723-6099
301-953-5042
301-953-5548 (FAX)
E-mail: julius@nansen.jhuapl.edu

Nassar Golshan
Jet Propulsion Laboratory
MS 161-241
4800 Oak Grove Dr.
Pasadena, CA 91109
818-354-0459
818-393-4643 (FAX)

Henry F. Helmken
Florida Atlantic University
P.O. Box 3091, MS SE/456
Boca Raton, FL 33431
407-367-3452
407-367-2336 (FAX)
helmkenh@acc.fau.edu

Hau H. Ho
TRW
MS R10/1356
One Space Park
Redondo Beach, CA 92647
310-812-1656
310-813-4719 (FAX)

James E. Hollansworth
NASA Lewis Research Center
21000 Brookpark Road, MS 54-2
Cleveland, OH 44135
216-433-3458
216-433-8705 (FAX)
E-mail: caholl@lims01.lerc.nasa.gov

Stephen Horan
New Mexico State University
P. O. Box 30001, Dept. SG
Las Cruces, NM 88003-3001
505-646-5870
505-646-1435 (FAX)
E-mail: shoran@nmsu.edu

Rafeh Hulays
University of British Columbia
2356 Main Mall
Vancouver, B.C.
Canada V6T 1Z4
604-822-2872
E-mail: acts@ee.ubc.ca

Louis J. Ippolito
Stanford Telecom.
1761 Business Center Drive
Reston, VA 22090
703-438-8061
703-438-8112 (FAX)
E-mail: lji@sed.stel.com

Shinichi Itoh
Nippon Motorola Ltd.
3-20-1 Minami-Azabu,
Minato-ku
Tokyo 106 Japan
81-3-3280-8550
81-3-3440-3108 (FAX)

Mark Jacobson
NOAA/ERL/WPL
325 Broadway
Boulder, CO 80303-3328
303-497-6497
303-497-6978 (FAX)
E-mail: jake@spopck.wpl.er.gov

Jeff Jenkins
New Mexico State University
P. O. Box 30001, Dept. 3-O
Las Cruces, NM 88003-3001
505-646-6287
505-646-1435 (FAX)
E-mail: jejenkn@nmsu.edu

Anil V. Kantak
Jet Propulsion Laboratory
MS-1708
4800 Oak Grove Drive
Pasadena, CA 91109
818-354-1825
818-393-0096 (FAX)
E-mail: kantak@java.jpl.nasa.gov

Ara Karahisar
Teleglobe Canada
625 Belmont St.
Montreal Quebec
Canada H3B 2M1
514-868-8322
514-868-8350 (FAX)

M. M. Z. Kharadly, Dept. of EE
University of British Columbia
2356 Main Mall
Vancouver, British Columbia
CANADA V6T 1Z4
604-822-2816
604-822-5949 (FAX)
E-mail: acts@ee.ubc.ca

John Kiebler
MITRE Corporation
409 Third Street, SW, Suite 300
Washington, DC 20024-3212
202-646-9113
202-646-9109/8 (FAX)
E-mail: jkiebler@mitre.org

Charles Kittiver
American Mobile Satellite Corp.
1150 Connecticut Ave. N.W.
Washington, DC 20036
202-872-7642
202-331-5861 (FAX)

John Koukos
Jet Propulsion Laboratory
MS T-1708
4800 Oak Grove Drive
Pasadena, CA 91109
818-354-1826
818-393-0096 (FAX)

Alexander Kukushkin
CSIRO, Div. of Radiophysics
P. O. 76
Epping NSW 2121
Australia
61 2 868 0269
61 2 868 0450 (FAX)
E-mail: akukushk@rp.csiro.au

Chuong Le
Jet Propulsion Laboratory
MS T-1708
4800 Oak Grove Dr.
Pasadena, CA 91109
818-354-7897
818-393-0096

Erich Lutz
DLR Oberpfaffenhofen
Institute for Communications
D-8031 Oberpfaffenhofen
Germany
49-8153-28-831
49-8153-28-1442 (FAX)

Charlie Mayer
University of Alaska, Dept.of EE
539 Duckering Bldg.
Fairbanks, AK 99775
907-474-6091
907-474-6087 (FAX)
E-mail: ffcem@aurora.alaska.edu

Jose Carlos Neves
Universidade de Aveiro
Dept. of Electronics and
Telecommunications
3800 Aveiro
Portugal
+351 34 25085/8
+351 34 381128 (FAX)

John J. O'Connor, Jr.
National Communications System
701 South Court House Rd.
Arlington, VA 22204
703-692-2814
703-746-7184 (FAX)

Michael Powers
Goddard Space Flight Center
Bldg. 19
Greenbelt, MD
301-286-4820
301-286-2929 (FAX)

Timothy Pratt
Virginia Tech.
Satcom Group
Blacksburg, VA 24061-0111
703-231-6681
703-231-3355 (FAX)

Will Remaklus
Virginia Tech.
Bradley Dept. of Electrical Engineering
Blacksburg, VA 24061-0111
703-231-6834
703-231-3355 (FAX)

David V. Rogers
Communications Research Centre
3701 Carling Avenue
Ottawa, Ontario
Canada K2H 8S2
613-998-5174
613-998-4077 (FAX)
E-mail: dave.rogers@crc.doc.ca

Jack Rubin
The Mitre Corp.
7525 Colshire Drive
McLean, VA 22102
703-883-7694
703-883-6389 (FAX)

Marco Rubin
Booz Allen & Hamilton
8283 Greenboro Drive
McLean, VA 22102-3838
703-902-4905
703-902-3354 (FAX)

Horst Salzwedel
Comdisco Systems. Inc.
919 E. Hillsdale Blvd.
Foster City, CA 94404
415-378-7537
415-358-3601 (FAX)
horst@csi.com

Mario Sforza
European Space Agency
Keplerlaan 1
Noordwijk 2200 AG
The Netherlands
+31 1719 83298
+31 1719 84999 (FAX)
E-mail: mario@xe.estec.esa.nl

Charles Sigler, Jr.
American Mobile Satellite Corp.
1150 Connecticut Ave, NW 4th Floor
Washington DC, 20036
202-872-7626
202-331-5861 (FAX)

Ernest K. Smith
ECE Department
Campus Box 425
University of Colorado
Boulder, CO 80309-0425
303 492-7123
303 492-2758 (FAX)
E-mail: smithek@boulder.colorado.edu

Victor Sparrow
National Communications System
701 S. Courthouse Road
Arlington, VA 22204
703-692-0635
703-746-7184 (FAX)

Robert H. Sternowski
Rockwell International - CACD
855 35th St. NE, MS 137-156
Cedar Rapids, IA 52498
319-395-5736
319-395-5742 (FAX)

Warren L. Stutzman
Virginia Tech.
Bradley Dept. of Electrical Engineering
Blacksburg, Virginia 24061-0111
703-231-6834
703-231-3355 (FAX)
E-mail: stutzman@vtvm1.cc.vt.edu

Tom Sullivan
Atlantic Research Corporation
8201 Corporate Drive, Suite 350
Landover, MD 20785
301-731-2200
301-731-2238 (FAX)

Krisjani S. Suwitra
Jet Propulsion Laboratory
4800 Oak Grove Drive, MS T-1708
Pasadena, CA 91109
818-354-9250
818-393-0096 (FAX)
E-mail: suwitra@java.jpl.nasa.gov

Yasutumi Takahashi
DDI Corporation
Ichibancho I-S Bldg. 8
Ichibancho Chiyoda-ku
Tokyo 102
Japan
81-3 3221-9681
81-3 3221-9694 (FAX)

K. Tomiyasu
Martin Marietta Corp.
MS C9\2188
P.O. Box 8048
Philadelphia, PA 19101
215-531-5740
215-644-8521 (FAX)

Joseph Turk
Colorado University
Dept. of Elec. Eng.
Fort Collins, CO 80523
303-491-7678
303-491-2249 (FAX)
E-mail: turk@longs.lance.colostate.edu

Wolf Vogel
E. E. Research Laboratory
University of Texas
10100 Burnet Road
Austin, TX 78758
512-471-8608
512-471-8609 (FAX)
E-mail: wvogel@chpc.utexas.edu

Hiromitsu Wakana
Kashima Space Research Center, CRL
893-1 Hirai, Kashima
Ibaraki 314
Japan
+81-299-84-4119
+81-299-84-4149 (FAX)

David B. Westenhaver
Auburn CCDS
746 Lioness Ct. S.W.
Stone Mountain, GA 30087-2855
404 925-1091
404-925-1091 (FAX)

Administrative Assistants

JPL:

Mardy Wilkins
818-354-1723
818-393-0096 (FAX)
E-mail: wilkins@java.jpl.nasa.gov

Virginia Tech:

Cynthia Marshall
703-231-6834
703-231-3355 (FAX)

ACTS Electronic Mailing List Address:

acts@java.jpl.nasa.gov

NAPEX-XVII AGENDA
NASA PROPAGATION EXPERIMENTERS MEETING
PASADENA CONVENTION CENTER (CONFERENCE BUILDING)
JUNE 15, 1993

8:00 **REGISTRATION**

8:30 **OPENING REMARKS**
F. Davarian and J. Kiebler

8:40 NEW CHALLENGES IN PROPAGATION RESEARCH IN THE U.S.
F. Davarian ***(JPL)***

SESSION 1. SLANT PATH PROPAGATION STUDIES AND EXPERIMENTS
E. K. Smith, Chairman

9:10 USER NEEDS FOR PROPAGATION DATA
T. Sullivan ***(ARC)***

9:25 STATISTICAL RESULTS FROM THE VIRGINIA TECH PROPAGATION EXPERIMENT USING THE OLYMPUS 12, 20, AND 30 GHz SATELLITE BEACONS
W. Stutzman, A. Safaai-Jazi, T. Pratt, B. Nelson, J. Laster, H. Ajaz ***(VPI & SU)***

9:55 RESULTS FROM A STUDY OF SCINTILLATION BEHAVIOR AT 12, 20, AND 30 GHz USING THE RESULTS FROM THE VIRGINIA TECH OLYMPUS RECEIVERS
T. Pratt and F. Haidara ***(VPI & SU)***

10:15 OLYMPUS EXPERIMENTS IN PORTUGAL
Jose Neves ***(University of Aveiro)***

10:25 ITELSAT PROPAGATION STUDIES
A. Bonati ***(Polytechnic of Milan)***

10:30 MORNING BREAK

10:40 RADIOMETRIC OBSERVATIONS OF ATMOSPHERIC ATTENUATION AT 20.6 AND 31.65 GHz: THE WAVE PROPAGATION LABORATORY DATA BASE
M. D. Jacobson, J. B. Snider, and E. R. Westwater ***(NOAA/ERL/WPL)***

10:55 LONG DURATION MEASUREMENTS OF FADING ON A LOW ELEVATION ANGLE, 11-GHz SATELLITE PATH
W. J. Vogel and G. W. Torrence ***(Texas)***

11:10 LARGE-SCALE RAINFALL DIVERSITY FOR ACTS
H. P. Lin and W. J. Vogel ***(Texas)***

11:40 RAIN-RATE DATA BASE DEVELOPMENT AND RAIN-RATE CLIMATE ANALYSIS
R. K. Crane ***(Oklahoma)***

12:00 LUNCH BREAK

1:30 A DATABASE FOR PROPAGATION MODELS
A. V. Kantak, K. Suwitra, and C. Le ***(JPL)***

SESSION 2. PROPAGATION STUDIES FOR MOBILE/PERSONAL COMMUNICATIONS
J. Kiebler, Chairman

2:00 CONTRIBUTION TOWARDS A DRAFT REVISION OF RECOMMENDATION 681: PROPAGATION DATA REQUIRED FOR THE DESIGN OF EARTH-SPACE LAND MOBILE TELECOMMUNICATIONS SYSTEMS
F. Davarian and D. Bishop ***(JPL)***

2:15 PROPAGATION ISSUES FOR EMERGING MOBILE AND PORTABLE COMMUNICATIONS, A SYSTEMS PERSPECTIVE
N. Golshan ***(JPL)***

2:35 PROPAGATION CONSIDERATIONS IN THE AMERICAN MOBILE SATELLITE SYSTEM DESIGN
C. Kittiver and E. Sigler ***(AMSC)***

2:55 CHARACTERISATION OF THE LMS PROPAGATION CHANNEL AT L- AND S-BANDS: NARROWBAND EXPERIMENTAL DATA AND CHANNEL MODELLING
M. Sforza and S. Buonomo ***(ESTEC)***

3:15 AFTERNOON BREAK

3:40 RESULTS OF MULTIBAND (L, S, Ku BAND) PROPAGATION MEASUREMENTS AND MODEL FOR HIGH ELEVATION ANGLE LAND MOBILE SATELLITE CHANNEL
M. A. N. Parks, G. Butt, B. G. Evans ***(University of Surrey)***, and M. Richharia ***(INMARSAT)***

4:00 EFFECTS OF THE EQUATORIAL IONOSPHERE ON L-BAND EARTH-SPACE TRANSMISSIONS
E. K. Smith and W. L. Flock ***(Colorado)***

4:15 TREE ATTENUATION AT 20 GHz: FOLIAGE EFFECTS
W. J. Vogel and J. Goldhirsh ***(Texas/APL)***

4:30 **CLOSING REMARKS**

5:00 **MEETING ADJOURNED**

ACTS PROPAGATION STUDIES MINIWORKSHOP
ADVANCED COMMUNICATIONS TECHNOLOGY SATELLITE
PASADENA CONVENTION CENTER (CONFERENCE BUILDING)
JUNE 14, 1993

SESSION 1. PROGRAM STATUS AND UPDATE
F. Davarian, Chairman

10:00 WELCOME
F. Davarian ***(JPL)***
10:05 ADVANCED COMMUNICATIONS TECHNOLOGY SATELLITE (ACTS) PROGRAM
R. Bauer (***NASA Lewis***)
10:15 STATUS OF ACTS PROPAGATION EXPERIMENTS
J. Kiebler ***(Mitre)***
10:20 THE ACTS PROPAGATION TERMINAL DELIVERY AND SUPPORT
W. Stutzman ***(VPI &SU)***
DATA COLLECTION WITH THE ACTS PROPAGATION TERMINAL
P.W. Remaklus ***(VPI&SU)***
PREPROCESSING DATA COLLECTED WITH THE ACTS PROPAGATION TERMINAL
D. Gaff ***(VPI&SU)***
11:20 ACTS DATA CENTER STATUS REPORT
A. Syed and W.J. Vogel ***(Texas)***

11:50 LUNCH BREAK

SESSION 2. EXPERIMENTER REPORTS
R. Crane and D. Rogers, Chairmen

1:30 PROPAGATION MEASUREMENT REQUIREMENTS BEYOND THE NEEDS OF THE CCIR
R.K. Crane ***(Oklahoma)***
1:40 ACTS PROPAGATION EXPERIMENT DISCUSSION
BRITISH COLUMBIA, COLORADO STATE, ALASKA, COMSAT LAB., NEW MEXICO AND STANFORD TELECOM., OKLAHOMA, SOUTH FLORIDA AND FLORIDA ATLANTIC , TELEGLOBE CANADA
3:30 BREAK
3:50 USING THE E-MAIL SYSTEM FOR INFORMATION EXCHANGE
K. Suwitra ***(JPL)***
4:00 UPLINK POWER CONTROL EXPERIMENT USING THE AMT
W. Stutzman ***(VPI&SU)***
4:10 A PLAN FOR ACQUIRING PROPAGATION DATA FROM ACTS COMMUNICATIONS EXPERIMENTS
A.G. Cha ***(JPL)***
4:25 NEW ISSUES AND ACTION ITEMS
5:00 MEETING ADJOURNED

OPENING REMARKS: CURRENT AND FUTURE ACTIVITIES

Faramaz Davarian

It is our custom to present the Propagation Program's recent accomplishments and future plans at the onset of a NAPEX meeting. The following is a summary of our report card.

The data analysis phase of the U.S. **Olympus Campaign** is nearing its end. The final report will be published by Virginia Tech by midsummer 1993. The report will comprise measurement analysis for 12 months. It will include monthly and annual attenuation statistics and statistics on scintillation effects. A number of prediction models will be presented. Two talks are scheduled on the Olympus experiments in the morning session.

The **ACTS** propagation experiment preparations are moving forward as expected. Since we devoted all of yesterday to this topic, I will not elaborate on ACTS any further.

The **mobile/personal** channel characterization efforts continued during the last year. Data collected by the University of Texas in 1992 are being analyzed and will become available by September 1993. We have recently started a study to characterize LEO mobile/personal channels. Topics such as indoor reception, tree shadowing, blockage, and delay spread will be investigated. These results will become available in one to two years from now. We have also collected Ka-band mobile data using Olympus 20 GHz beacon transmissions. Wolf Vogel will present a paper on this topic in the afternoon session. To reflect our radio satellite broadcast (DBS-R) interest, Nasser Golshan will discuss this topic in a paper that will be presented this afternoon.

The University of Texas has already collected five years of **low-elevation angle, 11-GHz** propagation data. This experiment is the subject of a paper that will be presented later this morning.

The work on **database for propagation models** has progressed very well. The first release is ready, and the participants of this meeting will receive a copy of the software. Kris Suwitra will present a demonstration of the software after lunch.

We had an active year where **CCIR** is concerned. An input document on land mobile satellite system (LMSS) propagation models was submitted to the U.S. national committee and was approved and sent to Geneva. This document will be used at the October 1993 meeting of Working Party 5B to produce CCIR recommendations. This CCIR input document will be discussed by Dennis Bishop later today. We have also submitted LMSS data to the CCIR data base. Bob Crane has developed a new rain rate data base for CCIR.

Last year Virginia Tech completed an uplink power control algorithm. This scheme will be tested using JPL's ACTS mobile terminal. The initial tests will be performed this fall, with more tests to follow in 1994.

For the last four years the NASA Propagation Program has supported the Wave Propagation Laboratory of NOAA to conduct radiometric measurements of the sky noise temperature at 20, 30, and 90 GHz. Due to budget restrictions, the program was unable to support this activity in the current year. However, NOAA was able to continue the effort using internal resources. We will hear a presentation on this topic today from Mark Jacobson.

Due to Ernie Smith's retirement and budgetary constraints, the NASA Propagation Information Center at the University of Colorado will close later this year. Although it is difficult to match Ernie Smith's and Warren Flock's quality work, we will try to continue this effort at JPL.

The NASA Propagation Handbooks are in need of revision. We have tried to attend to this need for the last two years; however, because of budget limitations we have not been able to do so. Regretfully, also due to funding limitations, the NASA Handbooks will not be revised next year either.

L-band ionospheric scintillation is of much concern to the FAA and the airlines. We are planning to investigate this problem and offer solutions. This will be a joint effort between our program and the FAA. It is expected that the initial results will be available for presentation at NAPEX XVIII.

We will also hear from two of our international guests, both members of the Olympus Propagation Experimenters (OPEX) group. Professor Jose Neves will discuss the Portuguese Olympus experiment, and Dr. Apolonia Bonati will introduce Itelsat millimeter wave propagation measurements in Italy.

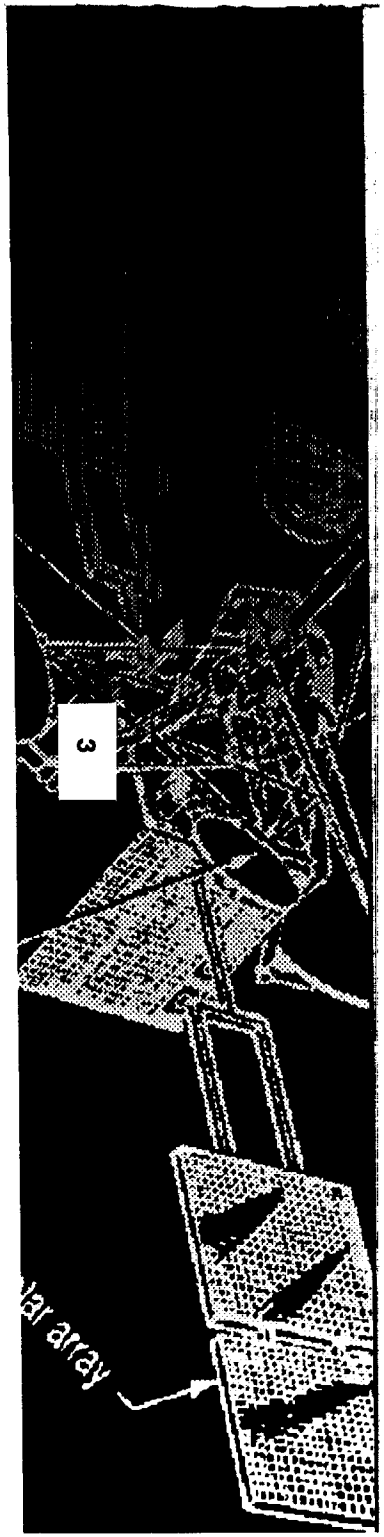

NASA Office of Advanced Concepts and Technology

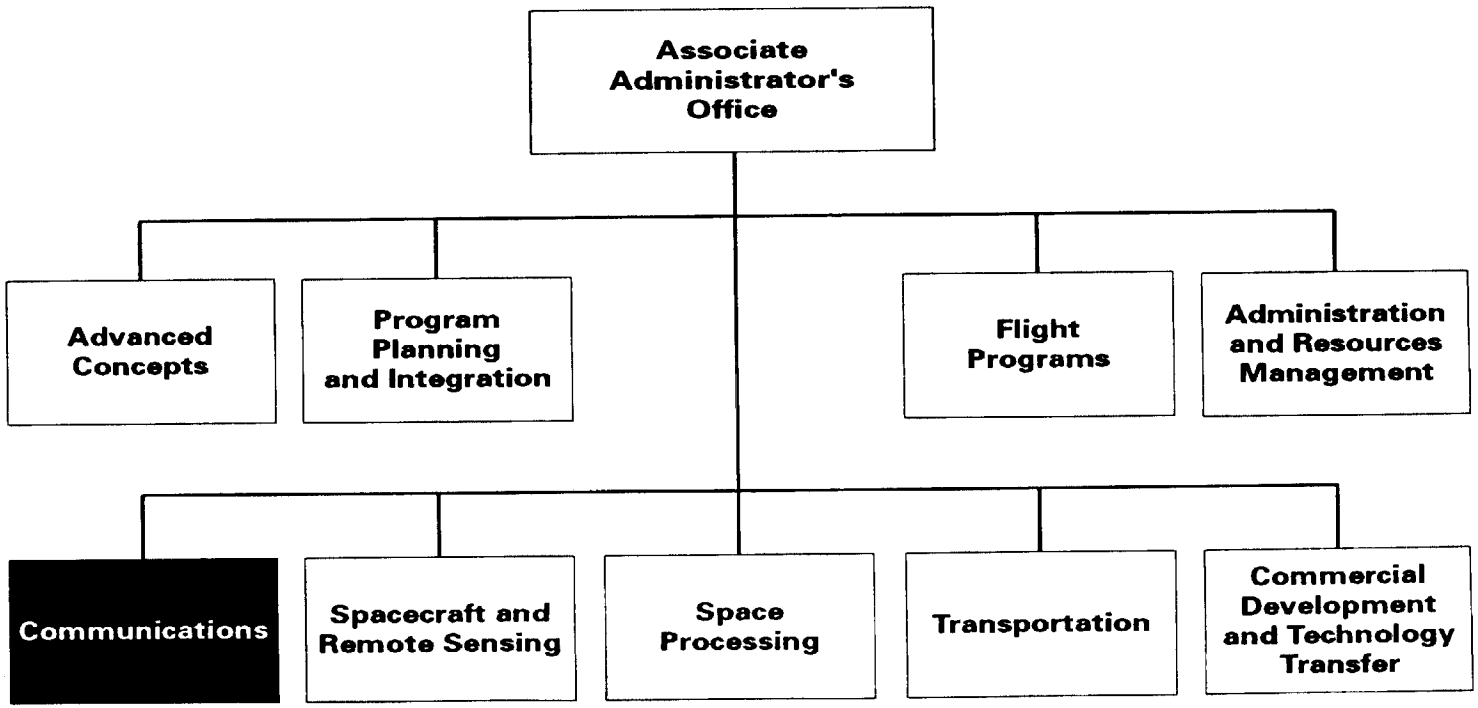

OPENING REMARKS
John Kiebler, MITRE Corporation

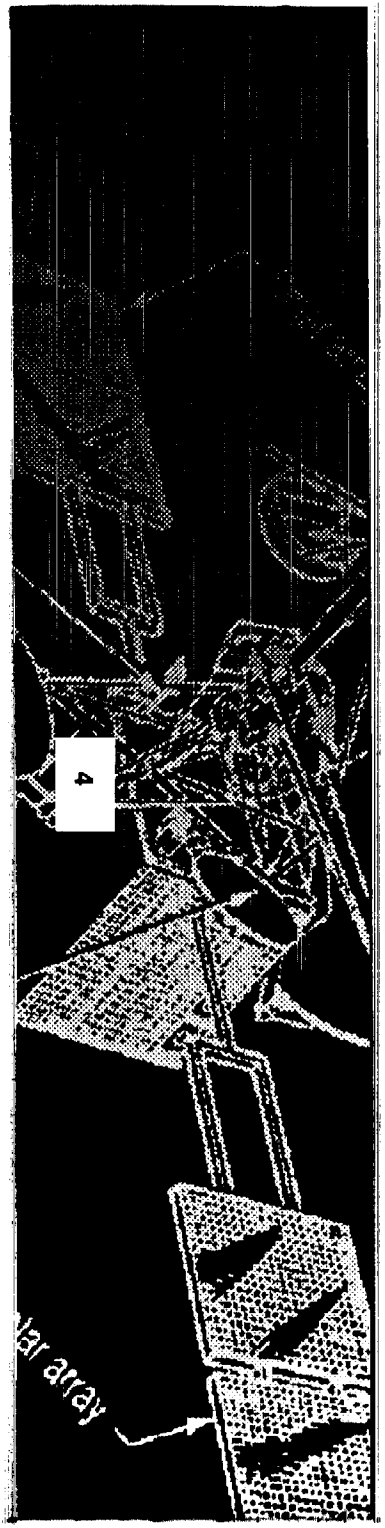

Communications Division

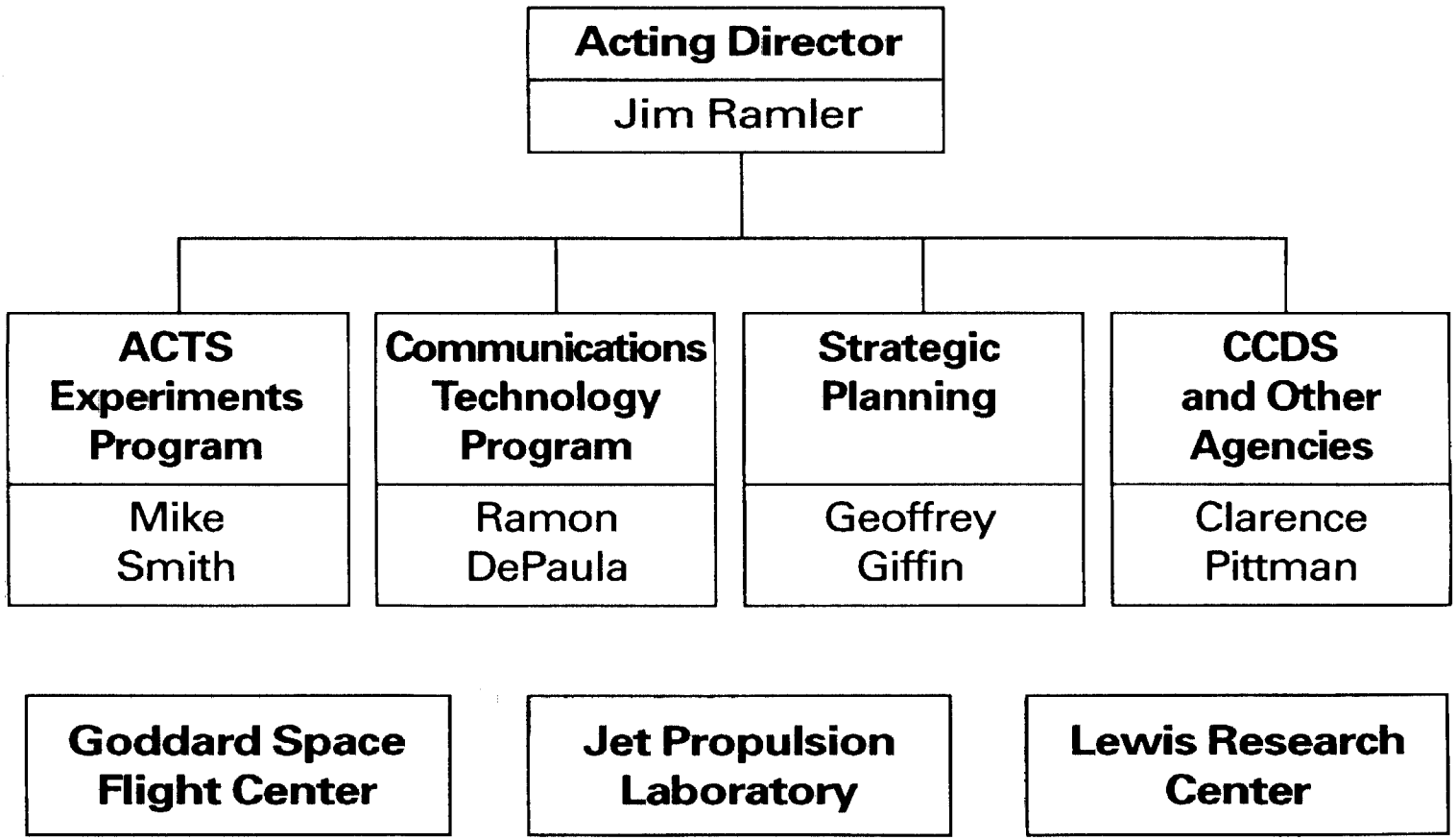

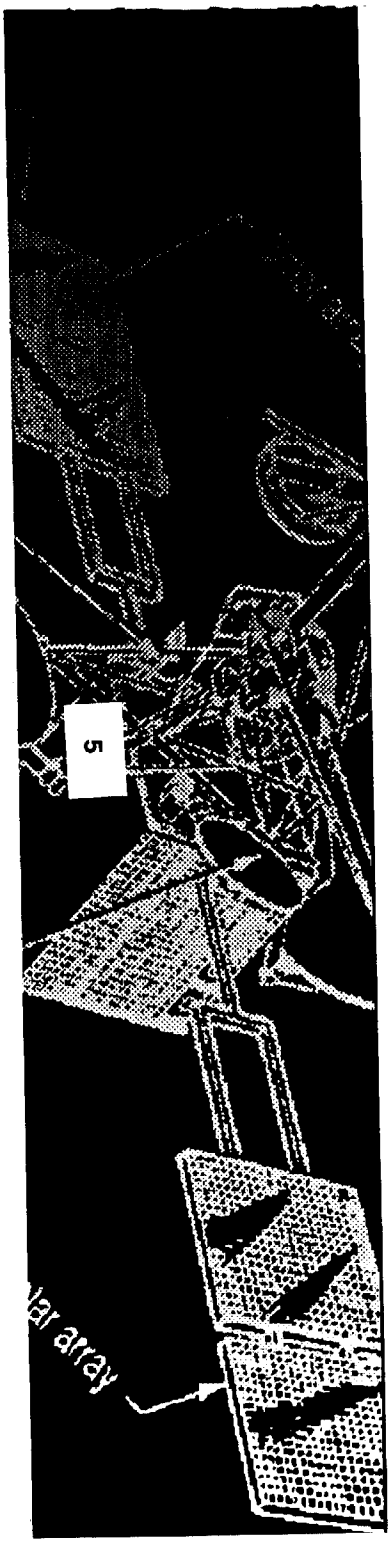

Mission

To pioneer innovative, customer-focused space communications concepts and technologies to enable advanced NASA missions and ensure U.S. competitiveness and preeminence in space communications

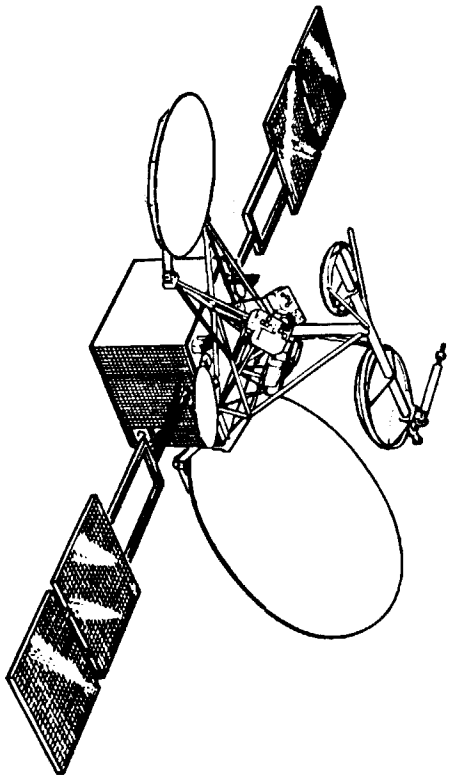

- Execute the ACTS Experiments Program as the centerpiece of the Nation's advanced communications development activities
  - Ensure strong participation by U.S. industry
  - Transfer ACTS technologies to U.S. industry
- Expand capability and reduce costs through technology advancements which increase U.S. competitiveness in communications and spacecraft performance in the areas of:
  - Near Earth communications
  - Deep space communications
  - Mobile communications
  - Fixed/broadband communications

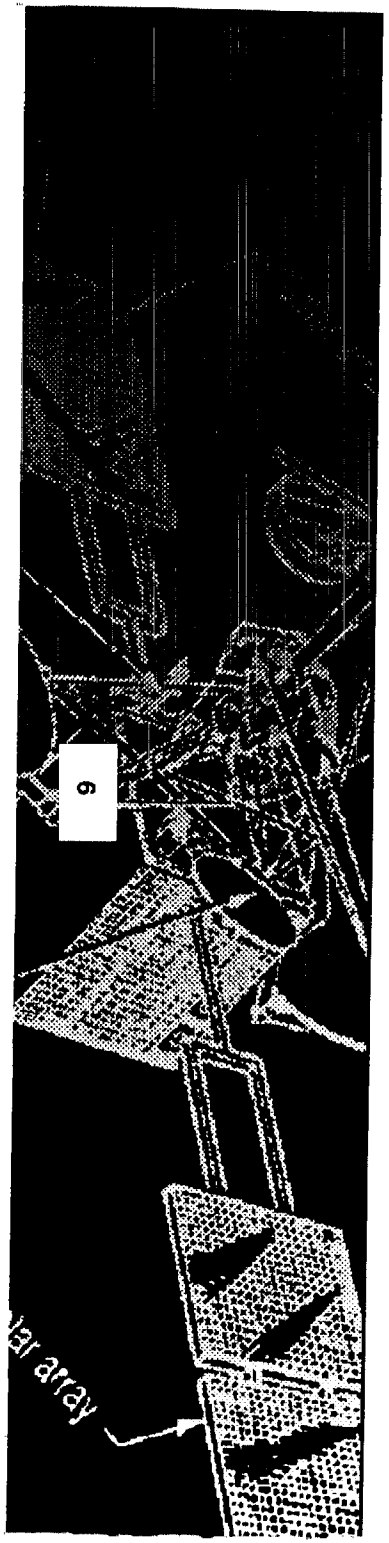

Major Elements

- Advanced Communications Technology Satellite (ACTS) Experiments Program
- Communications Technology Program
- Centers for the Commercial Development of Space (CCDS) in satellite communications
- Advanced Studies
- Strategic Planning Activity

Advanced Studies Program

Objective

Perform system and architecture studies to identify new communications technology needs and service strategies, propagation studies and experiments, and spectrum utilization analyses to determine optimum utilization and application of new frequency bands.

The program consists of the following elements:

- System studies
- Propagation studies
- Spectrum utilization studies

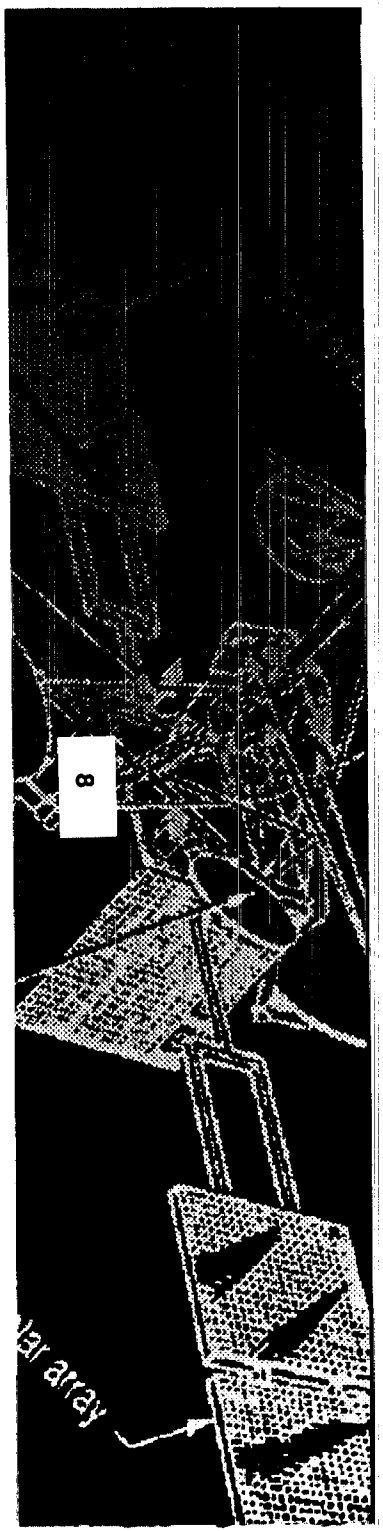

System Studies

- Identify and assess the needed technology developments for rapidly changing satellite communications market
- Provide basic requirements and design data from user/market, propagation, and regulatory studies. Define innovative concepts for satellites and systems to meet current and future needs of U.S. Industry
- Maintain current knowledge of state-of-the-art in communications technology

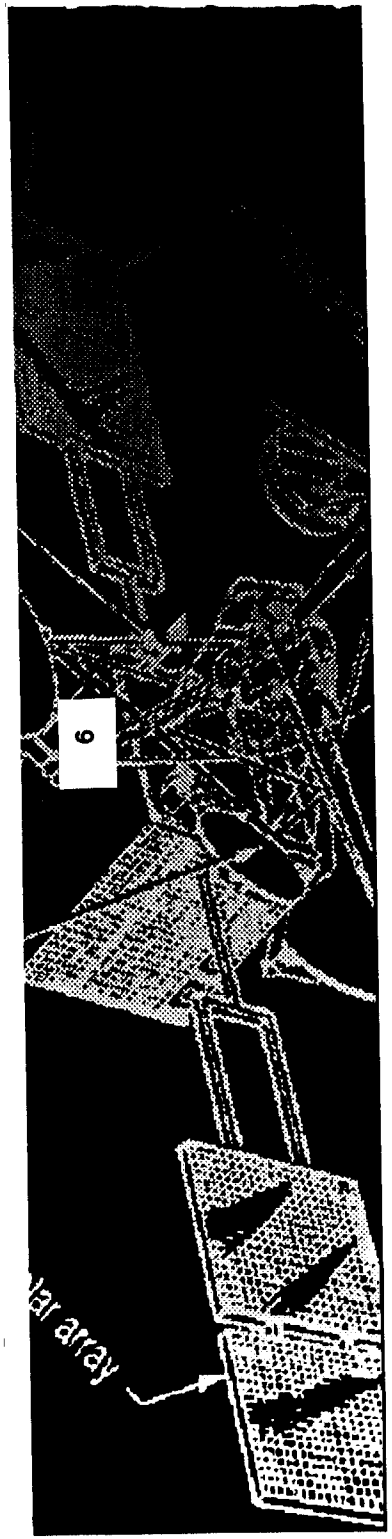

Propagation

- A coordinated NASA/University/Industry program which supports space communications science by conducting key propagation studies and experiments
- Perform analytical studies and conduct experiments to quantify impairments caused by: rain attenuation, depolarization, multi-path, scintillation, clouds, buildings and vegetation
- Develop mitigation techniques

ACTS Propagation Experiments

- *ACTS propagation experiments will be performed utilizing the 20 and 30 GHz beacons to characterize signal impairments and apply suitable compensation techniques*
- *Will conduct a series of workshops to establish requirements and coordinate experiment plans*

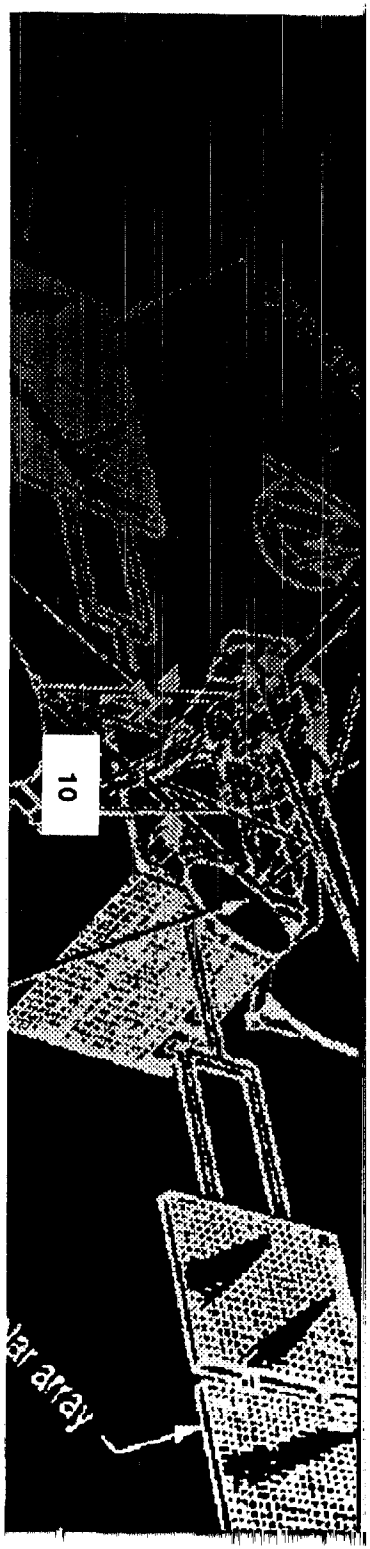

Orbit Spectrum Utilization

- Represent the interest of NASA and U.S. Industry in orbit/spectrum utilization for new and existing space services
- Participation in regulatory activities (CCIR meetings, World Administrative Radio Conferences [WARCs], etc.) to obtain necessary frequency allocations for future satellite services/applications
- Provide technical advice to NTIA and FCC
- Investigate new methods and concepts to utilize the existing orbit/spectrum resources more efficiently

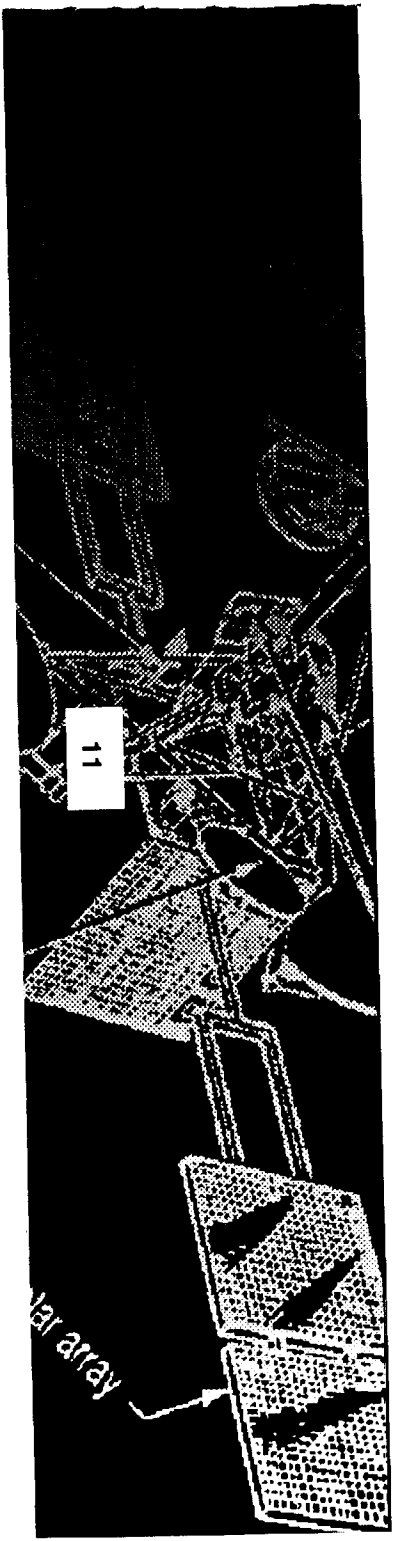

Summary

- The immediate future poses exciting, challenging and potentially world changing opportunities in the communications industry
  - Any time/anywhere personal communications
  - High data rate mobile communications
  - Integrated services (voice, FAX, video)
  - Ultra-high data rates for fixed services
- Major challenge to participants to take advantage of the technical opportunities, defense conversion and the new environment of innovative partnerships and alliances
- NASA intends to be a significant player in maintaining the leadership of the U.S. in the space communications business

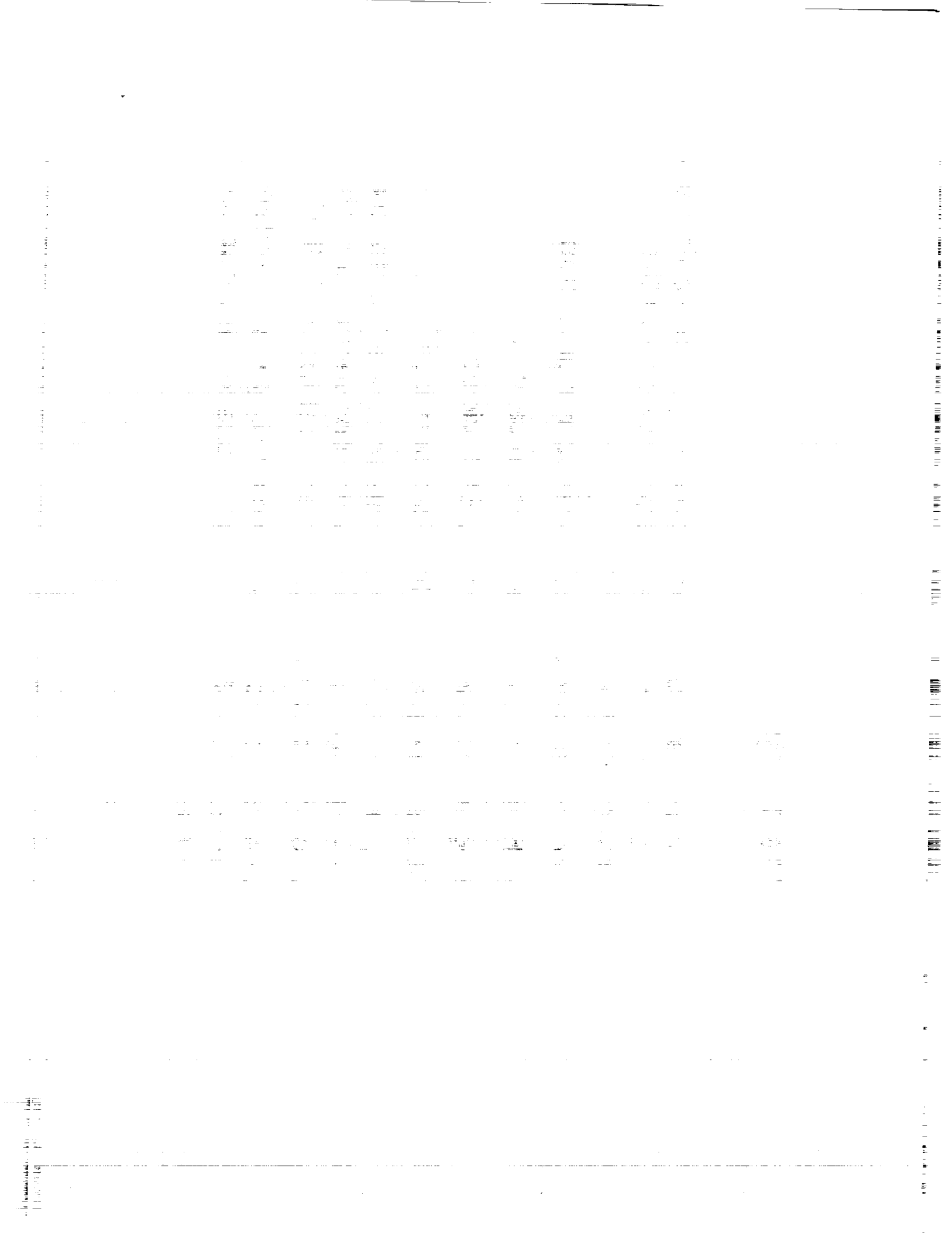

New Challenges in Propagation Research in the U.S.

Faramaz Davarian
Jet Propulsion Laboratory
California Institute of Technology

Introduction

Earth/space propagation research in the U.S. is tied to new developments in satellite communications. In spite of the fiber optics competition for trunked point-to-point communications, a host of emerging services are discovering the great potential of satellites for wireless communications. The application of satellites for radio communications appears to grow with a rapid pace in the areas of thin-route and mobile/personal communications.

An important factor influencing the future of satellite communications is the congestion of the spectral slots at Ku- and lower bands. This heavy usage of the spectrum gives rise to conflicts among the users and consequently forces regulatory organizations to relocate frequency assignments, a decision that, for obvious reasons, is unpopular with the relocated service. Because of this frequency shortage, frequencies in Ka- and higher spectral bands are currently viewed as good candidates for Earth/space communications in the future.

Therefore, new challenges in propagation research in the U.S. include the characterization of mobile/personal links and the investigation of higher bands for satellite communications. Figure 1 depicts the above radiowave propagation scenarios. This paper will briefly review the plans and the challenges of the propagation research in the U.S.

Mobile and Personal Applications

The use of satellites for mobile communications is not a new idea. This application was explored by NASA's Mobile Satellite Experiment (MSAT-X) at the Jet Propulsion Laboratory during the 1980s. It was soon realized that a good understanding of the channel characteristics is fundamental to the planning of mobile satellite

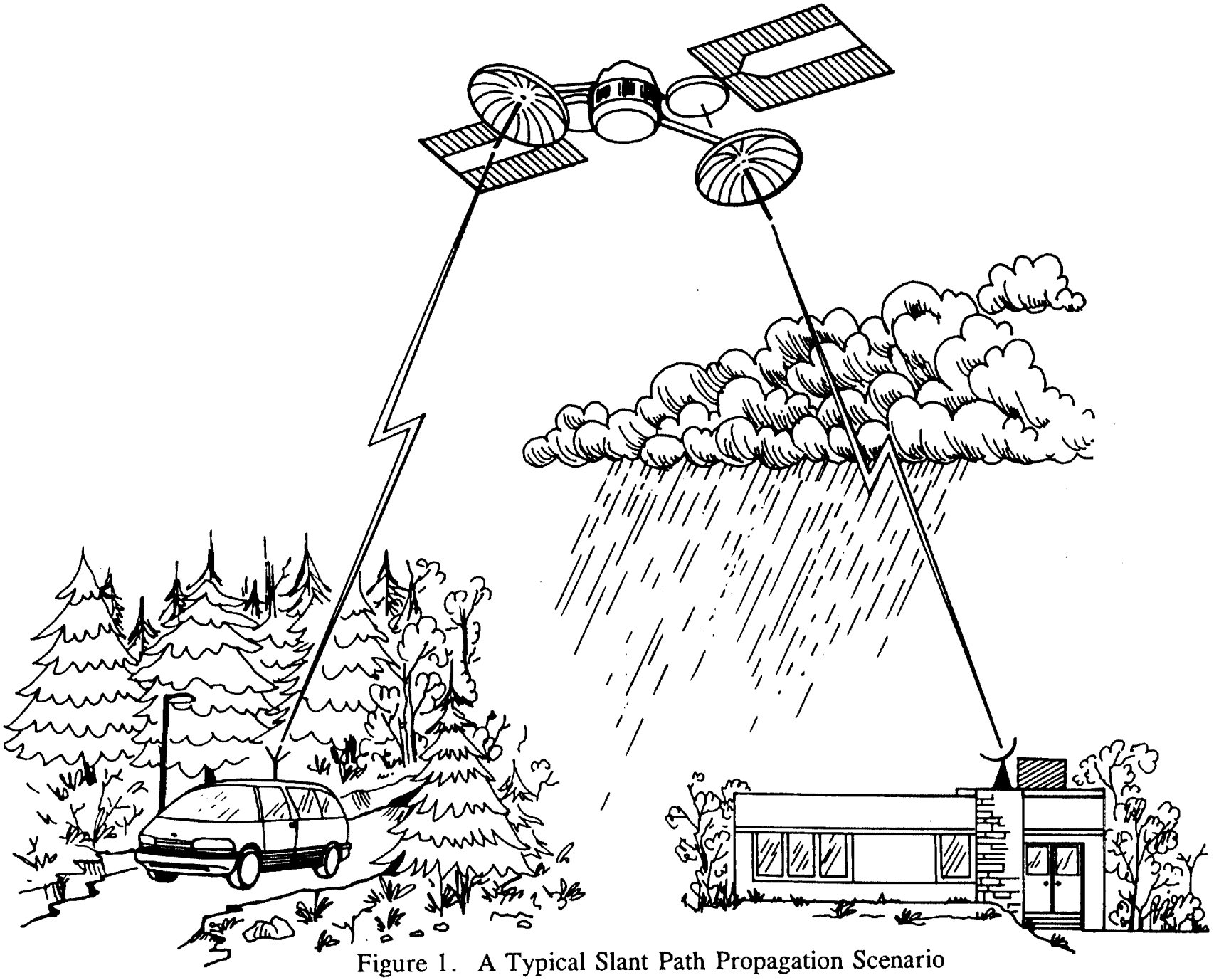

Figure 1. A Typical Slant Path Propagation Scenario

systems. To support the MSAT-X and the emerging mobile satellite technologies, the NASA Propagation Program funded a number of studies to examine the propagation effects of land mobile satellite channels. In addition to analytical work, these efforts included a considerable number of field measurements. In the early years of the endeavor, data were collected using simulated space platforms, such as balloons and helicopters, and in the later years, satellite transmissions were used. The mobile experiments in the U.S. were conducted primarily at UHF and L-bands, and they mostly employed omnidirectional ground antennas. The assumed satellite orbit for studies conducted in the U.S. was geostationary.

It is worth noting that in parallel with NASA's efforts, propagation researchers in other countries also investigated the vagaries of the mobile satellite channel. Notable efforts took place in Canada, Europe, and Japan. Some of these investigations also included aeronautical and maritime mobile satellite links. A compendium of results for land mobile satellite systems can be found in [1], and two CCIR recommendations address propagation in aeronautical and maritime mobile satellite systems [2].

Three recent events have influenced the future of mobile/personal applications.

First, in the 1980s Voice of America recognized the value of satellites in direct radio broadcasting to augment the less reliable shortwave broadcasting [3]. And more recently, the commercial use of DBS-R has attracted much attention [4].

Second, many potential service providers have lately considered the use of satellites for personal communications. Much attention is now being given to LEO as well as GEO satellites.

Third, WARC '92 deliberated mobile/personal applications and opened new regions of the spectrum for them. Although the L- and S-bands presently are the most popular spectral slots, allocation as low as 150 MHz and as high as 30 GHz exist for mobile/personal applications, and most of these frequencies are likely to be used sometime in the future.

The task that propagation researchers are faced with is the characterization of a vast region of the spectrum for mobile/personal links. This assignment is particularly challenging because the mobile

channel demonstrates a nonstationary behavior. Note that mobile/personal receivers may operate in a variety of propagation environments, including reception with or without a clear view -- tree shadowing, blockage, etc. In addition to the above effects, the Doppler-induced dynamics of the signal should also be taken into account.

Currently, data availability is limited to a few selected frequencies with only a limited number of physical and environmental attributes; therefore, future efforts should concentrate on expanding the existing propagation data base to all the bands of interest and include a broader selection of environmental parameters. It is also important that a diversity of satellite orbits, i.e., GEO, LEO, and HEO, be considered in the future studies. The following is a partial list of topics in propagation research which need to be addressed:

1. Conduct propagation measurements into buildings to determine the spatial, spectral, and temporal signal structure for indoor reception.

2. Perform mobile measurements in urban, suburban, and rural environments to derive statistical information, determine model parameters, and obtain data for channel simulation. Measurements through trees must receive much attention.

3. Make stationary and mobile measurements of the delay spread to model the wideband behavior of mobile/personal channels. Sites in city centers and mountainous areas are of special interest.

In addition to the above items, land mobile satellite service providers need detailed statistics on regions of interest to them. However, the collection of detailed information on all the regions of interest will be prohibitively expensive. A good compromise is presented in Item 4 below:

4. Optical blockage and shadowing measurements can be made to provide statistics on a given environment, for example, a given region, a particular highway, etc. It has been shown that optically based sensing systems can predict radio propagation impairments resulting from signal blockage and shadowing [5].

5. Develop service contour maps depending on frequency, orbit, land environment, coverage area, etc.

6. Develop a systematic method for evaluating ITU allotted spectral slots for different applications.

7. To enhance system performance, propagation effects should be mitigated or reduced. Examples are adaptive coding and power control, and smart antennas that can adapt their performance to match the propagation characteristics of the channel (multipath reception).

8. For applications near equatorial regions information is needed on the morphology of ionospheric scintillation at low latitudes, particularly as it affects L through C bands. Examples of services needing this type of information include direct broadcasting to low-latitude countries and aeronautical communications for oceanic flights.

The above studies should also consider the effect of polarization and antenna type on propagation.

In the future, the designers of mobile/personal satellite-based networks are likely to employ simulation schemes for system design and evaluation applications. Therefore, propagation data and models are needed to develop simulation tools. For such applications, time series data or data generated locally using known signal statistics can be used. Future propagation research should support the development of simulation tools.

Rain and Cloud Effects

Most rain attenuation prediction procedures depend on rain climate models. The available climate models are now about 15 years old, have not been updated in a consistent way to incorporate new observations, and are not dependent on measurable parameters such as annual and monthly rain accumulation, number of days with rain, synoptic conditions to be associated with rain, etc. Once the relationship between rain attenuation model and measurable climatological data is known, maps of the latter can be used to generate maps of the expected attenuation to be exceeded for a given fraction of time on a specific type of path such as from a mobile vehicle to a geostationary satellite. Future propagation research should include a revision of current rain climate models. Furthermore, rain-rate distribution models should be expanded to

represent seasonal behavior of the rain process. The annual/worst-month distribution relationships depend on the seasonality of the process, as do any models designed to explain the variability of the process.

Because most of the available data have been, or will be, used to provide the parameters for model distributions, more samples of the rain rate distributions for locations where observations have been made and for new locations are needed to provide an independent set to test the models.

An important component of most rain attenuation models is the rain height. For many applications the assumption of a fixed rain height is not realistic; therefore statistics on the variation of rain height with day, season, time of day, location within a storm, etc., are needed. For applications such as aeronautical mobile, the stochastic approach to rain height modeling is imperative. It is also important for receiver terminals in the mountains.

Some rain attenuation models depend on the expected correlation between rain rates at different locations along a path. For such applications an improved model for the correlation structure of rain rate can be useful.

By ignoring the microstructure of rain, the available models give rise to errors in signal attenuation prediction and discrepancies in frequency scaling. These problems become more intense for frequencies above about 17 GHz because of the sensitivity of these frequencies to changes in the drop size distribution at the smaller drop sizes. A basic problem lies in the difficulty of making reasonable drop size distribution measurements. Employing measurements at the higher frequencies, i.e., the 90- and 120-GHz windows, simultaneously with measurements at lower frequencies may unravel this problem. The microstructure problem is one that affects our ability to do "frequency scaling," an important component of the uplink power control problem.

Although the influence of clouds can be ignored for the lower frequencies, their effect is important at higher frequencies. The only simple measurement tools available for cloud sensing are multi-frequency radiometers similar to the ones NOAA operates in Boulder, Colorado. Since radiometers cannot determine the atmospheric liquid water versus distance, data from other remote sensing

measurements may need to be combined with radiometric data for cloud modeling. For propagation modeling this is virgin territory with no adequate models and very little data.

Characterization of the Spectral Bands above about 17 GHz

The congestion of the spectrum for radio communications will inevitably push some services to bands above about 17 GHz. Radiowave propagation at frequencies above 17 GHz is plagued with rain-induced signal attenuation, a factor that for small probability levels can be prohibitive. Therefore, services that require a low to moderate degree of link availability are likely to be attracted to frequencies above 17 GHz sooner than those demanding a very small probability of outage. The aeronautical mobile satellite service can use the Ka-band to its advantage considering that the cruising altitudes of most flights are high enough to either eliminate or considerably reduce the rain attenuation problem. Links in parts of the world with a low annual rainfall can use frequencies above about 17 GHz without significantly compromising link availability. For example, feeder links of mobile satellite systems can be placed in the relatively dry regions of the country to minimize rain attenuation at frequencies above about 17 GHz.

Link availability can be improved via the use of some form of fade mitigation technology. Hence, if tools to offset rain-induced effects are employed, the Ka-band can be used for services that require a moderate degree of link availability but cannot afford a large power margin. Lately, the VSAT industry is showing much interest in the Ka-band. A low margin VSAT can transmit in the Ka-band by either reducing its demand on link availability or employing a fade mitigation technique.

To accommodate low margin systems, future propagation research in the U.S. includes a measurement campaign using NASA's Advanced Communications Technology Satellite (ACTS). An experimental spacecraft, ACTS provides transponders and propagation beacons at 20- and 30-GHz bands. ACTS will also be used for Ka-band mobile/personal experiments. Plans for future research at the Ka-band call for the expansion of the current knowledge on Ka-band propagation with a focus on the following efforts:

- Develop attenuation prediction models for atmosphere-induced effects with attention to high-occurrence, low-attenuation factors, such as light rain, clouds, and fog.

- Refine the existing climatological maps.

- Develop fade mitigation tools.

- Develop a model for large-scale diversity.

- Provide a means of frequency scaling.

- Investigate propagation characteristics of ground and aeronautical mobile channels.

- Develop models for predicting impaired operation and outage duration statistics and the mean time between outages or impairments during a rain event.

The measurement phase of the ACTS campaign is likely to last four years with a total campaign period of five years, 1993 to 1998. Several sites, all equipped with dual frequency beacon receivers and radiometers, will collect data. Considering the complexity of the campaign, much thought has been given to data archiving logistics. It appears that the community will be served best if data archiving and dissemination takes place by a single organization, known as the ACTS Propagation Data Center. Table 1 shows the ACTS propagation measurement sites.

Table 1. Sites for ACTS Propagation Terminals

LOCATION	CCIR Rain Zone	LATITUDE (NORTH) Deg	LONGITUDE (WEST) Deg	AZIMUTH from North Deg	PATH EL Deg	SLANT RANGE Km
Vancouver, BC	D	49	123	150	30	38777
Ft. Collins, CO	E	40	105	173	43	37654
Fairbanks, AK	C	65	148	129	9	40905
Clarksburg, MD	K	39	077	214	39	37971
Las Cruces, NM	M/E	32	107	168	51	37075
Norman, OK	M	35	097	184	49	37242
Tampa, FL	N	28	082	214	52	37060
Montreal, PB	K	45	074	215	31	38583
Montreal, PB	K	46	075	214	31	38582

Since the ultimate goal is to provide design tools for system engineers, the ACTS campaign emphasizes interaction between the experimenters and industry. A forum known as the ACTS Propagation Studies Workshop, formed in 1990, brings together on an annual basis experts from industry, academia, and elsewhere to develop plans for the ACTS propagation campaign.

Regulatory Issues

The increased use of satellites by today's emerging services will result in new demands for the already scarce resource of the radiowave spectrum. These demands will inevitably result in a more aggressive approach toward revising existing allocations and generating new ones by the ITU. Therefore, regulatory bodies around the world will be in more need of propagation data than before. Hence, propagation research in the U.S. should continue the support of regulatory organizations with an emphasis given to

- Active participation in the CCIR efforts, particularly Study Group 5.
- Support of the ITU in providing spectrum for services which employ satellites for communications.
- Cooperation with other regulatory organizations, such as the NTIA, FCC, Space Frequency Coordination Group (SFCG), Consultative Committee on Space Data Systems (CCSDS), etc.

CCIR Study Group 5 activities entail mainly the development of recommendations for predicting propagation anomalies in communications systems. Many CCIR recommendations can be expanded to better serve system and design engineers.
In particular, recommendations dealing with propagation in mobile satellite channels (Rec. 680, 681, and 682 [2]), can greatly benefit from propagation research in the U.S. and elsewhere. For example, those recommendations will be enhanced by providing prediction models for signal attenuation, depolarization, and delay spread at all bands of interest with the elevation angle and the antenna type as parameters.

The inclusion of environmental descriptors in a model for mobile/personal applications is an important factor for the successful use of a prediction tool by system engineers. Examples are the

terrain type in land applications, the state of the sea surface in maritime applications, and the cruising altitude in aeronautical applications. Therefore, CCIR recommendations should be expanded to include models that accurately predict the propagation phenomena for the application of interest at the coverage of interest. Future efforts should include LEO and HEO configurations in addition to the GEO systems.

To predict slant path rain attenuation, CCIR provides prediction models and rain climate maps. The CCIR rain climate maps are in need of improvement; for example, the map for the U.S. places New Mexico, with its arid climate, in the same rain climate region as South Carolina, which has subtropical weather. Clearly future propagation research should correct such discrepancies.

Microclimatology is an important factor in the design and planning of fixed and broadcast services. CCIR models generally ignore this effect and hence give rise to prediction inaccuracies. This topic needs to be addressed by propagation researchers and the resulting data should be provided to CCIR.

Data Dissemination and Representation

The sophisticated satellite networks of the present day require automated techniques for link calculation and planning. Propagation prediction tools should be presented to the system engineer in an easy to use fashion. It is desirable that data and models be incorporated with computerized link calculation programs to save time and prevent user frustration. Therefore, the propagation community should provide engineers with user-friendly propagation software that can be easily implemented on popular personal computer systems and readily interfaced to the user's design control tables.

Simulation techniques are playing an increasingly important role in the planning, design validation, and implementation of communication systems. Since the collection of propagation data is often a time consuming effort, an alternate approach may be needed to meet the propagation needs of a system under design. In such a case, simulation can be an attractive alternative, assuming that adequate prior data can be applied to the system under consideration. Therefore, schemes to simulate propagation effects should be developed and provided to system designers. Again, to

enjoy widespread acceptance a simulation tool should use modern software technology and run on a personal computer.

Handbooks are useful tools for educational and system design purposes. In the U.S., NASA has published and maintains two handbooks on slant path propagation effects. NASA handbooks have been used by U.S. industry for many years. Currently CCIR Study Group 5 is also working on a handbook to complement some of its recommendations. Efforts to publish and update handbooks should continue and expand in the future. Such handbooks should be evolving documents with frequent revisions to ensure their vitality.

Conclusions

Some items in need of further research include

- Mobile/personal links in all the ITU allotted bands including the relevant choices of the propagation environment, ground antenna type and satellite orbit configuration as parameters.
- Rain climatology, including microstructure and seasonal effects.
- Rain attenuation models, including event duration distributions.
- Fade mitigation technology.
- Cloud effects for frequencies above about 30 GHz.
- Bands above about 17 GHz with emphasis given to low-margin applications.
- Low-latitude ionospheric scintillation effects (direct broadcast and aeronautical applications).
- Spectrum allocation for satellite applications via participation in regulatory processes.
- Computerized models for the prediction of propagation effects.
- Tools for the simulation of propagation effects.
- Maintenance and periodic revision of handbooks on slant path propagation.

The propagation community must stay abreast of the changing trends in the satellite communications market. This can be achieved by an ongoing dialogue with system planners and design engineers of satellite communication networks. The success of propagation research in the future will depend largely on how well the needs of the systems and engineering community are communicated to the propagation experts and experimenters.

Acknowledgment

The research conducted in this paper was funded by the Jet Propulsion Laboratory, California Institute of Technology, under a contract with the National Aeronautics and Space Administration. The author would like to thank many of the members of the NASA Propagation Program for providing him with useful comments.

References

1. J. Goldhirsh and W. Vogel, *Propagation Effects for Land Mobile Satellite Systems: Overview of Experimental and Modeling Results,* NASA Reference Publication 1274, Feb. 1992.

2. *Recommendations of the CCIR*, International Radio Consultative Committee, Geneva, Switzerland, Vol. V, 1990.

3. D. Messer, "BSS (Sound) Receiver Development Activities by the USA Government," paper presented at CITEL, August 24-28, b1992, Mexico City, Mexico.

4. D. Marcus, "Five More Companies Seek Audio Satellite Licenses from FCC," *Space News*, Jan 4-10, 1993.

5. W. Vogel, and U. Hong, "Measurements and Modeling of Land Mobile Satellite Propagation at UHF and L-band," *IEEE Trans on Ant and Prop., Vol 36, No. 5, May 1988, pp 707-719.*

NAPEX XVII

Session 1

SLANT PATH PROPAGATION STUDIES AND EXPERIMENTS

Chairman:

Ernest K. Smith

University of Colorado

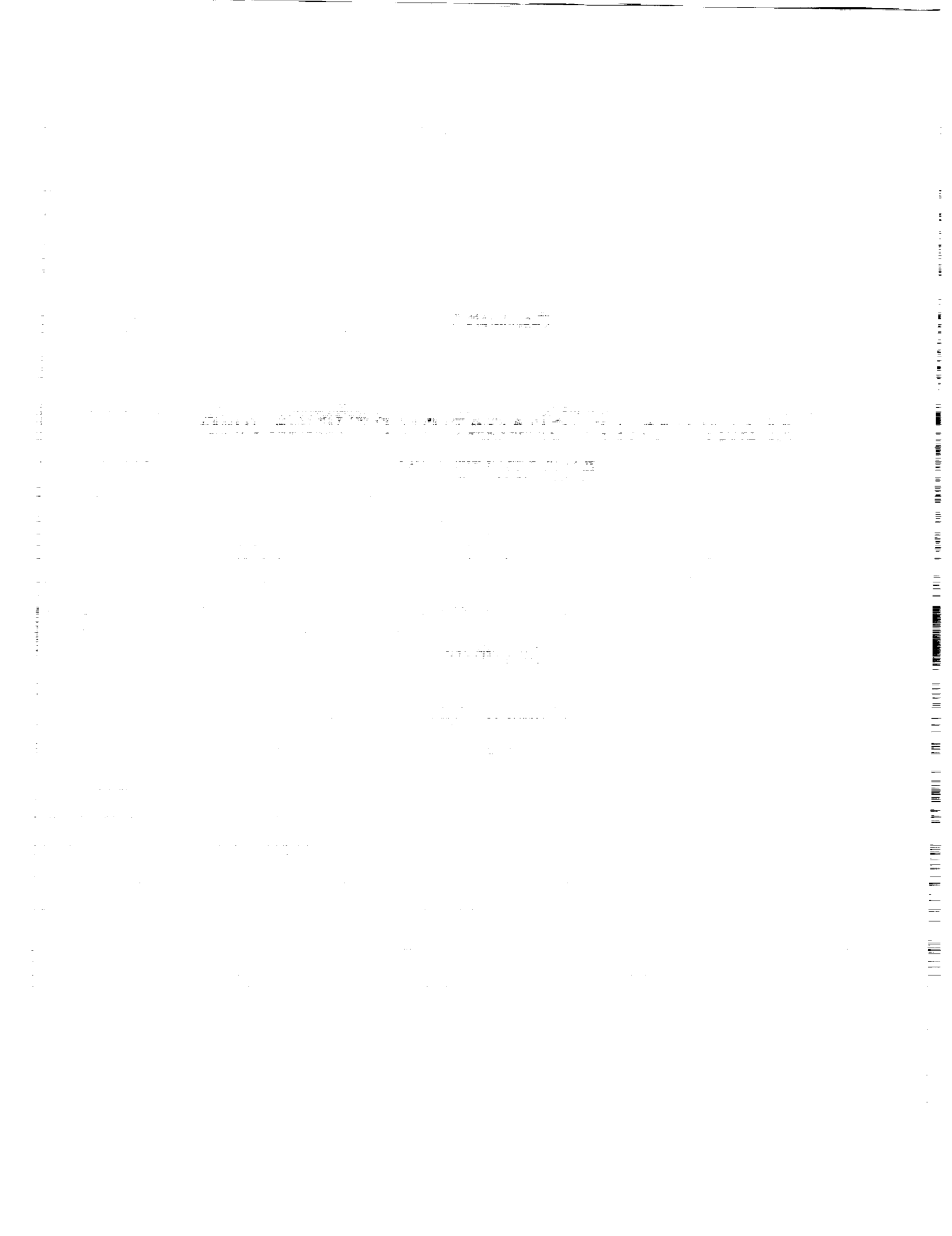

USER NEEDS FOR PROPAGATION DATA

Thomas M. Sullivan
Atlantic Research Corporation
Professional Services Group
8201 Corporate Drive, Suite 350
Landover, MD 20785

1. Introduction

New and refined models of radio signal propagation phenomena are needed to support studies of evolving satellite services and systems. Taking an engineering perspective, this paper reviews applications for propagation measurements and models in the context of various types of analyses that are of ongoing interest. Problems that have been encountered in the signal propagation aspects of these analyses are reviewed, and potential solutions to these problems are discussed.

The focus of this paper is on propagation measurements and models needed to support design and performance analyses of systems in the Mobile-Satellite Service (MSS) operating in the 1-3 GHz range.[1] These systems may use geostationary or non-geostationary satellites and Frequency Division Multiple Access (FDMA), Time Division Multiple Access Digital (TDMA), or Code Division Multiple Access (CDMA) techniques. Many of the propagation issues raised in relation to MSS are also pertinent to other services such as broadcasting-satellite (sound) at 2310-2360 MHz. In particular, services involving mobile terminals or terminals with low gain antennas are of concern.

2. Applications of Particular Concern

2.1 Form of Applied Propagation Factors

The engineering studies that require reliable predictions of signal propagation impairments include design and performance analyses that are described below. The analyses may be deterministic or use simulations, or may apply both simulation and deterministic techniques.[2] A deterministic approach is generally taken in cases where: baseband signal quality and availability are the dependent variables and simplicity is desired; initial estimates are sought; or accuracy sufficient for final results can be obtained. The more complex and costly simulation approach is taken when necessary for achieving the desired accuracy; performance in real time must be evaluated in detail; or it is desired to evaluate additional dependent variables such as loading on signaling channels. Consequently, suitable propagation models are needed for both analysis approaches.

---

1 The 1992 World Administrative Radio Conference (WARC-92) allocated the following bands to MSS in North America and elsewhere: 1492-1559 MHz (space-to-Earth); 1610-1660.5 MHz (Earth-to-space); 1613.8-1626.5 MHz (space-to-Earth); 1675-1710 MHz (Earth-to-space); 1930-2010 MHz (Earth-to-space); 2120-2200 MHz (space-to-Earth); 2483.5-2520 MHz (space-to-Earth); and 2670-2690 MHz (Earth-to-space).

2 Deterministic analyses address propagation factors in the form of cumulative time distributions. Simulations encompass propagation factors using Markov or Finite State Models (FSM).

2.2 Design Analyses

In the process of designing new systems, channels, or networks, analyses may be conducted to: develop an initial set of system requirements or specifications; identify optimal tradeoffs among candidate system parameters; investigate "sizing and timing" requirements for various system elements; or establish theoretical compliance of a design with the applicable specifications . Signal propagation impairments can be very influential upon the results of these analyses. Initial specifications for channel performance must not be overly ambitious in order to prevent unnecessarily high implementation costs. Those costs would result from improperly motivated tradeoff decisions, and the tradeoff evaluation process could in itself be flawed through application of erroneous propagation factors. Additional costs can be incurred, unnecessarily, if sizing or speed requirements for hardware or software are over estimated. Theoretical verification of compliance with specifications is of little value if the system ultimately does not perform as desired or expected. Thus, errors committed in addressing propagation factors can have serious consequences in the system design process.

2.3 Performance Analyses

Apart from design processes, performance analyses are conducted to determine: achievable system capacity; signal quality or availability; permissible or acceptable levels of aggregate and individual interfering signals[3]; the potential for sharing frequencies among MSS systems and between the MSS and other services; and the design and operating constraints necessary to complete coordination of proposed frequency assignments (i.e., to prevent mutual interference). The propagation data used in these applications can have consequences that are as dire as those associated with the design process.

In deciding the potential merits of a proposed domestic MSS frequency allocation or commercial MSS system, the Federal Communications Commission (FCC) must determine whether granting an allocation or a license is in the public interest. This can involve consideration of performance analyses (i.e., the analysis results filed as part of a petition for allocations or license application as well as independent analyses that may corroborate or refute those analyses), particularly where several competing applications are filed or there may be impact on incumbent systems. For example, the FCC recently convened a "Negotiated Rule Making Committee" to develop recommended technical rules for use of proposed domestic MSS allocations at 1610-1626.5/2483.5-2500 MHz, in which one of the contentious issues was the temporal-spatial average level of fading on downlinks (ill-substantiated values near 2 dB were used). This factor, when applied to contemplated CDMA systems, directly affects the potential peak capacity of individual systems and several such systems, collectively. The results of these analyses were presented to the FCC with results of similar analyses for competing MSS TDMA/FDMA technologies, and these may be compared and used as the basis for forthcoming FCC technical rules and licensing decisions. Consequently, much is at stake for the companies proposing these technologies.

On both the national and international levels, propagation factors may greatly influence: the frequency allocations adopted for MSS; MSS design and operating standards; and the implementation of MSS systems on an interference-free basis. Several MSS systems are proposed for each of the MSS frequency bands, and these bands already are used by services other than MSS. Thus, in accommodating growth in MSS spectrum requirements through enactment and implementation of new allocations, important factors are the degree to which incumbent systems may be displaced and the amount of spectrum resource in a shared band that may ultimately be available to MSS systems.

---

3 "Permissible" levels of interference are developed by the ITU Bureau of Radiocommunications (formerly the CCIR) in order to support frequency sharing studies and to establish the minimum level of interference that must be accepted by all system operators. For the MSS, this process is still at an early stage.

2.4 Summary of Applications

Much more could be said about the nature and importance of various applications for propagation data. The critical point, however, is to recognize that the work of propagation experts is vital to MSS and other radiocommunication services -- the results of that work can greatly influence many decisions, including decisions affecting business, design, operations, standards, and policy. Moreover, by virtue of being of a statistical nature, and because there are numerous relevant independent variables involved, it appears implausible that one will ever be able to conclude that there is no need for additional propagation measurements and new or refined propagation models for MSS in the 1 - 3 GHz range.

3. Difficulties Encountered in Applying Measurements and Models

3.1 Overview

A substantial number of publications provide relevant measurements and models; however, there are certain deficiencies in these publications. These deficiencies fall into two categories: (1) the necessary propagation information appears to be available but important facets are not documented, and (2) the desired data or models simply are not available. In addition, based on first hand experience in applying propagation data (or models) and in reviewing how other engineers have applied these data, there are numerous ways to misapply the available information that must be blamed on the principle that "a little knowledge can be dangerous." The latter problem is best addressed to engineers who apply propagation data and models; however, be it known that documentation of propagation phenomena should strive to leave nothing to the imagination.

3.2 Inadequate Documentation

There is an engineering requirement for full descriptions of measurements and models that are suitable for use by engineers in design and analytical processes. Specifically, all significant independent variables must be addressed and dependent variables must be specified in a usable form. It is suspected that in cases where deficiencies arise in these areas, they are, more often than not, the result of limitations on funding, schedule, or scope, rather than simply poor quality of documentation.

As the pace of reporting of the results of MSS propagation measurements escalated in the mid 1980s, potentially useful data were available but key measurement or model parameters were missing. For example, although it would seem that the characteristics of the antennas and antenna installations used during measurements would have a significant bearing on results, quite often little or no information was supplied on these parameters. Thus, the opportunity to incorporate measured data in models was hampered insofar as antenna parameters are important independent variables. One effort that was made to eliminate such deficiencies was the establishment of a standard form for reporting the results of propagation measurements in CCIR Study Group 5. (Although the author contributed to the development of this form, he has not ascertained that the adopted form is comprehensive.)

In many cases, measurements or models are documented using undefined measurement calibrations or parameter reference points. The best (or worst) example of this problem may be cumulative time distributions of fading, where fading levels are specified relative to "line of sight" (LOS) or a mean measured value. What is line of sight? Engineering studies must deal with absolute total levels of transmission loss, and so, fading relative to mean or LOS values can be applied only if the relationships between those values and transmission loss are known. (Of course, to allow for different path lengths, fading could perhaps be specified relative to free space loss.)

3.3 Inadequate Measurements/Models

It is the authors opinion that insufficient propagation measurements and models are available to support evaluation of the following phenomena:

- Spatial availability throughout a satellite service area - to support more comprehensive specification and analysis of performance objectives (i.e., signal quality, temporal availability, and spatial availability).

- Time diversity - the "gain" (dB) or "advantage" (probability) stemming from use of forward error correction, interleaving, and TDMA, as well as the performance of system control and error-mitigating network protocols.

- Spatial diversity - the diversity "gain" or "advantage" stemming from use of two antennas on the mobile earth station under various switching or combining approaches.

- Angle diversity - the diversity "gain" or "advantage" stemming from use of two satellites to serve the same mobile earth station under various switching or combining approaches..

- Correlation of signals on different paths - to support of studies of interference within and among MSS systems, and between transmissions in the MSS and other services (similar to angle diversity).

- Depolarization - to support studies of isolation between orthogonally polarized transmissions, to guide antenna design, and to enable analyses of various multipath and interference cancellation techniques.

4. Potential Solutions to Deficiencies

The following points are raised as tentative conclusions of this paper and, specifically, as solutions to the perceived deficiencies in available propagation information.

- Deficiencies can be mitigated through joint design of models by applications-engineers and propagation specialists.

- More funding is needed to support propagation measurements, modeling, and documentation.

- Private industry should contribute much of the necessary funds, insofar as it stands to save considerable money through these efforts and to accrue great profits.

- In order to avoid duplication of effort and to converge on defined goals, measurement efforts should be coordinated and centrally organized to the extent practical.

- The above could be accomplished in a joint NASA-industry program, using NAPEX as the forum for discussing the approach and reporting results.

USER NEEDS FOR PROPAGATION DATA

Presented to NAPEX

June 1993

Presented By

Thomas Sullivan
Atlantic Research Corporation

Tentative Conclusions of Paper

- New/Refined Mesurements and Models are Needed
- Engineering Applications Must Be Considered
- There Are Deficiencies in Available Data
  - Inadequate Reporting
  - Missing Measurements and Models
- Deficiencies Can Be Avoided
- A Renewed Program of MSS Measurements and Modeling Can Be Established

STATISTICAL RESULTS FROM THE VIRGINIA TECH PROPAGATION EXPERIMENT USING THE OLYMPUS 12, 20, AND 30 GHz SATELLITE BEACONS

W.L. Stutzman, A. Safaai-Jazi, T. Pratt, B. Nelson, J. Laster, and H. Ajaz
Satellite Communications Group
Bradley Department of Electrical Engineering
Virginia Polytechnic Institute and State University
Blacksburg, Virginia 24061-0111

1. INTRODUCTION

Virginia Tech has performed a comprehensive propagation experiment using the Olympus satellite beacons at 12.5, 19.77, and 29.66 GHz (which we refer to as 12, 20, and 30 GHz). Four receive terminals were designed and constructed, one terminal at each frequency plus a portable one with 20 and 30 GHz receivers for microscale and scintillation studies. Total power radiometers were included in each terminal in order to set the clear air reference level for each beacon and also to predict path attenuation. More details on the equipment and the experiment design are found in [1].

Statistical results for one year of data collection have been analyzed. In addition, the following studies were performed: a microdiversity experiment in which two closely spaced 20 GHz receivers were used [2]; a comparison of total power and Dicke switched radiometer measurements, frequency scaling of scintillations [3], and adaptive power control algorithm development. In this paper we report on statistical results.

2. THE DATABASE

Data were collected from August 1990 through September 1992. The initial few months of operation were used for calibration and equipment adjustment. Beacon data for the period June through August, 1991, could not be used because the Olympus spacecraft was out of its assigned geostationary orbit. Since fall 1992 the inclination angle of the satellite has been high due to fuel conservation measures, no N-S stationkeeping is performed. This leads to severe diurnal fluctuations at our location, which renders the data of poor quality. The analysis year uses the following 12 months:

January - May, 1991; June - August, 1992; September - December, 1991

3. ATTENUATION STATISTICS

Perhaps the most important aspect of the Olympus propagation experiment is the attenuation statistics. These statistics include exceedance data for attenuation with respect to free-space (AFS), attenuation with respect to clear air (ACA), and radiometer derived attenuation (ARD). The most important data sets are those for which data exist simultaneously on all three frequencies. This permits direct comparison, frequency scaling, etc. Numerous graphs and tables on attenuation statistics have been generated.

Figure 1 shows exceedance plots of AFS and ARD for the analysis year for 12, 20, and 30 GHz. As is typical of radiometer data, ARD values are not accurate above about 10 dB. Comparison of AFS and ARD data leads to the following conclusions: (1) For fades of less than 3 dB, attenuation data derived from total power radiometer measurements can match beacon attenuation measurements to within 0.1 dB. (2) For fades up to 10 dB, attenuation data derived from total power radiometer measurements match beacon attenuation measurements to within 1 dB. These data are for a common time base; that is, data are used only when valid data exist on all three frequencies. Exceedance plots for individual frequencies and pairs of frequencies 12/20, 12/30 and 20/30 have also been generated.

Measured clear air attenuation (ACA), which is the loss of signal strength due to gases and water vapor present in the earth's atmosphere, is shown in Fig. 2 for the analysis year. Clear air attenuation predicted (from the CCIR model) and measured (50% occurrence level for the analysis year) values are: 0.3 and 0.68 dB for 12.5 GHz, 1.53 and 1.58 dB for 19.77 GHz, and 1.36 and 1.42 dB for 29.66 GHz.

Table 1 shows attenuation data at many occurrence levels for all frequencies.

4. ATTENUATION RATIOS

A unique aspect of the experiment is the controlled frequency dependence, i.e., all variables across the 12, 20, and 30 GHz receivers are identical. Therefore, any differences are due to frequency effects. Frequency dependence is presented in terms of attenuation ratio (RA). Attenuation with respect to clear air is used in RA

calculations, because the clear air and rain frequency dependencies are much different and we wish to focus on the rain component. Plots of attenuation ratios for 30 to 20 GHz of a function of percent time of occurrence and as a function of the lower frequency attenuation level are shown in Fig. 3 for the analysis year. It is emphasized that RA is the instantaneous attenuation ratio and is obtained from the instantaneous data pairs at the two frequencies. This ratio relates directly to frequency scaling applications such as adaptive power control. It is noted that RA for 30/20 is very flat indicating potential application to adaptive control. Note from Fig. 3b that the median for the 30/20 ratio is about 2 at all levels with a spread from 1 to 99% between 1.4 and 2.6.

Statistical attenuation ratio (RAS), defined as the ratio of attenuation values obtained from cumulative attenuation statistics at the same level of occurrence, was also studied. The instantaneous nature of frequency scaling is not present in this parameter. Figure 4 compares the median values of RA to RAS for 30/20; similar results were obtained for 30/12 and 20/12. The excellent agreement between RA (50%) and RAS indicates that RAS, which is easily computed from separate exceedance statistics, is an accurate predictor of median instantaneous attenuation ratio.

5. SECONDARY STATISTICS

The secondary statistics include fade duration, interfade (non-fade) duration, fade slope, and ultimate fade depth. These statistics are valuable to system designers and also aid in the understanding of the nature of fading. Fade duration, FD, is defined as the length of time in seconds for which the attenuation with respect to clear air, ACA, exceeds a specified threshold level. Interfade duration is the complement of fade duration.

Fade and interfade durations statistics have been generated for threshold levels of -3, -1, 0, 1, 3, 5, 10, 15, 20, and 25 dB and durations exceeding 1, 6, 10, 20, 60, 600, and 3600 seconds. At each frequency, plots of the number of fade/non-fade events and the fade/interfade time as the percent time of the year for which data were collected versus fade/interfade duration are given for several threshold values. In order to eliminate the effect of scintillations on the number of fade/interfade events 10-second block averages of attenuation have been used. Fade duration statistics for the month of July 1992 are presented in Fig. 5 which illustrates the number of fades versus fade duration at 12, 20, and 30 GHz for several threshold levels. As an example, for a

threshold level of 5 dB the number of fades with fade durations exceeding 10 seconds is 34 at 12 GHz, 87 at 20 GHz, and 164 at 30 GHz. It is observed that for the same fade duration exceeded the number of fade events generally decreases with the threshold level. A deviation from this trend occurs at 20 GHz for fade durations less than 60 seconds and threshold levels of 1 and 3 dB. In other words, the number of fade events with duration exceeding 1, 6, 10, and 20 seconds at 3 dB exceeds that at 1 dB by few hundreds for the 20 GHz beacon. Such behavior at low threshold levels and short fade durations should not be surprising. Comparison of Figs. 5 a, b, and c, also indicates that for the same threshold level (>3 dB) and the same fade duration exceeded, the number of fade events at 12 GHz is less than that at 20 GHz which in turn is less that at 30 GHz. For threshold levels of 1 and 3 dB no consistent behavior prevails.

Fade slope is the time rate of change of attenuation in units of dB/second. The ESA definition of fade slope at a given threshold level fade is the difference between attenuations (in dB) 5 seconds before the threshold is crossed and 5 seconds after the threshold is crossed divided by 10 (seconds). In order to alleviate sensitivity to small variations in the received signal, 10-second block averages of attenuation are used here in the calculation of fade slope. Attenuation block average is calculated from stored values of attenuation in dB in the i^{th} 0.1-s interval from the beginning of the day (00:00:00 UT), AFS_i. The block averaged attenuation values are found from

$$AFSB_m = \frac{1}{100} \sum_{i=m-49}^{m+50} AFS_i \qquad [dB]$$

Fade slope is calculated from block averages at the i^{th} sample point as

$$FSB_i\left(\overline{AFS_i}\right) = \frac{\left(AFSB_{i+50} - AFSB_{i-50}\right)}{10} \qquad [dB/s]$$

where $\overline{AFS_i}$ is the threshold attenuation with respect to freespace at the i^{th} time sample obtained by averaging over the central 10-s period:

$$\overline{AFS_i} = \frac{1}{100} \sum_{j=i-49}^{i+50} AFS_j \qquad [dB]$$

At each frequency we determine fade slope FSB for attenuation (AFS) thresholds ranging from -8 to 39 dB in 1 dB steps. Fade slopes are sorted into 0.05 dB/second bins. Plots of fade slope statistics for each channel and for several threshold levels have been generated for the analysis year and are displayed in Fig. 6.

Figure 7 plots the fade slope and attenuation at 20 GHz in real time of one rain event that occurred on May 14, 1991. The fade slope and attenuation for this plot were generated using a 3-minute moving block average which eliminated small variations in attenuation and made the first derivative relation between fade slope and attenuation evident. Data points were plotted every 30 seconds beginning at 17:50 GMT and ending at 18:32 GMT on May 14, 1991.

6. CONCLUSIONS

Results from a comprehensive propagation experiment involving beacon and radiometric measurements at 12, 20, and 30 GHz for one year of data were presented. Radiometer derived attenuations agree well with beacon measured attenuations for fade levels below 10 dB. Attenuation statistics, attenuation ratios, fade and interfade durations, and fade slope for all three frequencies have been examined.

REFERENCES

[1] W.L. Stutzman et al., "Initial results from the 12, 20, and 30 GHz OLYMPUS propagation experiment in Blacksburg, Virginia," IEEE AP-S Inter. Symp. Digest (Chicago), pp. 736-739, July 1992.

[2] J.C. Cardoso, A. Safaai-Jazi, and W.L. Stutzman, "Microdiversity in satellite communications," to appear in IEEE Trans. on Ant. and Prop..

[3] F. Haidara and C.W. Bostian, "Preliminary results on scintillation intensity frequency scaling from the Virginia Tech OLYMPUS experiment," IEEE AP-S Inter. Symp. Digest (Chicago), pp. 301-304, July 1992.

[4] W.L. Stutzman and K.M. Yon, "A simple rain attenuation model for earth-space radio links operating at 10 - 35 GHz," Radio Science, vol. 21, pp. 65-72, Jan/Feb 1986.

napex.rpt
06/11/93

Table 1

Measured Attenuation Statistics for One Year of Data

Percent Time Exceeded	AFS			ARD			ACA		
	12	20	30	12	20	30	12	20	30
50.000	0.68	1.58	1.42	0.70	1.55	1.41	0.01	0.04	0.04
30.000	0.85	2.03	1.89	0.81	1.97	1.82	0.10	0.17	0.20
20.000	0.96	2.31	2.23	0.86	2.23	2.08	0.17	0.31	0.36
10.000	1.17	2.77	2.89	0.98	2.59	2.62	0.31	0.65	0.82
5.000	1.42	3.37	4.04	1.19	3.08	3.61	0.51	1.22	1.88
3.000	1.67	4.05	5.50	1.41	3.68	4.69	0.71	1.88	3.33
2.000	1.91	4.70	6.93	1.65	4.22	5.78	0.94	2.54	4.76
1.000	2.42	6.21	9.87	2.08	5.33	7.83	1.41	4.04	7.69
0.500	3.04	7.93	13.55	2.50	6.46	10.29	2.03	5.76	11.38
0.300	3.61	9.47	16.99	2.79	7.32	12.16	2.59	7.31	14.82
0.200	4.12	10.90	20.08	3.08	8.21	13.85	3.11	8.73	17.90
0.100	5.39	14.11	26.05	3.63	9.86	16.57	4.37	11.93	23.87
0.050	7.10	18.37	33.47	4.26	11.92	19.13	6.08	16.21	31.29
0.030	8.38	21.28	37.66	4.75	13.66	21.13	7.37	19.12	35.50
0.020	9.50	23.31		5.12	15.39	22.60	8.48	21.15	38.06
0.010	11.74	28.60		6.09	18.08	25.83	10.72	26.43	
0.005	13.92	33.55		7.47	20.72	28.39	12.90	31.37	
0.003	14.96	36.44		10.18	22.84	31.32	13.94	34.27	
0.002	15.67	38.56		18.05	24.39	31.39	14.65	36.39	
0.001	17.16				27.33		16.14		

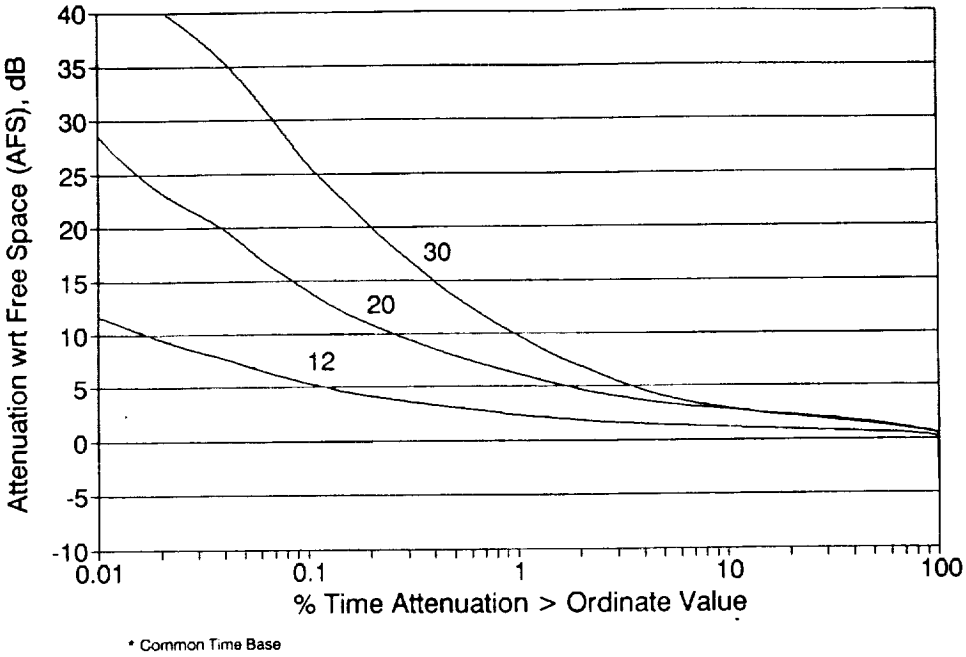

(a)

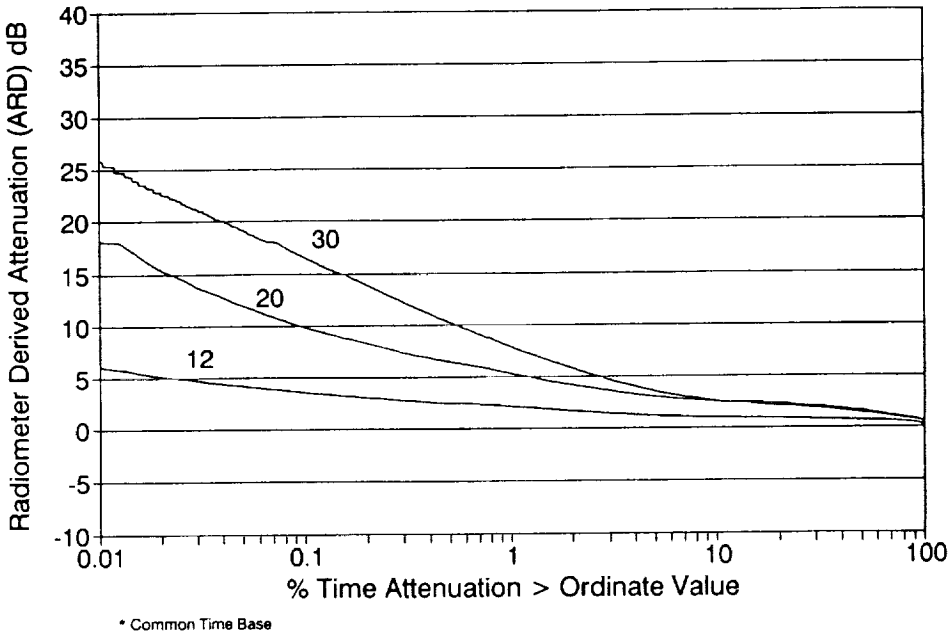

(b)

Figure 1. Measured results at 12, 20, and 30 GHz for the analysis year of Jan-May and Sep-Dec, 1991 and Jun-Aug, 1992: (a) Attenuation with respect to free space (AFS), (b) Attenuation derived from radiometer data (ARD). A common time base is used for all three frequencies.

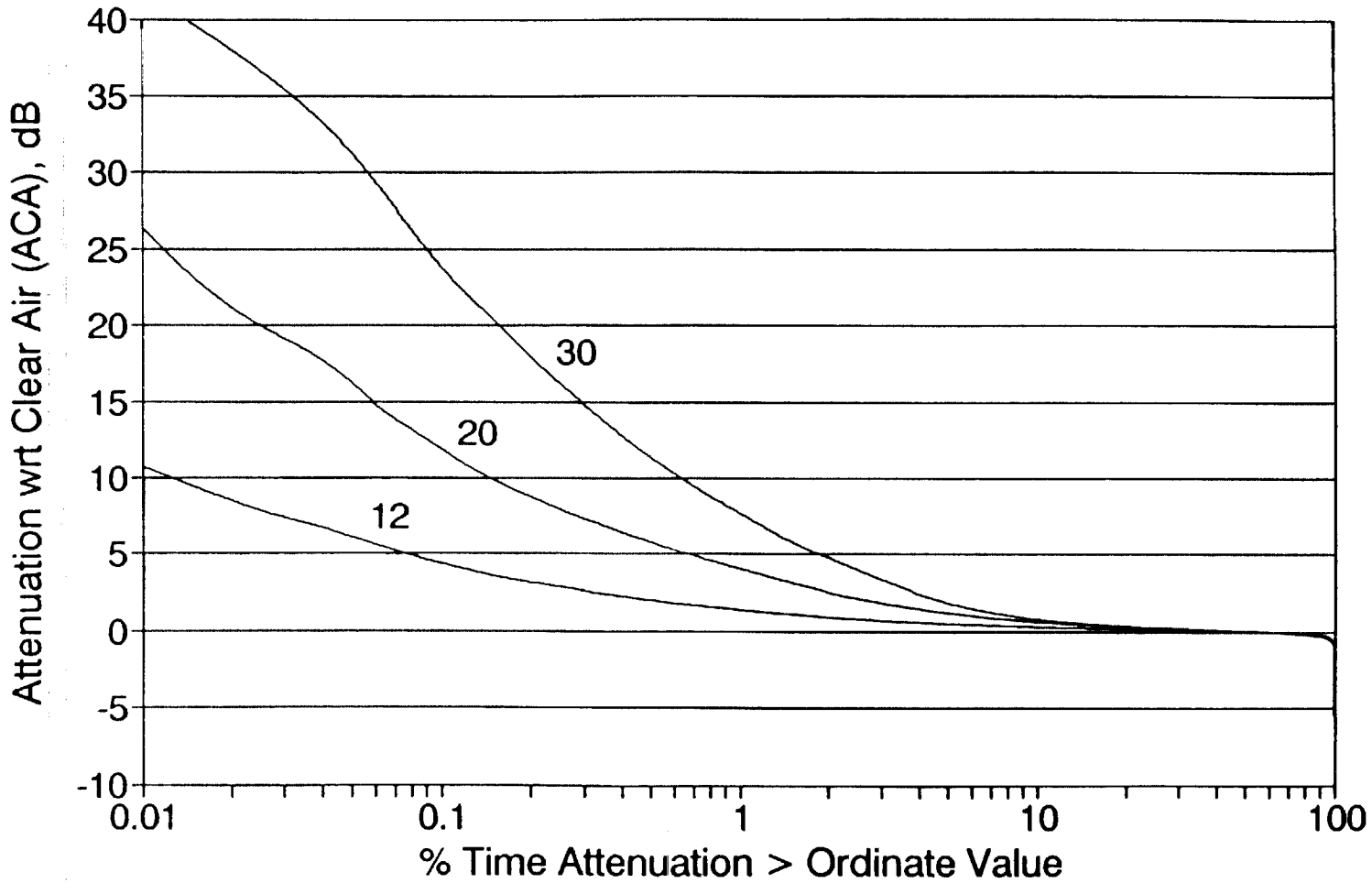

Figure 2. Measured results for ACA at 12, 20, and 30 GHz for the analysis year of Jan-May and Sep-Dec, 1991, and Jun-Aug, 1992. A common time base is used for all three frequencies.

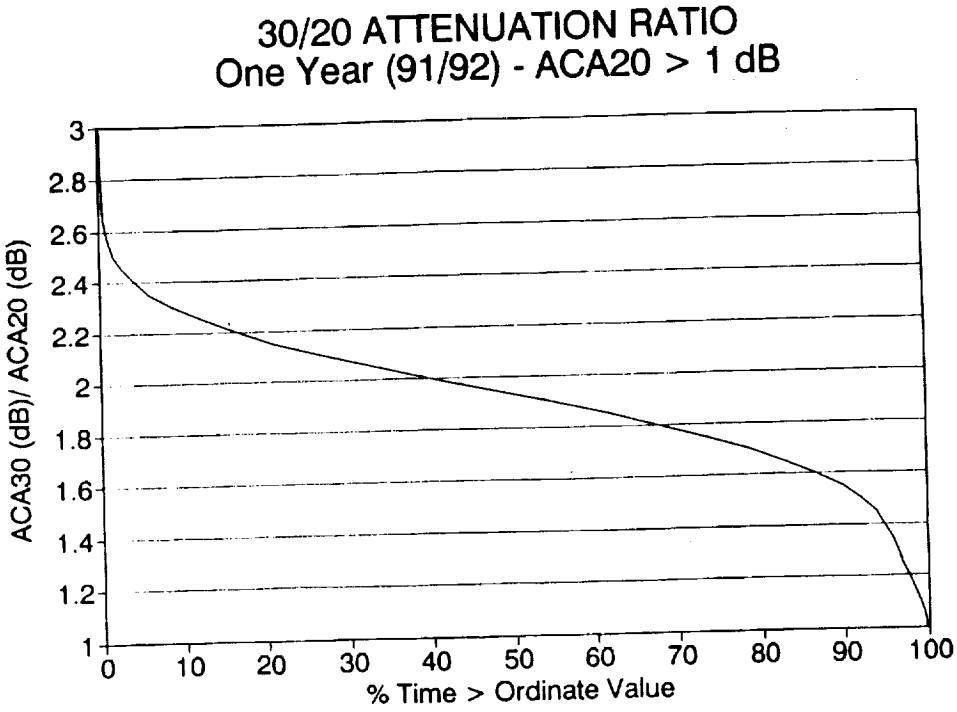

(a)

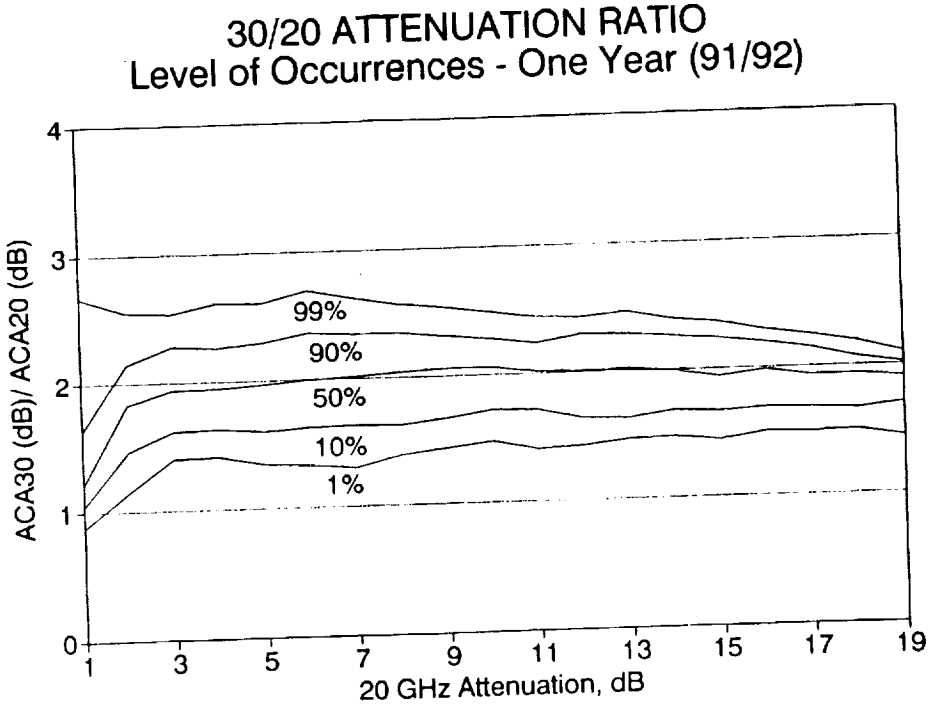

(b)

Figure 3. Attenuation ratio (RA) for frequency pairs 30/20 for the analysis year: (a) As a function of percent time, (b) As a function of 20 GHz attenuation.

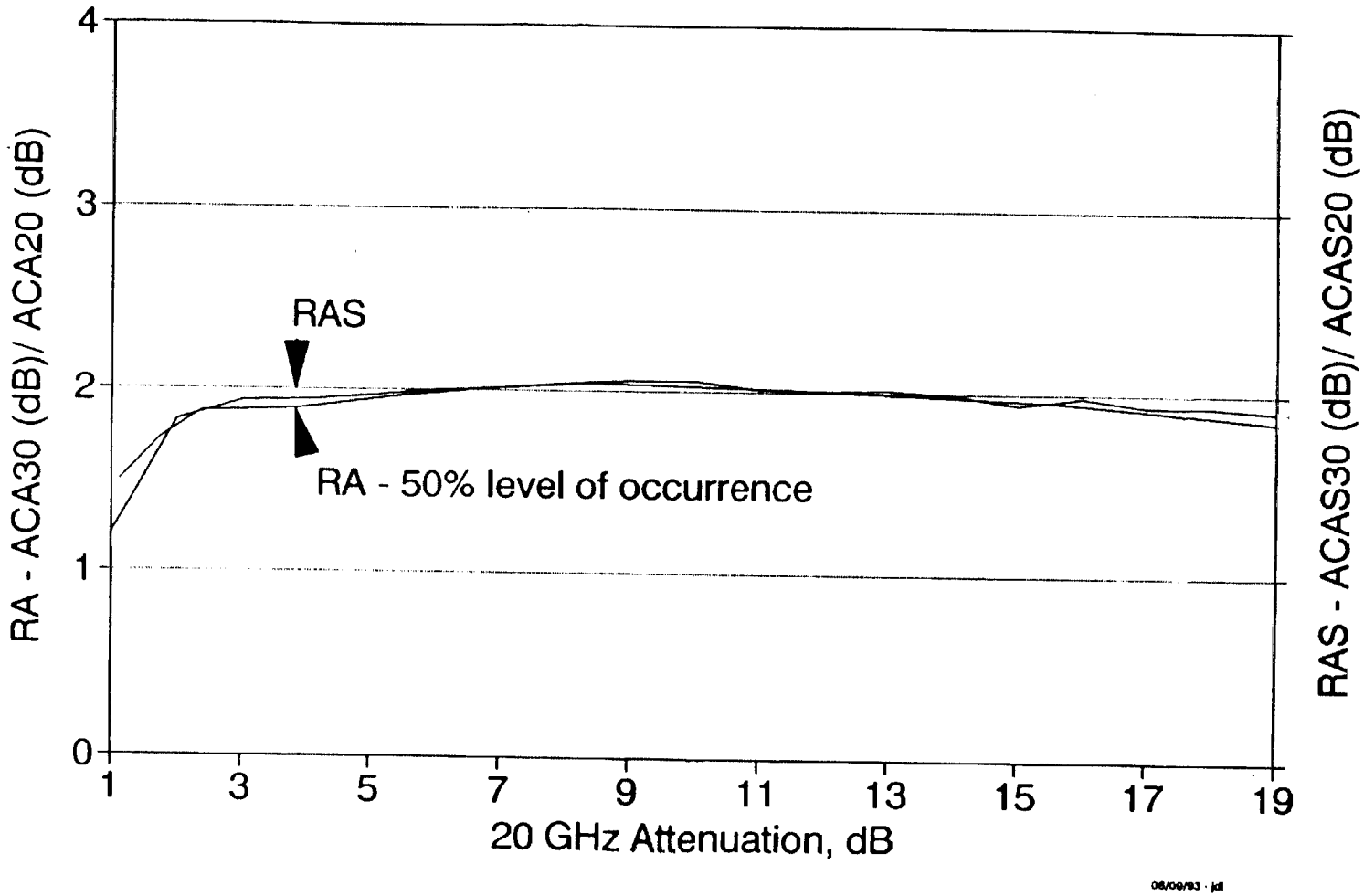

Figure 4. Comparison of statistical attenuation ratio (RAS) to median instantaneous ratio (RA) for 30/20.

(a)

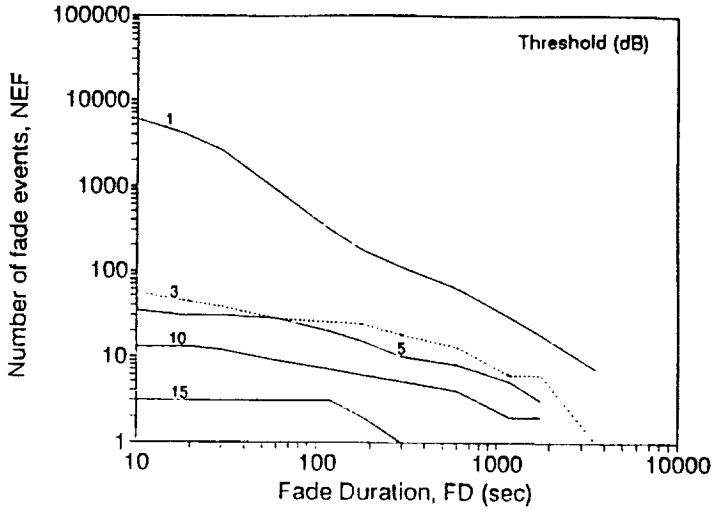

(b)

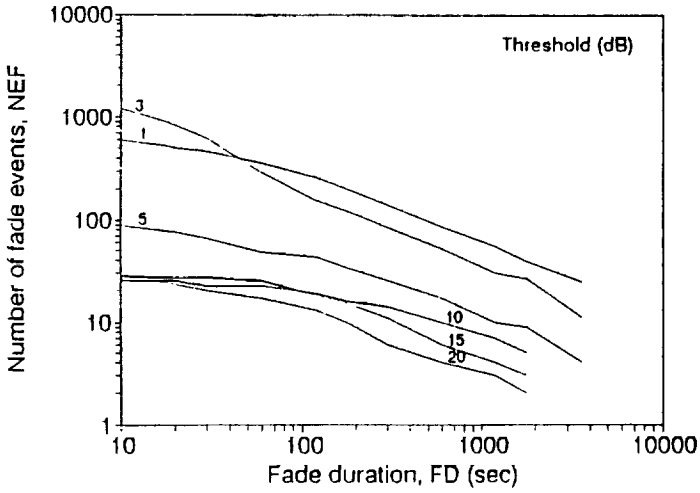

(c)

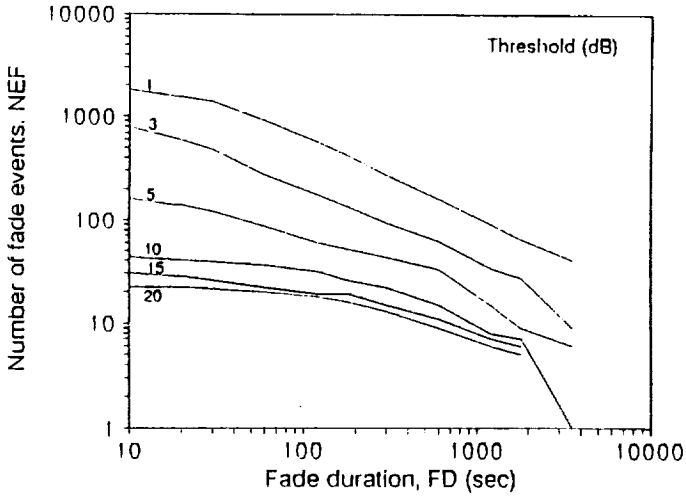

Figure 5. Number of fade events versus fade duration for the month of July 1992 at (a) 12 GHz, (b) 20 GHz, and (c) 30 GHz.

(a)

(b)

(c)

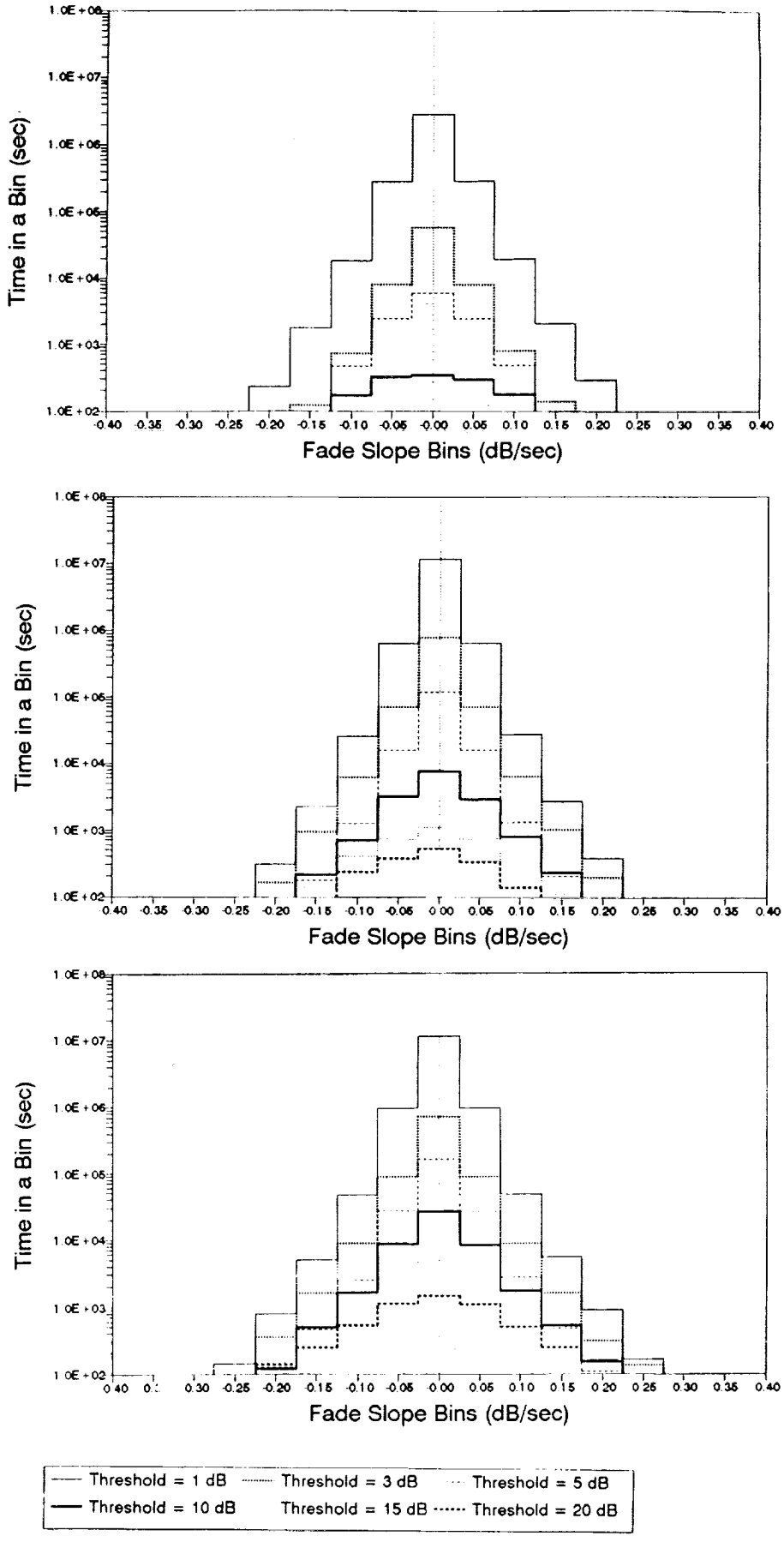

Figure 6. Fade slope ($\overline{FSB}$) for the analysis year for (a) 12 GHz, (b) 20 GHz, and (c) 30 GHz.

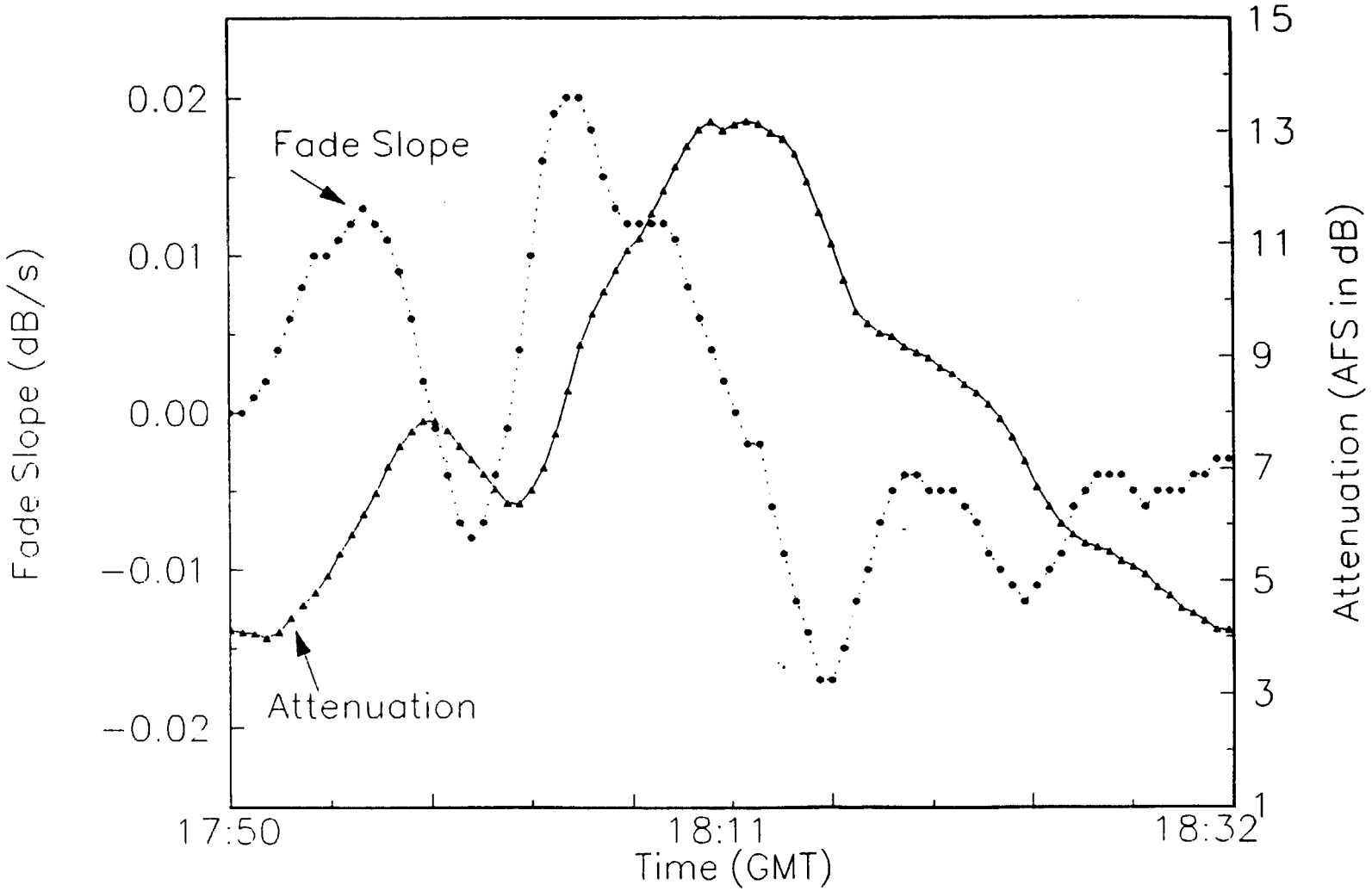

Figure 7. A typical rain event (May 14, 1991) showing fade and fade slope (3-minute block averaged).

RESULTS FROM A STUDY OF SCINTILLATION BEHAVIOR AT 12, 20 AND 30 GHz USING THE RESULTS FROM THE VIRGINIA TECH OLYMPUS RECEIVERS

T. Pratt* and F. Haidara
Virginia Polytechnic Institute and State University
Bradley Department of Electrical Engineering
Satellite Communication Group
Blacksburg, VA 24061-0111

1. INTRODUCTION

Tropospheric scintillations are rapid fluctuations of signal caused by multiple scattering from the small scale turbulent refractive index inhomogeneities in the troposphere. They can strongly impair satellite communications links operating at frequency above 10 GHz. The VA Tech OLYMPUS propagation experiment [1] which includes 12, 20, 30 GHz beacon receivers at an elevation angle of 14° provides us with valuable multifrequency scintillation data.

In this paper a long term analysis of tropospheric scintillation results from the VA Tech OLYMPUS experiment is presented. It includes statistics of both the scintillation intensity and the attenuation relative to clear air as well as seasonal, diurnal and meteorological trends. A comparison with the CCIR predictive model for scintillation fading is presented.

2. DATA ANALYSIS

The long term analysis conducted covers the following twelve months: January to May 1991, June to August 1992 and September to December 1991. This choice was imposed by the temporary loss of the satellite OLYMPUS between May and August 1991. The analysis is performed for "non rain" periods. The criterion used to discriminate these periods is based on the radiometric attenuation ARD and was chosen in order to avoid calculation of the scintillation intensity in rain. It is made of the set of conditions:

$$ARD30 < 3\ dB \text{ and } ARD20 < 2.7\ dB \text{ and } ARD12 < 1\ dB \quad (1)$$

These conditions allow us to eliminate most periods of rain and correspond to 73, 80.7, 80.4 % of the total period for respectively 12, 20 and 30 GHz. The scintillation intensity is computed for each frequency for successive 1 minute periods. The monthly cumulative distributions and PDF of both the scintillation intensity and the attenuation with respect to clear air as well as the seasonal and diurnal distributions of the scintillation intensity for the non rain periods, are produced.

3. STATISTICS OF SCINTILLATIONS

The long term distributions of the scintillation intensity were computed on a monthly basis. Figure 1 presents the PDF for May 1991 together with the Gamma and log-normal distribution constructed from the mean and variance of the measured data. The PDF of the scintillation intensity is best approximated by a log-normal distribution. The fit is better for the low scintillations, winter months, and the lowest frequencies. The cumulative distribution of the scintillation intensity for the total period is shown in Figure 2. During this one year period scintillation intensities of 0.8, 1, 1.2 dB were exceeded for 0.1% of the time at 12, 20, 30 GHz respectively. The monthly PDFs of the scintillation fading, exemplified for May 1991 in Figure 3 are not Gaussian, contrary to the short term distribution. The monthly PDFs show a very good agreement with the Mousley-Vilar model [2] which assumes that the attenuation has a Gaussian distribution with a variable variance. The model is excellent for enhancements but slightly underestimates our measured data at the higher fading. We explain this discrepancy in part by the choice of "non rain" threshold which does not eliminate all the rain from the analyzed data. In all cases the agreement between measured and predicted distributions is best at 12 GHz.

3. SEASONAL, DIURNAL AND METEOROLOGICAL TRENDS

The seasonal and diurnal variation of tropospheric scintillations are illustrated in Figure 4. It shows the increase of the monthly average of the scintillation intensity as the season shifts from winter to spring and summer.

There is little diurnal variation in winter scintillations and no well defined hour of peak scintillations. The spring and summer scintillation on the contrary show a strong diurnal trend with a maximum scintillations occurring in the afternoon between local times 13:00 and 15:00. The diurnal behavior of the scintillation intensity on a monthly basis is strongly correlated to the ground temperature and humidity as shown for June 1992 in Figure 5. The correlation coefficient obtained between the monthly average of the hourly ground temperature and humidity and the scintillation intensity at 12, 20, and 30 GHz are respectively 0.841, 0.835, 0.789 and -0.880, -0.870, -0.827. Note that temperature and humidity are mirror image of each other and that the scintillation intensity (regardless of the frequency) exhibitsa slightly higher correlation with the humidity than with the temperature.

The relation between scintillation and weather parameters is further investigated in Figure 6, in which the scatter plots of the monthly average scintillation intensity as a function of ground temperature, humidity and the wet refractive index are shown together with the best curve fit. The dependence between ground temperature and scintillation intensity was best approximated by using an exponential formula of the type $\sigma_\chi = ae^{bT}$; this is consistent with result found by Merlo et al. [3]. The scintillation intensity however is well represented by a linear function of the ground relative humidity and the ground wet refractive index. The coefficients of the curve fit are also given in Figure 6. Note the very good agreement between the data and the fits specially in the case of the wet refractive index N_{wet} . This confirms the results obtained by Karasawa et al. [4] on which the current CCIR model is based.

4. COMPARISON WITH CCIR MODEL

The CCIR model used to compute the long term (at least a month) statistics of amplitude scintillation for elevation angle higher than 4° described in [5] was compared to our measured data. The monthly average humidity and temperature of Roanoke (located 35 km from our experimental site) were used in the model for the period going from January 1991 to May 1991 because of a malfunction of our humidity sensor during that time. For June 1992, however the meteorological quantities measured at our experimental site were used. The

cumulative distribution of scintillation fade depths obtained using the CCIR technique are compared to the measured data as depicted in Figure 7. The average temperature and relative humidity used in the model are indicated on the graphs. There is a good agreement between measured and predicted scintillation fade depth on a monthly basis. In winter the CCIR model tends to underestimate the fade exceeded at low percentage (by a maximum of 0.2 dB at 30 GHz) but shows excellent agreement for the high percentage of time. The best fit is obtained at 12 GHz. In the spring and summer, on the contrary, the results obtained using the CCIR model exceed slightly the measured data at high percentages and match the experimental data at low percentages. The comparison of the CCIR model is not as good for the 6 month period of January-May 1991 combined with June 1992. The measured and predicted exceedance plots are very close at high percentages but diverge by as much as 1 dB at 30 GHz for low percentages. Globally, the difference between the CCIR model and measured scintillation fade depth is less than 0.5 dB for time percentages ranging between 0.1 and 10 %. For smaller percentages the rain attenuation would in any case be the dominant factor.

5. CONCLUSIONS

Scintillation results from the Virginia Tech OLYMPUS propagation experiment were presented. The statistics of both the scintillation intensity and the attenuation relative to clear air during dry weather were given and the seasonal, diurnal and meteorological trends were characterized. A comparison with the CCIR predictive model for scintillation fading was presented. The results presented here are unique in that they span the Ku, K and Ka frequency bands.

6. REFERENCES

[1] W.L. Stutzman et al., "Initial results form the 12, 20, and 30 GHz OLYMPUS propagation experiment in Blacksburg, Virginia," *IEEE AP-S Inter. Symp. Digest (Chicago)*, pp. 736-739, July 1992.

[2] T.J Mousley and E. Vilar, "Experimental and theoretical statistics of microwave amplitude scintillation on satellite down-link", *IEEE Trans. Ant. Propag.*, vol. AP 30, no. 6, pp. 1099-1106, Nov. 1982.

[3] U. Merlo, E. Fionda and P.G. Marchetti, "Amplitude scintillation cycles in

a SIRIO satellite link", *Electronics Letters,* vol. 21, no. 23, pp. , Nov. 1985.

[4] Y. Karasawa, K. Yasukawa, M. Yamada, "Tropospheric scintillation in the 14/11 GHz bands on earth-space paths with low elevation angles", *IEEE Trans. Ant. and Prop.*, vol. AP-36, no.4, pp. 563-569, Apr. 1988.

[5] Report of the CCIR 1990, Annex to vol. V, Report 718-3: "Effect of tropospheric refraction on radio wave propagation".

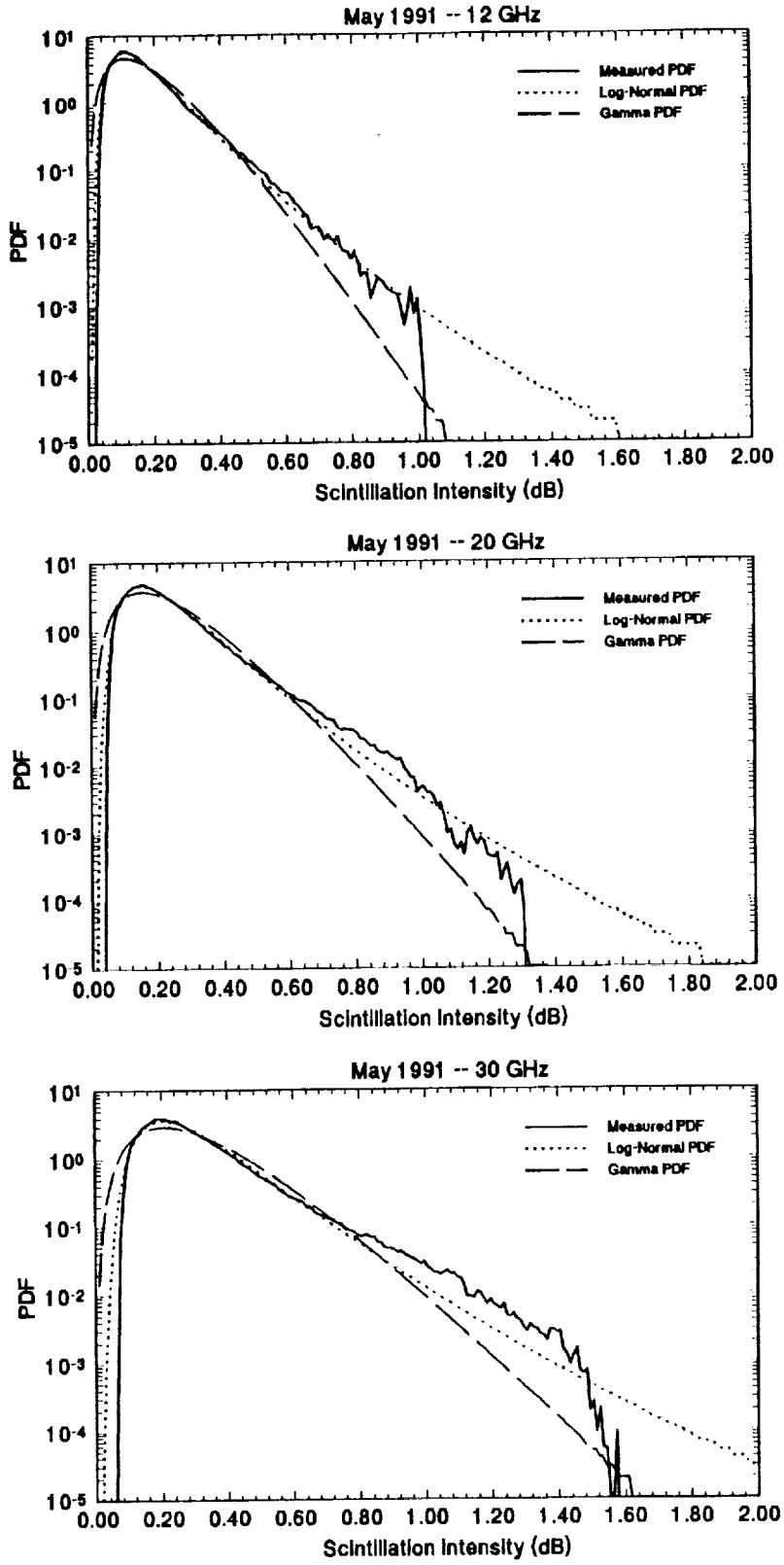

Figure 1: Monthly PDF of the scintillation intensity σ_χ for 12, 20 and 30 GHz compared to the corresponding Gamma and Log-normal distributions for May 1991.

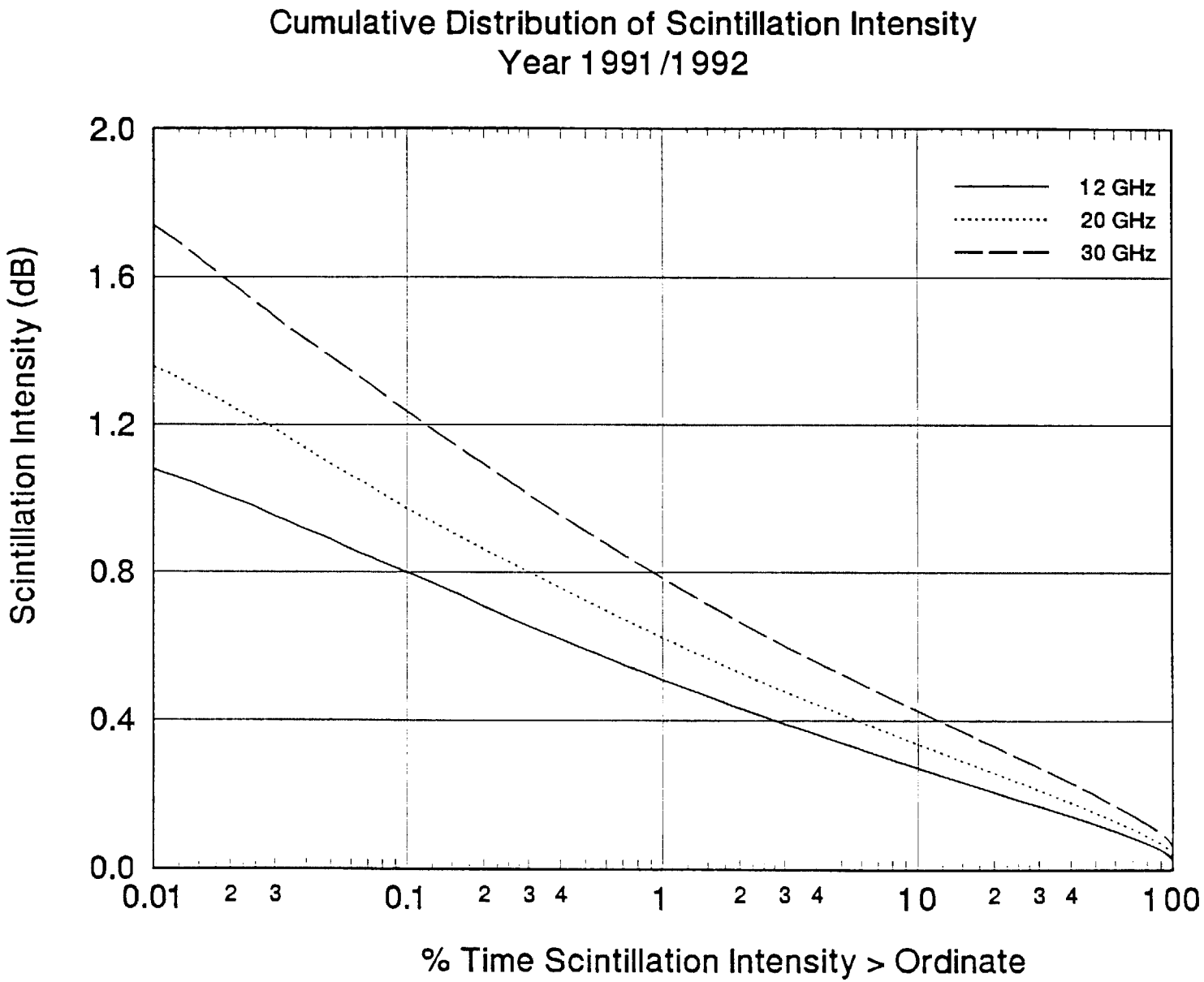

Figure 2. Monthly PDF of the scintillation fade depth for 12, 20 and 30 GHz compared to the corresponding Gaussian and Mousley-Vilar distributions for May 1991.

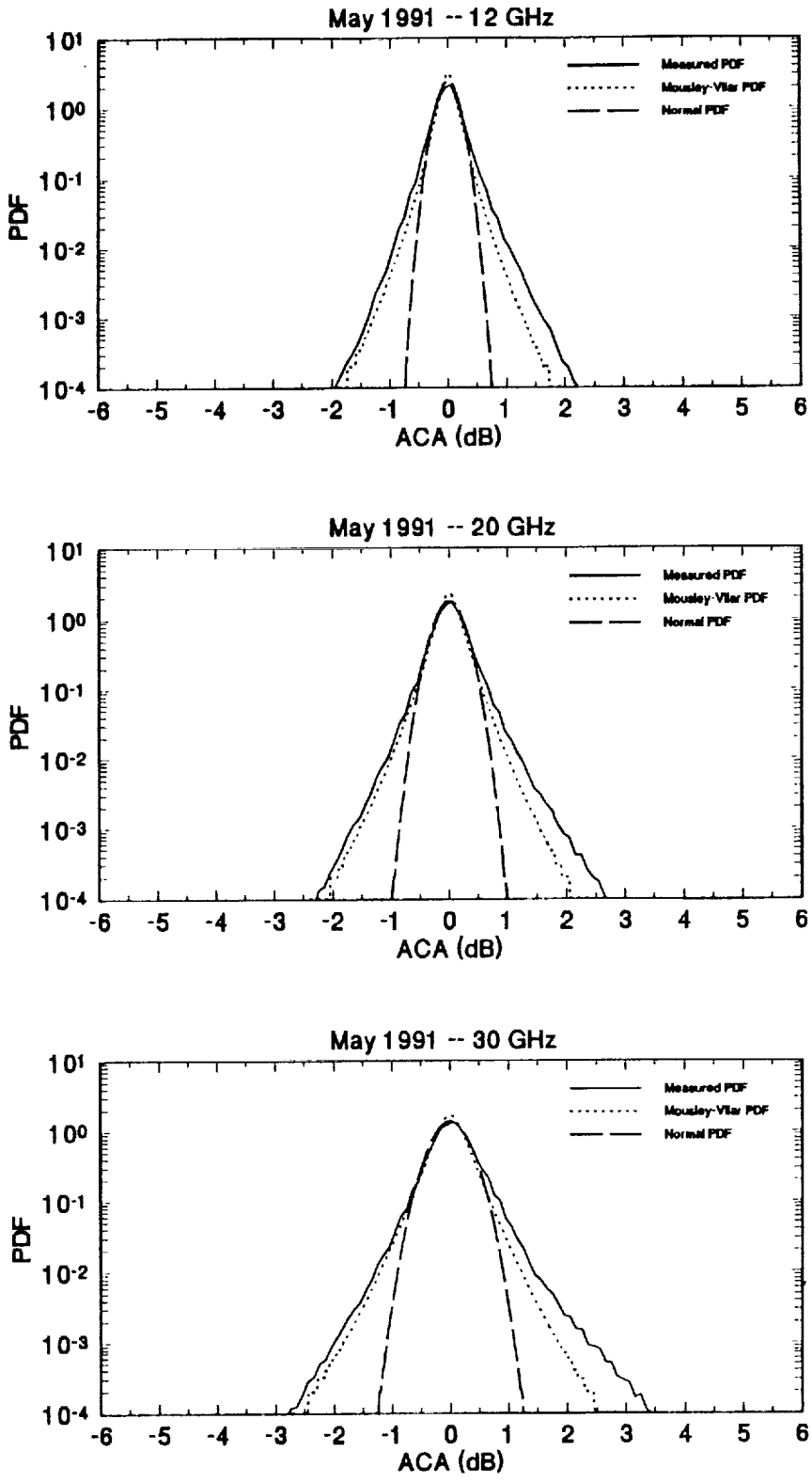

Figure 3: Monthly PDF of the scintillation fade depth for 12, 20 and 30 GHz compared to the corresponding Gaussian and Mousley-Vilar distributions for May 1991.

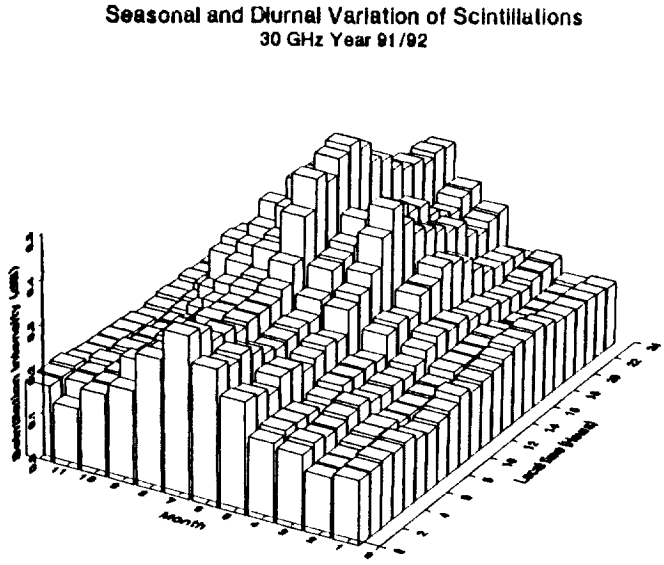

Figure 4: Diurnal and seasonal variation of the average monthly 12, 20, and 30 GHz scintillation intensities for one year of data. The scintillation intensities shown are the monthly average for of the scintillation intensity for each hour of the day.

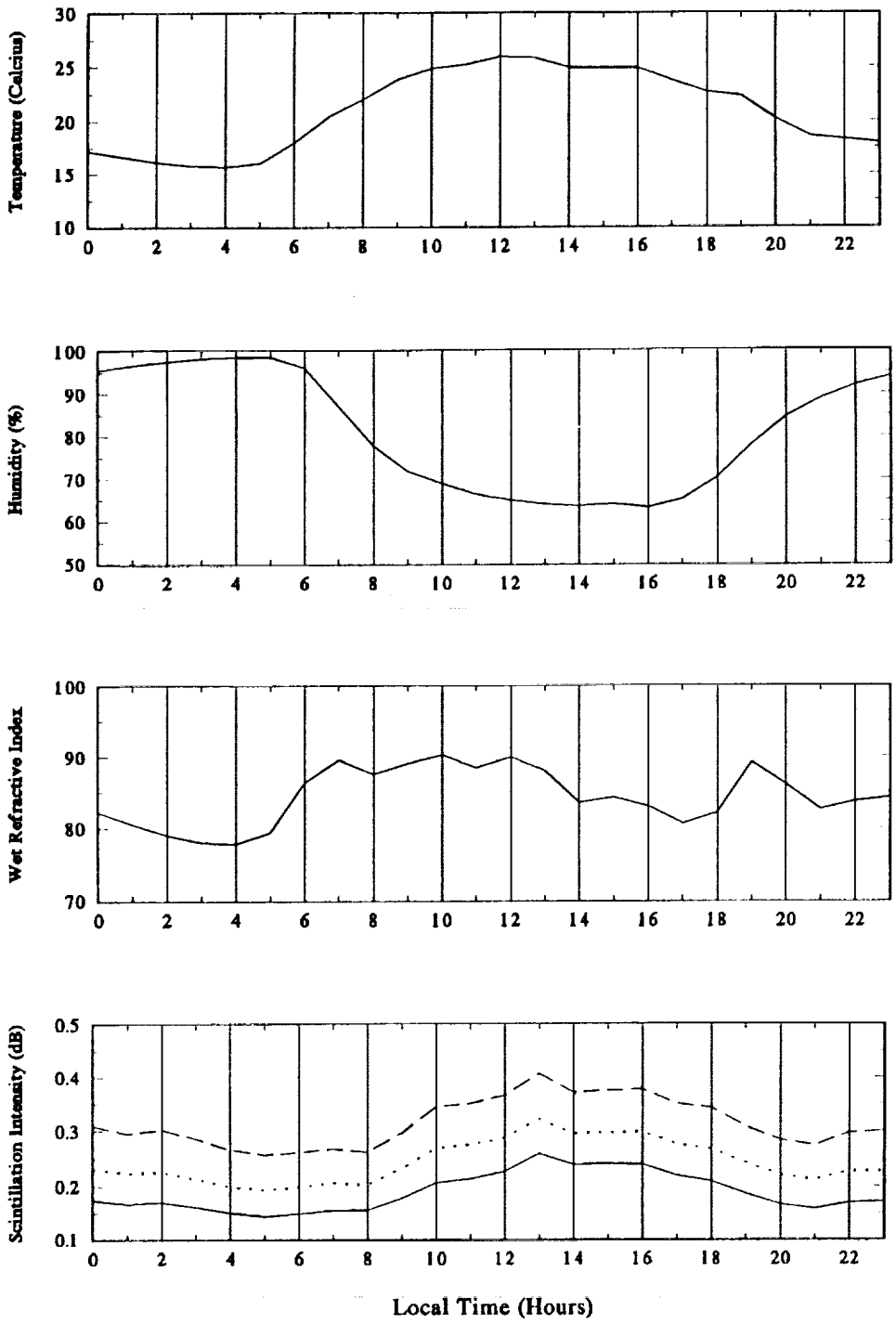

Figure 5: Diurnal variation of the average monthly ground temperature, ground relative humidity, ground wet refractive index and 12, 20, and 30 GHz scintillation intensities for June 1992. The quantities shown are monthly average for each hour of the day.

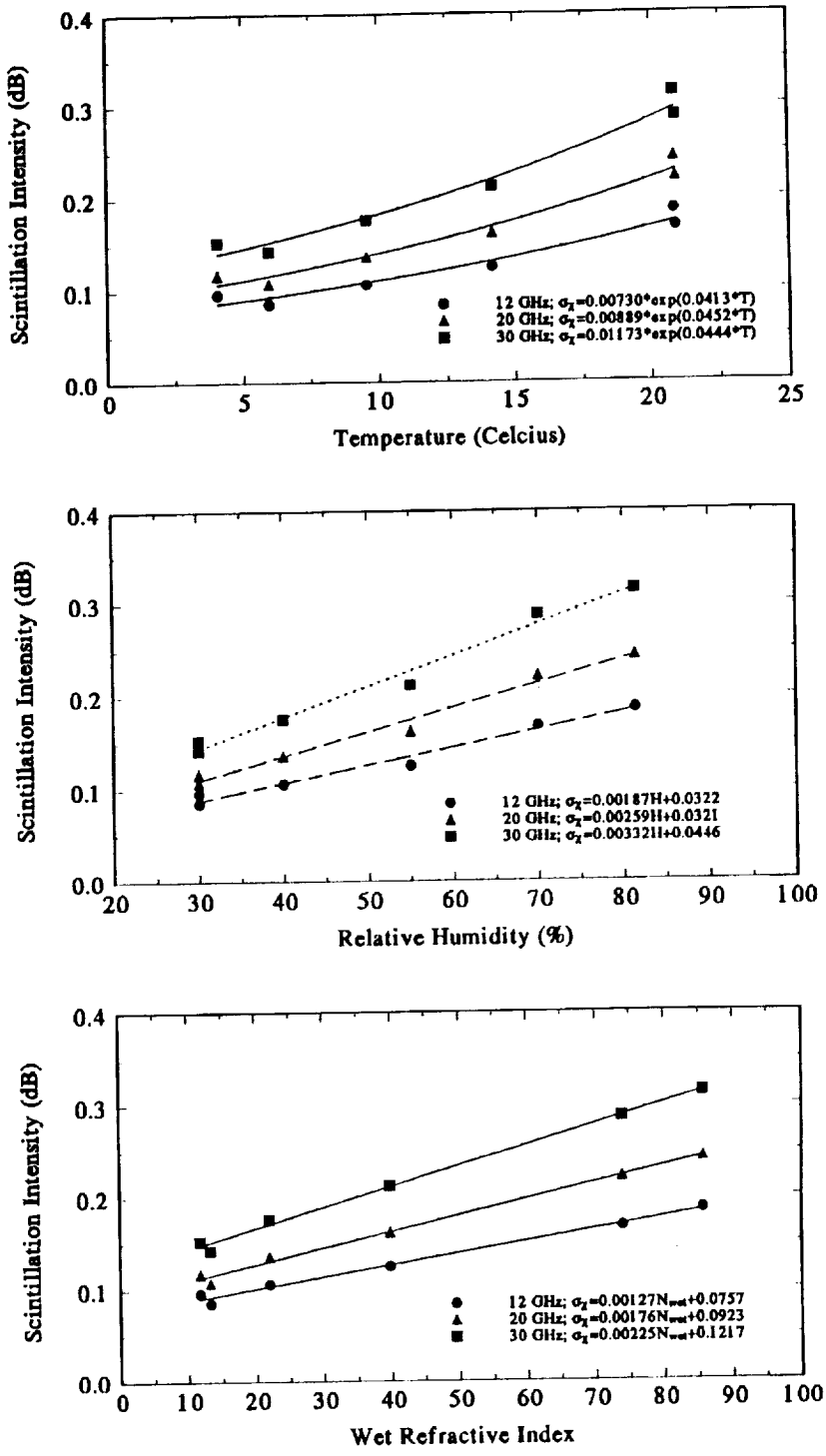

Figure 6: Scatter plot of the monthly average 12, 20 and 30 GHz scintillation intensities as a function of the monthly average of the ground temperature, ground relative humidity and ground wet refractive index for January to May 1991 and June 1992. The best fit curves and their equations are also shown.

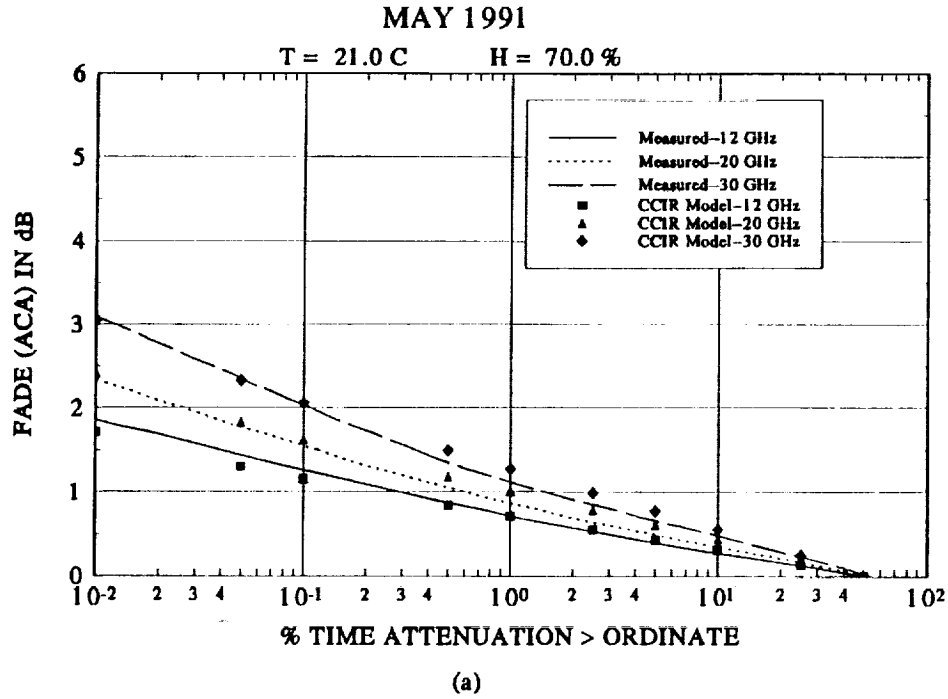

(a)

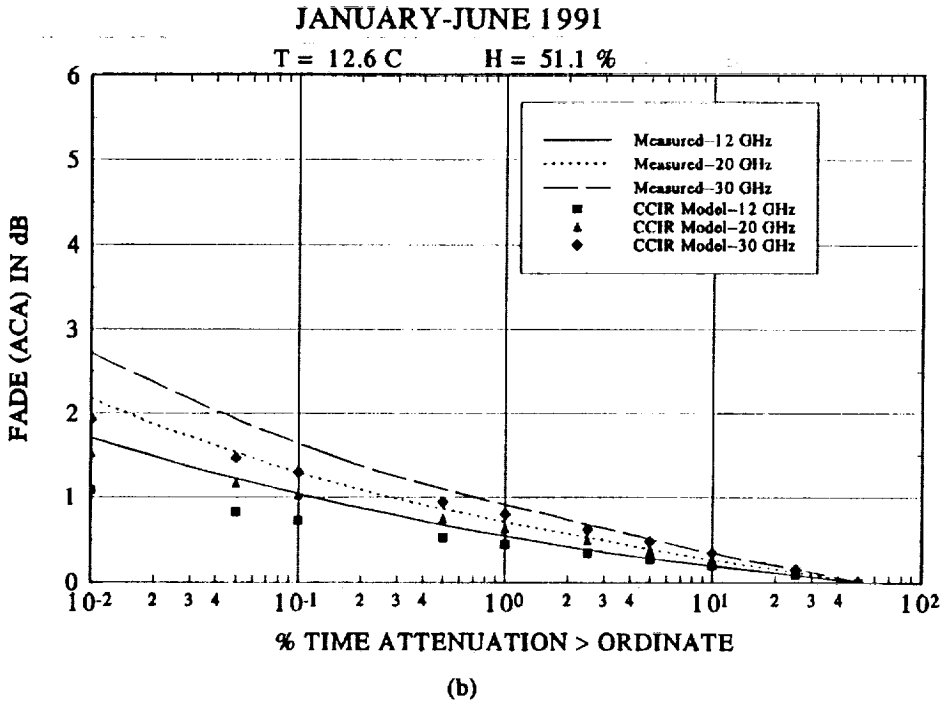

(b)

Figure 7: Comparison of the measured 12, 20 and 30 GHz scintillation fade depths to those obtained using the CCIR model with the ground temperature and relative humidity indicated on the graph: (a) May 1991 (b) January-May 1991.

The following papers were presented at NAPEX XVII but are not available for the proceedings:

OLYMPUS EXPERIMENTS IN PORTUGAL

Jose Carlos Neves
University of Aveiro

ITELSAT PROPAGATION STUDIES

Apolonia Pawlina Bonati
Polytechnic of Milan

Radiometric observations of atmospheric attenuation at 20.6 and 31.65 GHz: The Wave Propagation Laboratory data base

M. D. Jacobson, J. B. Snider, and E. R. Westwater
NOAA/ERL/Wave Propagation Laboratory
Boulder, Colorado 80303

Abstract

The National Oceanic and Atmospheric Administration (NOAA) Wave Propagation Laboratory (WPL) presently operates five dual-channel microwave radiometers, one triple-channel microwave radiometer, and one six-channel microwave radiometer. The dual-channel radiometers operate at frequencies of 20.6 or 23.87 GHz and 31.4 or 31.65 GHz. The triple-channel radiometer operates at 20.6, 31.65, and 90.0 GHz. The six-channel radiometer operates at frequencies of 20.6, 31.65, 52.85, 53.85, 55.45 and 58.8 GHz. Recent brightness temperature measurements and attenuation values from some of the above radiometers are presented here. These radiometric measurements, taken in different locations throughout the world, have given WPL a diverse set of measurements under a variety of atmospheric conditions. We propose to do a more complete attenuation analysis on these measurements in the future. In addition, a new spinning reflector was installed recently for the dual-channel radiometer at the Platteville, Colorado site. This reflector will extend our measurement capabilities during precipating conditions. We also discuss locating the three-channel and portable dual-channel radiometers at or near Greeley, Colorado to support the Advanced Communications Technology Satellite (ACTS) program.

I. Introduction

Between 1985 and 1988, WPL operated a limited network of four dual-channel microwave radiometers in northeastern Colorado. These radiometers, operating at 20.6 and 31.65 GHz, were deployed for meteorological purposes to measure precipitable water vapor (PWV) and integrated cloud liquid water (CLW). Data from ground-based microwave radiometers are also commonly used to derive attenuation statistics (Ortgies et al. 1990; Vogel et al. 1991; Fionda et al. 1991) useful to communication engineers. Using the radiometric technique, these authors have shown that attenuation levels up to about 12 dB can be derived with good accuracy.

Data from two of the Colorado stations, Denver and Platteville, have previously been used to derive single-station and two-station attenuation statistics for two 3-month periods during 1988 (Fionda et al. 1991). Recently, Westwater et al. 1992, greatly extended that work by deriving attenuation and attenuation-diversity statistics for an entire year's data taken between 1 November 1987 and 31 October 1988 at each of the four stations of

the Colorado network. We present the results of some new brightness temperature and attenuation measurements here.

A promising technique for measuring attenuation in precipating conditions is also discussed. This technique involves spinning the exposed reflector. This will help to minimize contaminated atmospheric data caused by the wet reflector (Jacobson et al. 1986) during precipating conditions.

Future attenuation studies that are related to the ACTS program are addressed.

Finally, WPL has also recently developed an airborne dual-channel radiometer which can view up and down (Fedor et al. 1988). The first experiment for this instrument will occur in September 1993, near San Clemente Island, California.

II. Description of Radiometers in WPL

A. *Radiometer characteristics*

WPL's radiometers were designed, constructed, and field-tested by WPL (excluding the portable radiometer which was designed and built by Radiometrics Corporation); a complete description of the systems is given by Hogg et al.(1983) and Westwater et al. (1987). A sketch of the triple-channel system is shown in Fig. 1. The WPL instruments were designed to operate continuously, unattended, in almost all weather conditions. The salient characteristics of the instruments are shown in Table 1. Note that the antenna beamwidths for the Denver radiometer, the three-channel radiometer, and one of the transportable radiometers differ from those of the other four stations. Field experiments (Snider et al. 1988), in which the three-channel radiometer with a beamwidth of 2.5 degrees was compared with the network radiometers with their beamwidths of 5 degrees, showed a correlation of 0.99 between the systems. The receivers of all seven radiometers are of the same construction. The radiometers are internally calibrated by switching between the antenna and two hot blackbody loads, and are externally calibrated approximately every two weeks using the "tipping curve" method (Hogg et al. 1983; Decker and Schroeder, 1991).

B. *Methodology to derive attenuation from emission*

The basic quantity measured by a radiometer is brightness temperature, T_b, which is closely related to input power present at the antenna (Ulaby et al. 1981). Although the probability distributions of T_b are of interest in themselves, the quantities needed by communication engineers are the distributions of attenuation. We derive the attenuation, τ(dB), from T_b by using the well-known formula (Westwater et al. 1990)

$$\tau(\mathrm{dB}) = 4.34 \ln\{(T_m - T_c)/(T_m - T_b)\} \quad , \qquad (1)$$

where

T_m = mean radiating temperature (K),

and

T_c = cosmic background temperature = 2.75 K.

In deriving τ, we used monthly mean values of T_m calculated from our radiative transfer and cloud models.

C. Single-station attenuation statistics

Data are taken by radiometers that operate unattended, although bimonthly, on-site calibrations are made. For the most part, the data are of high quality, although occasional outliers have to be removed. Such outliers can arise from liquid and ice buildup on the antennas, spurious signals of electromagnetic origin, calibration drifts in the receivers, and data transmission errors.

After the quality control methods discussed by Westwater et al. (1992) are applied to the data, cumulative distributions of brightness temperature and radiometrically derived attenuation are obtained for each station. An example of the four-station composite values of the Colorado Research Network are shown in Fig. 2. It is interesting to compare these radiometrically derived values of attenuation with forthcoming beacon measurements from ACTS (Chakraborty and Davarian, 1991).

III. Recent Radiometric Data

A. *Data from Norman, Oklahoma*

We operated a dual-channel radiometer at Norman, Oklahoma from February 1991 through February 1992 at frequencies of 20.6 and 31.65 GHz. Brightness temperature measurements for one month, October 1991, are shown in Fig. 3. Attenuation statistics for this period are currently being derived. An infrared radiometer, with a wavelength of operation around 10.6 micrometers, was also operated here. This instrument can sense clouds and is used to estimate cloud base temperature. Initial tests have shown agreement with radiosonde indications of cloud base temperature to within a degree Celsius (Shaw et al. 1993).

B. *Data from Coffeyville, Kansas*

We operated the three-channel radiometer near Coffeyville, Kansas from November through mid-December 1991 at frequencies of 20.6, 31.65, and 90.0 GHz. Attenuation measurements for three days are shown in Fig. 4. Notice the high attenuation measured by the 90.0 GHz channel relative to the attenuation at the two lower frequencies. This increased attenuation is due to the factor of five increase in cloud liquid attenuation coefficient (Westwater et al., 1990). An infrared radiometer, with a wavelength of operation around 10.6 micrometers, was also operated here. Furthermore, we operated our infrared spectrometer system (Shaw et al, 1991), known as FIRS (Fourier-transform InfraRed Sounder), at this location.

This instrument measures the atmospheric temperature and humidity profiles.

C. *Data from Porto Santo, Portugal*

This location provided attenuation measurements for the marine environment in the north Atlantic Ocean. We operated the three-channel radiometer on Porto Santo Island, Portugal, in June 1992. One of the transportable dual-channel radiometers made measurements aboard the NOAA ship Malcom Baldridge in June 1992. This ship cruised across the North Atlantic Ocean during this trip. The radiometer was then taken off the Malcom Baldridge ship and located on Porto Santo Island, Portugal in July 1992. It will be operating there until the end of June 1993, The dual-channel frequencies are 20.6 and 31.65 GHz. Two days of attenuation measurements from the three-channel system are shown in Fig. 5. As before, the 90.0 GHz attenuation measurements are much greater than the other two channels. Infrared radiometers, with a wavelengths of operation around 10.6 micrometers, were also operated in these locations.

D. *Data from Kavieng, Papua New Guinea*

This location provided an extremely high water vapor environment for the marine environment in the South Pacific Ocean. We operated one of the transportable dual-channel radiometers in Kavieng, Papua New Guinea during January and February 1993 at frequencies of 23.87 and 31.65 GHz. Two days of these attenuation measurements are shown in Fig. 6. In addition, we operated our FIRS instrument at this location.

IV. Spinning reflector

A dry reflector surface is required during precipating conditions to avoid contamination of the atmospheric data (Jacobson et al., 1986 and Stankov et al., 1992). Although a high velocity air stream has been used successfully to prevent rain from falling on small optical apertures of a few inches diameter, the technique is impractical for the large apertures used by WPL the microwave radiometers. An alternate solution is to spin the exposed reflector so that particles falling on the rapidly rotating disk will be thrown off, thereby reducing the liquid water layer buildup on the exposed flat. The Desert Research Institute (DRI), and the Commonwealth Scientific and Industrial Research Organization (CSIRO), which is located in Melbourne, Australia, both have implemented spinning disks on their radiometric systems. DRI has found that the spinning reflector has been effective in shedding liquid water and snow accumulations (Demoz et al. 1993).

We have recently designed and built a spinning flat reflector for the Platteville radiometer. The exposed circular flat is positioned at 45° with respect to the horizontal (see Fig. 7). The flat reflector is 3 feet in diameter and is currently rotating at 300 revolutions per minute (RPM), although the speed can be

adjusted. A controlled experiment will be performed in the near future to determine how well the spinning flat sheds water.

V. Future Plans

We propose to analyze and publish attenuation statistics for the locations listed in Section III. In addition, we propose to locate the triple-channel radiometer near Greeley, Colorado, adjacent to the radar operated by the University of CHicago and the ILLinois State Water Survey (CHILL), beginning in the fall of 1993 for a period not to exceed 1 year. We plan to locate the portable dual-channel radiometer next to the ACTS receiver in Greeley, Colorado, also in the fall of 1993 for a maximum of one year. Measurements from this instrument would provide valuable information for the ACTS project.

VI. Acknowledgements

The authors wish to thank Duane Hazen, Bill Madsen, Anthony Francavilla, Mike Nunnelee and Paul Schmidt for their work on the hardware and software for the various radiometric systems.

References

Chakraborty, D., and F. Davarian, " The ACTS Propagation Program," Proc. NAPEX XV, JPL Publ. 91-31, pp. 50-54, 1991.

Decker, M. T., and J. A. Schroeder, "Calibration of ground-based microwave radiometers for atmospheric remote sensing," NOAA Tech. Memo. ERL WPL-197, 16 pp., 1991.

Demoz, B. B., A. W. Huggins, J. A. Warburton, and R. L. Smith, "Field performance of a spinning-reflector microwave radiometer," J. Atmos. Oceanic Tech., vol. 10, no. 3, pp. 420-427, 1993.

Fedor, L. S., M. D. Jacobson, A. J. Bedard, Jr., E. R. Westwater, D. C. Hogg, and R. T. Nishiyama, "Dual-channel microwave radiometer for airborne meterological applications," NOAA Tech. Memo. ERL WPL-157, 1988.

Fionda, E., M. J. Falls, and E. R. Westwater, "Attenuation statistics at 20.6, 31.65, and 52.85 GHz derived from emission measurements by ground-based microwave radiometers," IEE Proc.-H, vol. 138, pp. 46-50, 1991.

Hogg, D. C., M. T. Decker, F. O. Guiraud, K. B. Earnshaw, D. A. Merritt, K. P. Moran, W. B. Sweezy, R. G. Strauch, E. R. Westwater, and C. G. Little, "'An automatic profiler of the temperature, wind, and humidity in the troposphere," J. Appl. Meteor., vol. 22, pp. 807-831, 1983.

Jacobson, M. D., D. C. Hogg, and J. B. Snider, "Wet Reflectors in Millimeter-Wave Radiometry-Experiment and Theory," IEEE Trans. Geosci. Remote Sensing, vol. GE-24, no. 5, pp. 784-791, 1986.

Ortgies, G., F. Rucker, and F. Dintelmann, "Statistics of clear air attenuation on satellite links at 20 and 30 GHz," Electron. Lett., vol. 26, pp. 358-360, 1990.

Shaw, J. A., J. H. Churnside, and E. R. Westwater, "An infrared spectrometer for ground-based profiling of atmospheric temperature and humidity," Proc. SPIE, vol. 1540, Infrared Tech. XVII, pp.681-686, 1991.

Shaw, J. A, L. S. Fedor, "Improved calibration of infrared radiometers for cloud temperature remote sensing," Optical Engineering, vol. 32, no. 5, pp. 1002-1010, 1993.

Snider, J. B., "Verification of the accuracy of a network of water-vapor radiometers," Proc. IGARSS '88 Symposium, Edinburgh, Scotland, 13-16 September, 1988, pp. 19-20, 1988.

Stankov, B. B., E. R. Westwater, J. B. Snider, and R. L. Weber, "Remote measurements of supercooled integrated liquid water during WISP/FAA aircraft icing program," Jour. Aircraft, vol. 29, no. 4, pp. 604-611, 1992.

Ulaby, F. T., R. K. Moore, and A. K. Fung, *Microwave Remote Sensing: Active and Passive;* Volume I: Microwave Remote Sensing Fundamentals and Radiometry. Reading, MA: Addison-Wesley, 456 pp., 1981.

Vogel, W. J., G. W. Torrence, and J. E. Allnutt, "Estimating satellite beacon attenuation from radiometer data: error statistics based on two year's low elevation angle measurements at 11.2 GHz," Proc. ICAP 31, York (UK), pp. 362-365, 1991.

Westwater, E.R.,and J.B. Snider, "Microwave Radiometer Facilities at the Wave Propagation Laboratory," Proc. NAPEX XI, Virginia Polytechnic Institute and State University, Blacksburg, Virginia, pp. 24-27, 1987.

-------- J. B. Snider, and M. J. Falls, "Ground-based radiometric observations of atmospheric emission and attenuation at 20.6, 31.65, and 90.0 GHz: A comparison of measurements and theory," IEEE Trans. Antennas Propagat., vol. 38, pp. 1569-1580, 1990.

-------- M. J. Falls, and E. Fionda, "Brightness Temperature and Attenuation Diversity Statistics at 20.6 and 31.65 GHz for the Colorado Research Network," Proc. NAPEX XVI, Houston, Texas, pp. 81-96, 1992.

Figure and Table Captions:

Fig. 1. Side view of the transportable triple-channel radiometer.

Fig. 2. Composite brightness temperature (A) and zenith attenuation (B) statistics for the four stations of the Colorado Research Network. These measurements were taken between November 1987 and October 1988 at frequencies of 20.6 and 31.65 GHz.

Fig. 3. Dual-channel radiometer observations at Norman, Oklahoma, taken for the month of October 1991 at frequencies of 20.6 and 31.65 GHz.

Fig. 4. Triple-channel radiometer observations near Coffeyville, Kansas. These measurements were taken during 1991, on (a) November 15, (b) November 19, and (c) November 21, at frequencies of 20.6, 31.65, and 90.0 GHz.

Fig. 5. Dual-channel radiometer observations from Porto Santo Island, Portugal. These measurements were taken on (a) 15 June 1992 and (b) 27 June 1992, at frequencies of 20.6 and 31.65 GHz.

Fig. 6. Dual-channel radiometer observations at Kavieng, Papua New Guinea. These measurements were taken on (a) 23 January 1993 and (b) 27 January 1993 at frequencies of 23.87 and 31.65 GHz.

Fig. 7. The spinning reflector structure, designed and built by WPL.

Table 1. Characteristics of the WPL radiometers.

WPL MICROWAVE RADIOMETER FACILITIES
(January 3, 1993)

LOCATION	EQUIPMENT (ν in GHz)	VIEWING	STATUS
Stapleton International Airport Denver, CO	6-channel (20.6, 31.65 52.85, 53.85 55.45, 58.8)	Zenith, equal beamwidths at all channels (2.5°)	Operating (50 GHz channels to be replaced by MARK II)
Platteville, CO	2-channel (20.6, 31.65)	Zenith, equal beamwidths at both channels (5.0°)	Operating
Transportable: Porto Santo Island, Portugal	2-channel (20.6, 31.65)	Zenith, equal beamwidths at both channels (5.0°)	Operating
Transportable: Shipboard	2-channel 23.87, 31.4)	Zenith	Operating on RV Ala Moana
Airborne	2-channel (23.87, 31.65)	Zenith	Operating on NOAA P3 and NOAA King Air
Transportable	3-channel (20.6, 31.65, 90.0)	Steerable Full Sky Coverage, equal beam-widths (2.5°)	Operating in Erie, CO
Transportable	2-channel (23.87, 31.65)	Zenith equal beam-widths (2.5°)	Operating in Kavieng Papua NG

Table 1.

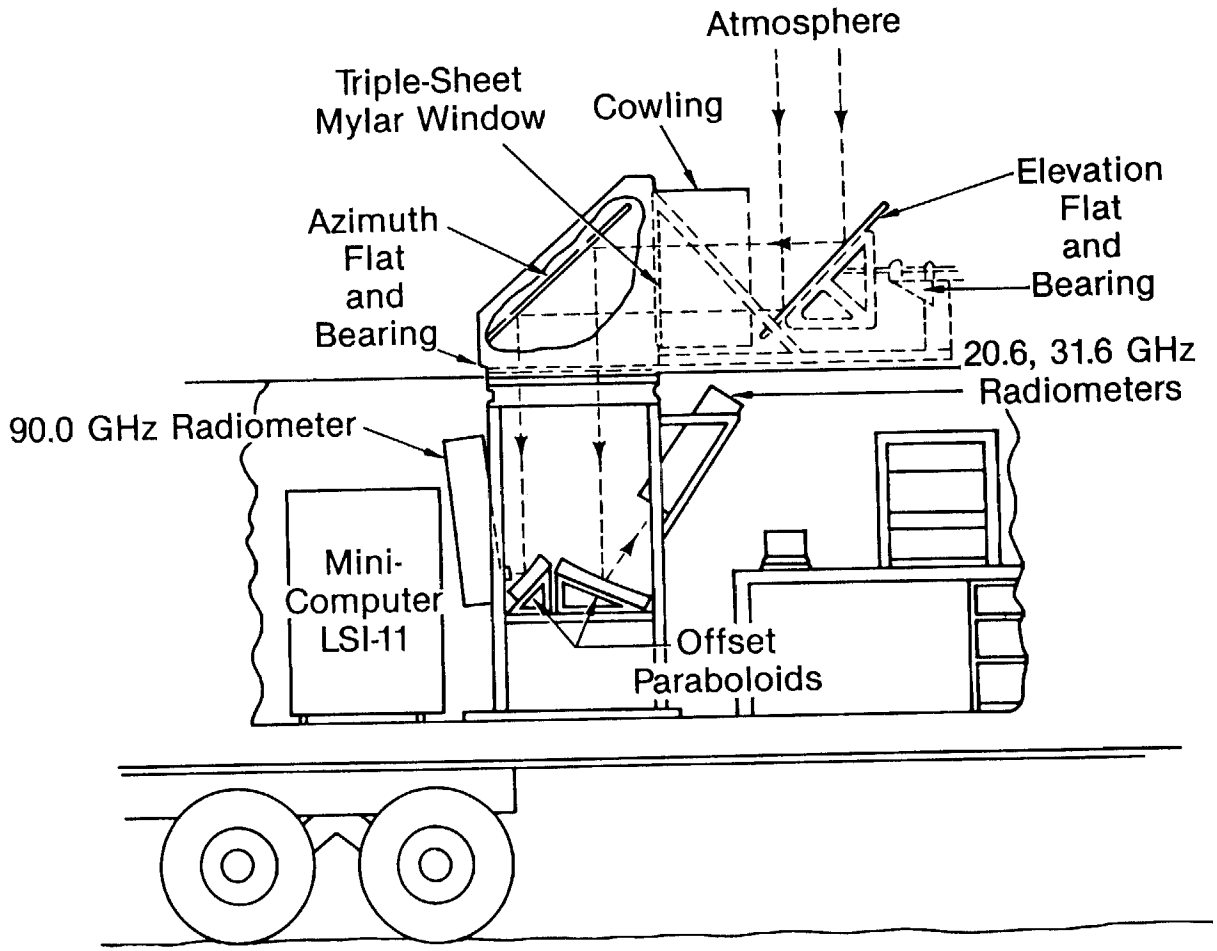
Atmosphere
Triple-Sheet
Mylar Window
Cowling
Elevation
Flat
and
Bearing
Azimuth
Flat
and
Bearing
20.6, 31.6 GHz
Radiometers
90.0 GHz Radiometer
Mini-
Computer
LSI-11
Offset
Paraboloids

Figure 1.

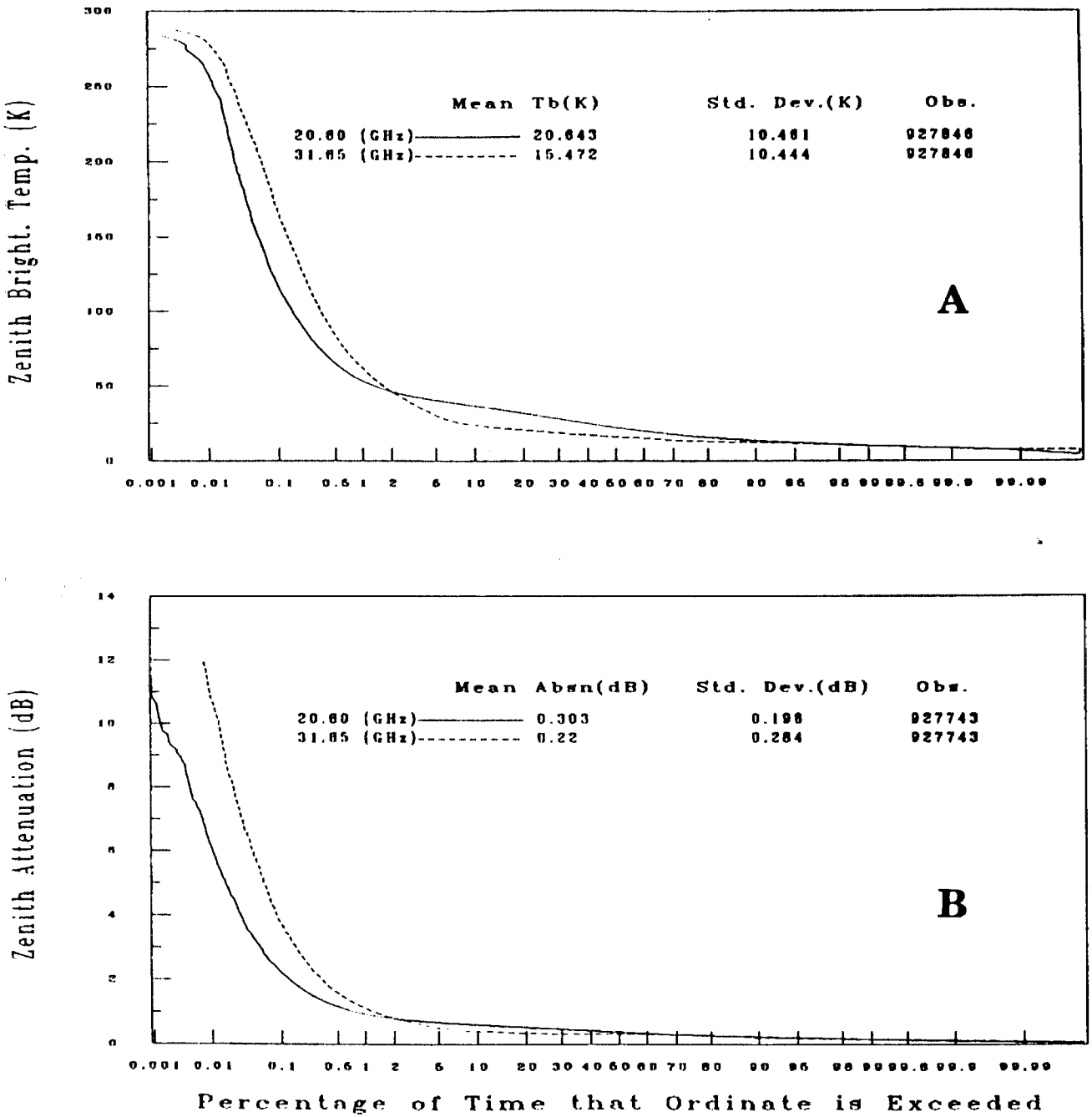
Zenith Bright. Temp. (K)
Mean Tb(K)
Std. Dev.(K)
Obs.
20.60 (GHz)—— 20.643 10.461 927846
31.65 (GHz)---- 15.472 10.444 927846
A
Zenith Attenuation (dB)
Mean Absn(dB)
Std. Dev.(dB)
Obs.
20.60 (GHz)—— 0.303 0.198 927743
31.65 (GHz)---- 0.22 0.284 927743
B
0.001 0.01 0.1 0.5 1 2 5 10 20 30 40 50 60 70 80 90 95 98 99 99.5 99.9 99.99
Percentage of Time that Ordinate is Exceeded

Figure 2.

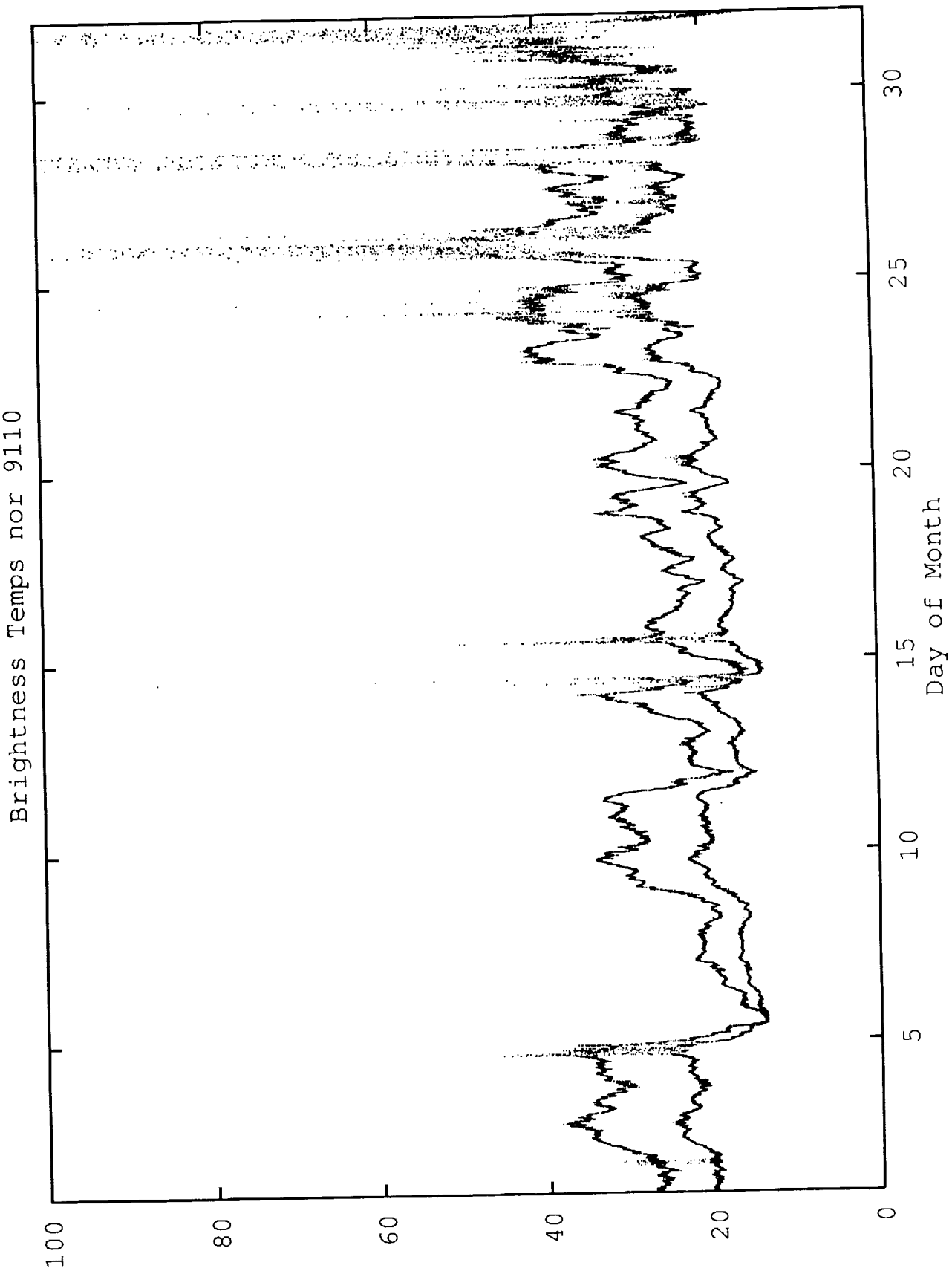
Brightness Temps nor 9110
Day of Month
0
20
40
60
80
100
5
10
15
20
25
30

Figure 3.

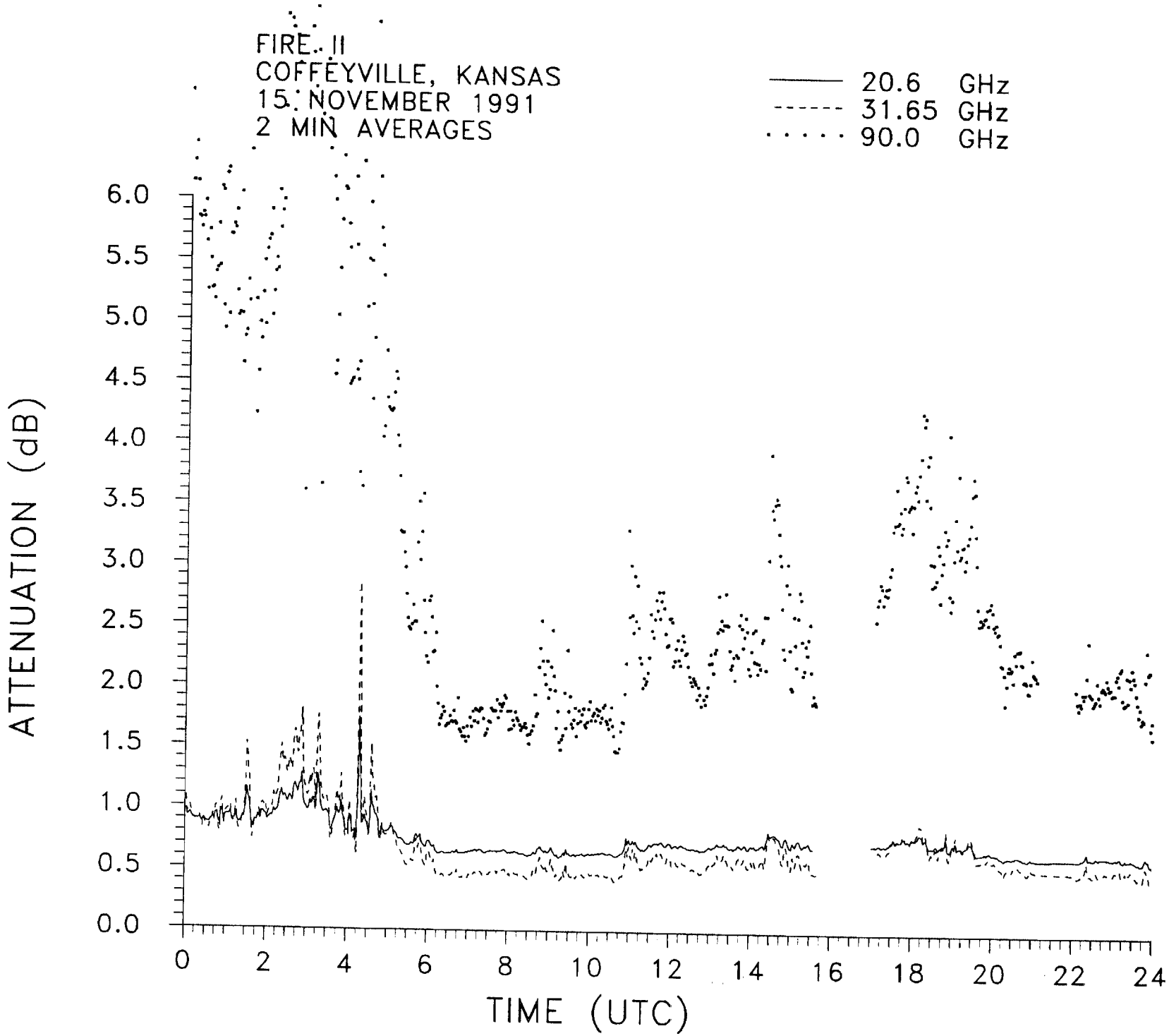
FIRE II
COFFEYVILLE, KANSAS
15 NOVEMBER 1991
2 MIN AVERAGES
20.6 GHz
31.65 GHz
90.0 GHz
ATTENUATION (dB)
6.0
5.5
5.0
4.5
4.0
3.5
3.0
2.5
2.0
1.5
1.0
0.5
0.0
0
2
4
6
8
10
12
14
16
18
20
22
24
TIME (UTC)

Figure 4a.

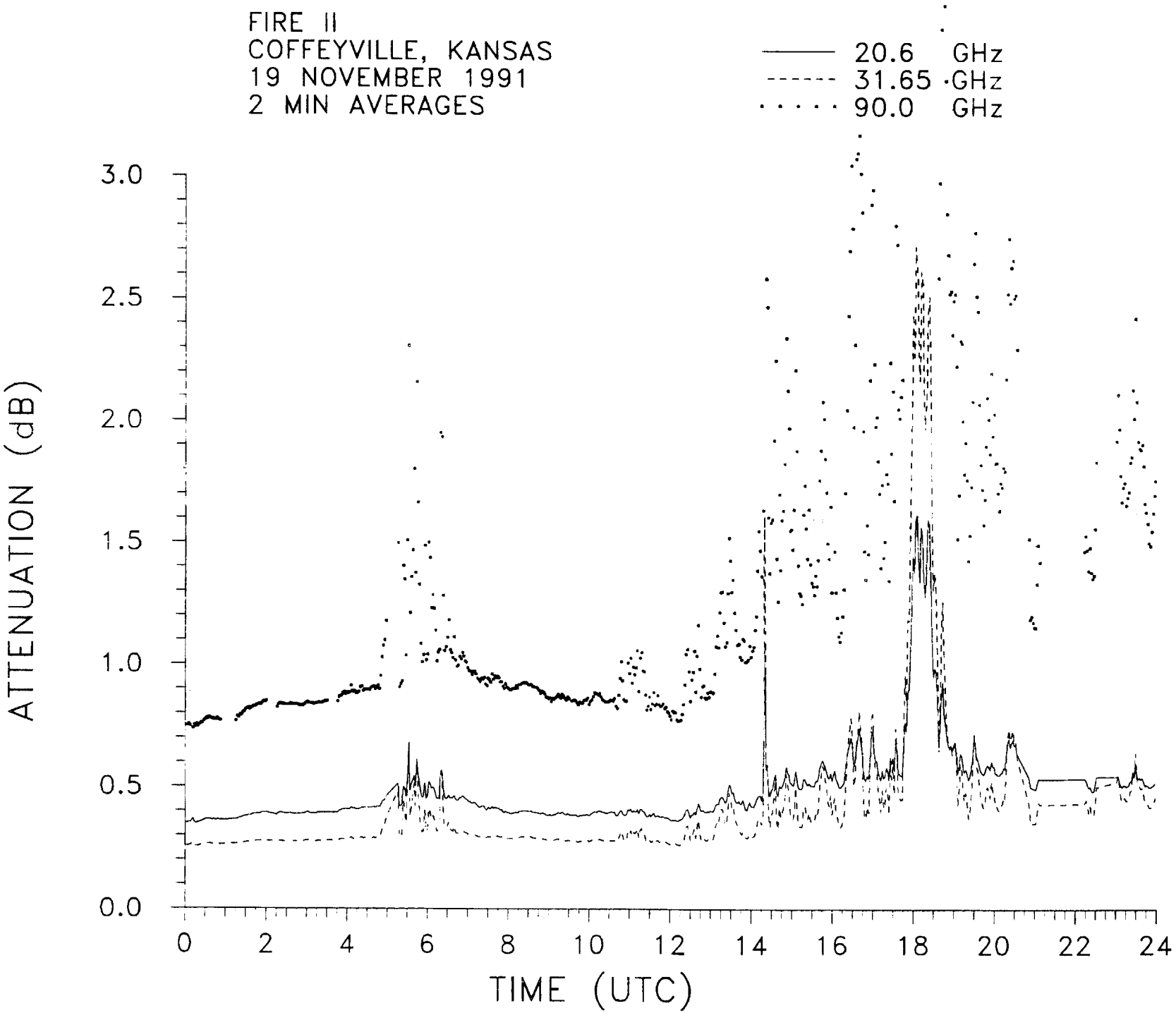
FIRE II
COFFEYVILLE, KANSAS
19 NOVEMBER 1991
2 MIN AVERAGES
20.6 GHz
31.65 GHz
90.0 GHz
ATTENUATION (dB)
3.0
2.5
2.0
1.5
1.0
0.5
0.0
0
2
4
6
8
10
12
14
16
18
20
22
24
TIME (UTC)

Figure 4b.

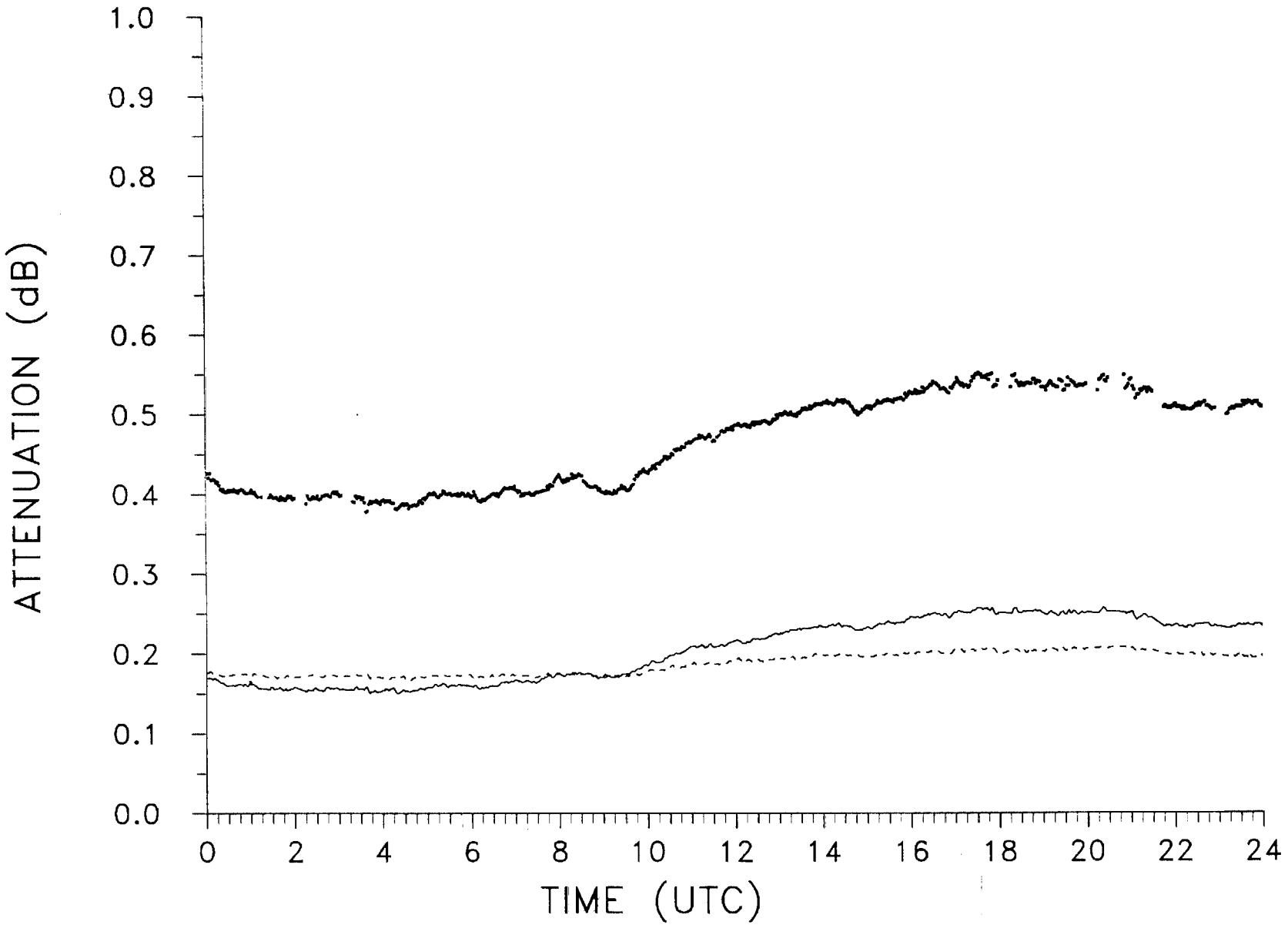
FIRE II
COFFEYVILLE, KANSAS
21 NOVEMBER 1991
2 MIN AVERAGES
20.6 GHz
31.65 GHz
90.0 GHz
ATTENUATION (dB)
1.0
0.9
0.8
0.7
0.6
0.5
0.4
0.3
0.2
0.1
0.0
0
2
4
6
8
10
12
14
16
18
20
22
24
TIME (UTC)

Figure 4c.

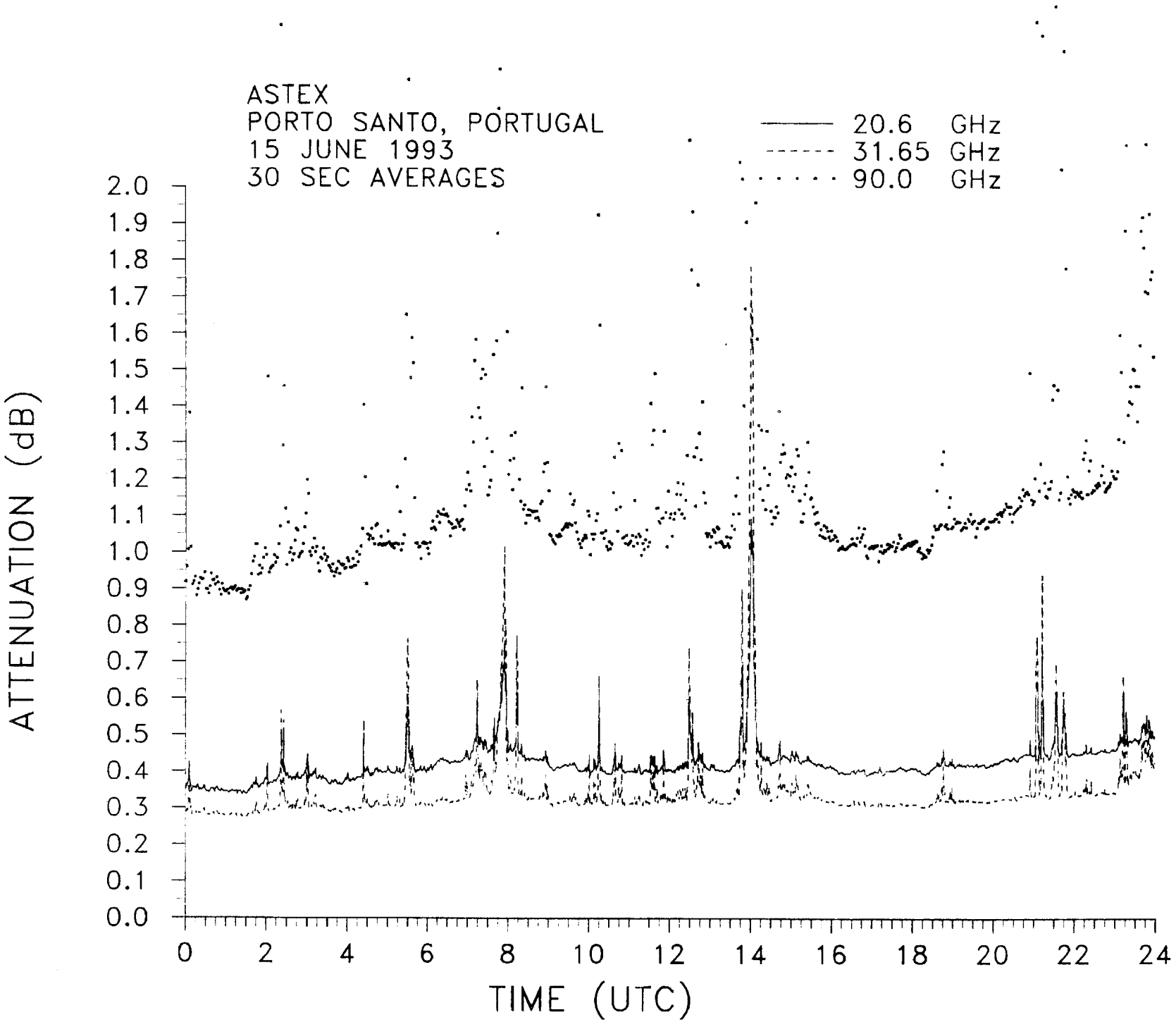
ASTEX
PORTO SANTO, PORTUGAL
15 JUNE 1993
30 SEC AVERAGES
20.6 GHz
31.65 GHz
90.0 GHz
ATTENUATION (dB)
2.0
1.9
1.8
1.7
1.6
1.5
1.4
1.3
1.2
1.1
1.0
0.9
0.8
0.7
0.6
0.5
0.4
0.3
0.2
0.1
0.0
0
2
4
6
8
10
12
14
16
18
20
22
24
TIME (UTC)

Figure 5a.

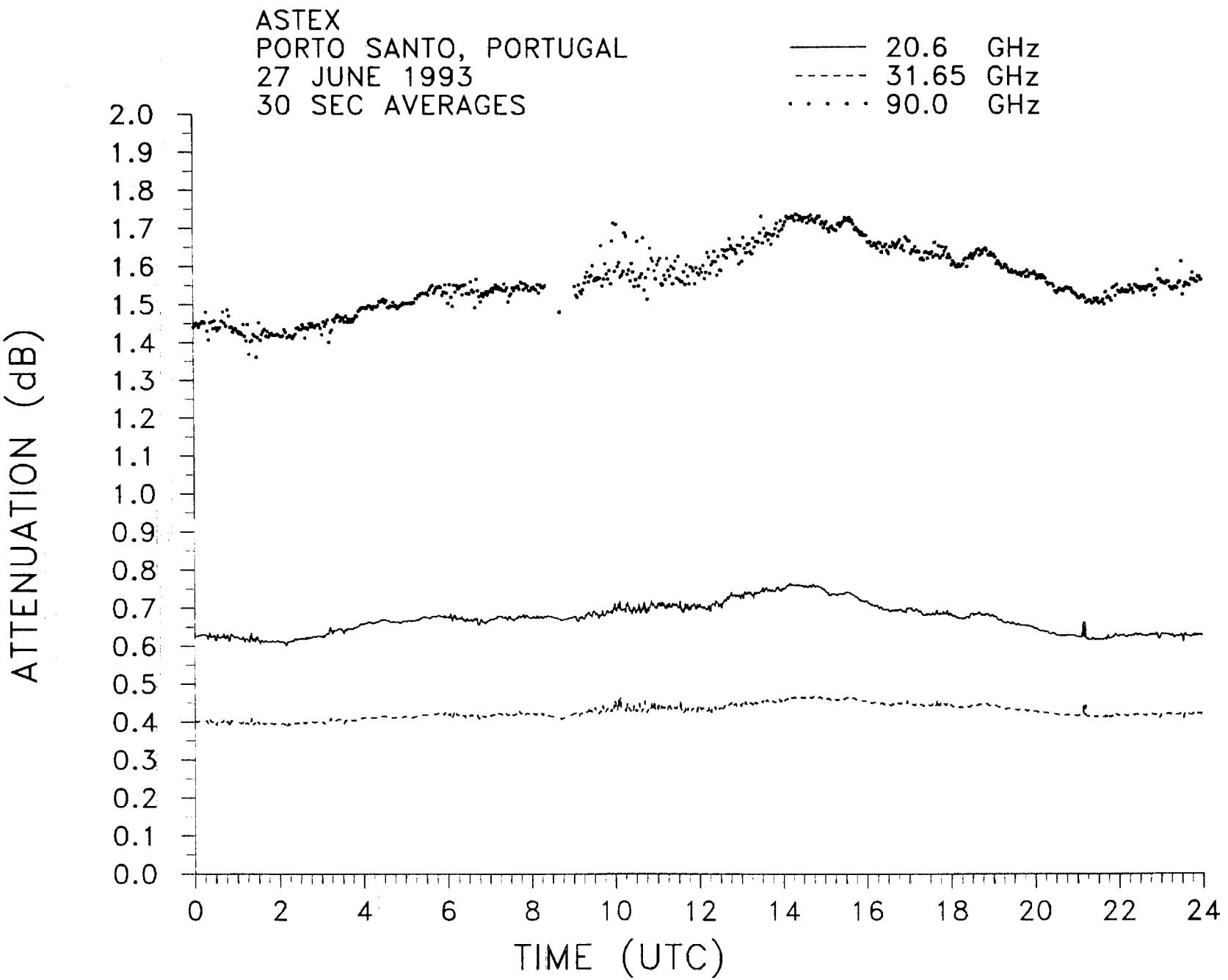
ASTEX
PORTO SANTO, PORTUGAL
27 JUNE 1993
30 SEC AVERAGES
20.6 GHz
31.65 GHz
90.0 GHz
ATTENUATION (dB)
2.0
1.9
1.8
1.7
1.6
1.5
1.4
1.3
1.2
1.1
1.0
0.9
0.8
0.7
0.6
0.5
0.4
0.3
0.2
0.1
0.0
0
2
4
6
8
10
12
14
16
18
20
22
24
TIME (UTC)

Figure 5b.

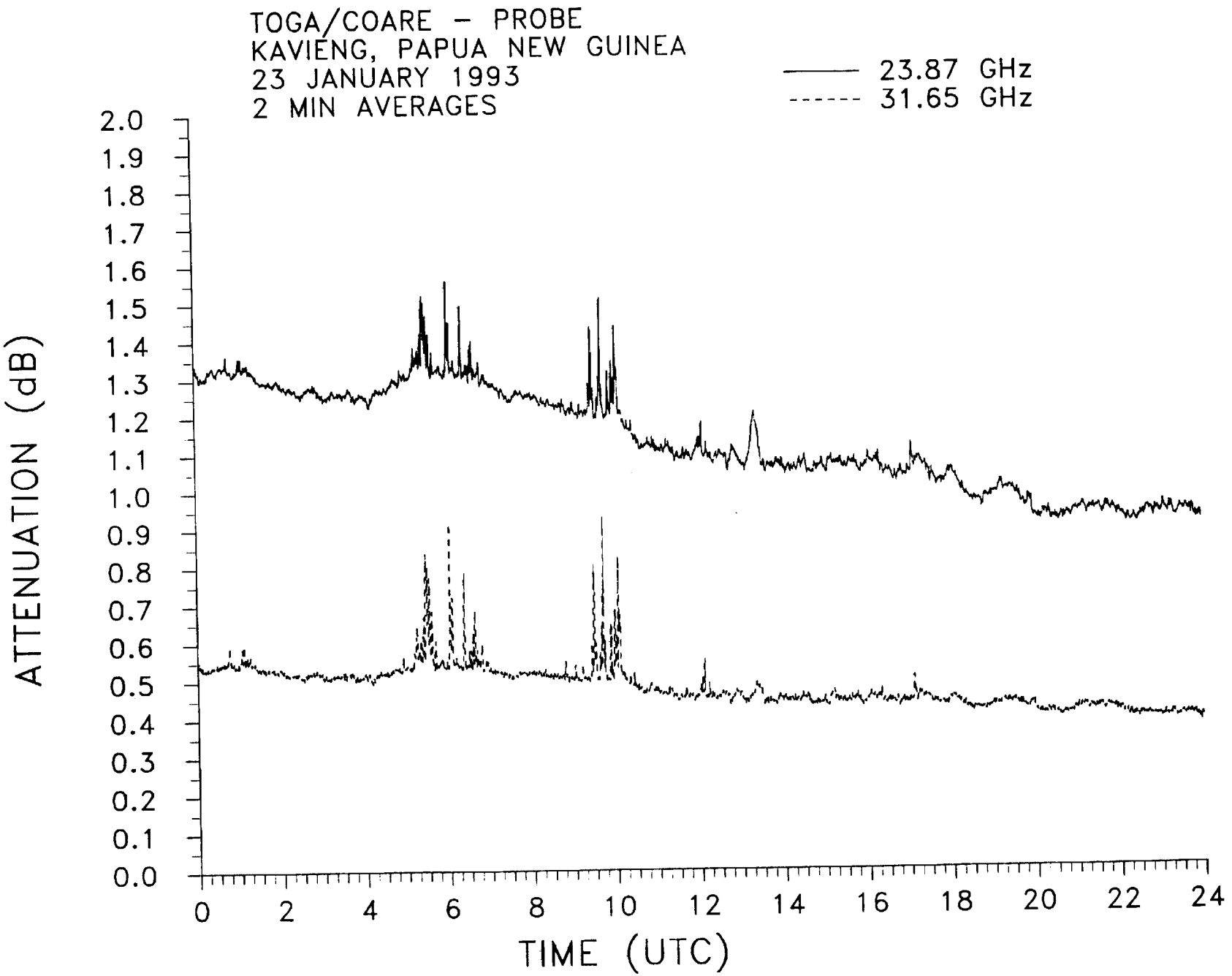
TOGA/COARE – PROBE
KAVIENG, PAPUA NEW GUINEA
23 JANUARY 1993
2 MIN AVERAGES
23.87 GHz
31.65 GHz
ATTENUATION (dB)
2.0
1.9
1.8
1.7
1.6
1.5
1.4
1.3
1.2
1.1
1.0
0.9
0.8
0.7
0.6
0.5
0.4
0.3
0.2
0.1
0.0
0
2
4
6
8
10
12
14
16
18
20
22
24
TIME (UTC)

Figure 6a.

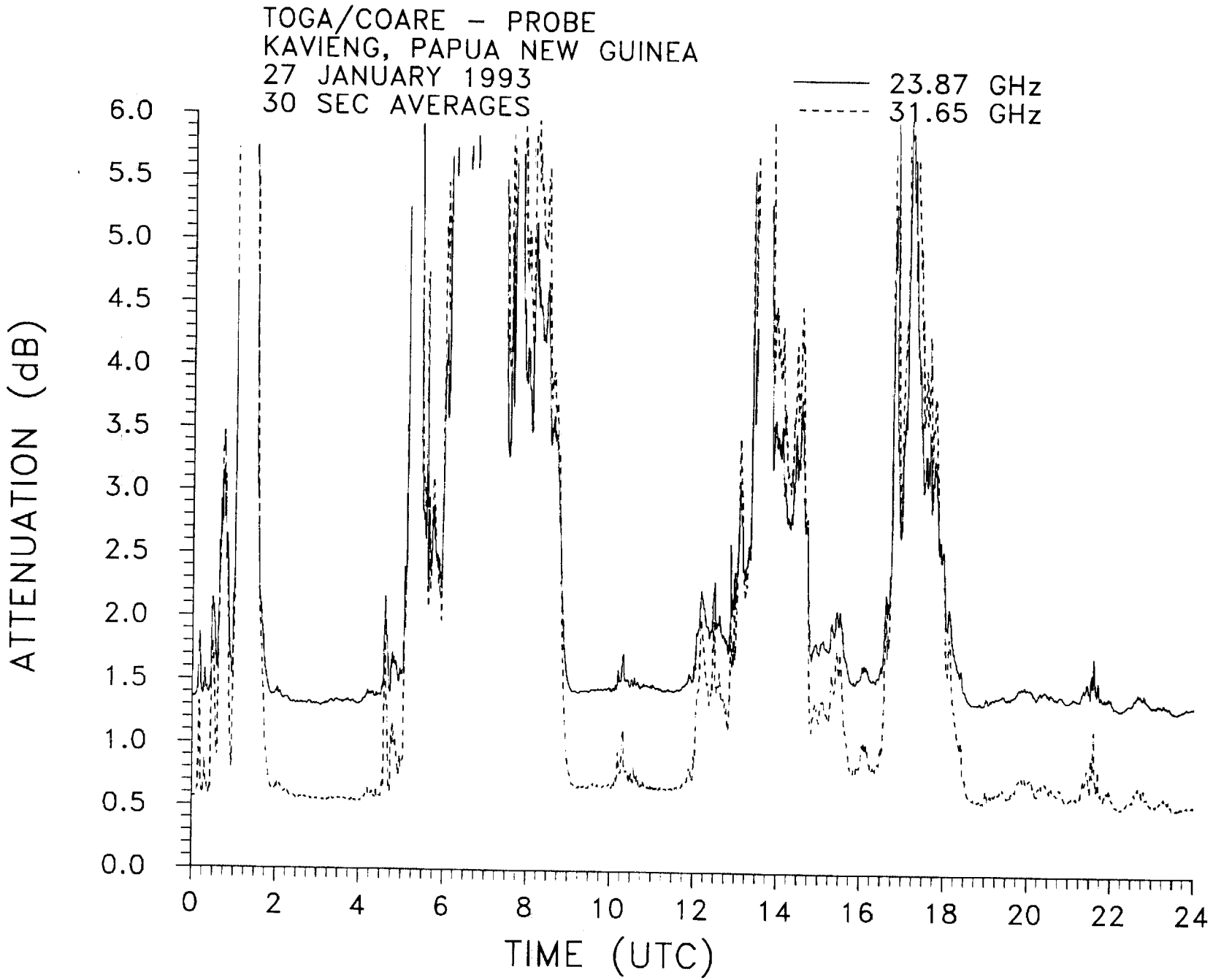
TOGA/COARE – PROBE
KAVIENG, PAPUA NEW GUINEA
27 JANUARY 1993
30 SEC AVERAGES
23.87 GHz
31.65 GHz
ATTENUATION (dB)
6.0
5.5
5.0
4.5
4.0
3.5
3.0
2.5
2.0
1.5
1.0
0.5
0.0
0
2
4
6
8
10
12
14
16
18
20
22
24
TIME (UTC)

Figure 6b.

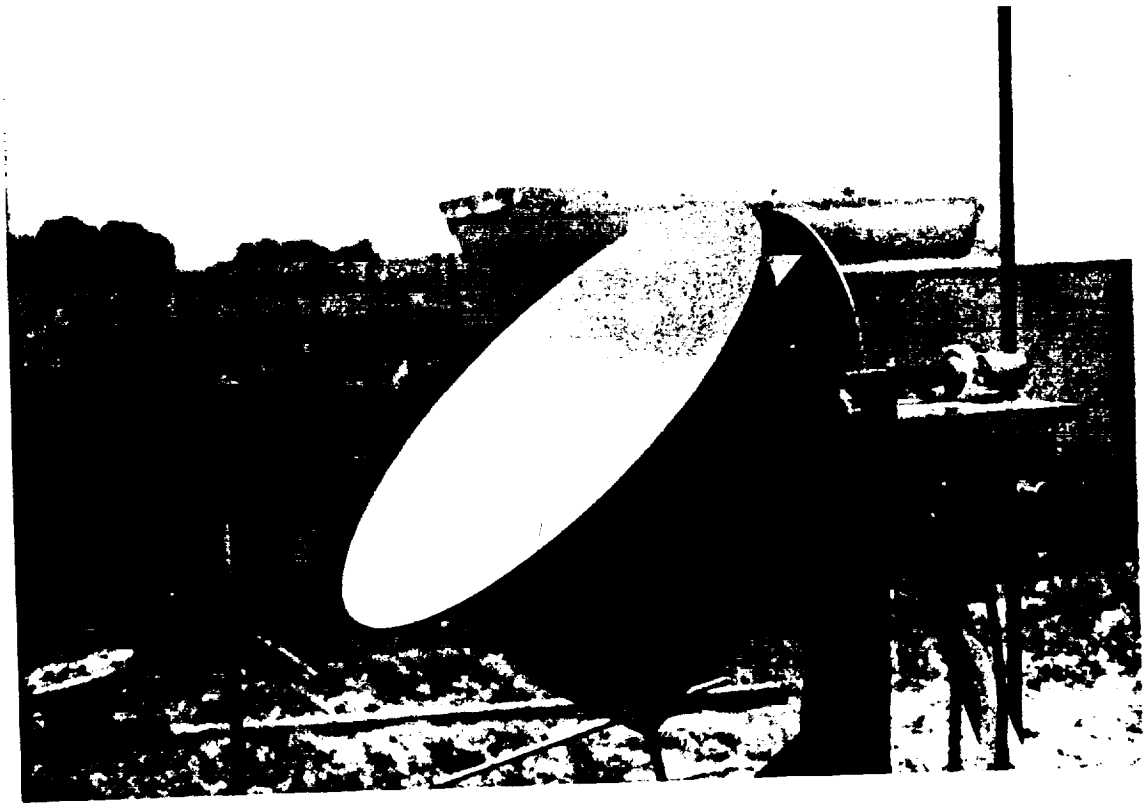

Figure 7.

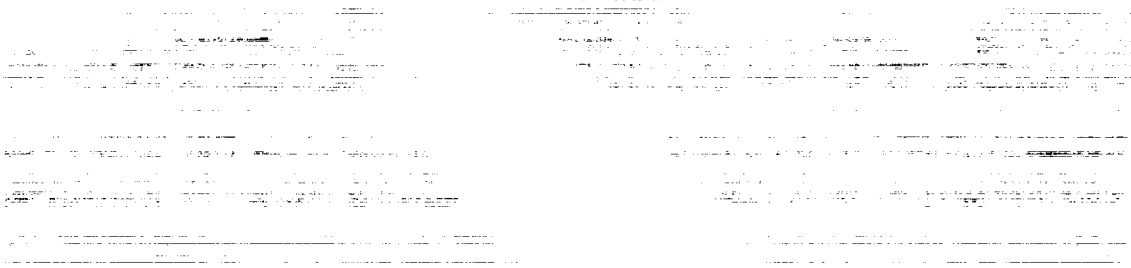

LONG DURATION MEASUREMENTS OF FADING ON A LOW ELEVATION ANGLE, 11-GHZ SATELLITE PATH

Wolfhard J. Vogel and Geoffrey W. Torrence
Electrical Engineering Research Laboratory
The University of Texas at Austin
Austin, Texas 78758-4445

Abstract - **Some rainfall rate and beacon fade results from the first 5 years of continuous observations of an 11.2 GHz satellite beacon with a 5.8° elevation angle in Austin, Texas are presented and compared to CCIR predictions.**

INTRODUCTION

Systematic measurements of satellite beacon rain attenuation have been carried out since late 1960s in the US, Europe, and Japan. Their results have been used to develop and verify the many prediction methods now in worldwide use, of which the CCIR and Global models may be the most familiar. These models predict the annual cumulative probability of exceeding a given fade on a specific satellite link, taking into account such parameters as the ground location, the frequency, and the elevation angle.

The prediction models have reached a reasonable state of maturity and perform with adequate average accuracy on links with non-extreme conditions, i.e., for elevation angles above about 30° and in temperate climate zones. The modeling interest, therefore, has shifted towards trying to forecast the year-to-year variability of fading, using approaches such as *Worst Month* predictions and other statistical approaches.

Characterizing the natural variability, return period, or prediction risk associated with rain attenuation requires data obtained over a sufficiently long period of time [1]. Most of the data sets available in the CCIR data base, the official repository for beacon fade data, however, do not exceed 2 to 3 years and this is not adequate to test variability model designs. As a remedy, the 11.2 GHz beacon observations in progress in Austin, Texas, since June 1988, are being continued [2] and this paper summarizes some of the results from the first 5 years of the experiment.

EXPERIMENTAL DETAILS

Data Collection

The experimental equipment for the measurements at Austin, Texas (30.39°N lat., 97.73°W long., 185 m alt., CCIR Climate Region M), incorporates a 2.4 m diameter receiving antenna feeding both a beacon receiver and a radiometer, a tipping bucket rain gauge, and sensors for wind, relative humidity, and pressure. Employing a single antenna ensures the alignment of the volume from which the thermal radiation emanates with the path of the beacon signal. Its measured sky coupling efficiency, h, is 0.98. A block diagram of the receiving equipment is shown in Figure 1.

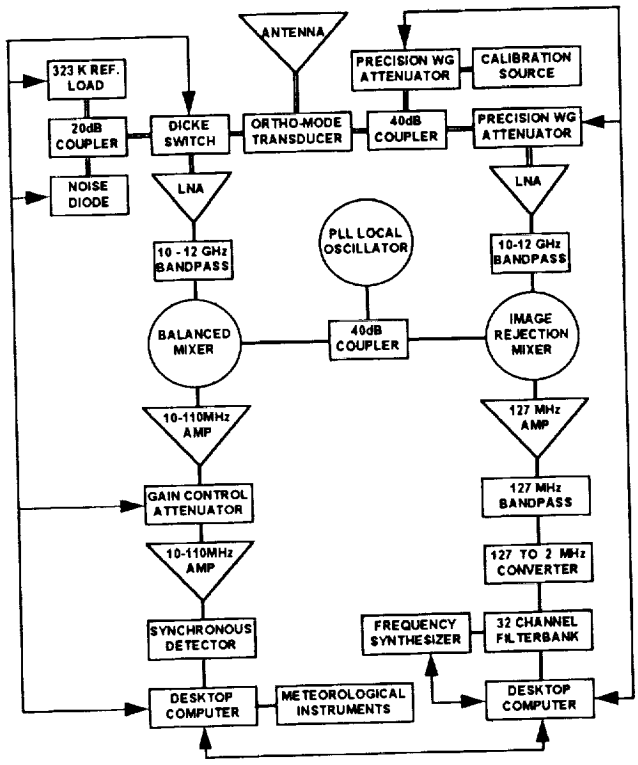

Fig. 1 11.2 GHz Beacon Receiver and Radiometer Block Diagram.

The data reported pertain to the five-year period from June 1988 to May 1993, during which the right-hand circularly polarized (RHCP) 11.198 GHz signal from a succession of three INTELSAT geostationary satellites located at 335.5°E was monitored, with a path elevation angle of 5.8°. Salient features of the beacon receiver are a K_u-Band low-noise amplifier and a 32 channel frequency-

tracking filter bank with 100 Hz bandwidth (BW) and a 0.9 Hz post detection BW, resulting in a fade margin of 25 dB. The receiver output is sampled at a 2 Hz rate. The radiometer implements a gain controlled, continuously self-calibrating Dicke-switched design with a total noise BW of 200 MHz centered at 11.325 GHz (LHCP), a 1 s integration time, and a sensitivity of less than 0.1 K. The radiometer and meteorological sensors are sampled at a 0.1 Hz rate; rain gauge tipping times are recorded asynchronously with a resolution of 0.06 s. Both experiment control and data acquisition are personal computer driven.

Beacon receiver calibrations were performed approximately quarterly by the signal injection method to allow for the characterization of the receiver in the enhancement region and to avoid having to rely on rare periods with low scintillations for a constant reference signal. The calibrations verified that receiver gain changes were negligible. The radiometer noise diode was calibrated against liquid nitrogen at the beginning of the experiment and diode aging appears to be insignificant, as the lowest sky temperature observed during dry winter nights repeated from year to year.

Data loss through equipment malfunction was minimized by careful system design, built-in redundancy, and daily operator inspection. During the five year period only one failure occurred during a fade event, but the data could be recovered from simultaneous strip-chart recordings. Data gaps caused by calibration or maintenance are judged to have negligible impact on the statistical results.

Data Processing

Calibration verified both constant gain and linearity of the receiver, but several factors contribute to a time varying offset. These need to be separated by post-acquisition data processing to derive the level of the received signal with respect to free space or clear air. The radiometer derived attenuation for non-rain fade periods is the most important ingredient in this procedure.

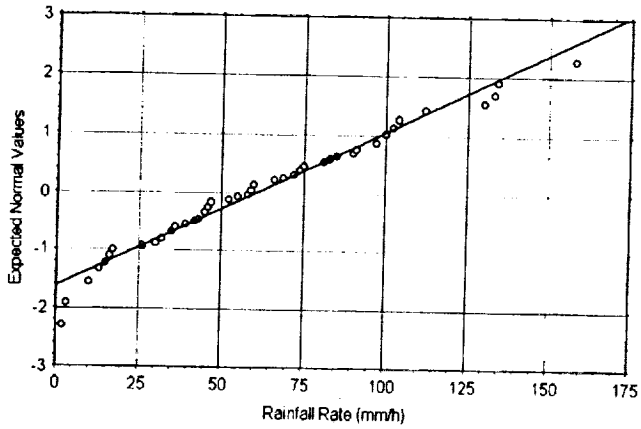

Fig.2 The 0.01% Rainfall Rate for the 60 Month Measurement Period Indicates Normal Behavior.

At the low elevation angle of this experiment, scintillations of the beacon level (±5 dB at 0.01% of time) were observed nearly always, even during rain fades, as verified by comparing the variations of beacon and radiometer time series. To separate rain fading from scintillation fading it is therefore not sufficient to just extract beacon data for time periods during which the radiometer is above a threshold (e.g., 110 K); the scintillations have to be removed by low-pass filtering of A_{fs} or A_{ca}. For the results presented here, we chose a moving averager window width of 3 min, which rejects about 80% of the scintillation power without causing overshoots after rapidly-decaying rain fades, based upon a graphical inspection of fade events.

RESULTS

Rainfall Rate

The rainfall rate at 0.01% annual probability for CCIR Climate Region M is 62.5 mm/hr, but for the 5-year measurement it averages 73.6 mm/hr, indicating that the CCIR classification does not fully account for Austin's subtropical climate in which rainfall often occurs in very heavy showers. The mean monthly 0.01% rainfall rate over the 60 month measurement period, however, is 60.7 mm/hr. A chi-squared fit performed on the data indicates that the monthly 0.01% rainfall rate is normally distributed with a standard deviation of 36.2 mm/hr, as depicted in Figure 2.

The month-by-month tabulation of the measured rainfall statistics has been included in Appendix A. Cumulative distributions of the rainfall rate observed for each of the 5 years, the overall period, and the *worst month* have been plotted in Figure 3.

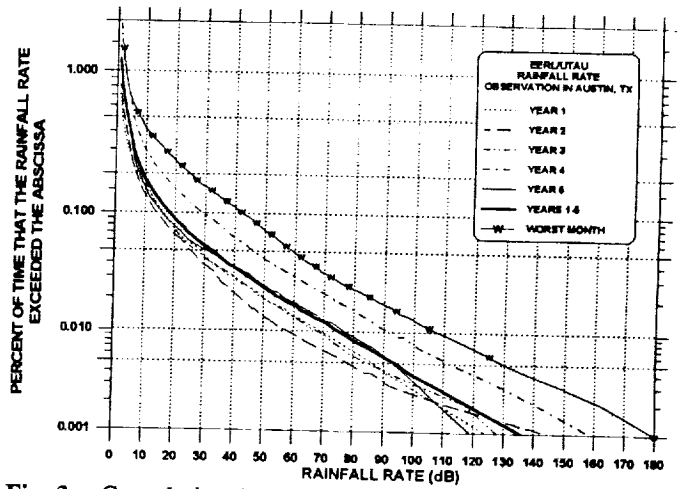

Fig. 3 Cumulative Distributions of the Annual Rainfall Rate for the 5 Years of Observation in Austin, Texas.

Fading

Figure 4 plots the percentage of time that the unfiltered clear air attenuation exceeded the values drawn on the abscissa for each of the 5 observation years, as well as the overall period. Note that the ordinate has a normal probability scale. Fades predicted by the CCIR method as given in Report 564 have also been included and are represented by the symbol **C**. There are two distinct domains in the graph. Fades less than about 5 dB are dominated by scintillations symptomatic for a low-elevation angle path. As scintillations are present for almost all of the time, year-to-year variations are very small. The higher fades are due to rain attenuation, are relatively rare events, and therefore exhibit much higher year-to-year variability. It is obvious, however, that the CCIR prediction method seriously underestimates rain fading.

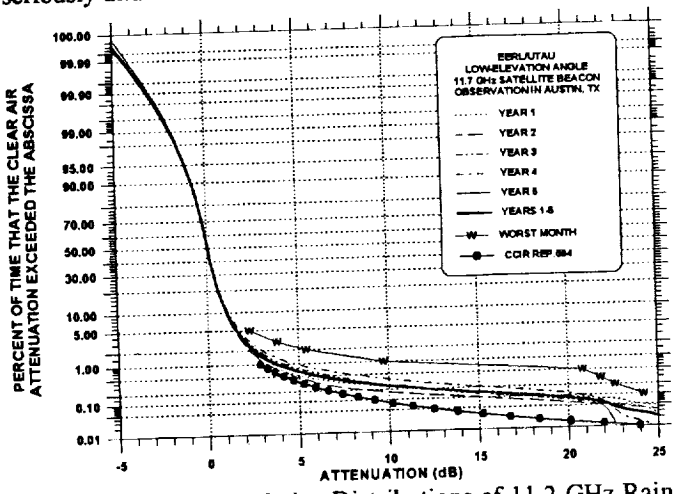

Fig. 4 Annual Cumulative Distributions of 11.2 GHz Rain Fades Measured in Austin, Texas, over a 60 Month Period.

The experiment's dynamic range of less than 25 dB is not adequate to characterize the 0.01% fades. During the *worst month*, 20 dB fades were exceeded for about 1% of the time. The average difference between monthly and 5-year fades exceeded at percentages between 0.1 and 1 has been plotted in Figure 5 along with the standard deviation. The average difference at 0.1% is about -4 dB, i.e., the monthly average 0.1% fade is about 14 dB, as opposed to the annual 0.1% fade value of 18 dB. Common sense would indicate that the average difference ought to be 0 dB. The discrepancy can be blamed on an apple/orange comparison. When comparing cumulative distributions, one has to have the same timebase. As an example, assume a month to have 100 hours and a year to consist of 2 months. During the first month, let fades exceed 5 dB for 1 hour, during the second month, fades exceed 5 dB for 2 hours and 10 dB for 1 hour. Assume fades were 0 dB at all other times. The two 1% fade levels are then 5 dB and 10 dB, with an average of 7.5 dB. The year, consisting of 200 hours, had 197 hours at 0 dB, 3 hours exceeding 5 dB, and 1 hour exceeding 10 dB. At 1% (2-hours), the annual fade exceeded only 5 dB. A table of the monthly and annual rain attenuation in excess of clear air, lowpass filtered with a 180 s window, has been added in Appendix B.

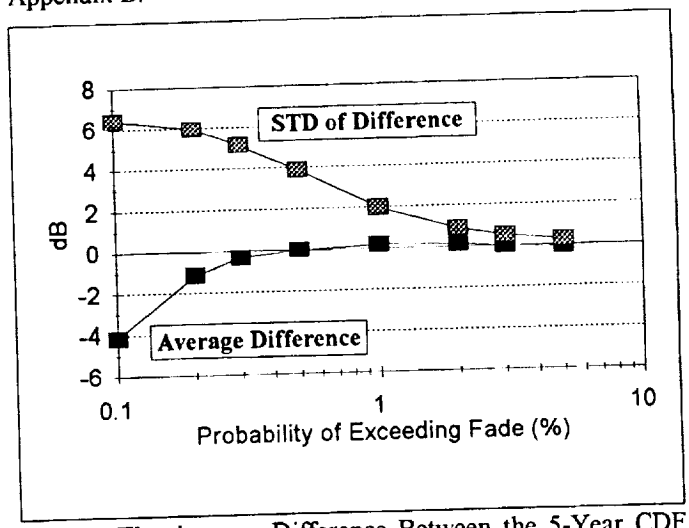

Fig. 5 The Average Difference Between the 5-Year CDF and the 60 Monthly CDFs.

Radiometric Medium Temperature

The 60 monthly values of the radiometric medium temperature, used for converting sky temperature to fades, are normally distributed and have a mean value of 266.7 K and a standard deviation of 5.5 K. Figure 6 shows a time series of the medium temperature estimates. The first 15 months have a lower average than the later months. At this time the cause for this trend is not known, however, it merits further investigation.

CONCLUSION

Observations of beacon rain fades on an 11.2 GHz path with 5.8° elevation have been performed for 5 years and are still continuing. The value of the long, uninterrupted and homogeneous data set will be for the modeling of the variability of rain fading. The results so far show that the CCIR prediction method consistently underestimates the attenuation due to rain fading on this link.

REFERENCES

[1] R. K. Crane, "Worst-month rain attenuation statistics: A new approach," *Radio Science*, vol. 26, no. 4, pp. 801-820, 1991.

[2] Vogel, W. J., G. W. Torrence, and J. E. Allnutt, "Rain Fades on Low Elevation Angle Earth-Satellite Paths: Comparative Assessment of the Austin, Texas 11.2 GHz Experiment," (invited), to be published in IEEE Proceedings, June 1993

APPENDIX A: Monthly and Annual Rain Rates (mm/h) Exceeded with Time Percentages from 0.5 to 0.001 in Austin, Texas, During the Five Year Period from June 1988 to May 1993.

Time	Rain Rate at Percentage											
yymm	0.5	0.3	0.2	0.1	0.05	0.03	0.02	0.01	0.005	0.003	0.002	0.001
8806	2	6	12	31	55	70	79	90	99	110	121	126
8807	2	6	13	22	31	36	40	45	47	52	53	55
8808	0	1	2	9	16	27	33	60	81	99	108	111
8809	1	3	4	6	9	12	20	43	51	69	82	87
8810	0	0	2	3	16	25	48	69	81	84	92	96
8811	0	0	0	1	2	5	7	10	20	24	27	32
8812	1	2	3	4	6	8	8	10	12	13	14	15
8901	4	8	11	16	21	25	29	35	41	46	47	50
8902	0	1	2	4	7	9	10	13	15	16	23	24
8903	2	8	12	23	37	47	55	85	136	144	152	172
8904	1	3	8	20	52	74	94	112	132	138	144	151
8905	8	17	24	39	56	64	68	81	98	105	108	129
Year1	1	4	7	15	28	39	49	70	88	101	111	137
8906	1	4	6	15	25	34	40	59	78	84	87	94
8907	0	0	0	0	0	0	0	3	7	7	8	16
8908	4	9	15	27	38	43	50	66	96	111	115	140
8909	0	0	0	1	9	14	17	32	69	74	76	77
8910	3	4	4	7	13	17	19	26	44	56	57	61
8911	2	2	3	5	6	9	11	17	21	22	28	30
8912	0	0	0	0	1	1	2	2	3	3	3	4
9001	1	1	2	3	7	11	13	16	21	22	28	29
9002	5	7	11	18	28	35	39	46	53	58	65	66
9003	4	6	8	12	18	24	28	30	35	36	38	39
9004	4	6	7	15	27	36	47	98	182	194	199	199
9005	10	21	31	47	67	82	96	134	180	199	199	199
Year2	2	4	6	13	24	34	42	59	79	97	125	173
9006	0	0	1	11	53	80	105	130	159	172	178	194
9007	4	5	8	15	27	39	50	59	69	72	73	75
9008	0	0	0	0	3	5	7	10	14	18	19	21
9009	2	4	8	20	41	54	69	75	84	95	102	130
9010	5	7	9	14	20	31	36	58	75	82	87	89
9011	4	7	9	13	21	27	32	47	51	57	61	68
9012	0	1	1	7	19	26	31	46	70	76	82	94
9101	9	12	16	21	29	37	42	47	55	57	60	66
9102	5	6	7	9	17	29	32	44	62	65	75	77
9103	0	1	2	3	7	12	17	42	58	71	75	77
9104	3	5	7	11	30	49	65	91	117	129	133	153
9105	3	12	19	32	50	61	72	100	115	124	127	139
Year3	3	6	8	15	26	40	50	68	86	109	118	140
9106	3	6	10	22	34	43	56	74	98	121	150	170
9107	0	1	4	8	31	46	60	83	92	95	98	105
9108	8	17	25	42	88	114	128	158	193	193	199	199
9109	1	5	12	25	37	44	48	60	71	80	83	98
9110	1	7	15	33	62	77	89	104	135	147	150	167
9111	0	1	4	11	20	30	35	45	52	63	64	65
9112	17	24	33	49	67	78	83	91	100	101	103	110
9201	4	5	5	7	8	9	12	15	18	19	19	20
9202	7	8	11	19	34	43	52	60	75	88	108	121
9203	6	10	16	28	45	57	65	75	84	88	99	110
9204	3	4	5	7	13	21	38	52	63	99	106	112
9205	12	22	35	54	72	90	102	133	156	168	177	186
Year4	5	9	15	28	46	61	73	93	115	134	147	171
9206	3	6	12	27	46	65	82	97	105	111	113	117
9207	0	2	2	3	6	7	11	16	20	21	21	28
9208	0	2	4	11	15	19	26	39	48	50	52	56
9209	3	5	9	41	68	83	92	100	110	116	120	127
9210	0	0	0	13	31	42	54	73	88	96	107	120
9211	6	10	14	37	61	75	85	104	131	143	150	174
9212	4	6	8	12	19	23	27	33	45	49	53	55
9301	5	6	8	10	16	22	24	36	44	50	55	62
9302	4	6	7	12	17	22	25	35	44	59	84	96
9303	2	5	8	15	23	33	44	55	62	67	80	87
9304	4	6	10	18	27	42	57	72	79	83	86	92
9305	5	7	10	28	47	56	77	102	119	128	135	140
Year5	3	5	7	15	30	46	57	78	94	104	111	127
Yrs1-5	3	6	9	18	32	45	56	75	95	111	125	148

APPENDIX B: Monthly and Annual Rain Attenuation (dB) in Excess of Clear Air (50% @ 0dB) Measured in Austin, Texas, at a Frequency of 11.2 GHz with an 5.8° Elevation Angle. The Fade Margin of the System was Nearly 25 dB. The Data have been Low-Pass Filtered with a 180 s Window.

Time	Attenuation at Percentage															
yymm	5	3	2	1	0.5	0.3	0.2	0.1	0.05	0.03	0.02	0.01	0.005	0.003	0.002	0.001
8806	0.8	1.1	1.6	3.5	8.4	15.6	20.1	23.1								
8807	1.0	1.4	1.8	3.1	5.2	7.5	10.3	17.9	23.1							
8808	1.0	1.2	1.5	2.7	5.1	7.1	10.8	16.6	21.3	23.8						
8809	1.0	1.3	1.6	2.8	5.8	9.0	13.5	17.3	20.8	23.2						
8810	0.6	0.7	0.9	1.2	1.8	3.0	4.8	8.4	13.0	22.3						
8811	0.6	0.7	0.8	1.0	1.4	1.8	2.4	4.5	10.1	14.9	16.7	18.2	20.5	21.2	21.5	21.7
8812	0.8	1.0	1.2	1.5	2.1	2.6	2.8	3.0	3.4	3.6	3.7	4.0	5.9	6.4	6.6	6.7
8901	1.0	1.3	1.7	2.8	4.2	5.9	8.1	12.6	16.6	20.3						
8902	0.7	0.8	0.9	1.1	1.3	1.6	2.0	2.8	6.1	9.0	10.2	11.5	13.1	13.8	14.1	14.3
8903	0.8	1.1	1.7	3.7	6.1	8.4	10.7	16.9	20.4	22.2	23.1					
8904	0.8	1.1	1.3	2.0	4.6	7.4	9.5	16.3	22.7							
8905	0.8	1.3	2.1	8.6	18.6											
Year1	0.9	1.1	1.4	2.4	4.8	7.7	11.6	18.9	23.5							
8906	0.9	1.3	1.9	4.0	6.1	10.2	21.5									
8907	0.8	1.0	1.2	1.6	2.5	4.0	6.4	12.2	15.2	16.6	17.7					
8908	1.0	1.2	1.5	2.3	4.6	7.0	10.4	16.5	20.8							
8909	0.9	1.1	1.2	1.5	1.9	2.4	3.7	6.1	10.9	16.2	17.5	21.4				
8910	0.8	1.1	1.3	2.6	5.2	6.2	7.1	15.2	23.9							
8911	0.7	0.9	1.1	1.6	3.0	4.1	4.9	6.1	7.3	7.8	8.4	9.9	10.6	10.8	10.8	10.9
8912	0.5	0.6	0.6	0.8	0.9	1.0	1.2	1.4	1.5	1.6	1.6	1.7	1.7	1.7	1.8	1.8
9001	0.8	1.0	1.2	1.4	1.7	2.0	2.2	2.8	3.6	4.0	4.3	5.1	8.9	9.6	9.9	10.1
9002	0.9	1.4	2.2	3.8	5.6	8.1	11.1	15.1	17.3	19.1	20.8	21.5	22.1	22.6	22.9	23.0
9003	0.8	1.1	1.3	2.1	4.3	5.4	6.1	7.0	8.1	9.6	12.0	14.6	17.2	18.2	18.5	18.8
9004	0.7	1.0	1.4	4.5	6.6	9.7	12.3	22.3								
9005	0.8	1.1	1.6	4.0	11.9	16.9	19.5	23.8								
Year2	0.9	1.1	1.4	2.3	4.4	6.1	8.2	15.1	21.7							
9006	0.7	0.8	1.0	1.2	1.7	2.3	3.9	13.9	20.3	23.2	23.7	24.2				
9007	1.2	1.8	2.6	4.1	6.6	9.6	11.8	15.2	18.8	20.3	21.6	22.8	23.4			
9008	0.9	1.2	1.4	1.9	2.7	4.3	7.1	12.2	19.0	22.2	24.0	24.1				
9009	1.2	1.6	2.2	4.0	5.5	7.4	9.1	12.4	15.7	19.8	21.8	23.2	24.0			
9010	0.9	1.1	1.5	4.1	6.7	9.0	11.8	21.9	24.3							
9011	0.8	1.2	1.7	3.4	5.5	6.7	8.3	16.9	22.4	23.8	24.3					
9012	0.7	0.9	1.0	1.3	1.6	1.9	2.3	3.3	4.6	5.6	6.2	7.7	8.2	8.7	8.8	8.9
9101	1.4	2.7	4.1	7.5	10.0	12.1	13.7	16.1	19.3	20.5	21.3	23.9	24.3			
9102	0.7	1.0	1.3	2.9	8.3	10.2	11.6	14.2	17.2	19.1	23.1	24.3				
9103	0.7	0.9	1.2	2.0	3.1	4.2	5.4	9.1	11.5	13.3	14.6	15.5	15.8	16.6	16.9	17.0
9104	1.0	2.2	3.9	6.5	9.6	17.6	22.6	24.2								
9105	1.0	1.5	2.2	4.6	8.8	14.7	18.9	22.9	24.1							
Year3	1.0	1.3	1.8	3.7	6.5	8.9	11.2	17.0	22.4	24.2						
9106	1.0	1.6	2.3	4.1	6.4	10.2	12.3	18.5	24.0							
9107	0.9	1.2	1.6	2.7	6.0	9.9	12.1	15.7	18.1	19.2	19.9	20.4				
9108	1.1	1.6	2.3	4.7	10.7	15.7	19.6	23.1	24.0							
9109	1.3	1.7	2.3	3.9	6.0	8.1	9.6	11.7	16.2	19.6	20.7	23.9				
9110	0.9	1.3	1.8	4.6	11.0	15.0	17.9	20.5	21.4	22.0	22.2	22.4				
9111	0.8	1.0	1.1	1.4	1.9	2.4	3.3	9.1	13.1	18.7	21.0	22.4	22.7			
9112	2.3	3.8	5.4	8.9	12.5	17.0	19.3	21.6	22.1	22.2	22.2					
9201	1.1	1.4	1.6	2.3	3.1	3.7	4.1	4.6	5.1	5.7	5.9	6.3	7.8	8.4	8.8	9.0
9202	1.6	2.2	2.8	4.8	7.4	8.7	9.8	11.2	15.1	23.0	23.1					
9203	0.9	1.4	2.8	5.3	8.4	11.7	14.5	18.5	21.2	22.1	22.5					
9204	0.7	1.1	1.7	3.5	5.3	6.5	7.1	8.3	9.4	10.4	10.8	12.6	15.7	16.6	16.8	17.0
9205	1.4	1.4	3.9	9.7	20.8	21.8	22.0	22.4	22.6	22.7	22.8	23.0				
Year4	1.2	1.7	2.4	4.5	7.9	11.5	14.9	20.5	22.1	22.5	22.9	24.2				
9206	1.0	1.7	2.7	6.1	11.2	20.9	22.2	22.6								
9207	0.8	1.0	1.2	1.5	2.1	2.9	4.0	5.4	8.7	10.2	11.7	14.9	15.8	16.1	16.2	16.3
9208	0.9	1.3	1.6	2.9	5.5	8.4	10.1	14.9	21.7							
9209	0.9	1.1	1.5	3.7	7.4	14.1	18.4	21.5	22.0	22.3						
9210	0.7	0.8	1.0	1.3	2.2	4.4	11.8	20.0	22.0							
9211	1.0	1.7	2.7	5.6	8.9	11.2	13.2	16.9	18.8	20.7	21.3	22.2				
9212	0.9	1.2	1.6	2.6	3.5	5.0	6.3	7.6	8.5	9.2	9.8	11.8	14.6	15.2	15.4	15.7
9301	0.9	1.1	1.4	2.4	4.4	6.0	7.5	12.2	14.9	16.3	18.2	19.7	21.0	21.5	21.8	22.0
9302	0.9	1.2	1.6	2.6	3.9	5.4	6.4	9.1	12.3	15.8	17.3	21.2	21.8			
9303	0.9	1.2	1.5	2.0	3.2	5.1	7.0	9.9	13.8	17.9	19.9	22.1				
9304	0.9	1.1	1.5	3.1	5.4	7.5	10.3	17.6	21.6	22.0						
9305	1.0	2.0	3.5	5.8	8.8	15.2	19.0	21.2	21.8							
Year5	0.9	1.2	1.6	3.1	5.7	8.4	11.1	18.2	21.8	22.1	22.3	22.7				
Yrs1-5	1.0	1.3	1.7	3.2	5.9	8.7	11.7	18.4	22.1	23.3	24.3					

LARGE-SCALE RAINFALL DIVERSITY FOR ACTS

H. P. Lin and W. J. Vogel

Electrical Engineering Research Laboratory
The University of Texas at Austin

Abstract *- From the NOAA 15 minute precipitation file for the US, data were selected for a set of 23 stations spanning a 5 year period. The selection covers the spot beam locations for ACTS and the propagation experiment sites. There is a 2% probability of having any simultaneous rain at 3 or more stations, but this reduces to less than 0.001% at a rainfall rate of 40 mm/hr.*

Introduction

Satellite communications systems operating at frequencies above 10 GHz are vulnerable to rain attenuation. For elevation angles above about 10° this effect is performance limiting and therefore has to be well understood, both from the perspective of the systems operator, the user, as well as the designer. Much work has already been performed to measure and model satellite propagation through rain [1] in order to develop reliable outage predictions or fade mitigation techniques for currently operating satellites.

The advent of the next generation of satellites at K-Band, such as Olympus, ACTS, and others invites a study of the large scale statistics of rain attenuation, because these satellites introduce new technologies that can make use of the fact that rainfall at any time is limited in spatial extent and has location dependent probabilities on a continental scale. Two examples of these techniques are beam-shaping for satellites with CONUS coverage, such as broadcast satellites, and uplink power control and adaptive transmission rate control for multi-beam communications satellites. An example of the latter is ACTS, which will offer a certain amount of pooled resources to overcome, on demand, rain fading in a limited number of its beam locations [2].

The objective of this study is to predict the probable demand on shared rain fade mitigation resources of multi-beam satellites operating in the CONUS region. Similar to studies that have been pursued in Italy, the UK, and Japan [3-5], the investigation is based on available rainfall data. In order to derive ACTS specific information, precipitation data for 23 stations were extracted from the NOAA 15 minute precipitation data base. The stations are either at locations served by the ACTS spot beams, or are at sites chosen for beacon propagation experiments. The data base yielded 5 years of concurrent information, covering the period of Jan. 1, 1984 to Dec. 31, 1988. The data were used to determine individual rain statistics, as well as joint statistics for pairs and triplets of stations as a function of separation. The number of stations with rainfall rate exceeding a given threshold was also determined. In order to assess the effect of the integration time of the rainfall on the results, four years of rain gauge data obtained in Austin, Texas were used to derive scaling parameters. Where appropriate, the results are compared to those found for Italy.

Precipitation Data Base

Description

Rainfall data with the highest resolution collected in the US are those in the NOAA data file TD 3260. It contains 15 minute precipitation information. According to NOAA, the data were taken by qualified observers at primary, secondary, and cooperative stations operated by the National Weather Service and the Federal Aviation Agency. Approximately 2,700 stations have recorded precipitation data in the file, although not all stations cover the entire period starting in 1970. The data are in the form of variable length ASCII records, giving each station's accumulated rainfall for 15 minute intervals, the daily total, and error flags. For most of the stations rainfall is quantized in increments of 0.1 inches. Error flags indicate abnormal conditions, such as deleted, incomplete, or missing data. The files, a total of about 275 MBytes, are available on magnetic tape. The stations are listed by station identification numbers only, therefore another data tape, the Station Historical File (TD 9767), is also needed for location and operations information.

Selection of Stations

The selection of ACTS stations is summarized in Table 1 and their location (with the exception of the Alaska station) has been plotted in Figure 1. The selected stations include the seven Class I propagation experiment sites, namely:

Fort Collins, Colorado; Tampa, Florida; Baltimore, Maryland; White Sands, New Mexico; Oklahoma City, Oklahoma; Blaine, Washington; and Fairbanks, Alaska.

The other 16 selected stations are covered by ACTS spot beams. In Table 1, the column labeled BAD% gives the percentage of defective records in the data base for each station.

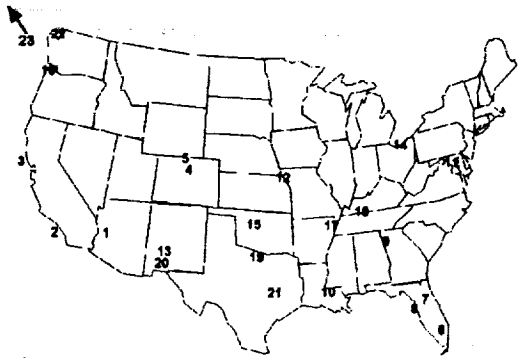

Fig.1 Location of the 23 stations selected for ACTS coverage.

Table 1: Stations Selected For ACTS Prediction

NO	ID	CITY	STATE	BAD %	LAT(°)	LON(°)	ELEV(m)
1	026481	PHOENIX WB AP	ARIZONA	0.0%	33.26	112.02	111
2	047740	SAN DIEGO WB AP	CALIFORNIA	0.0%	32.44	117.10	2
3	047772	SAN FRANCISCO WB CITY	CALIFORNIA	0.0%	37.47	122.25	5
4	052220	DENVER WB AP	COLORADO	0.0%	39.46	104.53	529
5	053005	FORT COLLINS	COLORADO	12.5%	40.35	105.05	500
6	085663	MIAMI WB AIRPORT	FLORIDA	0.0%	25.49	80.17	1
7	086628	ORLANDO (MC COY AFB)	FLORIDA	0.0%	28.26	81.19	10
8	088788	TAMPA WB AIRPORT	FLORIDA	0.0%	27.58	82.32	2
9	090451	ATLANTA WB AIRPORT	GEORGIA	0.2%	33.39	84.25	98
10	166660	MOISANT INT AP	LOUISIANA	0.0%	29.59	90.15	0
11	180465	BALTIMORE WB AIRPORT	MARYLAND&DC	0.0%	39.15	76.32	2
12	234358	KANSAS CITY WSMO AP	MISSOURI	0.0%	39.17	94.43	101
13	299686	WHITE SANDS NATL	NEW MEXICO	12.3%	32.47	106.10	400
14	331657	CLEVELAND WB AP	OHIO	0.0%	41.24	81.51	79
15	346661	OKLAHOMA CITY WB AP	OKLAHOMA	0.0%	35.24	97.36	128
16	356751	PORTLAND WB AP	OREGON	0.0%	45.36	122.36	2
17	405954	MEMPHIS WB AP	TENNESSEE	0.8%	35.03	89.59	26
18	406402	NASHVILLE WB AP	TENNESSEE	0.0%	36.07	86.41	58
19	412242	FORT WORTH INTL WSO	TEXAS	0.9%	32.50	97.03	54
20	412797	EL PASO WB AP	TEXAS	0.0%	31.48	106.24	392
21	414300	HOUSTON WSMO AP	TEXAS	1.5%	29.58	95.21	10
22	450729	BLAINE	WASHINGTON	5.1%	48.59	122.45	4
23	502968	FAIRBANKS WB AP	ALASKA	0.3%	64.50	147.43	44

Rain Statistics for Selected Stations

The probability of having rain for each of the 23 stations has been plotted in Figure 2. In this plot the area of the circle is proportional to the average annual rain probability, defined as the number of 15 minute intervals with precipitation divided by the number of quarter hours per year. The largest value in this selection is 2.37% for Station 16 (Portland, Oregon), and the smallest is 0.34% for station 13 (White Sands, New Mexico). The average annual rain amount for the stations has been plotted in Figure 3, in which the area of each circle is proportional to the rain amount.

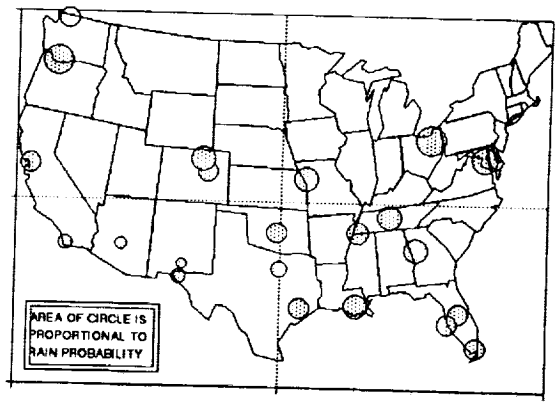

Fig. 2: The probability of having rain at the 23 ACTS stations derived from five years of precipitation data.

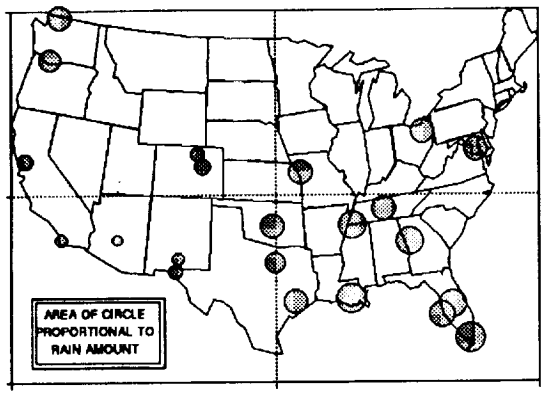

Fig. 3: The average annual rain amount at the 23 ACTS stations.

The site at New Orleans, Louisiana, had the most rain, with 60.03", while Phoenix received the least amount, with only 9.21". By comparing the relative size of the circles for individual stations, one can get some indication about the typical rain intensity. In the case of Florida vs. the Northwest, for instance, the probability of having rain is smaller in Florida, but the total amount at both locations is similar. This is due to Florida's heavy showers and the Northwest's frequent drizzle rain.

Despite the fact that only 23 stations are in the ACTS station set, occasionally a significant fraction of these stations can experience rain at the same time. An example of this is shown in Figure 4, which demonstrates simultaneous rain (within

Fig. 4: Due to the structure of weather fronts, on rare occasions many stations report rain during the same 15 minute interval. In this case, 7 stations have precipitation.

the same quarter hour) at 7 of the stations. The statistical significance of this event will be characterized in the following section.

Simultaneity of Rain

Station Count

For a satellite system with many beams and spare capacity for fade mitigation, the most important quantity is the probability that rainfall above a given rate threshold is observed simultaneously at several stations. The count of stations with simultaneous rainfall from 0 to 10 mm/quarter-hour for the ACTS set of 23 stations has been plotted in Figure 5.

The probability that two or more of these stations have simultaneous precipitation of $\geq$ 2.5 mm/quarter-hour was found to be 0.5%. Increasing the rainfall rate threshold to 10 mm/quarter-hour decreases that probability to 0.02%. Comparing these results to the case in which 128 approximately equal-distant CONUS stations were selected, one finds that for the lower rainfall rates the probability of simultaneous precipitation at a given number of stations is larger in the ACTS case.

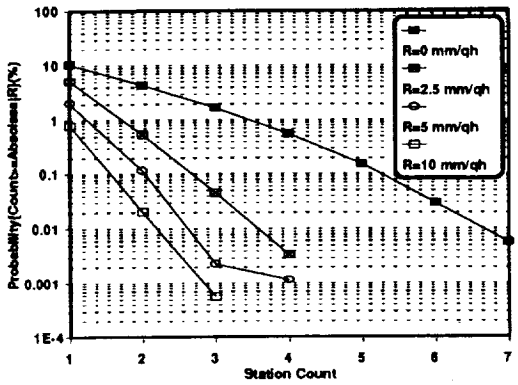

Fig. 5 The probability that rainfall above a threshold rate occurs simultaneously at several of the 23 ACTS stations, for rainfall rates of 0, 2.5, 5, and 10 mm/quarter-hour.

For example, 5% of the ACTS stations have rain exceeding 2.5 mm per quarter-hour for 5% of the time, as opposed to only 1% of the 128 station set. This difference is caused by the large spatial correlation between rainfall events. Both sets of stations are distributed all over the US, but because of the higher density for the set of 128, there is more correlation among the set of 23. Therefore, no linear scaling of the station count is found. This result also indicates that 128 stations are a sufficient number to characterize the large scale behavior of precipitation.

A second difference between the results from the two sets of stations can be attributed to the fact that the National Weather Service has changed the resolution of the rain gauges from 0.1" to 0.01". Most of the 128 station data is based on tenths of inch resolution, whereas the ACTS rain data mostly have 0.01" resolution. This explains the

difference in probability between the two station sets. For the 128 stations, low rates cannot be resolved adequately and the 2.5 and 3 mm/quarter-hour station counts merge. At 10 mm/quarter-hour the resolution is adequate and the probabilities are similar.

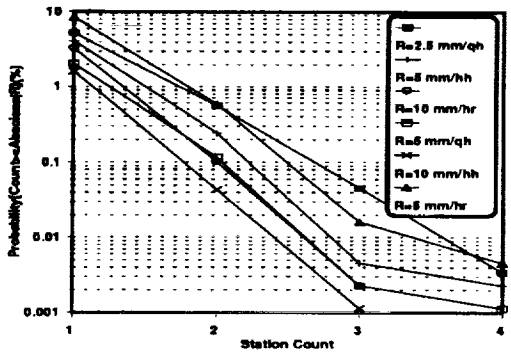

Fig. 6: Comparison of the probability of simultaneity of rain for time bases of 15, 30, and 60 minutes.

Figure 6 displays the probability of rain at several stations for time bases of 15, 30, and 60 minutes. As in the 128 station case, the results for thresholds of 2.5 mm/quarter-hour, 5 mm/half-hour, and 10 mm/hour are not equivalent because most rain events are of short duration.

Joint Probability

More insight is gained into the large scale structure of precipitation when the joint probability of rainfall is determined as a function of station separation. Plotted in Figure 7 are the two-station joint probabilities for rainfall rates in excess of 0, 2.5, 5, and 10 mm/quarter-hour. A probability minimum exists for the case of rain > 0 mm/quarter-hour at a distance of about 1000 to 1500 mile separation, where the joint probability of rain at two of the selected stations is about 0.025%. For the higher rainfall rates, the probabilities are lower and noisier because only 23 stations are considered.

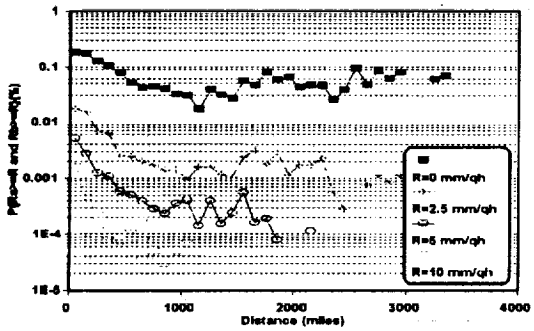

Fig. 7: Joint probability of rain at two of the ACTS stations.

Statistical Dependence

A statistical dependence index has been defined [2] by the ratio of the joint probability to the product of the single station probabilities as

$$\chi = \frac{P_{ab}}{P_a P_b} \qquad (1)$$

and

$$\chi = \frac{P_{abc}}{P_a P_b P_c} \qquad (2)$$

for 2 and 3 stations, respectively. For the case of statistical independence, $\chi = 1$. If rain at the stations is correlated, then $\chi > 1$. If $\chi < 1$, negative correlation exists.

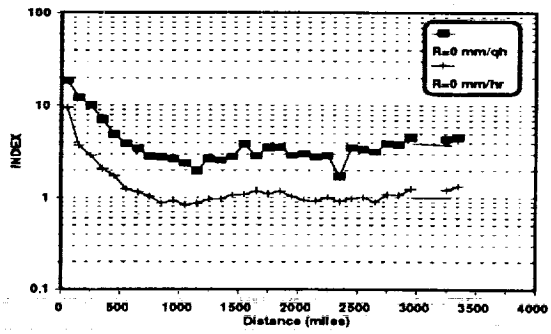

Fig. 9: Average conditional probability of the rain rate at any other station exceeding the threshold value R, given that it rains with rate>R at a specific station.

For the 23 ACTS stations, values of χ for two stations and for rainfall greater than 0 mm per quarter-hour and per full hour have been plotted in Figure 8; the curves for three stations and for R>2.5 mm/quarter-hour are very noisy due the limited set of data and have not been included in the graph. The statistical dependence index has a minimum for pairs of stations separated by 1000 miles and slowly increases for separations greater than 1500 miles, with a peak near 2000 miles, and a second minimum near 2500 miles. The first peak can be explained by the coast-to-coast effect and the second one by the correlation between Alaska and Florida. The result for hourly data is consistent with the 128 station case, but for the quarter hour time base the statistical dependence index is larger. This is a consequence of the typical short duration of rain. If most rain events consist of only 1/4 hour with rain in one hour, then the probability of rain for the 1/4 hour timebase will be 1/4 of the probability for the one hour timebase. The joint probability, P_{ab}, will have the same ratio. Then, according to (1), χ can

be up to four times as large for the shorter timebase.

Conditional Probability

Another useful quantity characterizing large-scale rain diversity is the conditional probability of the rainfall rate at any station i exceeding R, given that the rainfall rate at station n also exceeds the same threshold. This can be expressed by

$$P_c(n) = P\{R_i > R \mid R_n > R\} \qquad (3)$$

and has been plotted in Figure 9 for the ACTS stations for rainfall rate thresholds of 0, 2.5, 5, and 10 mm/quarter-hour. As expected, the conditional probability decreases with increasing rainfall rate. At the threshold of 2.5 mm/quarter-hour, the conditional probability varies between about 10 to 30% for all the stations. Curiously, some stations have significantly lower conditional probabilities than others, namely stations 5, 13, and 22, i.e., Fort Collins, White Sands, and Blaine, Washington. In the case of station 22, it is furthest removed from all other stations except station 16 and has a lower probability of rain than station 16. The low conditional probability for stations 5 and 13 can be explained with the aid of Figure 7, in which the joint probability of rain is lower for a mid-continent-to-coast geometry than a coast-to-coast one. The reason that neighboring central stations 4 and 20 don't show the same behavior may be that frontal weather systems are more likely to exist near coastlines than mid-continent, making weather in those regions less highly correlated with distance.

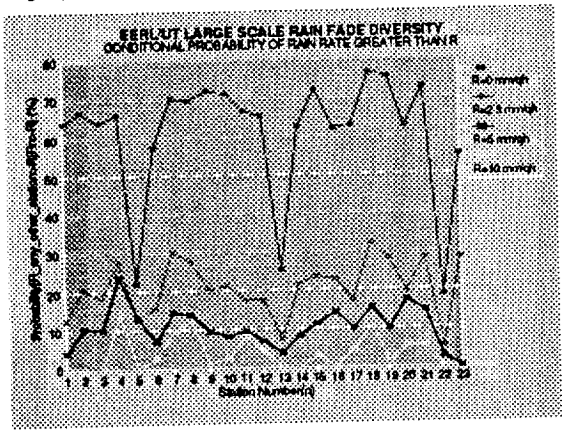

Fig. 9 The average conditional probability of the rain rate at any other station exceeding the threshold value R, given that it rains with rate>R at a specific station.

Conclusions

The NOAA 15 minute precipitation data are the highest resolution rainfall data available for the US for a large number of stations and for a period of about 20 years.

For the 23 ACTS stations, there is a 2% probability of having any simultaneous rain at 3 or more stations, but this reduces to less than 0.001% at a rainfall rate of 40 mm/hr (Fig. 5).

Bibliography

[1] Ippolito, L. J., "Propagation Effects Handbook for Satellite Systems Design," NASA Reference Publication 1082(04), February 1989

[2] NASA, "ACTS, The Blueprint for Future Telecommunications," ACTS Program Support Office, 600 Maryland Ave. S.W., Suite 220, Washington, D.C. 20004, June 1990

[3] Barbaliscia, F., G. Ravaioli, and A. Paraboni, "Characteristics of the Spatial Statistical Dependence of Rainfall Rate Over Large Areas," *IEEE Trans. Ant. and Prop.*, Vol. 40, No. 1, pp. 8-12, January 1992

[4] Fukuchi, H., "Correlation properties of rainfall rates in the United Kingdom," *Proc. IEE*, 135, pt H, pp. 83-88, 1988

[5] Otsu, Y., Y. Takahashi, and T. Kozu, "Simultaneous occurrence probabilities of rainfall among nine locations in Japan," *Electronics Letters*, Vol. 22, pp. 937-938, 1986

[6] Goldhirsh, J., V. Krichevski, and N. Gebo, "Rain Rate Statistics and Modeled Slant Path Fade Distributions at 20 GHz and 30 GHz Derived from a Rain Gauge Network in the Mid-Atlantic Coast of the United States over a Five Year Period," Report S1R92U-006, The Johns Hopkins University, Applied Physics Laboratory, Johns Hopkins Road, Laurel, MD 20723-6099, March 1992

[7] Lin, H. P. and W. J. Vogel, "Large Scale Rainfall Diversity for ACTS," EERL Report 23 December 1992, 10100 Burnet Rd., Austin, TX 78758

Rain Rate Duration Statistics Derived from the Mid-Atlantic Coast Rain Gauge Network

Julius Goldhirsh
The Johns Hopkins University, Applied Physics Laboratory
Johns Hopkins Road, Laurel Maryland, 20723-6099

Abstract

A rain gauge network comprised of 10 tipping bucket rain gauges located in the Mid-Atlantic coast of the United States has been in continuous operation since June 1, 1986. Rain rate distributions and estimated slant path fade distributions at 20 GHz and 30 GHz covering the first five year period have been derived from the gauge network measurements, and these results have been described by Goldhirsh et al. [1]. In this effort, we present rain rate *time duration* statistics. The rain duration statistics are of interest for better understanding the physical nature of precipitation and to present a data base which may be used by modelers to convert to slant path fade duration statistics. Such statistics are important for better assessing optimal coding procedures over defined bandwidths.

1.0 Review of Experimental Configuration

The rain gauges are of the tipping bucket type described by Goldhirsh and Gebo [2] and Gebo and Goldhirsh [3]. Each rain gauge is interfaced with an individual PC which records the tipping times from which the rain rates are derived. The gauges are located within a rectangular grid whose north-south and east-west distances are 70 km and 47 km, respectively. The gauge locations are shown on the map of Figure 1 and are numbered from 1 to 10. Calibrations are performed twice per year and the system is maintained with errors of less than 5% in rainfall at rates of 12 to 15 mm/h.

2.0 Review of Rain Rate Distributions

For purpose of completeness, we review the previously reported pertinent cumulative fade distributions. In Figure 2 are given the individual network average rain rate distributions for years 1 through 5, where year 1 covered the period 1 June 1986–31 May 1987, and subsequent year numbers covered the respective contiguous 12 month periods. Site #6 operated during the first three years and Site #4 operated during the latter four year period. These intervals were accounted for in determining the resultant network and yearly averages. We note years 1, 2, 3, and 5 show similar distributions, whereas year 4 shows significantly higher probabilities. The combined distribution, which is the spatial and temporal average, is given by the circled points and represents the equivalent of 47 site-years of measurements. This set of distributions indicates that it took four years before an extreme rain rate distribution was noted. As of this writing, approximately seven years of network data have been accumulated,

and it is the intent to reexamine the annual variability after 10 years of network data are available. Figure 3 shows distributions for each of the 10 sites, where each corresponds to the five year temporal average (with the exception of Sites #4 and #6). The combined spatial and temporal average is given by the distribution with the circled points. We note the spatial variability of the distributions (Figure 3) is significantly smaller than the temporal variability (Figure 2).

3.0 Rain Rate Durations

3.1 Methodology of Formulation

Consistent with the definition of Vogel et al. [4], a rain rate *episode* represents the continuous time interval a designated rain rate threshold level is exceeded. The conditional probability of exceeding a rain rate duration for a given rain episode level is defined as follows

$$P(D > D_q | R > R_q) = \frac{N(D > D_q | R > R_q)}{N_T(R > R_q)} \tag{1}$$

where

R	Rain rate in mm/h
R_q	Designated threshold rain rate value or episode threshold
D	Duration of rain rate episode
D_q	Designated threshold duration pertaining to rain rate episode level
$N(D > D_q \mid R > R_q)$	Number of episodes for which $D > D_q$ given $R > R_q$
$N_T(R > R_q)$	Total number of episodes for which $R > R_q$

Cumulative probability distributions of the type given by (1) were obtained from density distributions containing 150 contiguous duration bins whose bin size was one minute.

3.2 Temporal and Spatial Average

In Figure 4 are given a family of distributions pertaining to a temporal and spatial average of the rain rate site data for rain rate thresholds of 5, 10, 20, 50, 100, and 125 mm/h. We note that for any given probability the rain rate durations decrease with increasing rain rate, and conversely. This characteristic is amplified in Figure 5 where the duration is plotted versus rain rate for fixed probability levels (solid levels). The curves follow an approximate power law curve in the range 5 mm/h to 50 mm/h, and thereafter the durations tend to fall off more rapidly with increasing rain rate. By expressing each curve by it's best fit power curve (for the indicated range of rain rates), we obtain

$$D = A(P)\, R^{-B(P)} \qquad 5 \leq R \leq 50 \tag{2}$$

where D is the rain rate duration in minutes and R is the rain rate in mm/h. A family of A and B values were derived for each percentage level and best fit functional forms were determined which fit the A versus P and B versus P relations [5]. The functions are given by

$$A(P) = \left(a + b\ P^{0.5}\ \ln P\right)^{-1} \tag{3}$$

$$B(P) = c + d\ \exp\left(P/e\right) \tag{4}$$

where

$$\begin{cases} a = 3.28322 \times 10^{-3} \\ b = 9.17138 \times 10^{-4} \\ c = 9.31395 \times 10^{-1} \\ d = 1.16276 \times 10^{-2} \\ e = 2.31520 \times 10^{1} \end{cases} \tag{5}$$

where P is the probability of exceeding the duration D and is expressed in percent. The resultant set of empirically derived fits are given by the dashed curves in Figure 6. We note that the expression (2) fits the measured levels very well for all probabilities indicated. The difference between the measured and empirically derived durations at 50 mm/h for the 50% case is less than 0.3 min. The overall average of the absolute differences between the measured durations and empirically derived durations is 0.5 min with the RMS being 1.3 min for the system of curves.

3.3 Site-to-Site Variability

In Figure 7 we compare the site-to-site variability of the rain duration distributions for the 10 sites for the different rain rate thresholds, where each site is averaged over the five year period. The peak spread was determined for a series of fixed probabilities in Figure 7 and the resultant equi-probability values versus distribution spread is plotted in Figure 8 for the series of rain rate thresholds. The curve for the threshold value of 100 mm/h, which not shown in Figure 7, is also plotted in Figure 8.

We glean the following characteristics from Figures 7 and 8: [1] The distributions are grouped into bundles associated with the indicated rain rate threshold (Figure 7). [2] The spread of distributions (for any given rain rate threshold), increases monotonically with increasing rain rate duration (Figure 7). [3] The distribution spread increases monotonically with decreasing rain rate threshold (Figure 8).

The narrowness of the distribution spread for probabilities above 10% is indicative of the fact that the spatial structure of the rain cells and its dynamics are similar statistically for each rain rate threshold over the lateral scale dimensions defining the separations of the ten sites.

3.4 Year-Year Variability

In Figure 9 is plotted a family of curves representing the network average distribution for each year of the five year period. The resultant set of curves is a manifestation of the

year to year variability of the rain rate durations. In Figure 10 are plotted the corresponding equi-probability values versus the distribution spread for the family of rain rate thresholds considered. The characteristics are similar to those described in the previous section. The narrowness of the distribution spread for probabilities greater than 10% is indicative of the fact that the spatial structure of the rain cells and its dynamics are statistically similar for any given rain rate threshold from year to year. What differs from year to year is the frequency of occurrence of the rain rate threshold. However, once the rain events occur, the conditional statistics are relatively invariant.

4.0 Comparison with Other Investigators

We compare here the rain rate duration distributions examined here with those recently published for Austin, Texas over the four year period from June 1988–May 1992 [4]. Figure 11 presents a comparison of the cumulative rain rate distributions of Austin, Texas and the Mid-Atlantic coast combined average case, and Figure 12 shows the corresponding rain duration distributions. We note that although the rain rate distributions are considerably different (Figure 11), the rain duration distributions are remarkable similar (Figure 12); especially at probabilities greater than 10% for all rain rate thresholds. Excellent agreement is noted for probabilities of 1% and greater for rain rate thresholds larger than 10 mm/h. The equal probability differences are well within the spread durations for the individual sites denoted in Figure 8. The proximity of the duration distributions indicate that for the two regions, the statistics associated with the structure and dynamics of rain cells are relatively invariant, although the absolute probability of occurrence varies.

5.0 Summary and Conclusions

Rain rate time durations were analyzed employing a data base covering the first five years of measurements from the Mid-Atlantic coast tipping bucket rain gauge network comprised of 10 gauges. An empirical rain rate model was developed which characterizes the combined network average (temporal and spatial) of the probability of time duration of rain rate episodes to within an overall average error of 0.5 minutes (equation (2)). The narrowness of the spread of distributions for the year-to-year and site-to-site cases are indicative that given a rain rate threshold, the duration statistics are relatively invariant. A comparison of the the Mid-Atlantic coast rain rate duration distributions with those from Austin, Texas showed close agreement. The above results demonstrate that although the frequency of occurrence of a rain rate threshold may vary from year to year and location to location, once the threshold is exceeded, the dynamics and rain cell structures are generally statistically invariant.

6.0 Acknowledgements

The author is grateful to Norman Gebo who manages the rain gauge network and to Vladimir Krichevsky who developed the rain duration software and reduced the five year data set. This work was supported by the NASA Propagation Program directed by the Office of Commercial Programs under Contract NOO39-91-C-001.

7.0 References

1 Goldhirsh, J. V. Krichevsky, and N. E. Gebo, "Rain Rate Statistics and Fade Distributions at 20 and 30 GHz Derived from a Network of Rain Gauges in the Mid-Atlantic Coast over a Five Year Period," *IEEE Trans. Ant. & Prop.*, Vol. 40, No. 11, pp. 1408–1415, November, 1992.

2 Goldhirsh, J. and N. E. Gebo, "A Comparative Assessment of R. M. Young and Tipping Bucket Rain Gauges," *JHU/APL Technical Report S1R-92U-018*, June 1992.

3 Gebo, N. E. and J. Goldhirsh, "Operation, Calibration, and Data Acquisition for Capacitive and Tipping Bucket Rain Gauges," *JHU/APL Technical Report S1R93U-004*, March 1993.

4 Vogel et al., "Rain Fades on Low Elevation Angle Earth-Satellite Paths: Comparative Assessment of the Austin, Texas 11.2 GHz Experiment," *Proceedings of the IEEE*, June, 1993.

5 Jandel Scientific, "TableCurve, Automated Curve Fitting Software," Jandel Scientific, San Rafael, CA 94901.

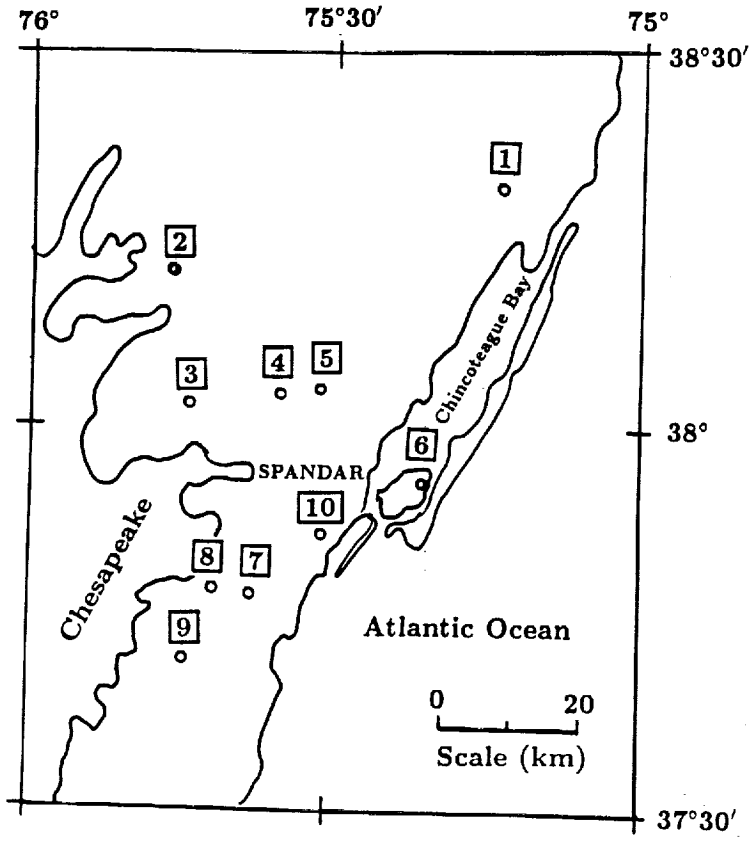

Figure 1: Map of Mid-Atlantic coast region designating rain gauge site locations.

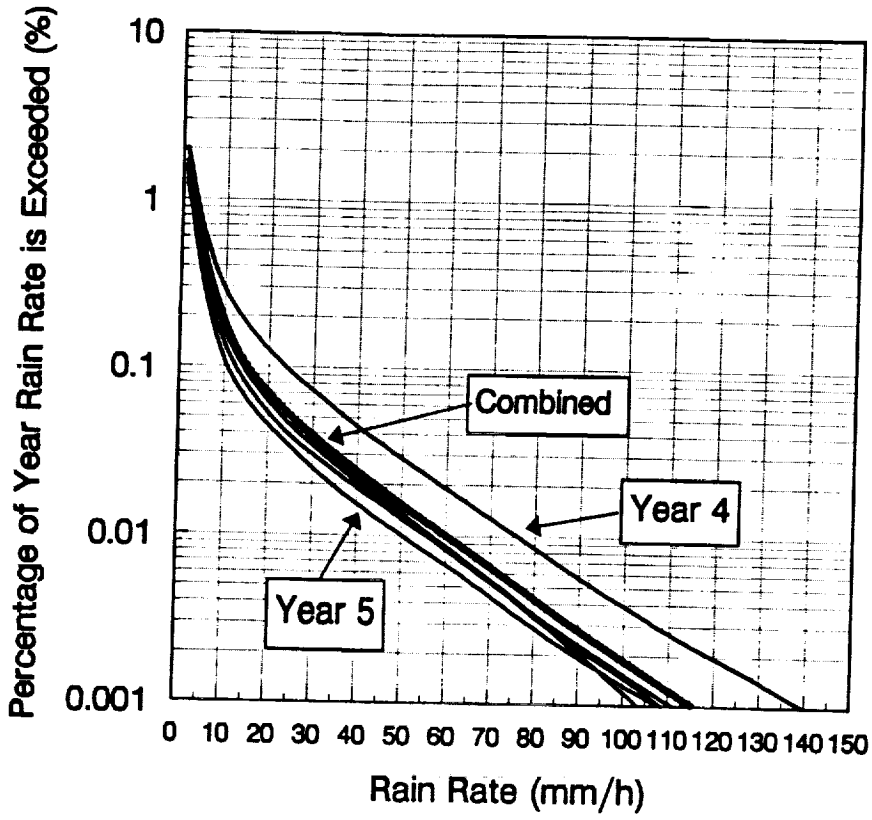

Figure 2: Year-to-year rain rate distributions of network average [1].

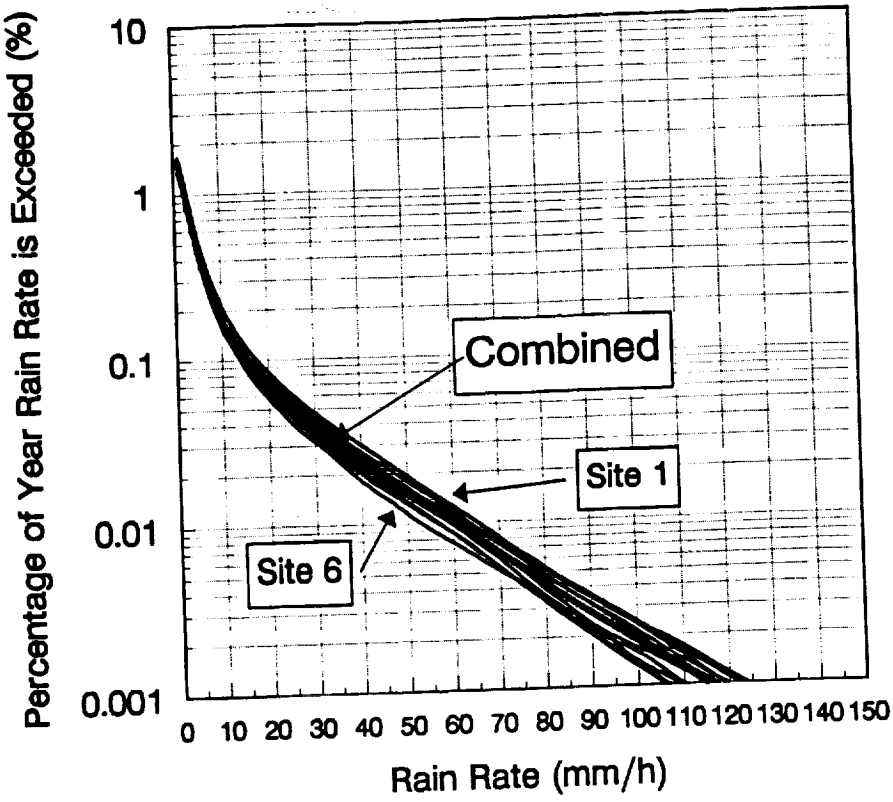

Figure 3: Site-to-site rain rate distributions of five year average [1].

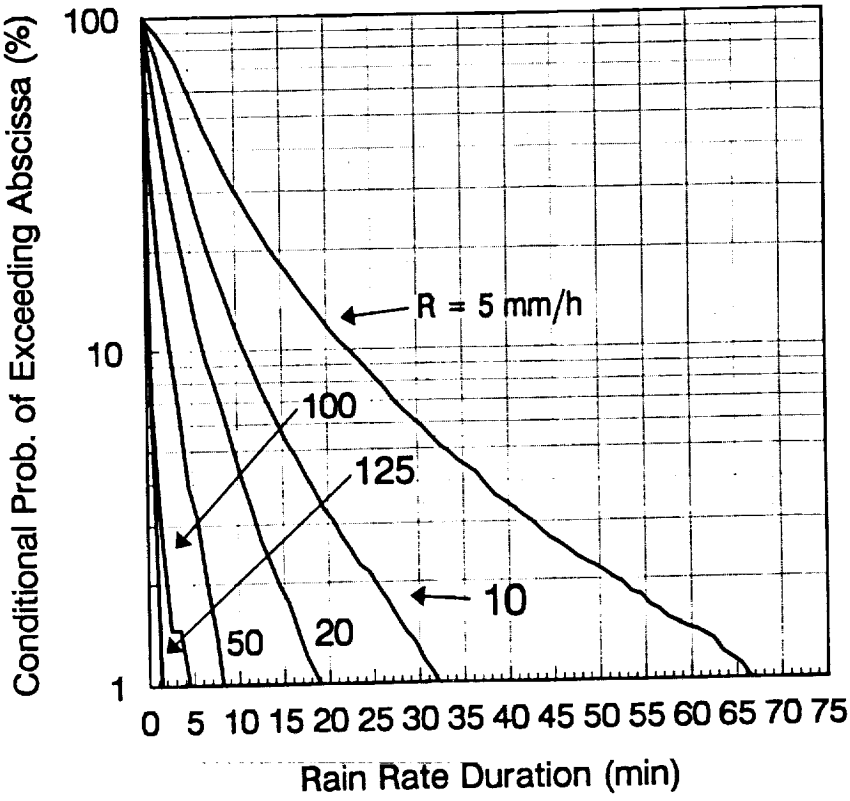

Figure 4: Rain rate duration distributions of combined spatial and temporal average.

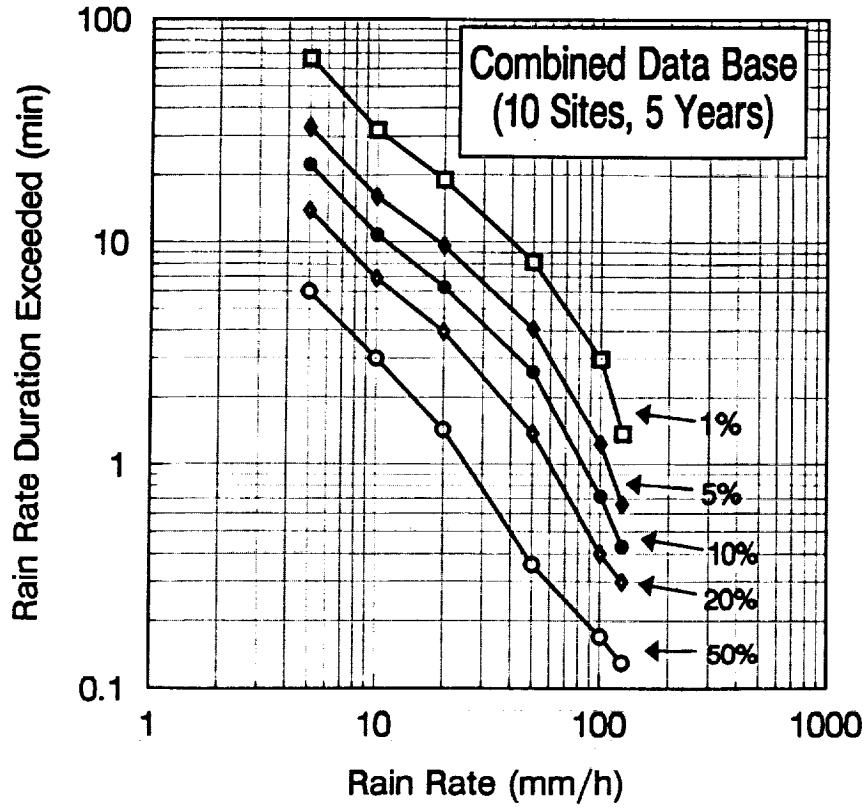

Figure 5: Rain rate duration versus rain rate threshold at equal probability levels.

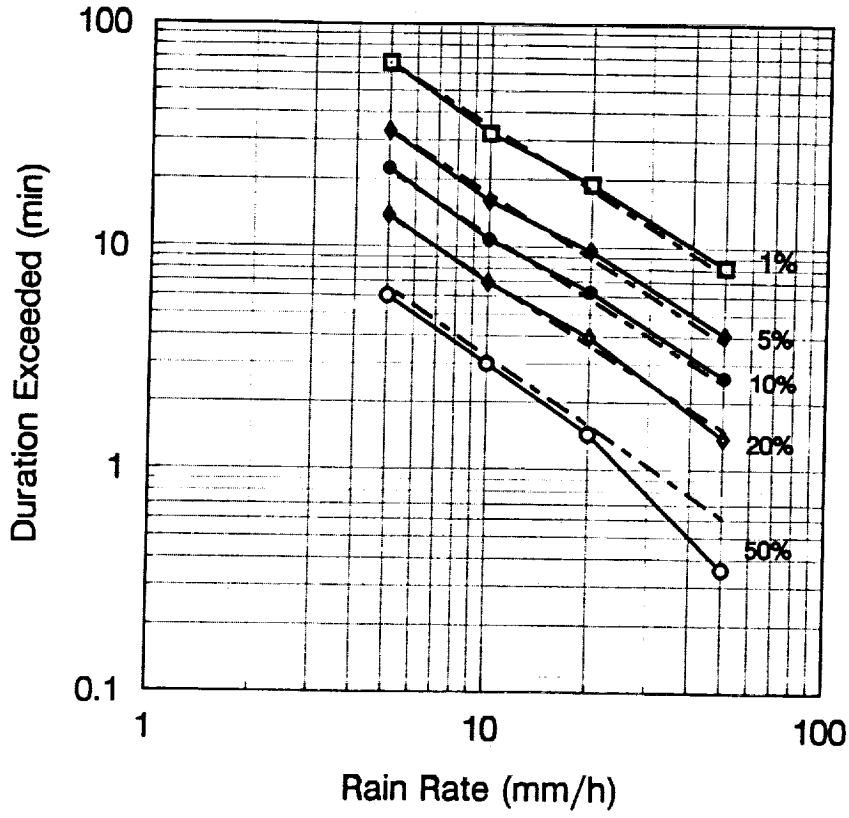

Figure 6: Comparison of measured (solid curve) and empirical model (dashed curve) of rain rate duration versus rain rate threshold at equal probability levels.

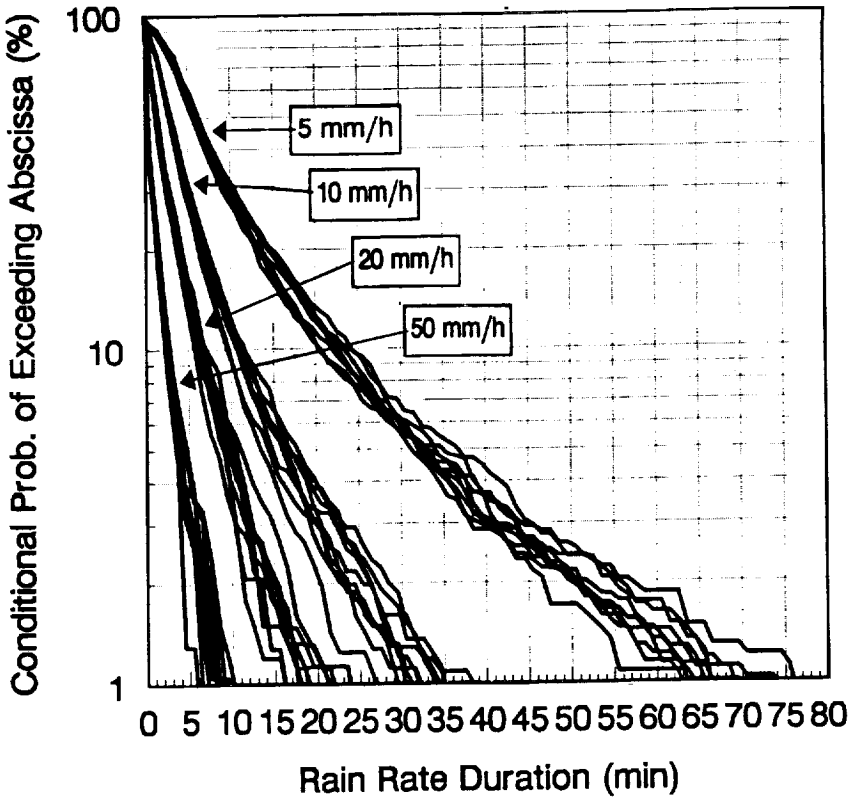

Figure 7: Site-to-site rain rate duration distributions of five year average [1].

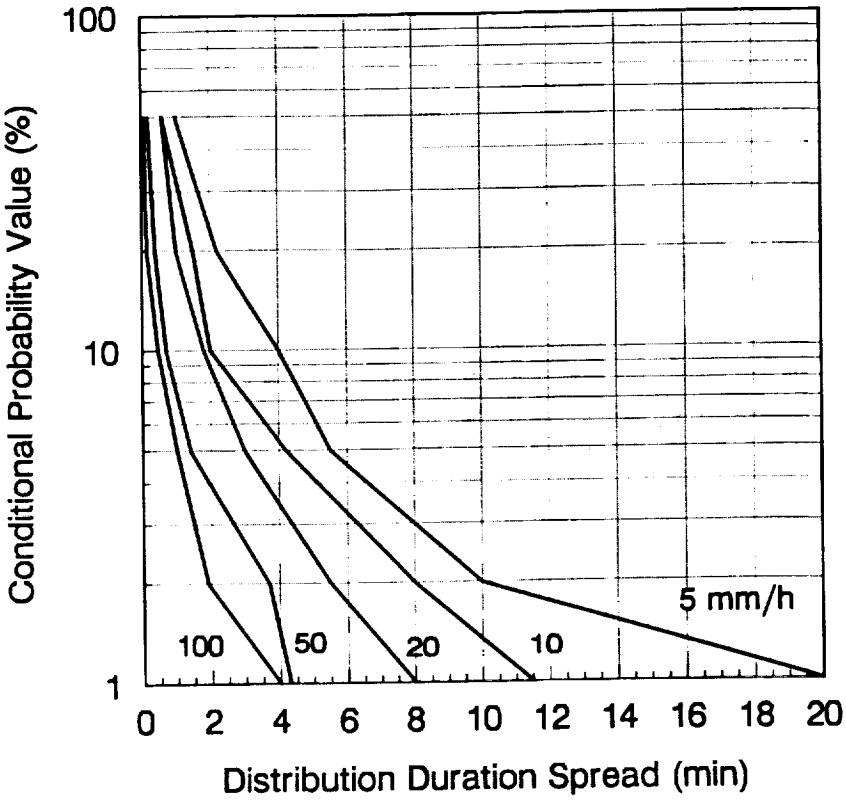

Figure 8: Site-to-site rain rate duration peak spread as a function of probability.

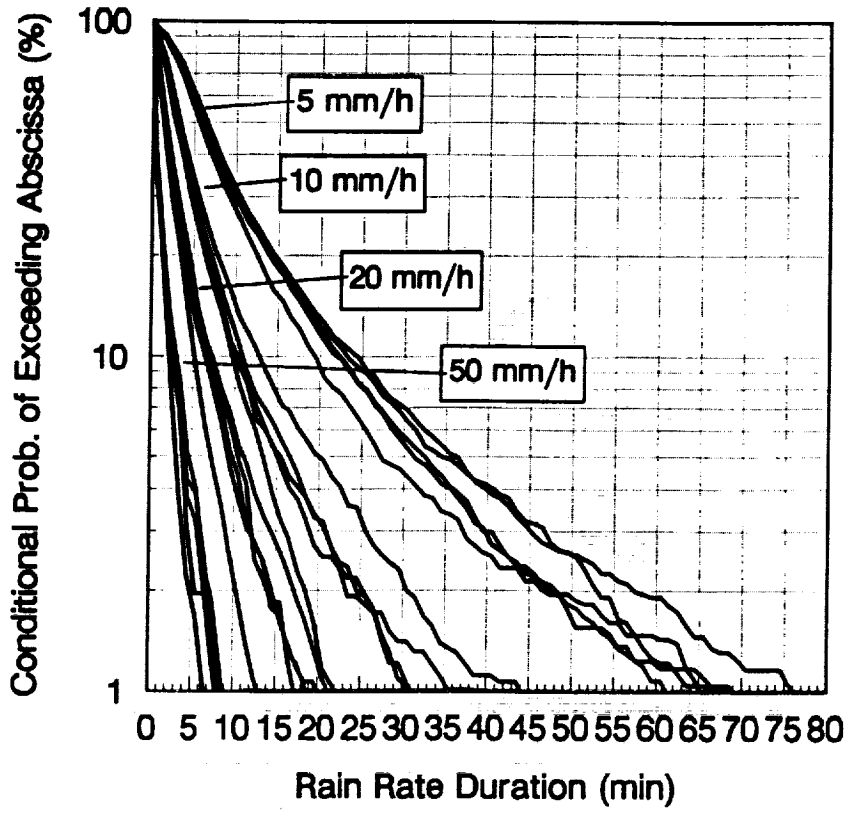

Figure 9: Year-to-year rain rate duration distributions of network average.

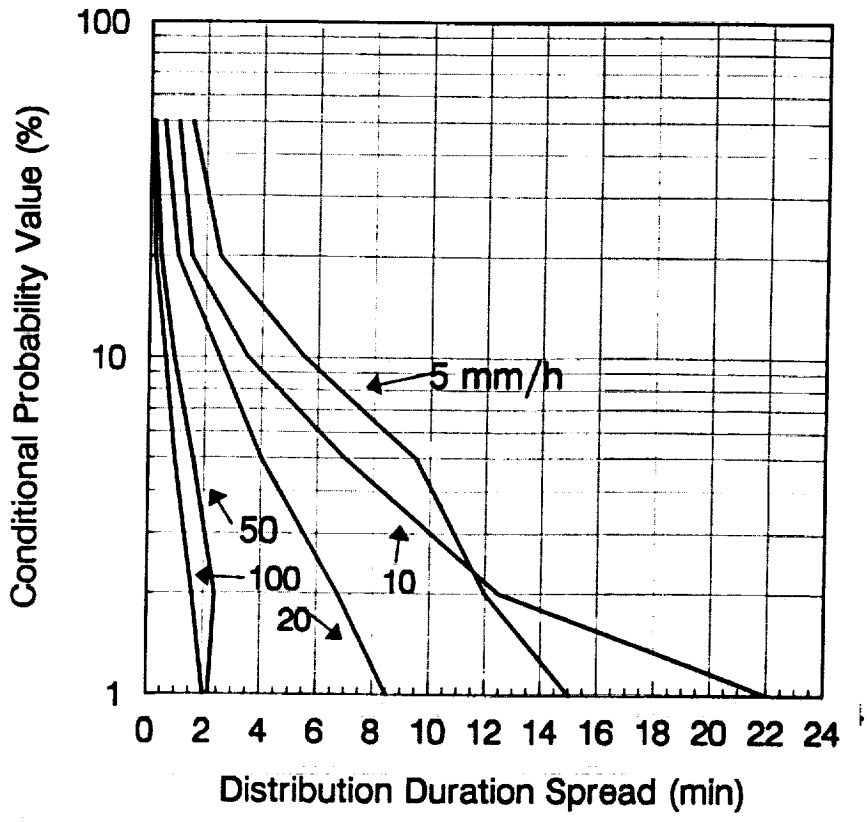

Figure 10: Year-to-year rain rate duration peak spread as a function of probability.

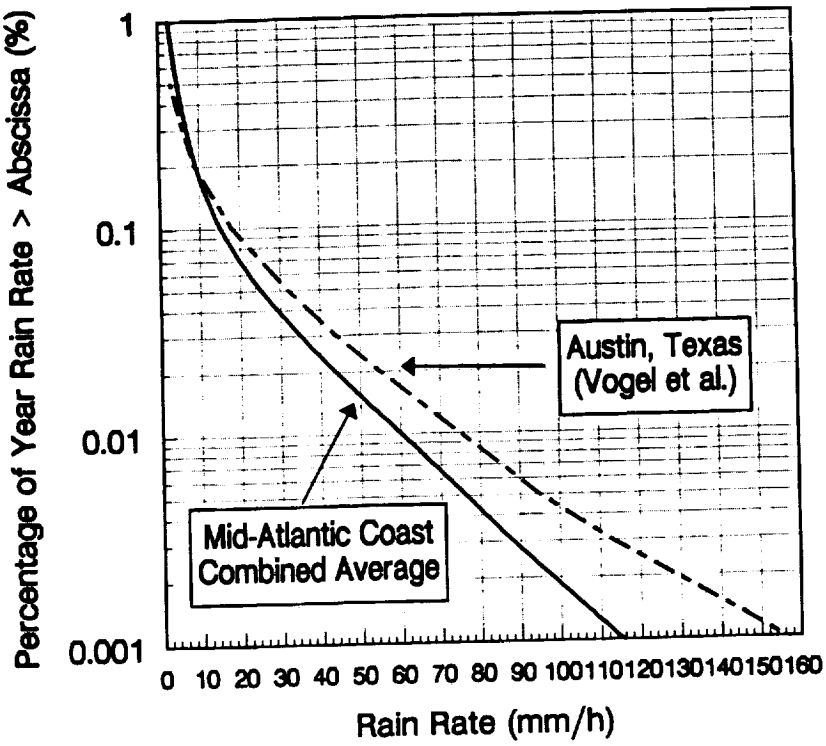

Figure 11: Comparison of cumulative rain rate distributions from Mid-Atlantic coast and Austin, Texas [4].

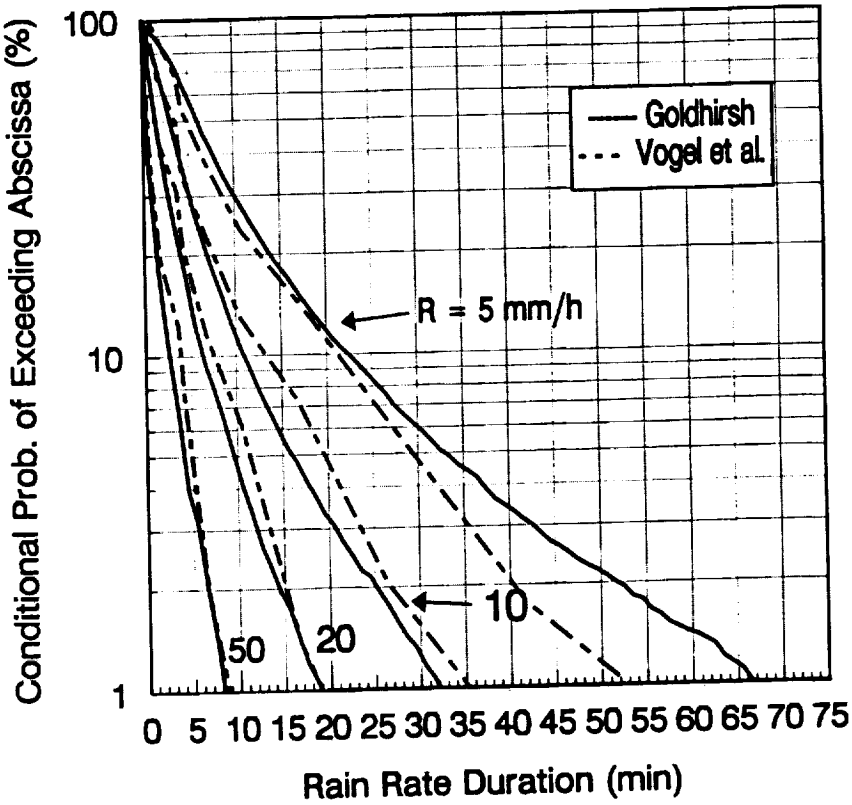

Figure 12: Comparison of cumulative rain rate *duration* distributions from Mid-Atlantic coast and Austin, Texas [4].

Rain-Rate Data Base Development and Rain-Rate Climate Analysis

Robert K. Crane
University of Oklahoma
June 14, 1993

Report to the NAPEX-17 Meeting
Pasadena, California

Abstract

The single-year rain-rate distribution data available within the archives of CCIR Study Group 5 have been compiled into a data base for use in rain-rate climate modeling and for the preparation of predictions of attenuation statistics. The four year set of tip-time sequences provided by J. Goldhirsh for locations near Wallops Island were processed to compile monthly and annual distributions of rain rate and of event durations for intervals above and below preset thresholds. A four-year data set of tropical rain-rate tip-time sequences were acquired from the NASA TRMM program for 30 gauges near Darwin, Australia. They have also been processed for inclusion in the CCIR data base and the expanded data base for monthly observations at the University of Oklahoma.

The empirical rain-rate distributions (edfs) accepted for inclusion in the CCIR data base were used to estimate parameters for several rain-rate distribution models: the lognormal model, the Crane two-component model, and the three parameter model proposed by Moupfuma. The intent of this segment of the study is to obtain a limited set of parameters that can be mapped globally for use in rain attenuation predictions. If the form of the distribution can be established, then perhaps available climatological data can be used to estimate the parameters rather than requiring years of rain-rate observations to set the parameters. The two-component model provided the best fit to the Wallops Island data but the Moupfuma model provided the best fit to the Darwin data.

Rain-Rate Data Base Development and Rain-Rate Climate Analysis

1. The data banks

Rain-rate observations from the CCIR data banks, the measurements made by J. Goldhirsh at Wallops Island, and the archives of the TRMM observation program for Darwin, Australia were combined to compile a new rain-rate data base. The format of this data base is displayed in Table 1 for observations from Wallops Island. The categories indicated in the headings for each column were agreed by Study Group 5 at their last set of meetings in Geneva. It is noted that no observers have as yet provided all the data that are requested. An output from the ACTS Propagation Experiment should be complete entries for the data base.

Table 2 displays information stored in the OU data base that are used for rain-rate climate analysis but go beyond the requests of the CCIR. They include the model parameters for several different models employed to represent the empirical distribution function (edfs) and the errors that result from using the models.

Summary plots are available for each gauge site. Figures 1 and 2 display the summary data for Wallops Island Gauge #1 and for the Darwin data from Annaburro. The columns G and C give the root-mean-square difference in the natural logarithms between predictions, for the Global and CCIR rain-rate climate zones. From the figure for Wallops Island, it is evident that the climate zone models fit the observations quite closely and only a small seasonal variation is present. For Annaburro, the climate zone models do not fit very well and a large seasonal variation is present.

The new data bank includes both annual and worst month edfs and monthly data at 0.01%, 0.1% and 1% of a month for displaying seasonal variations. These data can be readily compared with models as illustrated in Figure 3. Two plots are given, one for the annual distribution and the other for the worst month. For the Crane "Global" model and the expected year-to-year and location-to-location variability of observations relative to that model, the annual data fit well within the expected distribution bounds. For the worst month observations, the rain-rate values are larger than expected but still within the expected bounds for a single year of observation (a single sample).

The data from Wallops Island and from Australia were also used to prepare empirical distributions of times above and below selected rain rate thresholds. These data were fit to exponential distributions by month to explore their dependence on year, season, etc. The exponential model was used instead of the lognormal model that is often quoted in the literature because, if the correlation time for the rain process is fixed and the process is assumed stationary, theory predicts the exponential form. Empirically, it also provides a good fit to the observations. As with most statistical problems, insufficient data are available to select one model over the other, but the theoretical argument is compelling. Sample results from monthly exponential distribution fits are displayed in Figures 4 and 5 for Wallops Island Gauge #1. The average duration of intervals with rain rates in excess of 10 mm/h is 6 minutes and the distribution of average durations may be approximated as normal. The average duration of a rain event (above 0.1 mm/h) is 5 hours (300 minutes).

2. Models for observed rain-rate distributions

The observed rain-rate distributions are samples from a random process. Figure 3 displays two such samples and model predictions that bound the expected range (5% to 95%) for the observed distributions. The expected distributions are shown to be smooth functions of percent time (or of rain rate). The observed random variables are only constrained to be monotonically increasing with decreasing percentage of time. A model to represent the observed distribution should depend on few parameters to provide a maximum of smoothing (or averaging) to reduce the statistical variations. Three such models were employed to represent the observed distributions, the Crane two-component model (5 parameters), the lognormal model (3 parameters), and the Moupfuma model (3 parameters). The latter is a function that performs well in least squares curve fitting over a partial range of the reported distributions. The two component model is constrained to mimic weather radar observations. It often performs less well than the simpler lognormal model. In this case, more parameters do not automatically provide for a better fit.

The results of the use of these models on the Wallops Island observations, the Darwin observations and the entire CCIR data base are presented in Table 3. For the data from Wallops Island, the two-component model performed best with a root-mean-square fitting error in the natural logarithm of the rain rate of 0.06 (-> 6.2%). For the data from Australia the Moupfuma model performed the best with an error of 0.17 (-> 18.5%). For all the other data in the CCIR data banks the lognormal model did the best (-> 17.5%) followed by the two-component model then the Moupfuma model.

Currently, the CCIR is intent on selecting a model to be used to parameterize rain-rate observations. Study Group 5 is pushing the use of the Moupfuma model. It works better than the other models for data from the tropics but works less well at mid-latitudes. It has the advantage over the two-component model of using only three parameters. However, the Moupfuma model is strictly a curve fitting procedure and does not provide a probability distribution. The other two models are constrained to provide probability distributions.

Although the physically based two-component model performs well at mid-latitudes, an improved model is needed for tropical regions. Work at OU continues to find a model that performs well in both tropical and mid-latitude regions, produces a probability distribution, and has integral constraints such that the parameters of the model can be readily estimated from climatological data. For the lognormal and two-component model, one of the parameters can be set using the total annual accumulation of rain fall. It should be possible to set a second parameter based on the statistics of the monthly accumulations. Finally, extreme value information may be useful in setting a third parameter. The intent is not to find a statistical relationship between the parameters and climatological data but to find integral constraints that directly determine the parameters. The parameters can then be mapped based on the available mappings of climatological data.

Wallops Is_VA-1

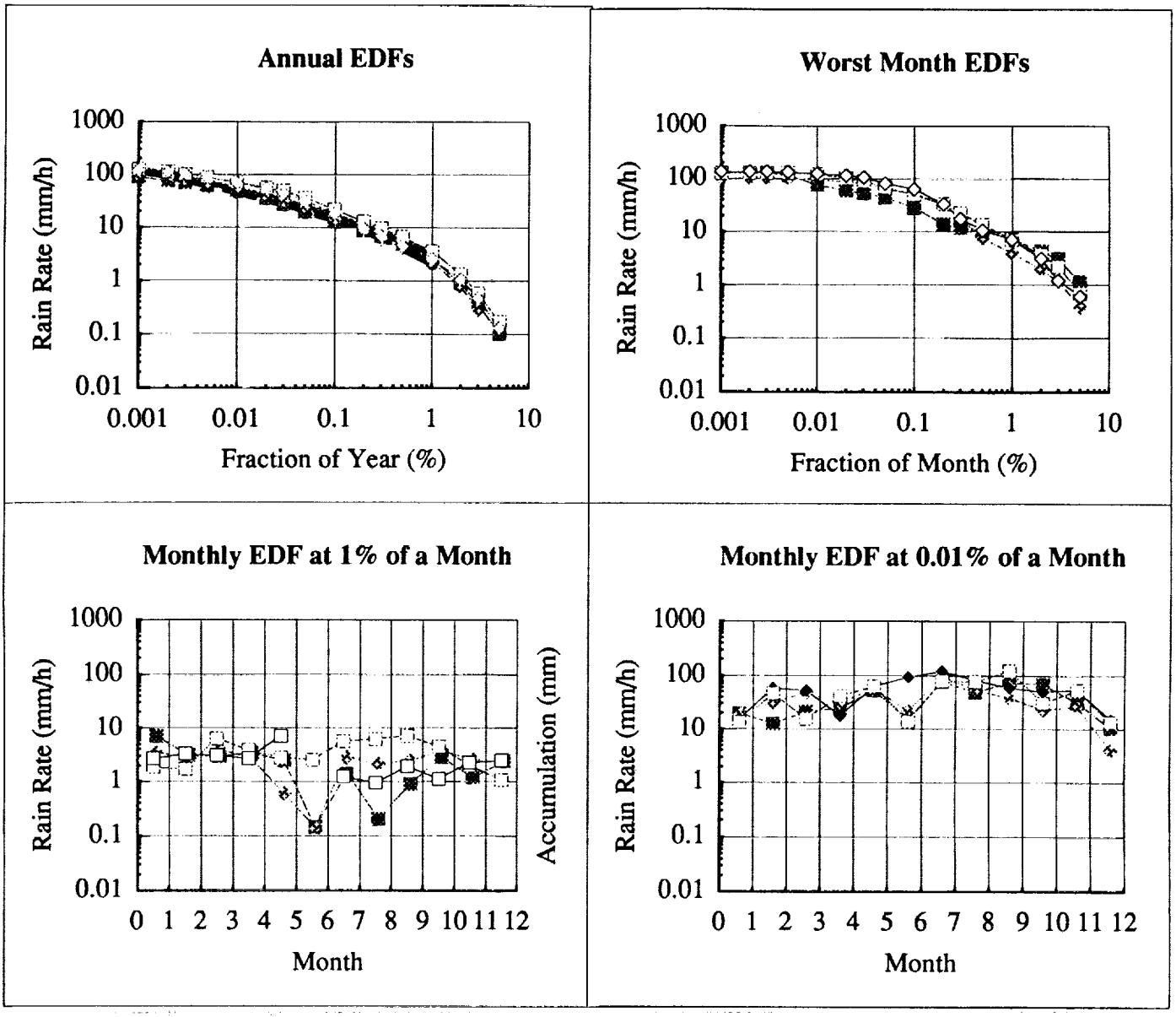

	Year (%	0.001	0.002	0.003	0.005	0.01	0.02	0.03	0.05	0.1	0.2	0.3	0.5	1	2	3	5	G	C
RWI0101	87_01	86	76	70	60	48	34	26	19	13	8.9	7.1	5.0	2.7	0.9	0.4	0.1	0.22	0.22
RWI0102	88_01	94	87	80	66	54	39	32	24	15	8.7	6.3	4.2	2.3	0.8	0.3		0.21	0.21
RWI0103	89_01	126	111	101	86	69	56	47	36	22	12.8	9.6	6.7	3.6	1.4	0.6	0.2	0.27	0.27
RWI0104	90_01	120	109	102	87	68	54	43	31	18	9.6	6.8	4.5	2.5	1.1	0.5	0.1	0.23	0.23

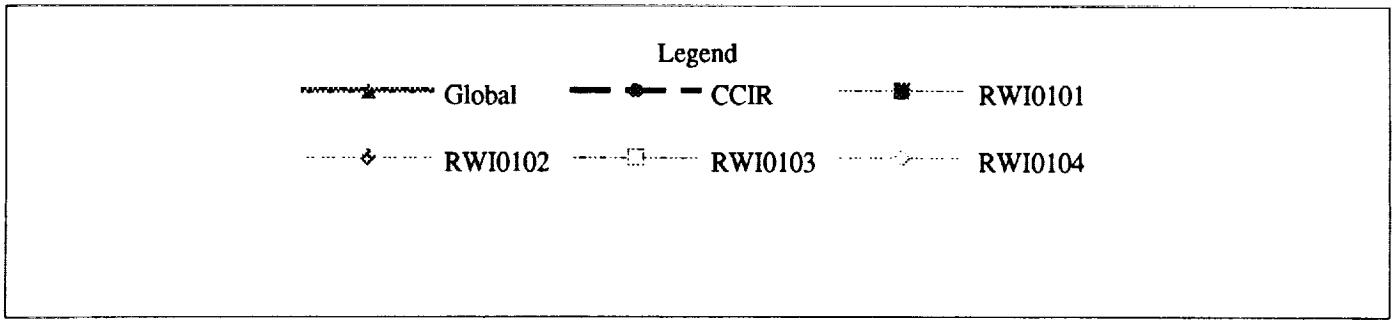

Figure 1

Annaburroo_AU

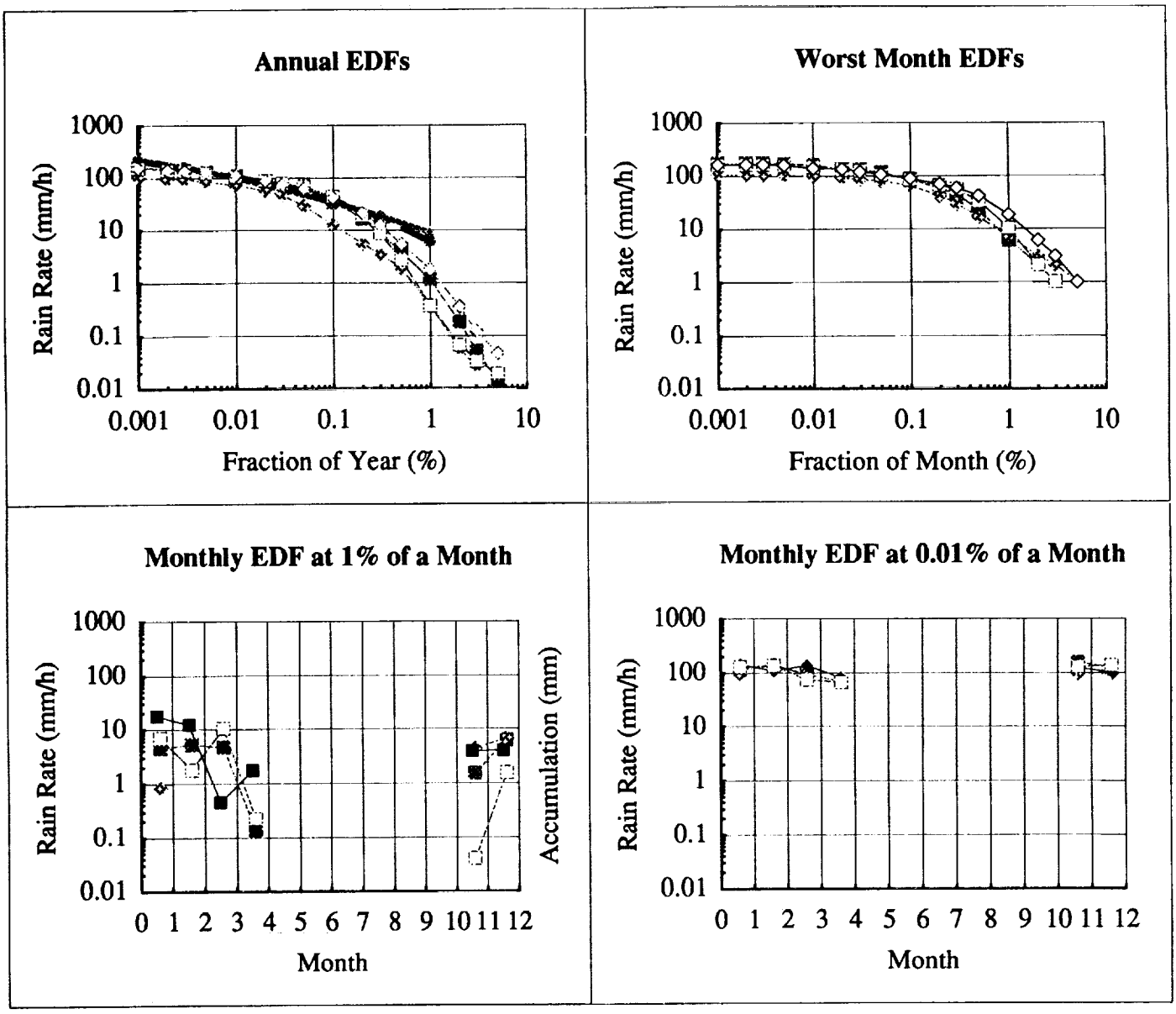

	Year	0.001	0.002	0.003	0.005	0.01	0.02	0.03	0.05	0.1	0.2	0.3	0.5	1	2	3	5	G	C
XAU0101	87_11	160	145	139	129	108	89	79	63	37	16	9	4	1.2	0.2	0.1	0.0	0.87	0.71
XAU0102	88_11	103	96	93	85	71	57	46	29	13	6	3	2	0.4	0.1	0.0		0.98	0.97
XAU0103	89_11	152	143	135	125	103	88	79	68	44	19	9	3	0.4	0.1	0.0	0.0	0.39	0.34
XAU0104	90_11	153	141	136	128	112	89	76	62	41	21	13	5	1.8	0.4	0.1	0.0	0.65	0.48

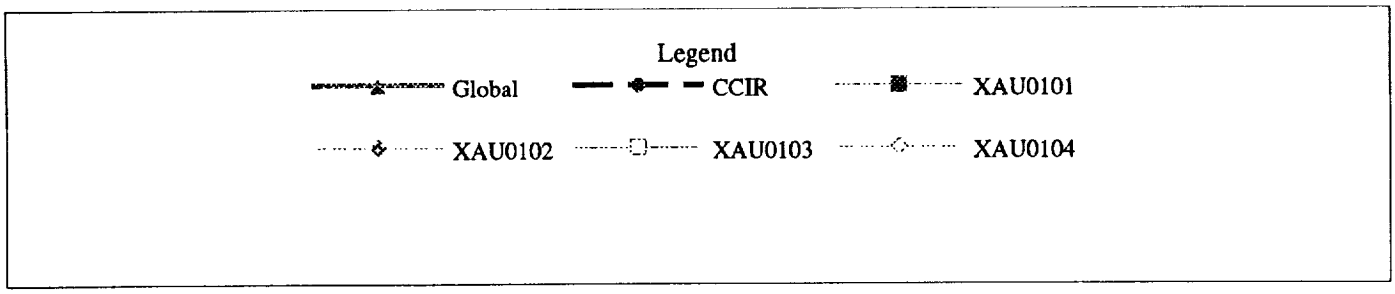

Figure 2

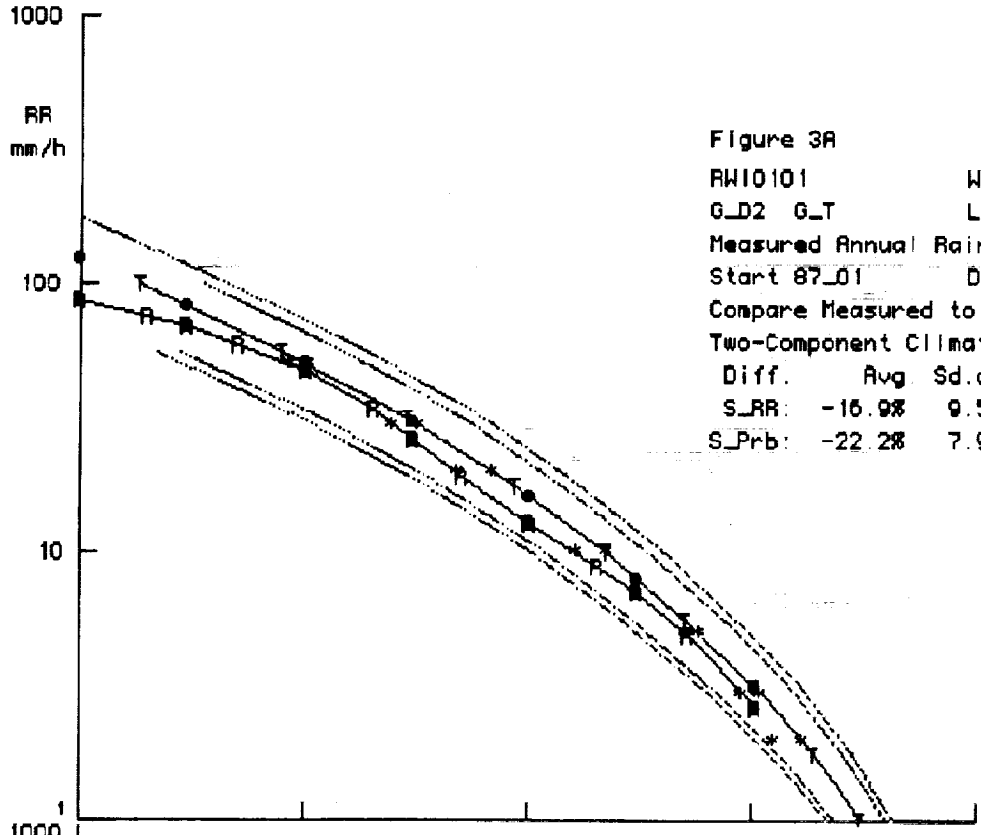

Figure 3A
RWI0101 WALLOPS_IS_VA
G_D2 G_T Lat = 0.0 deg
Measured Annual Rain Rate EDF
Start 87_01 Dur. 12 Months
Compare Measured to Expected Model
Two-Component Climate Model

Diff.	Avg	Sd.dv.	RMSD	#
S_RR:	-16.9%	9.5%	22.9%	7
S_Prb:	-22.2%	7.9%	30.0%	7

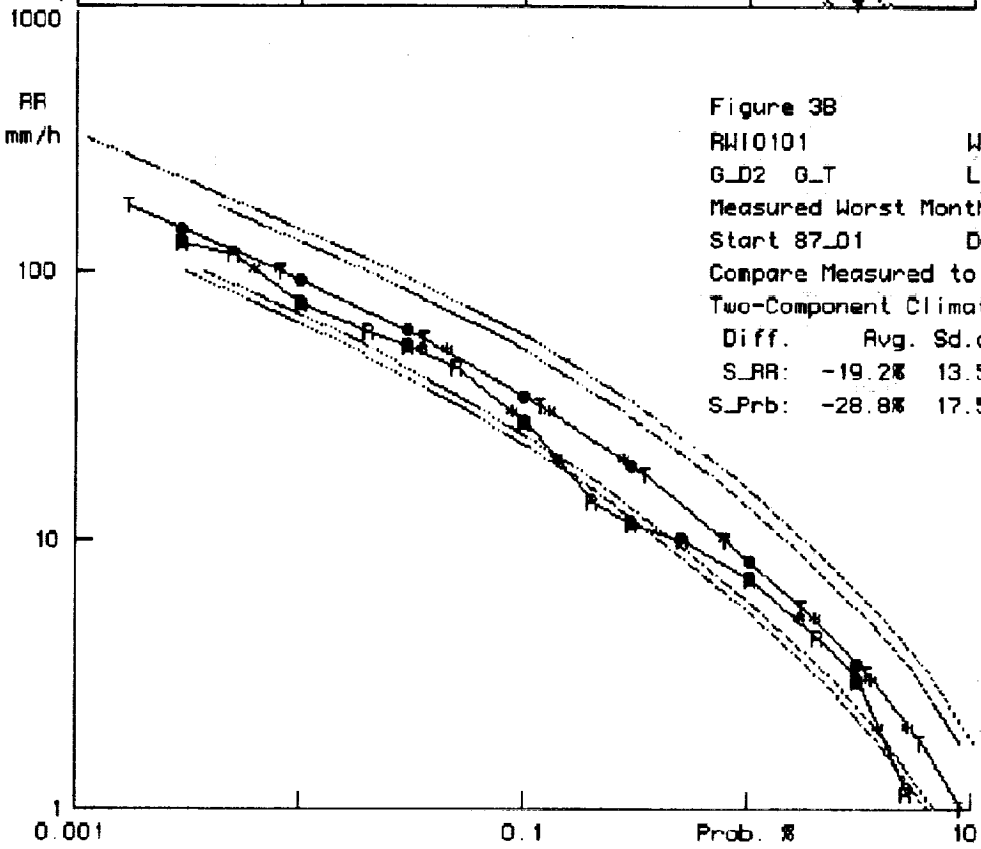

Figure 3B
RWI0101 WALLOPS_IS_VA
G_D2 G_T Lat = 0.0 deg
Measured Worst Month Rain Rate EDF
Start 87_01 Dur. 12 Months
Compare Measured to Expected Model
Two-Component Climate Model

Diff.	Avg.	Sd.dv.	RMSD	#
S_RR:	-19.2%	13.5%	28.1%	7
S_Prb:	-28.8%	17.5%	45.6%	8

WIGauge1_60_Avg_Dur_10.0

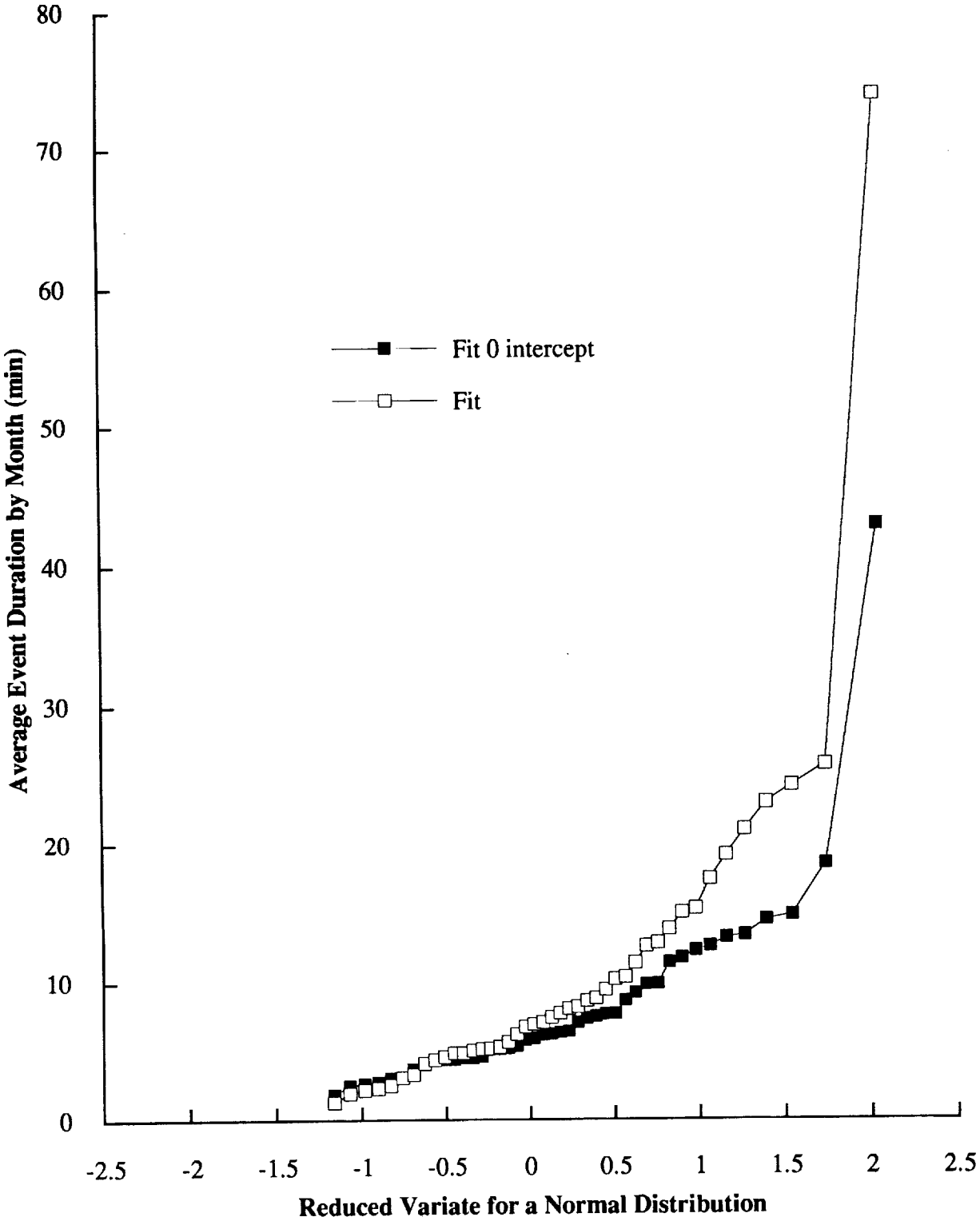

Figure 4

WIGauge1_60_Avg_Dur_0.1

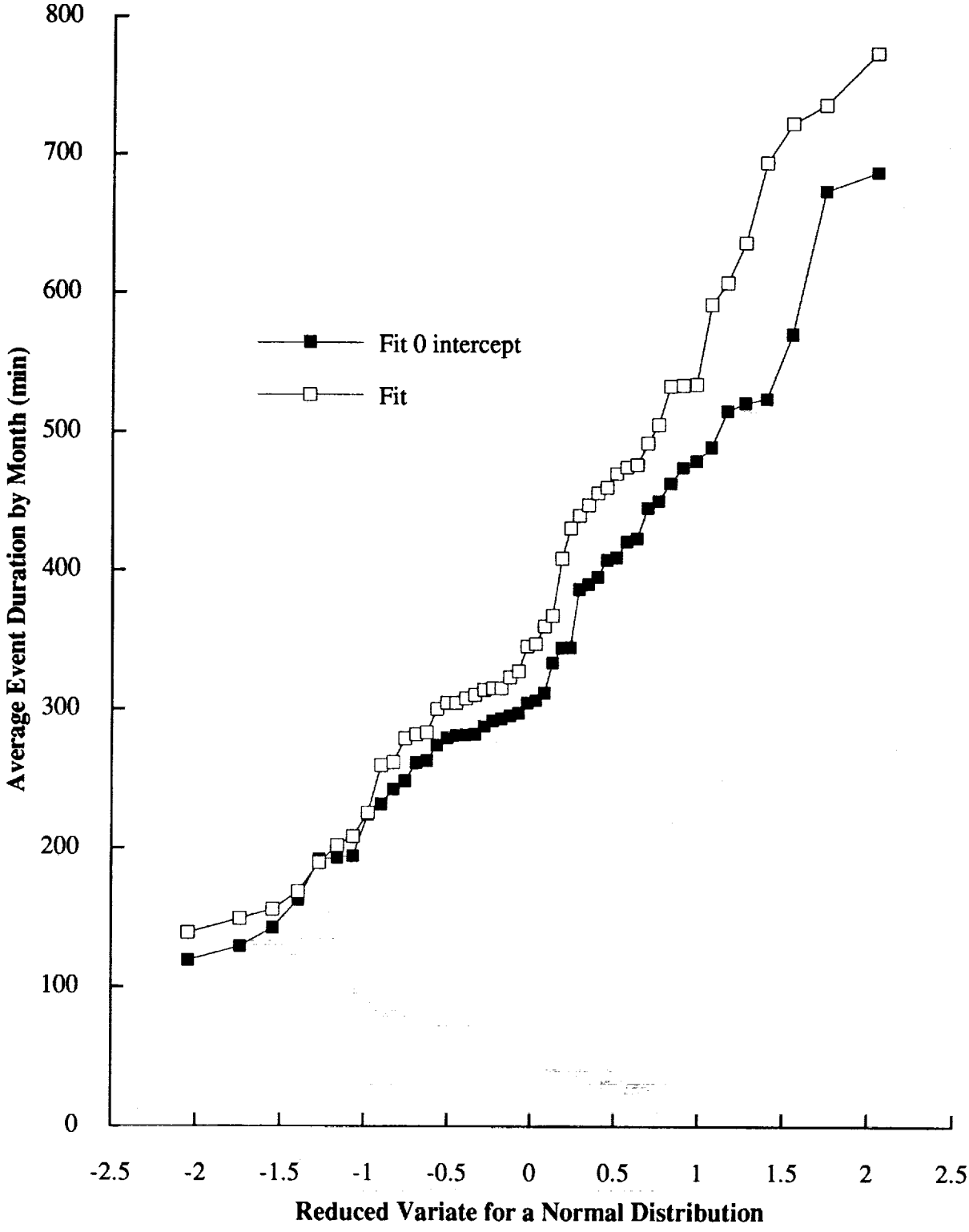

Figure 5

Table 1 WI RR dBase.2

Experiment Number	RG Site Name	RG Country	RG Latitude [deg] N	RG Longitude [deg] E	RG Altitude amsl [m]	CCIR Rain Zone	Rain Gauge Type	RG Resolution [mm/h]	RG Integration Time [s]	RG Accumulation [mm/tip]	RG Aperture [cm^2]	Start Date	End Date	Duration [days]	Fraction of Year R > 0.5 mm/h [%]
RWI0101	WALLOPS_IS_VA	US	0	0	0	K						87_01	87_12	365	
RWI0102	WALLOPS_IS_VA	US	0	0	0	K						88_01	88_12	366	
RWI0103	WALLOPS_IS_VA	US	0	0	0	K						89_01	89_12	365	
RWI0104	WALLOPS_IS_VA	US	0	0	0	K						90_01	90_12	365	
RWI0201	WALLOPS_IS_VA	US	0	0	0	K						87_01	87_12	365	
RWI0202	WALLOPS_IS_VA	US	0	0	0	K						88_01	88_12	366	
RWI0203	WALLOPS_IS_VA	US	0	0	0	K						89_01	89_12	365	
RWI0204	WALLOPS_IS_VA	US	0	0	0	K						90_01	90_12	365	
RWI0301	WALLOPS_IS_VA	US	0	0	0	K						87_01	87_12	365	
RWI0302	WALLOPS_IS_VA	US	0	0	0	K						88_01	88_12	366	
RWI0303	WALLOPS_IS_VA	US	0	0	0	K						89_01	89_12	365	
RWI0304	WALLOPS_IS_VA	US	0	0	0	K						90_01	90_12	365	
RWI0402	WALLOPS_IS_VA	US	0	0	0	K						88_01	88_12	365	
RWI0403	WALLOPS_IS_VA	US	0	0	0	K						89_01	89_12	366	
RWI0404	WALLOPS_IS_VA	US	0	0	0	K						90_01	90_12	365	
RWI0501	WALLOPS_IS_VA	US	0	0	0	K						87_01	87_12	365	
RWI0502	WALLOPS_IS_VA	US	0	0	0	K						88_01	88_12	366	
RWI0503	WALLOPS_IS_VA	US	0	0	0	K						89_01	89_12	365	
RWI0504	WALLOPS_IS_VA	US	0	0	0	K						90_01	90_12	365	
RWI0601	WALLOPS_IS_VA	US	0	0	0	K						87_01	87_12	365	
RWI0602	WALLOPS_IS_VA	US	0	0	0	K						88_01	88_12	366	
RWI0701	WALLOPS_IS_VA	US	0	0	0	K						87_01	87_12	365	
RWI0702	WALLOPS_IS_VA	US	0	0	0	K						88_01	88_12	366	
RWI0703	WALLOPS_IS_VA	US	0	0	0	K						89_01	89_12	365	
RWI0704	WALLOPS_IS_VA	US	0	0	0	K						90_01	90_12	365	
RWI0801	WALLOPS_IS_VA	US	0	0	0	K						87_01	87_12	365	
RWI0802	WALLOPS_IS_VA	US	0	0	0	K						88_01	88_12	366	
RWI0803	WALLOPS_IS_VA	US	0	0	0	K						89_01	89_12	365	
RWI0804	WALLOPS_IS_VA	US	0	0	0	K						90_01	90_12	365	
RWI0901	WALLOPS_IS_VA	US	0	0	0	K						87_01	87_12	365	
RWI0902	WALLOPS_IS_VA	US	0	0	0	K						88_01	88_12	366	
RWI0903	WALLOPS_IS_VA	US	0	0	0	K						89_01	89_12	365	
RWI0904	WALLOPS_IS_VA	US	0	0	0	K						90_01	90_12	365	
RWI1001	WALLOPS_IS_VA	US	0	0	0	K						87_01	87_12	365	
RWI1002	WALLOPS_IS_VA	US	0	0	0	K						88_01	88_12	366	
RWI1003	WALLOPS_IS_VA	US	0	0	0	K						89_01	89_12	365	
RWI1004	WALLOPS_IS_VA	US	0	0	0	K						90_01	90_12	365	

Table 1 WI RR dBase.2

Experiment Number	% year 0.001 RR >	% year 0.002 RR >	% year 0.003 RR >	% year 0.005 RR >	% year 0.01 RR >	% year 0.02 RR >	% year 0.03 RR >	% year 0.05 RR >	% year 0.1 RR >	% year 0.2 RR >	% year 0.3 RR >	% year 0.5 RR >	% year 1 RR >	% year 2 RR >	% year 3 RR >	% year 5 RR >
RWI0101	86.23	75.55	70.06	59.67	47.68	34.02	26.47	19.27	12.75	8.86	7.07	4.97	2.66	0.9	0.37	0.1
RWI0102	93.99	87.45	79.78	66.24	53.82	39.18	32.21	23.59	14.56	8.73	6.3	4.2	2.29	0.78	0.29	
RWI0103	125.65	110.66	101.23	86.07	69.26	55.94	46.98	35.81	21.73	12.83	9.57	6.65	3.63	1.35	0.58	0.17
RWI0104	120.49	108.97	102.28	86.6	68	53.5	43.47	30.93	18.27	9.57	6.81	4.52	2.52	1.07	0.47	0.13
RWI0201	83.63	73.66	67.6	59.34	46.42	30.15	22.5	15.62	9.76	6.71	5.37	3.93	2.08	0.65	0.24	
RWI0202	77.02	72	69.38	62.86	49.4	35.31	28.71	20.74	12.91	7.49	5.58	3.79	1.89	0.66	0.21	
RWI0203	99.57	88.12	77.92	64.84	52.04	40.49	34.77	25.84	17.68	10.14	7.52	5.22	2.86	1.23	0.57	0.16
RWI0204	115.32	90.72	82.3	72.86	62.52	47.36	36.21	25.16	14.91	8.17	6.06	4.22	2.37	1.01	0.48	0.13
RWI0301	110.97	92.95	84.96	76.02	62.49	41.85	29.53	18.36	10.67	7.34	5.86	4.24	2.18	0.71	0.3	
RWI0302	96.81	87.45	77.83	63.19	49.54	38.66	31.71	22.94	13	8.15	6.3	4.3	2.28	0.83	0.34	
RWI0303	132.12	115.04	107.76	100.06	79.36	57.42	45.73	33.46	19.47	11.03	8.44	6.05	3.15	1.27	0.48	0.12
RWI0304	120.49	100.44	78.7	67.84	54.16	38.68	31.97	22.48	13.08	7.55	5.55	3.91	2.1	0.94	0.44	
RWI0402	119.8	104.36	89.95	77.2	63.23	46.1	35.62	23.4	13.61	8.09	6.1	4.13	2.08	0.68	0.28	
RWI0403	127.01	117	106.03	86.16	66.37	50.37	44.27	32.62	21.15	12.03	8.34	5.68	2.97	0.87	0.33	0.1
RWI0404	102.91	94.56	87.33	72.44	53.37	35.9	27.73	19.95	12.11	7.34	5.84	4.09	2.16	0.83	0.32	
RWI0501	108.81	82.74	76.65	69.29	53.88	36.74	27.71	18.9	12.18	8.56	6.64	4.57	2.36	0.76	0.33	
RWI0502	84.52	75.51	71.49	64.91	56.93	43.73	33.53	21.85	12.29	7.89	6.11	4.24	2.34	0.79	0.34	
RWI0503	163.46	134.33	110.45	84.94	65.77	49.86	41.6	32.77	18.59	10.63	7.81	4.9	2.57	1.09	0.57	0.16
RWI0504	118.55	91.39	81.06	67.16	45.16	33.01	25.01	18.28	11.25	7.32	5.73	4.01	2.07	0.81	0.33	
RWI0601	109.21	94.77	82.3	72.86	58	42.16	34.66	24.6	14.25	9.33	6.85	4.5	2.09	0.67	0.28	
RWI0602	50.68	44.1	41.34	35.98	27.23	20.19	16.65	12.85	9.3	6.41	5.15	3.74	1.99	0.59	0.22	
RWI0701	114.48	94.97	90.12	75.62	58.13	33.03	24.98	18.06	12.09	8.13	6.29	4.21	2.17	0.7	0.28	
RWI0702	76.92	70.68	62.02	52.47	40.26	29.59	23.59	18.08	12.06	7.67	5.94	4.23	2.21	0.71	0.3	
RWI0703	136.3	121.36	116.49	100.89	85.24	67.7	55.54	42.42	27.65	14.63	9.79	6.51	3.43	1.44	0.7	0.19
RWI0704	93.21	79.6	64.54	58.34	46.33	35.82	29.95	23.34	14.14	7.33	5.24	3.82	2.24	0.93	0.4	
RWI0801	108.81	98.27	82.58	62.52	48.77	33.65	28.28	20.49	12.51	8.1	6.18	4.29	2.19	0.78	0.25	
RWI0802	81.53	74.42	68.51	64.11	50.35	35.04	27.43	18.45	11.92	7.61	5.7	3.85	1.96	0.56	0.23	
RWI0803	134.44	127.49	109.01	101.35	81.21	68.9	59.73	46.42	27.21	14.39	9.5	5.95	2.82	1.01	0.43	
RWI0804	77.04	68.17	62.37	53.98	44.11	34.46	28.7	20.92	12.07	7.24	5.4	3.71	2.26	1.01	0.49	0.13
RWI0901	109.29	96.62	85.6	71.34	57.5	40.45	31.24	21.93	12.86	8.25	6.33	4.41	2.33	0.8	0.28	
RWI0902	72.58	66.25	61.51	52.47	41.73	30.32	24.26	17.56	11.13	7.21	5.73	4.15	2.23	0.74	0.31	
RWI0903	98.79	88.64	82.3	70.65	61.87	49.62	41.8	31.67	17.34	9.88	7.19	4.76	2.43	1.05	0.47	0.13
RWI0904	87.95	79.77	73.52	62.84	50.17	34.77	27.55	19.06	10.36	6.3	4.67	3.22	1.71	0.58	0.2	
RWI1001	74.45	62.94	58.13	51.11	38.87	28.11	21.95	15.57	10.62	7.01	5.3	3.73	1.9	0.58	0.2	
RWI1002	74.42	65.54	59.55	50.68	37.03	27.81	22.4	16.95	10.77	7.19	5.44	3.7	1.94	0.65	0.23	
RWI1003	108.01	94.56	87.33	79.05	66.67	49.51	38.67	29.81	18.52	11.15	8.21	5.57	2.78	0.95	0.39	
RWI1004	91.39	79.53	73.97	64.66	48.09	36.33	29.39	20.55	12.87	7.84	5.86	3.98	2.33	1.02	0.42	

Table 1 WI RR dBase.2

Experiment Number	% wM 0.001 RR >	% wM 0.002 RR >	% wM 0.003 RR >	% wM 0.005 RR >	% wM 0.01 RR >	% wM 0.02 RR >	% wM 0.03 RR >	% wM 0.05 RR >	% wM 0.1 RR >	% wM 0.2 RR >	% wM 0.3 RR >	% wM 0.5 RR >	% wM 1 RR >	% wM 2 RR >	% wM 3 RR >	% wM 5 RR >
RWI0101	127.5	127.5	127.5	114.5	75.24	59.07	52.64	43.68	27.53	13.72	11.43	10.04	7.16	4.32	2.98	1.13
RWI0102	101.93	101.93	101.93	101.93	94.5	85.25	79.09	63.72	50.19	32.23	17.85	7.49	3.92	1.96	1.16	0.38
RWI0103	129.47	129.47	129.47	129.47	119.8	101.5	87.91	67.12	49.24	32.9	22.6	13.38	7.08	3.72	2.21	0.69
RWI0104	136.6	136.6	136.6	132.96	122.5	114	104.9	80.6	62.4	32.93	17.56	10.43	7.11	3.14	1.21	0.6
RWI0201	101.96	101.96	101.96	99.24	85.62	75.89	68.1	48.43	25.17	9.13	8.12	6.73	4.93	3.06	2.21	1.42
RWI0202	89.95	89.95	89.95	86.37	82.65	70.21	64.82	60.96	42.67	25.17	19.06	9.77	3.77	1.63	0.87	0.25
RWI0203	102.14	102.14	102.14	99.41	84.52	64.32	56.74	49.17	38.74	23.17	19.37	10.85	5.24	2.96	1.82	0.71
RWI0204	151.8	151.8	151.8	145.43	134.6	89.58	74.29	64.41	40.08	24.6	17.45	10.56	6.19	2.86	1.38	0.62
RWI0301	129.23	129.23	129.23	129.23	111.6	88.74	73.22	63.87	39.88	21.67	12.32	6.86	5.53	3.47	2.36	1.3
RWI0302	108.06	108.06	108.06	105.18	94.95	82.21	64.49	49.24	34.19	23.68	16.12	9.05	3.16	1.79	0.99	0.4
RWI0303	143.23	143.23	143.23	137.22	127	110	105.8	91.58	61.6	34.21	19.89	12.53	8.43	4.75	2.2	0.65
RWI0304	170.52	170.52	170.52	144.49	106.7	66.98	60.62	44.59	30.85	15.5	9.62	6.06	3.46	1.85	1.37	0.64
RWI0402	135.13	135.13	135.13	128.62	108	93.9	85.39	72.75	52.93	27.9	16.64	8.53	3.45	1.72	0.85	0.35
RWI0403	144.53	144.53	144.53	140.67	128.6	104	78.88	61.81	47.09	30.39	22.92	11.7	6.88	3.85	1.1	0.39
RWI0404	102.6	102.6	102.6	102.6	96.59	80.43	66.13	48.31	25.45	15.37	11.43	8.51	5.81	2.79	1.24	0.56
RWI0501	136.97	136.97	136.97	136.97	85.25	73.14	65.73	50.62	24.71	11.91	10.62	9.54	7	3.8	2.49	1.19
RWI0502	101.04	101.04	101.04	96.17	84.12	76.22	71.73	62.85	49.94	27.47	14.71	8.2	3.88	2.05	1.07	0.4
RWI0503	173.15	173.15	173.15	173.15	162.3	116.5	82.9	63.12	44.2	26.29	19.02	12.99	6.79	2.59	1.61	0.79
RWI0504	143.23	143.23	143.23	122.15	91.14	80.43	68.48	59.25	30.85	17.21	12.55	9.29	6.37	3.12	1.35	0.4
RWI0601	120.3	120.3	120.3	114.5	100.6	82.16	70.99	48.16	29.99	15.61	12.1	10.37	7.33	4.64	3.34	1.56
RWI0602	71.48	71.48	71.48	68.17	50.51	28.93	25.09	21.74	13.89	9.57	8.5	5.8	3.69	1.94	0.86	0.34
RWI0701	151.8	151.8	151.8	128.62	113	87.32	72.45	56.81	23.85	15.28	10.18	8.72	6.39	3.92	2.75	1.45
RWI0702	80.52	80.52	80.52	72.54	69.42	54.84	47.51	36.01	23.89	13.64	8.75	6.41	3.81	1.66	0.86	0.38
RWI0703	162.35	162.35	162.35	158.02	122.3	116.4	103.1	93.86	76.92	55.84	40.5	26.76	10.07	4.08	1.99	1
RWI0704	96.63	96.63	96.63	96.63	85.25	63.74	55.21	46.44	37.9	28.47	22.66	15.39	6.79	2.35	1.48	0.68
RWI0801	160.89	160.89	160.89	121.36	101.9	82.84	58.87	49.24	29.01	13.49	8.94	7.56	5.57	3.59	2.57	1.35
RWI0802	80.94	80.94	80.94	78.78	68.29	61.6	55.21	44.96	29.01	16.51	10.26	5.76	3.32	1.47	0.54	0.19
RWI0803	143.23	143.23	143.23	137.22	124.2	105.6	101.7	90.66	71.9	57.79	46.37	30.09	10.28	3.86	1.62	0.39
RWI0804	101.04	101.04	101.04	75.21	73.35	58.12	52.41	46.56	37.9	27.13	21.27	13.51	6.9	2.86	1.47	0.79
RWI0901	135.13	135.13	135.13	109.3	105.4	87.8	68.97	49.91	37.06	20.5	11.74	7.72	5.61	3.79	2.83	1.61
RWI0902	143.23	143.23	143.23	136.32	84.52	58.12	44.82	31.13	18.72	11.48	7.78	6.32	4.2	1.93	1.01	0.26
RWI0903	96.2	96.2	96.2	93.63	87.6	78.87	70.09	64.32	55.31	43.44	35.31	22.8	7.04	2.46	1.67	0.62
RWI0904	135.51	135.51	135.51	86.18	81.42	77.47	65.73	56.38	42.24	26.07	17.5	9.77	4.91	1.95	1.21	0.68
RWI1001	101.32	101.32	101.32	76.58	64.32	55.14	40.93	30.43	19.28	11.21	9.92	8.16	5.51	3.58	2.59	1.53
RWI1002	85.1	85.1	85.1	72.38	67.85	51.74	42.29	35.76	25.82	18.32	12.59	6.05	3.33	1.61	0.94	0.36
RWI1003	160.89	160.89	160.89	128.62	93.73	71.91	67.85	61.8	45.22	33.48	26.87	17.12	9	3.6	1.47	0.56
RWI1004	128.66	128.66	128.66	125.23	89.58	74.41	63.2	51.04	37.6	20.39	15.79	11.47	6.62	2.87	1.59	0.69

Table 1 WI RR dBase.2

Experiment Number	Jan R 0.01 mm/h	Feb R 0.01 mm/h	Mar R 0.01 mm/h	Apr R 0.01 mm/h	May R 0.01 mm/h	Jun R 0.01 mm/h	Jul R 0.01 mm/h	Aug R 0.01 mm/h	Sep R 0.01 mm/h	Oct R 0.01 mm/h	Nov R 0.01 mm/h	Dec R 0.01 mm/h
RWI0101	19.75	12.75	21.21	24.43	53.08	14.90	75.24	49.26	73.73	66.98	31.72	10.25
RWI0102	19.75	31.17	47.87	31.05	56.99	21.91	94.50	53.77	38.11	23.13	26.65	4.05
RWI0103	15.40	57.77	52.21	17.74	63.20	93.73	119.81	81.13	58.86	50.08	53.54	14.77
RWI0104	13.32	45.78	15.65	41.06	63.20	14.06	78.43	75.24	122.49	30.93	52.40	13.15
RWI0201	15.58	15.18	18.64	32.01	46.47	59.51	85.62	5.7	56.74	23.13	20.67	10.02
RWI0202	6.97	50.96	40.2	31.72	24.93	14.06	82.65	42.07	29.93	50.08	29.93	6.63
RWI0203	10.56	24.15	84.52	40.52	33.34	70.85	56.99	21.21	35.96	34.64	71.6	2.05
RWI0204	17.81	18.07	15.86	39.18	134.6	51.21	64.02	79.85	23.72	20.94	32.91	23.52
RWI0301	19.48	13.51	26.88	17.9	29.68	111.6	5.11	80.78	83.5	29.19	20.1	11.24
RWI0302	18.64	44.62	49.39	25.14	23.13	63.74	94.95	56.26	25.14	23.52	40.03	3.43
RWI0303	16.59	43.2	51.06	21.37	26.42	101.5	127	64.02	50.51	40.2	80.43	9.28
RWI0304	17.81	26.29	18.33	85.25	106.7	33.93	72.38	55.99	23.72	44.59	41.98	13.87
RWI0402	13.71	36.13	67.85	22.58	71.91	58.86	108	60.4	29.93	46.47	39.18	13.15
RWI0403	13.94	30.47	60.4	16.39	75.24	108.9	128.6	63.2	19.92	35.33	44.97	2.9
RWI0404	18.64	16.10	10.37	56.74	96.59	66.12	63.20	78.43	50.51	26.88	38.89	9.96
RWI0501	28	13.52	24.93	19.71	35.79	85.25	80.78	56.26	58.86	25.05	37.58	12.2
RWI0502	13.15	37.48	60.66	24.43	47.25	31.72	84.12	39.69	26.08	33.34	66.12	3.73
RWI0503	17.59	45.78	63.2	16.38	69.82	120.8	162.3	48.07	66.12	32.79	29.93	8.26
RWI0504	14.12	17.04	13.09	42.43	91.14	40.39	53.08	35.33	80.43	13.15	37.77	9.12
RWI0601	37.27	3.16	38.1	29.93	48.18	76.81	39.5	100.6	57.26	69.82	60.14	17.59
RWI0602	14.96	25.36	16.59	42.43	14.53	5.12	33.77	30.94	50.51	30.06	18.8	8.26
RWI0701	18.96	6.14	25.98	26.37	31.86	80.43	113	89.58	22.65	51.75	13.26	25.25
RWI0702	17.78	40.59	47.25	22.38	44.59	42.43	31.45	69.42	47.66	35.33	31.72	4.34
RWI0703	13.94	55.78	79.75	23.22	70.99	114	122.3	83.13	46.31	33.34	85.25	28
RWI0704	24.93	37.26	28	50.51	70.99	85.25	31.86	27.3	8.83	46.47	19.92	18.96
RWI0801	16.59	19.14	33.77	31.05	29.68	99.34	101.9	26.42	52.02	49.85	31.05	25.25
RWI0802	16.94	26.88	34.75	26.65	64.02	63.74	66.67	68.29	52.4	35.33	28.5	6.17
RWI0803	12.41	36.32	84.52	21.12	63.2	55.54	124.2	119.8	66.12	47.25	56.74	13.15
RWI0804	21.82	37.26	24.93	44.01	73.35	8.16	50.08	45.16	40.03	44.59	18.4	26.42
RWI0901	16.81	28.75	25.25	29.93	44.59	70.85	83.13	23.82	105.4	26.42	37.77	23.52
RWI0902	14.18	24.09	29.68	14.06	35.95	44.01	49.85	84.52	50.51	42.61	39.18	17.59
RWI0903	13.63	35.03	60.4	18.8	69.82	51.13	87.6	39.69	66.12	15.86	54.02	18.64
RWI0904	28.36	32.3	17.43	14.06	81.42	47.66	46.47	39.04	29.93	63.2	18.4	15.4
RWI1001	20.84	15.32	23.82	14.9	43.85	60.14	26.42	21.82	64.32	57.36	25.37	27.54
RWI1002	17.3	27.75	23.52	12.51	33.34	11.14	67.85	54	35.96	26.76	23.22	5.19
RWI1003	9.46	34.78	80.78	23.72	50.08	93.73	76.55	79.75	79.59	31.45	42.43	35.33
RWI1004	25.98	27.13	20.59	25.37	89.58	3.89	75.24	39.5	16.89	15.86	16.89	42.07

Table 1 WI RR dBase.2

Experiment Number	Jan R 0.1 mm/h	Feb R 0.1 mm/h	Mar R 0.1 mm/h	Apr R 0.1 mm/h	May R 0.1 mm/h	Jun R 0.1 mm/h	Jul R 0.1 mm/h	Aug R 0.1 mm/h	Sep R 0.1 mm/h	Oct R 0.1 mm/h	Nov R 0.1 mm/h	Dec R 0.1 mm/h
RWI0101	13.70	8.53	10.48	11.66	15.95	2.02	21.81	7.87	19.67	27.53	14.72	6.42
RWI0102	12.61	12.50	19.31	6.58	15.49	1.63	50.19	21.27	13.01	13.67	7.47	2.70
RWI0103	5.64	6.82	21.72	9.28	15.61	38.42	49.24	31.73	27.10	25.28	13.88	4.27
RWI0104	7.06	11.49	5.76	19.50	24.57	6.15	22.99	20.75	62.40	9.45	34.22	6.98
RWI0201	10.81	7.66	7.71	12.23	10.8	15.17	25.17	3.19	17.31	9.92	7.05	6.08
RWI0202	3.34	15.24	15.49	11.04	6.96	2.28	42.67	20.07	10.35	10.43	10.38	2.92
RWI0203	5.84	7.17	19.95	16.23	6.11	38.74	31.36	10.39	20.18	14.83	23.36	1.4
RWI0204	7.4	8.59	6.5	12.29	39.57	10.66	27.76	40.08	9.22	5.37	15.55	7.53
RWI0301	12.3	8.92	7.92	9.47	9.3	28.48	1.71	23.07	39.88	9.67	8.67	7.02
RWI0302	8.96	12.1	18.28	8.99	8.83	19.47	34.19	20.88	8.81	12.09	9.8	2.68
RWI0303	6.47	6.41	24.64	9.92	8.7	38.31	61.6	32.47	14	19.23	18.37	2.02
RWI0304	8.92	9.51	7.67	16.21	23.43	5.33	30.85	20.47	5.42	8.94	23.18	8.18
RWI0402	7.58	11.4	20.39	10.26	11.95	7.92	52.93	9.73	8.2	15.78	9.41	6.68
RWI0403	5.64	5.79	22.42	11.1	9.24	47.09	39.85	20.47	9.62	11.51	11.2	2.33
RWI0404	8.17	9.52	6.27	16.67	25.45	7.43	10.78	13.38	6.15	6.21	24.13	6.49
RWI0501	13.5	9.17	10.17	8.85	12.52	24.1	24.71	12.13	14.28	13.74	11.35	7.04
RWI0502	7.31	13.38	23.73	10.62	8.23	2.2	49.94	13.44	9.53	11.07	12.25	2.82
RWI0503	6.95	6.17	19.31	10.3	6.88	40.76	44.2	15.14	34.69	14.06	13.37	3.5
RWI0504	7.64	6.47	7.63	20.09	30.85	6.28	10.02	10.55	6.79	4.58	21.13	5.85
RWI0601	16.42	2.2	14.2	12.95	14.52	29.99	8.14	17.87	8.4	26.97	13.74	7.9
RWI0602	10.91	6.75	6.31	10.82	7.74	0.89	13.89	12.82	7.37	13.44	9.3	2.82
RWI0701	13.01	2.47	7.59	14.02	11.75	23.85	22.55	5.39	10.29	18.57	7.17	8.58
RWI0702	11.95	9.77	10.48	8.23	18.19	7.39	8.83	23.89	11	16.02	12.29	2.87
RWI0703	5.57	9.3	24.32	11.82	17.19	18.73	76.92	47.65	21.22	12.69	8.46	3.39
RWI0704	9.36	11.99	7.21	14.71	37.9	20.56	7.76	9.59	2.77	9.73	8.88	6.78
RWI0801	11.85	8.09	8.66	14.31	12.81	21.29	29.01	4.15	14.93	22.41	9.32	8.73
RWI0802	10.51	7.97	9.8	9.6	11.11	6.69	10.22	29.01	10.97	16.69	13.43	2.99
RWI0803	5.72	9.12	20.43	9.43	16.31	11.32	71.9	61.47	20.74	15.48	10.6	2.2
RWI0804	8.86	11.31	7.33	12.49	37.9	2.31	14.64	7.64	2.59	11.49	7.9	7.3
RWI0901	12.57	9.48	7.71	11.07	11.28	37.06	18.72	4.69	29.82	13.58	10.68	9.21
RWI0902	8.38	8.95	10.15	8.1	12.82	4.98	17.52	18.72	12.91	16.65	13.37	3.42
RWI0903	5.55	10.02	21.44	10.75	15.91	11.54	55.31	15.05	12.36	9.84	11.16	4.01
RWI0904	9.67	14.56	9.33	5.79	42.24	1.75	4.99	11.26	3.04	11.09	6.72	3.9
RWI1001	13.61	10.16	9.05	2.89	14.4	14.5	2.26	6.02	12.72	19.28	7.42	8.53
RWI1002	10.43	7.36	8.59	7.56	11.58	1.44	20.64	25.82	10.59	12.61	10.24	2.51
RWI1003	5.36	9.73	16.94	10.78	14.06	26.25	12.08	45.22	24.84	15.28	8.7	5.85
RWI1004	8.45	9.96	7.85	9.19	32.2	2.35	37.6	15.72	4.28	8.12	8.72	9.14

Table 1 WI RR dBase.2

Experiment Number	Jan R 1 mm/h	Feb R 1 mm/h	Mar R 1 mm/h	Apr R 1 mm/h	May R 1 mm/h	Jun R 1 mm/h	Jul R 1 mm/h	Aug R 1 mm/h	Sep R 1 mm/h	Oct R 1 mm/h	Nov R 1 mm/h	Dec R 1 mm/h
RWI0101	7.16	3.10	2.96	3.45	2.44	0.14	1.41	0.20	0.90	2.85	1.19	2.42
RWI0102	3.57	2.67	3.92	2.68	0.59	0.14	2.84	2.13	2.46	3.75	2.53	
RWI0103	1.86	1.71	6.40	3.84	2.83	2.58	5.71	6.18	7.08	4.48	2.00	1.06
RWI0104	2.68	3.26	3.10	2.69	7.11		1.23	0.94	1.89	1.12	2.27	2.46
RWI0201	4.93	3.27	2.05	3.23	1.02	0.72	0.3	0.25	1.03	0.72	1.14	2.13
RWI0202	1.5	3.05	2.94	3.48	1.28	0.17	3.77	1.27	2.05	1.64	2.83	0.15
RWI0203	1.67	2.23	5.24	4.27	1.56	2.3	2.75	4.84	2.68	3.53	2.45	0.3
RWI0204	2.67	3.55	2.82	2.91	6.19	0.36	1.56	1.82	0.41	0.45	1.28	2.53
RWI0301	5.53	3.18	2.19	3.42	1.14	1.37	0.1	0.02	2.42	1.09	1.28	2.55
RWI0302	2.33	3.16	3.02	3.07	2.44	0.37	2.46	1.37	2.43	2.81	2.89	
RWI0303	1.51	1.9	6.1	4.02	2.49	1.4	2.56	8.43	3.03	4.28	2.18	0.05
RWI0304	2.92	3.46	2.7	2.82	2.67		0.78	1.65	0.86	0.72	2.08	2.73
RWI0402	1.51	2.91	3	3.45	1.77	0.24	3.33	0.12	0.62	1.81	1.51	2.72
RWI0403	0.88	0.96	4.97	3.51	1.84	2.81	2.98	1.45	2.25	2.46	3.11	
RWI0404	3.08	2.71	1.92	2.97	5.81		0.65	1.20	0.65	0.65	2.06	2.79
RWI0501	7	2.79	2.36	2.03	1.8	0.82	0.63	0.16	1.34	1.01	2.3	2.97
RWI0502	3.15	3.09	2.75	3.88	1.33	0.22	3.36	1.34	1.95	2.61	3.34	
RWI0503	1.29	1.94	4.96	2.51	1.42	0.63	3.38	2.28	6.79	3.36	2.48	1.09
RWI0504	3	1.88	2.31	3.8	6.37	0.06	0.62	0.96	0.72	0.33	1.85	2.39
RWI0601	7.33	0.18	2.17	1.96	2.39	0.42	0.85	0.24	0.76	1.47	1.04	2.17
RWI0602	3.69	1.75	0.57	3.4	1.3	0.11	0.91	1.76	2.26	3.03	3.19	0.4
RWI0701	6.39	0.17	1.61	2.97	2.05	1.62	1.54	0.14	1.13	1.47	1.34	2.46
RWI0702	2.91	2.49	1.07	3.44	3.56	0.58	0.8	2.06	2.24	2.78	3.81	
RWI0703	0.89	1.85	5.99	4.83	2.16	1.75	7.06	10.07	3.9	3.53	2.92	1.13
RWI0704	3.18	2.1	3.23	2.33	6.79	0.15	0.78	1.9		0.91	1.48	2.64
RWI0801	5.57	2	1.75	2.45	2.18	1.51	1.6	0.16	1.71	1.35	0.91	2.23
RWI0802	2.59	2.25	1.63	1.97	2.34	0.64	0.9	2.69	2.27	2.49	3.32	0.21
RWI0803	1.08	0.99	5.15	3.52	1.71	0.25	9.03	10.28	3.14	2.98	2.93	0.73
RWI0804	3.19	2.18	2.92	2.62	6.9		1.09	1.93	0.51	1.07	1.42	2.74
RWI0901	5.61	1.76	1.72	2.49	2.05	2.07	0.18	0.16	0.58	1.56	2.12	2.64
RWI0902	2.09	2.57	1.62	3.73	4.2	0.52	0.75	2.02	2.21	2.93	3.45	0.68
RWI0903	1.18	1.78	4.75	3.74	1.77	0.68	7.04	4.11	1.67	2.3	2.94	1.3
RWI0904	2.91	2.18	3.08	1.53	4.91		0.07	2.15	0.28	0.9	0.98	0.31
RWI1001	5.51	2.43	2	0.09	2.19	1.34		0.18	0.61	0.22	1.27	2.07
RWI1002	2.81	2.35	1.54	3.23	2.1	0.18	0.44	2.18	1.99	2.9	3.33	0.16
RWI1003	1.17	1.51	4.44	4.08	1.76	0.87	0.68	9	5.23	3.1	3.51	0.28
RWI1004	3.12	2.44	3.01	1.67	6.62		1.9	0.93	0.55	0.84	1.86	2.92

Table 1 WI RR dBase.2

Experiment Number	Jan Rain [mm]	Feb Rain [mm]	Mar Rain [mm]	Apr Rain [mm]	May Rain [mm]	Jun Rain [mm]	Jul Rain [mm]	Aug Rain [mm]	Sep Rain [mm]	Oct Rain [mm]	Nov Rain [mm]	Dec Rain [mm]
RWI0101												
RWI0102												
RWI0103												
RWI0104												
RWI0201												
RWI0202												
RWI0203												
RWI0204												
RWI0301												
RWI0302												
RWI0303												
RWI0304												
RWI0402												
RWI0403												
RWI0404												
RWI0501												
RWI0502												
RWI0503												
RWI0504												
RWI0601												
RWI0602												
RWI0701												
RWI0702												
RWI0703												
RWI0704												
RWI0801												
RWI0802												
RWI0803												
RWI0804												
RWI0901												
RWI0902												
RWI0903												
RWI0904												
RWI1001												
RWI1002												
RWI1003												
RWI1004												

Table 1 WI RR dBase.2

Experiment Number	Jan Snow ?	Feb Snow ?	Mar Snow ?	Apr Snow ?	May Snow ?	Jun Snow ?	Jul Snow ?	Aug Snow ?	Sep Snow ?	Oct Snow ?	Nov Snow ?	Dec Snow ?
RWI0101												
RWI0102												
RWI0103												
RWI0104												
RWI0201												
RWI0202												
RWI0203												
RWI0204												
RWI0301												
RWI0302												
RWI0303												
RWI0304												
RWI0402												
RWI0403												
RWI0404												
RWI0501												
RWI0502												
RWI0503												
RWI0504												
RWI0601												
RWI0602												
RWI0701												
RWI0702												
RWI0703												
RWI0704												
RWI0801												
RWI0802												
RWI0803												
RWI0804												
RWI0901												
RWI0902												
RWI0903												
RWI0904												
RWI1001												
RWI1002												
RWI1003												
RWI1004												

Table 1 WI RR dBase.2

Experiment Number	Jan Uptime [%]	Feb Uptime [%]	Mar Uptime [%]	Apr Uptime [%]	May Uptime [%]	Jun Uptime [%]	Jul Uptime [%]	Aug Uptime [%]	Sep Uptime [%]	Oct Uptime [%]	Nov Uptime [%]	Dec Uptime [%]
RWI0101												
RWI0102												
RWI0103												
RWI0104												
RWI0201												
RWI0202												
RWI0203												
RWI0204												
RWI0301												
RWI0302												
RWI0303												
RWI0304												
RWI0402												
RWI0403												
RWI0404												
RWI0501												
RWI0502												
RWI0503												
RWI0504												
RWI0601												
RWI0602												
RWI0701												
RWI0702												
RWI0703												
RWI0704												
RWI0801												
RWI0802												
RWI0803												
RWI0804												
RWI0901												
RWI0902												
RWI0903												
RWI0904												
RWI1001												
RWI1002												
RWI1003												
RWI1004												

Table 2 WI RR dBase.2

Experiment Number	References	Comments	Update	Global Rain Zone	Annual Rain [mm]	Jan Rain [mm]	Feb Rain [mm]	Mar Rain [mm]	Apr Rain [mm]	May Rain [mm]	Jun Rain [mm]	Jul Rain [mm]	Aug Rain [mm]	Sep Rain [mm]	Oct Rain [mm]	Nov Rain [mm]	Dec Rain [mm]
RWI0101	Goldhirsh	Gauge	6/11/93	G_D2													
RWI0102	Goldhirsh	Gauge	6/11/93	G_D2													
RWI0103	Goldhirsh	Gauge	6/11/93	G_D2													
RWI0104	Goldhirsh	Gauge	6/11/93	G_D2													
RWI0201	Goldhirsh	Gauge	6/11/93	G_D2													
RWI0202	Goldhirsh	Gauge	6/11/93	G_D2													
RWI0203	Goldhirsh	Gauge	6/11/93	G_D2													
RWI0204	Goldhirsh	Gauge	6/11/93	G_D2													
RWI0301	Goldhirsh	Gauge	6/11/93	G_D2													
RWI0302	Goldhirsh	Gauge	6/11/93	G_D2													
RWI0303	Goldhirsh	Gauge	6/11/93	G_D2													
RWI0304	Goldhirsh	Gauge	6/11/93	G_D2													
RWI0402	Goldhirsh	Gauge	6/11/93	G_D2													
RWI0403	Goldhirsh	Gauge	6/11/93	G_D2													
RWI0404	Goldhirsh	Gauge	6/11/93	G_D2													
RWI0501	Goldhirsh	Gauge	6/11/93	G_D2													
RWI0502	Goldhirsh	Gauge	6/11/93	G_D2													
RWI0503	Goldhirsh	Gauge	6/11/93	G_D2													
RWI0504	Goldhirsh	Gauge	6/11/93	G_D2													
RWI0601	Goldhirsh	Gauge	6/11/93	G_D2													
RWI0602	Goldhirsh	Gauge	6/11/93	G_D2													
RWI0701	Goldhirsh	Gauge	6/11/93	G_D2													
RWI0702	Goldhirsh	Gauge	6/11/93	G_D2													
RWI0703	Goldhirsh	Gauge	6/11/93	G_D2													
RWI0704	Goldhirsh	Gauge	6/11/93	G_D2													
RWI0801	Goldhirsh	Gauge	6/11/93	G_D2													
RWI0802	Goldhirsh	Gauge	6/11/93	G_D2													
RWI0803	Goldhirsh	Gauge	6/11/93	G_D2													
RWI0804	Goldhirsh	Gauge	6/11/93	G_D2													
RWI0901	Goldhirsh	Gauge	6/11/93	G_D2													
RWI0902	Goldhirsh	Gauge	6/11/93	G_D2													
RWI0903	Goldhirsh	Gauge	6/11/93	G_D2													
RWI0904	Goldhirsh	Gauge	6/11/93	G_D2													
RWI1001	Goldhirsh	Gauge	6/11/93	G_D2													
RWI1002	Goldhirsh	Gauge	6/11/93	G_D2													
RWI1003	Goldhirsh	Gauge	6/11/93	G_D2													
RWI1004	Goldhirsh	Gauge	6/11/93	G_D2													

Table 2 WI RR dBase.2

Experiment Number	Jan Ex 5 [mm]	Feb Ex 5 [mm]	Mar Ex 5 [mm]	Apr Ex 5 [mm]	May Ex 5 [mm]	Jun Ex 5 [mm]	Jul Ex 5 [mm]	Aug Ex 5 [mm]	Sep Ex 5 [mm]	Oct Ex 5 [mm]	Nov Ex 5 [mm]	Dec Ex 5 [mm]
RWI0101												
RWI0102												
RWI0103												
RWI0104												
RWI0201												
RWI0202												
RWI0203												
RWI0204												
RWI0301												
RWI0302												
RWI0303												
RWI0304												
RWI0402												
RWI0403												
RWI0404												
RWI0501												
RWI0502												
RWI0503												
RWI0504												
RWI0601												
RWI0602												
RWI0701												
RWI0702												
RWI0703												
RWI0704												
RWI0801												
RWI0802												
RWI0803												
RWI0804												
RWI0901												
RWI0902												
RWI0903												
RWI0904												
RWI1001												
RWI1002												
RWI1003												
RWI1004												

Table 2 WI RR dBase.2

Experiment Number	Error G_Climate	Error C_Climate	Error T-C fit	Error LN fit	Error Mpf fit	TC [1]	TC [2]	TC [3]	TC [4]	TC [5]	LN [1]	LN [2]	LN [3]	Rrate01	Rrate1	Mpf [1]	Mpf [2]	Mpf [3]
RWI0101	0.46078	0.17661	0.06507	0.07522	0.14077	0.04849	19.41876	3.49305	1.27686	1.18391	3.66989	1.1496	1.29609	47.7	12.7	0.38027	-0.71169	-0.04749
RWI0102	0.37858	0.17413	0.06455	0.10375	0.11254	0.05677	22.45515	2.68284	1.51253	1.17215	2.96135	1.30758	1.32617	53.8	14.6	0.42235	-0.74966	-0.03917
RWI0103	0.39378	0.54762	0.05888	0.11051	0.06782	0.11085	23.37817	3.95207	1.40242	1.25567	3.76164	1.62043	1.32238	69.3	21.7	0.69838	-0.66885	-0.03464
RWI0104	0.43137	0.41003	0.06206	0.14992	0.08455	0.209	22.88533	4.36234	0.83335	1.15121	4.58319	0.80647	1.51497	68	18.3	0.47003	-0.69574	-0.03168
RWI0201	0.49333	0.12504	0.06325	0.11695	0.17717	0.05575	21.49345	2.68284	1.3292	1.07146	2.96135	1.07404	1.3207	46.4	9.8	0.27007	-0.84529	-0.03898
RWI0202	0.5018	0.13714	0.05901	0.12513	0.12545	0.15416	16.594	2.88913	1.11994	1.05456	1.99484	1.72053	1.24229	49.4	12.9	0.2667	-0.6845	-0.04878
RWI0203	0.29374	0.35218	0.03379	0.08604	0.05632	0.11052	18.75558	4.58319	0.95591	1.26394	4.15214	1.18939	1.32063	52	17.7	0.61643	-0.737	-0.04197
RWI0204	0.38854	0.30682	0.06165	0.13588	0.08983	0.11169	22.08683	5.86687	0.54313	1.37599	4.93559	0.68056	1.50851	62.5	14.9	0.43875	-0.75264	-0.034
RWI0301	0.4144	0.20219	0.09131	0.1565	0.17312	0.0648	26.94233	3.43426	1.0552	1.16675	2.96135	1.10374	1.39776	62.5	10.7	0.35429	-0.84941	-0.02819
RWI0302	0.33725	0.16868	0.06587	0.10089	0.10579	0.0446	22.80532	2.88913	1.34447	1.2165	2.96135	1.31552	1.3128	49.5	13	0.48163	-0.81955	-0.03646
RWI0303	0.46666	0.512	0.06264	0.1287	0.11091	0.10052	28.86915	3.85568	1.28083	1.22287	3.95207	1.25351	1.41685	79.4	19.5	0.5393	-0.66512	-0.03053
RWI0304	0.30059	0.232	0.08131	0.10961	0.06894	0.03764	29.36974	1.99484	1.65269	1.19506	1.99484	1.66032	1.31864	54.2	13.1	0.56469	-0.96208	-0.02465
RWI0402	0.43492	0.24612	0.07527	0.1198	0.12495	0.04095	28.27268	2.88913	1.15348	1.3193	2.96135	1.12588	1.42612	63.2	13.6	0.3378	-0.78003	-0.02886
RWI0403	0.52342	0.42696	0.07744	0.11221	0.07973	0.08679	23.56835	3.58038	1.22652	1.3287	3.58038	1.27059	1.41285	66.4	21.2	0.43325	-0.64427	-0.03244
RWI0404	0.36917	0.16407	0.04345	0.09233	0.12517	0.05824	26.42555	3.60812	1.00481	1.19346	4.39615	0.66167	1.50193	53.4	12.1	0.42882	-0.89341	-0.02833
RWI0501	0.34973	0.15681	0.05303	0.08961	0.14851	0.06052	24.70998	2.74991	1.49594	1.10452	2.96135	1.28507	1.32087	53.9	12.2	0.47074	-0.87449	-0.03166
RWI0502	0.36764	0.19988	0.09411	0.1601	0.15768	0.21441	15.92008	1.94619	1.83961	0.74853	2.96135	1.29053	1.31448	56.9	12.3	0.4407	-0.72308	-0.0446
RWI0503	0.38546	0.46889	0.06409	0.08598	0.09062	0.03339	34.02688	4.93559	0.74464	1.48539	4.93559	0.77157	1.54171	65.8	18.6	0.56222	-0.83889	-0.02107
RWI0504	0.37365	0.12999	0.03613	0.11163	0.12407	0.05279	28.40248	2.61741	1.53411	1.01457	1.99484	1.59938	1.29774	45.2	11.2	0.44405	-0.98883	-0.02362
RWI0601	0.41066	0.21717	0.04078	0.08651	0.10553	0.09109	23.05816	2.88913	1.22708	1.20155	1.99484	1.96605	1.2695	58	14.3	0.38133	-0.74389	-0.03472
RWI0602	0.67882	0.37417	0.04015	0.04587	0.15062	0.02251	14.15361	2.43052	1.55312	1.00714	2.55357	1.41613	1.09305	27.2	9.3	0.29629	-0.76322	-0.08312
RWI0701	0.41864	0.16138	0.05014	0.11507	0.17954	0.0503	30.21863	2.43052	1.76067	1.0044	2.96135	1.13299	1.38061	58.1	12.1	0.35219	-0.88924	-0.02587
RWI0702	0.4192	0.11002	0.03219	0.05619	0.12379	0.05405	18.87779	2.68284	1.4773	1.08453	2.96135	1.25843	1.25391	40.3	12.1	0.42382	-0.82601	-0.04718
RWI0703	0.46976	0.67272	0.05492	0.16806	0.12259	0.2582	25.2026	4.58319	1.09631	1.13343	4.15214	1.43497	1.40385	85.2	27.7	0.74923	-0.63184	-0.03171
RWI0704	0.32177	0.18317	0.08667	0.12686	0.09426	0.08493	20.19956	2.81866	1.37573	1.07734	1.99484	1.80694	1.23451	46.3	14.1	0.52955	-0.8563	-0.03912
RWI0801	0.4133	0.1149	0.04237	0.0778	0.14871	0.05964	26.76718	2.55357	1.65499	1.02513	2.96135	1.22689	1.33832	48.8	12.5	0.36633	-0.8691	-0.02934
RWI0802	0.50207	0.13469	0.0667	0.11114	0.14748	0.07467	19.5917	2.61741	1.28737	1.13618	2.74991	1.19271	1.32488	50.3	11.9	0.25104	-0.72475	-0.04475
RWI0803	0.49756	0.60879	0.07901	0.17465	0.09889	0.2487	25.52555	2.96135	1.60346	1.02403	1.80723	3.28116	1.24076	81.2	27.2	0.61694	-0.58627	-0.03249
RWI0804	0.41325	0.23406	0.05018	0.12471	0.08303	0.15356	15.70376	3.66989	1.14105	0.96143	4.93559	0.69846	1.40074	44.1	12.1	0.43639	-0.74028	-0.05217
RWI0901	0.38362	0.1881	0.05204	0.08868	0.13881	0.05467	26.21303	3.52012	1.04904	1.25003	3.88555	0.84202	1.45744	57.5	12.9	0.40977	-0.81625	-0.03108
RWI0902	0.42407	0.13632	0.04909	0.08648	0.12857	0.08799	16.44335	2.81866	1.34551	1.0653	2.96135	1.25039	1.24899	41.7	11.1	0.4247	-0.81045	-0.05007
RWI0903	0.39572	0.35867	0.06028	0.16874	0.10331	0.20915	18.86593	4.36234	0.84457	1.18736	4.05087	1.05212	1.39973	61.9	17.3	0.52284	-0.63287	-0.04366
RWI0904	0.56335	0.17931	0.07517	0.13839	0.14519	0.11347	19.68048	2.25698	1.58159	0.8221	2.96135	0.91183	1.41147	50.2	10.4	0.13976	-0.75917	-0.03855
RWI1001	0.56372	0.16425	0.03998	0.06624	0.15209	0.05644	17.48039	2.68284	1.25005	1.11721	2.88913	1.10262	1.28063	38.9	10.6	0.21833	-0.77013	-0.05132
RWI1002	0.51817	0.13463	0.02746	0.05654	0.13332	0.06045	17.06933	2.88913	1.16109	1.14312	2.96135	1.12083	1.27394	37	10.8	0.28404	-0.80118	-0.04966
RWI1003	0.3243	0.36815	0.05058	0.10758	0.09582	0.13727	21.93354	2.96135	1.58634	1.11545	1.85241	2.87417	1.1719	66.7	18.5	0.60922	-0.69776	-0.03794
RWI1004	0.28391	0.19773	0.05811	0.11203	0.09064	0.11097	20.05514	2.37124	2.05007	0.82802	1.99484	1.87127	1.22817	48.1	12.9	0.58565	-0.88827	-0.03641

Table 3 Model Compare

	Global Climate	CCIR Climate	Two Component	Lognormal	Moupfuma
All					
Average	1.09	0.70	0.37	0.29	0.13
Standard Deviation	0.78	0.51	0.25	0.20	0.22
Root-Mean-Square-Error	1.33	0.86	0.45	0.35	0.26
Number of EDFs	207	207	182	195	201
Sample Dispersion					
Wallops Island					
Average	0.42	0.26	0.06	0.11	0.12
Standard Deviation	0.08	0.15	0.02	0.03	0.03
Root-Mean-Square-Error	0.43	0.30	0.06	0.11	0.12
Number of EDFs	37	37	37	37	37
Sample Dispersion					
Darwin. Australia					
Average	1.83	1.09	0.58	0.45	0.16
Standard Deviation	0.34	0.44	0.11	0.10	0.06
Root-Mean-Square-Error	1.87	1.18	0.59	0.46	0.17
Number of EDFs	100	100	100	100	100
Sample Dispersion					
All from CCIR					
Average	0.37	0.36	0.18	0.11	0.10
Standard Deviation	0.23	0.21	0.12	0.11	0.38
Root-Mean-Square-Error	0.43	0.42	0.22	0.16	0.39
Number of EDFs	70	70	45	58	64
Sample Dispersion					

Table 3 Model Compare

	Two-Component P cell	R cell	P debris	R debris	StDev debris
All					
Average	0.224	39.7	2.41	2.45	1.35
Standard Deviation	0.211	77.5	1.22	3.63	0.40
Root-Mean-Square-Error					
Number of EDFs	182	182	182	182	182
Sample Dispersion	0.94	1.95	0.51	1.48	0.30
Wallops Island					
Average	0.097	22.5	3.20	1.31	1.13
Standard Deviation	0.062	4.7	0.87	0.32	0.15
Root-Mean-Square-Error					
Number of EDFs	37	37	37	37	37
Sample Dispersion	0.64	0.21	0.27	0.24	0.13
Darwin. Australia					
Average	0.359	24.4	2.91	1.03	1.63
Standard Deviation	0.192	13.7	0.70	0.89	0.26
Root-Mean-Square-Error					
Number of EDFs	100	100	100	100	100
Sample Dispersion	0.54	0.56	0.24	0.87	0.16
All from CCIR					
Average	0.027	87.8	0.65	6.55	0.89
Standard Deviation	0.047	145.3	0.35	5.43	0.21
Root-Mean-Square-Error					
Number of EDFs	45	45	45	45	45
Sample Dispersion	1.72	1.65	0.53	0.83	0.24

Table 3 Model Compare

	Lognormal P rain	R rain	StDev rain
All			
Average	2.24	3.33	1.48
Standard Deviation	1.31	5.47	0.45
Root-Mean-Square-Error			
Number of EDFs	195	195	195
Sample Dispersion	0.58	1.64	0.31
Wallops Island			
Average	3.17	1.33	1.34
Standard Deviation	0.92	0.53	0.10
Root-Mean-Square-Error			
Number of EDFs	37	37	37
Sample Dispersion	0.29	0.40	0.07
Darwin. Australia			
Average	2.87	0.91	1.83
Standard Deviation	0.73	1.11	0.24
Root-Mean-Square-Error			
Number of EDFs	100	100	100
Sample Dispersion	0.25	1.21	0.13
All from CCIR			
Average	0.55	8.76	0.94
Standard Deviation	0.44	7.52	0.24
Root-Mean-Square-Error			
Number of EDFs	58	58	58
Sample Dispersion	0.79	0.86	0.25

Table 3 Model Compare

	CCIR RR 0.01%	RR 0.1%	Moupfuma LnA	Bex	Uex
All					
Average	72.1	23.7	0.25	-0.67	-0.034
Standard Deviation	30.6	13.4	1.04	0.49	0.020
Root-Mean-Square-Error					
Number of EDFs	207	200	201	201	201
Sample Dispersion	0.42	0.57	4.08	0.73	0.59
Wallops Island					
Average	55.2	14.5	0.44	-0.78	-0.038
Standard Deviation	12.5	4.5	0.13	0.09	0.011
Root-Mean-Square-Error					
Number of EDFs	37	37	37	37	37
Sample Dispersion	0.23	0.31	0.31	0.12	0.30
Darwin. Australia					
Average	97.9	33.3	0.00	-0.35	-0.033
Standard Deviation	13.3	10.6	0.46	0.06	0.006
Root-Mean-Square-Error					
Number of EDFs	100	100	100	100	100
Sample Dispersion	0.14	0.32	343.11	0.17	0.18
All from CCIR					
Average	44.2	13.7	0.55	-1.10	-0.033
Standard Deviation	23.4	9.4	1.69	0.63	0.034
Root-Mean-Square-Error					
Number of EDFs	70	63	64	64	64
Sample Dispersion	0.53	0.69	3.09	0.57	1.02

A Database for Propagation Models

Anil V. Kantak, Krisjani Suwitra and Choung Le
Jet Propulsion Laboratory,
California Institute of Technology
Pasadena, California 91109.

1.0 Introduction

The National Aeronautics and Space Administration's (NASA) Propagation Program supports academic research that models various propagation phenomena in the space research frequency bands. NASA supports such research via schools and institutions prominent in the field. The products of such efforts are particularly useful for researchers in the field of propagation phenomena and telecommunications systems engineers.

The systems engineer usually needs a few propagation parameter values for a system design. Published literature on the subject, such as the CCIR publications, may help somewhat, but often times, the parameter values given in such publications use a particular set of conditions which may not quite include the requirements of the system design. The systems engineer must resort to programming the propagation phenomena model of interest and to obtain the parameter values to be used in the project. Furthermore, the researcher in the propagation field must then program the propagation models either to substantiate the model or to generate a new model. The researcher or the systems engineer must either be a skillful computer programmer or hire a programmer, which of course increases the cost of the effort. An increase in cost due to the inevitable programming effort may seem particularly inappropriate if the data generated by the experiment is to be used to substantiate the already well-established models, or a slight variation thereof.

To help the researcher and the systems engineers, it was recommended by the participants of NASA Propagation Experimenters (NAPEX) XV held in London, Ontario, Canada on June 28 - 29, 1991, that propagation software should be constructed which will contain models and prediction methods of most propagation phenomenon. Moreover, the software should be flexible enough for the user to make slight changes to the models without expending a substantial effort in programming.

2.0 Properties of the Propagation Database

The database described in this paper produces a user-friendly environment with sufficient freedom for the users to model and predict propagation effects. The salient features of the software are as follows:

1. The database contains most, if not all, propagation phenomena models accepted by the propagation community. Access to the models is quite simple and requires only basic computer skills.

2. The database provides a summary description of the model with the parameters and the units of the parameters present therein.

3. The database models contain, where possible, default values for parameters of the model under consideration so that the user does not need to search for the already defined and known values of the parameters. The user can change the default values to more appropriate values.

4. Longer, more involved models are subdivided into steps. Descriptions of each step are available.

5. Extensive charting capabilities are available to the user. Where feasible, the actual charting process is made transparent to the user and involves the user only when a choice must be made between the possible outputs.

6. The user can override any choice made by the program and obtain an output that is appropriate for the application of interest.

7. The database allows changes to the model being run, i.e., changes in mathematical functions and operations using already existing parameters in the model. However, no new definitions of parameters will be permitted.

8. The data to be passed through the model is easily accessed in a straightforward manner with minimal user interface.

9. The database contains, when possible, default data that can be used to run the model and possibly produce the plots. This will be useful in comparing the data generated from a new experiment with already existing data.

10. Every model in the database has the same overall instructions and operating procedure. The user needs to learn how to use only one model in order to use the entire database effectively.

11. All the necessary precautions to ensure the correct use of the database are incorporated in the program. When incorrect inputs are made or when an action conflicts with the general directives of the program, the user is alerted with a warning.

12. User-friendly procedures are used to call the available mathematical functions of Excel software, such as the curve fitting, statistical analysis, etc. This allows the user to apply these functions to the data whenever needed.

13. The database is provided free of cost to the user.

3.0 Software Selection to Host the Propagation Database

A small study was conducted to evaluate the advantages and disadvantages of hosting the Propagation Database Software using a compiler-based program versus a spreadsheet-based program. The results indicate that a final product, such as the database spreadsheet software, has distinct advantages over the compiler-based software.

Of the many commercially available spreadsheet programs, Microsoft Excel was selected to host the Propagation Database software. Excel provides an extensive list of database and mathematical functions necessary to implement the propagation models. Excel also provides charting capabilities that include many versions of two- and three-dimensional charts. Excel also offers the dialog box utility, which can be effectively used for input and output functions of the Propagation Database. Another notable advantage of Excel is that it can call any executable programs written in C, which is a compiler-based program. This arrangement is ideal because it combines the advantages of a spreadsheet environment with the speed of the compiler-based software for number-crunching purposes.

4.0 Software and Hardware Requirements

To run the Propagation Database, Microsoft Windows 3.1 and Microsoft Excel 4.0 or later are required. The following figure shows how the Propagation Database Software interacts with Windows and Excel in the block diagram form. The software is kept under a file called "PRPDBS.XLA"

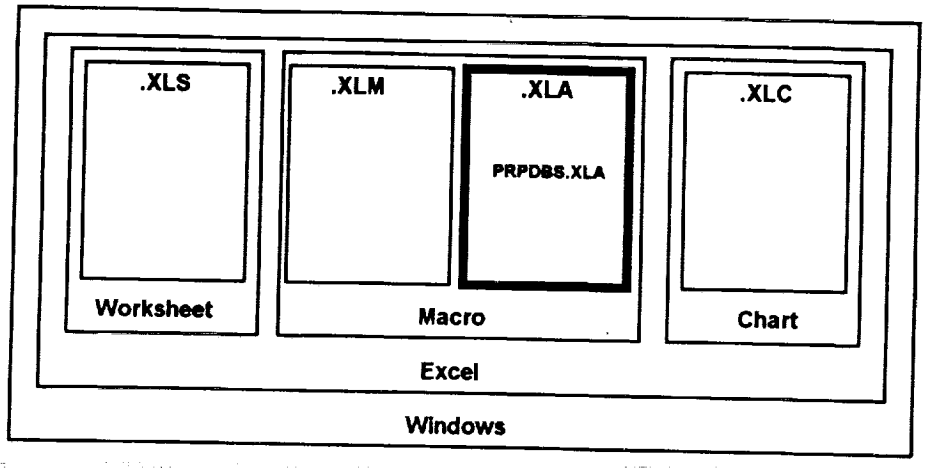

By the way of hardware requirements, a reasonable PC to run the software would be the 80386 machine accompanied by its math coprocessor chip, 80387, with at least 4 Mbytes of RAM. The clock speed should be at least 20 MHz or more. An 80486-based system with a higher clock speed would be better. Any other computer, such as the 80286-based PC etc., with sufficient RAM will run the software; however, it will be very slow. It is recommended that a color monitor be used so that the charting can be done more effectively. Also, a hard disk having a reasonable storage space (a few megabytes) available for the software is needed. The software is developed for IBM PCs and compatibles. The Macintosh version will also be available soon.

5.0 The Propagation Database

The Propagation Database is divided into six categories: the Ionospheric models, the Tropospheric models, the Land Mobile Systems models, the Effects of Small Particles models, the Rain models, and the Radio Noise models. These six categories are further divided into subcategories to include all the models to be housed in the software.

Ionospheric Models:
Absorption Model, and Scintillation Model

Tropospheric Models:
Index of Refraction Profile Model, Gaseous Attenuation Model, Refraction and Fading Model

Land Mobile Satellite System Models:
Cumulative Distribution of Fade Duration Model, Cumulative Distribution of Non Fade Duration Model, Cumulative Distribution of Phase Fluctuation Model, Diffusely

Scattering Model, Empirical Regression Models, Empirical Roadside Shadowing Model, Large Scale - Small Scale (LS-SS) Coverage Model, Fade State Transition Model, Faraday Rotation Model, Frequency Scattering Model, Geometric Analytic Models, Single Object Model, Multiple Object Scattering Model, Loo's Distribution Model, Log normal Shadowing Model, Raleigh Model, Reflection Coefficient Model, Simplified Log normal Shadowing Model, and Total Shadowing Model

Effect of Small Particles Models:
Cloud Model

Rain Models:
CCIR Model, CCIR Model (Proposed Modification), Global Model, Dutton Dougherty Model, Lin Model, Rice Holmberg Model, and Simple Attenuation Model

Radio Noise Models:
Noise Model

The access to any model is carried out using Excel's dialog box user interface. Each dialog box is divided into six distinct areas to help the user to provide the inputs easily.

The six areas of the dialog box are described below. The first area is used to provide general information about the model selected by the user. This step describes any particular conditions required by the model, the parameter ranges as well as the number of steps the model has, and so on. The second area is used to display formulas describing the model selected. The formula can be modified by the users to a certain extent using legal expressions in Excel. Once the formula is created, the software will use this formula for the current run only. Loading the software again will bring back the original formula. The third area is the input area. This area is used to acquire input parameter(s) for the model. The fourth area is used to display definitions of the input and output parameter(s) used by the model. The fifth area is used to display intermediate or final result(s) of the particular model. The sixth area has a few buttons to help the user and to produce the output(s) of the model (or step). For some models, this area also has buttons to allow creation of a table of output values of the model as a function of the range of the selected input parameter. The following figures show the run of the CCIR rain attenuation model included in the database software.

6.0 Conclusion

A database of various propagation phenomena models that can be used by telecommunications systems engineers to obtain parameter values for systems design is presented. This is an easy-to-use tool and is currently implemented on a PC using Excel software under Windows environment; a Macintosh version of the software will also be available by the end of the year. Anyone desiring a copy of the software should contact the authors.

A Sample Run of the CCIR Rain Attenuation Model

Step 1: Calculates hR, the effective rain height in kilometers. The model used for the effective rain height, h_R, is as follows:

$$h_R = 3.0 + 0.028 * Phi \qquad 0 \le Phi < 36^0$$
$$h_R = 4.0 - 0.075 * (Phi - 36) \qquad Phi \ge 36^0$$

where *Phi* is the station's latitude in degrees, which the user must input (e.g., 37 degrees). The user may then click the output button to see the effective rain height, h_R. Clicking the Step 2 button takes the user to the next step.

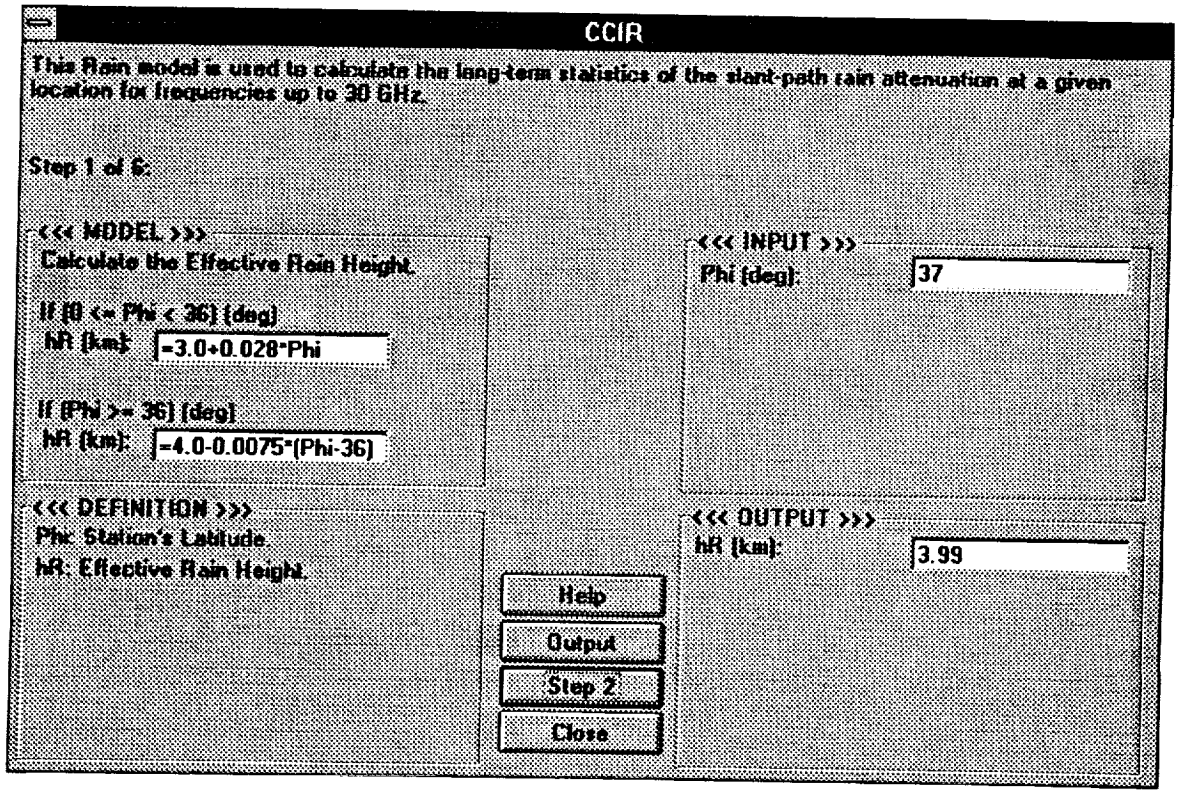

Step 2: Calculates L_S, the slant-path length below rain height in km. The model used for the slant-path length, L_S, is as follows:

$$L_s = \frac{(h_R - h_s)}{\sin(Theta)} \qquad Theta \geq 5^0$$

$$L_s = \frac{2(h_R - h_s)}{\left(\sin^2(Theta) + \frac{2(h_R - h_s)}{R_e}\right)^{1/2} + \sin(Theta)} \qquad Theta < 5^0$$

where h_R is the effective rain height in kilometers, h_S is the height mean sea level of the earth station in km supplied by the user (e.g. 0.632 km.), *Theta* is the elevation angle in degrees, which the user supplies (e.g., 14 degrees), and R_e is the modified earth radius (defaulted to 8500 kilometers), which may be changed if the user desires it. Clicking the output button shows L_S (the slant-path length). Then clicking step 3 takes the user to the next step.

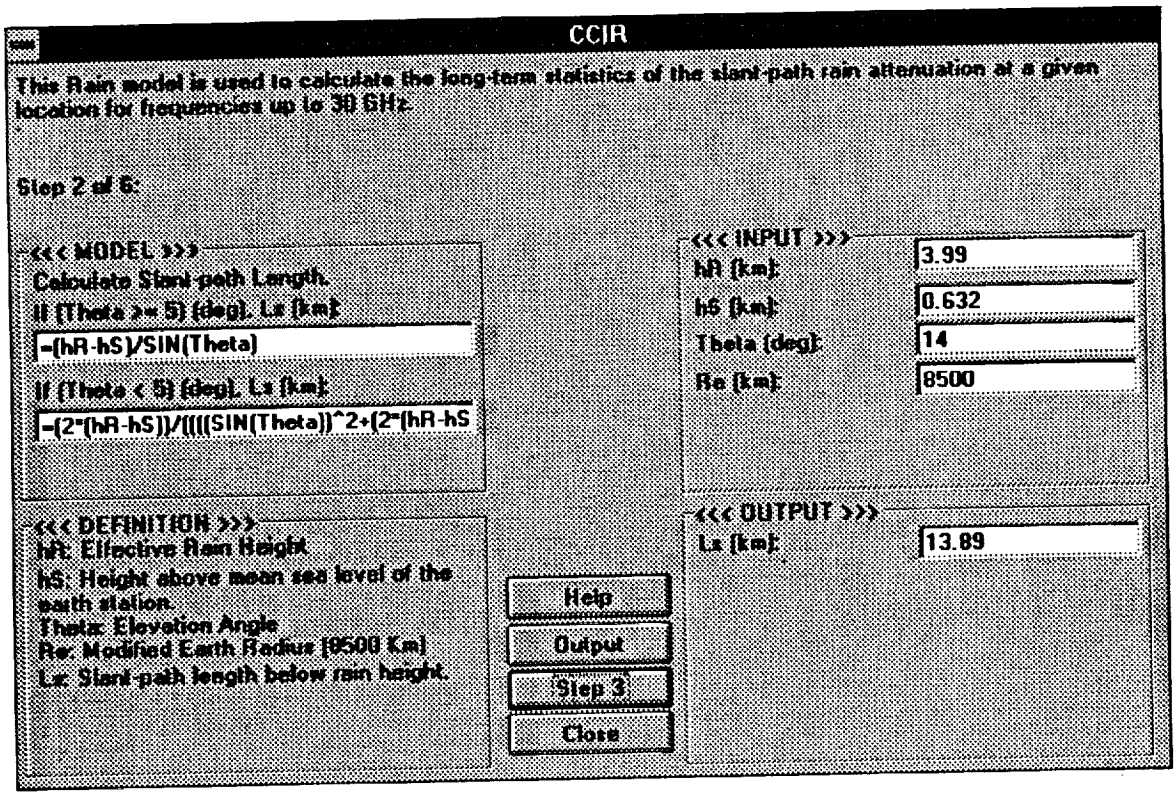

Step 3: Calculates L_g, the horizontal projection of the slant-path length in kilometers. The model used for the horizontal projection of the slant-path length, L_g, is

$$L_s = L_s \cos(Theta)$$

where, L_S is the slant-path length below rain height in kilometers, *Theta* is the elevation angle in degrees. Clicking the Output button shows L_g (the horizontal projection of the slant-path length). Clicking the Step 4 button takes the user to the next step.

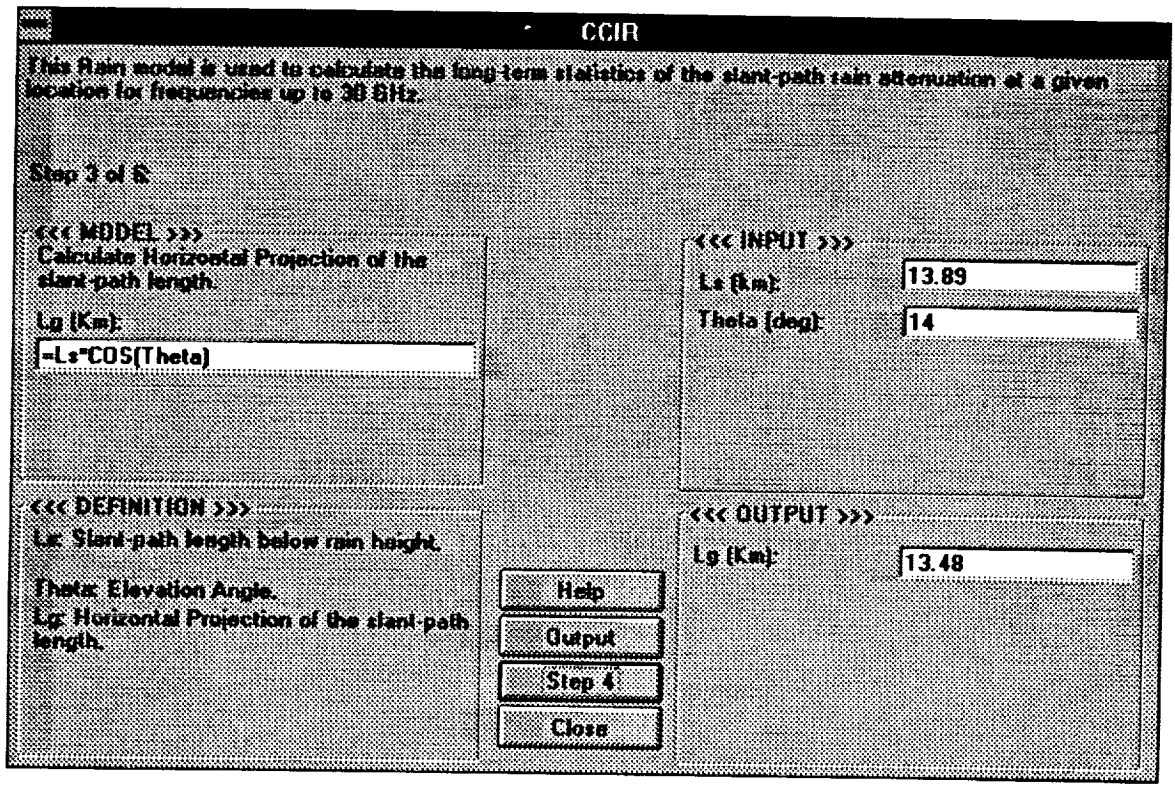

Step 4: Obtains $R_{0.01}$ (dB), the rain intensity exceeded for 0.01% of an average year and calculates $r_{0.01}$, the reduction factor. The model used for the reduction factor, $r_{0.01}$, is

$$r_{0.01} = \frac{1}{1 + L_o / L_o}, \quad L_o = 35\exp(-0.015 R_{0.01})$$

where, $R_{0.01}$ is the rain intensity exceeded for 0.01% of an average year in mm/hr and $r_{0.01}$ is the reduction factor. The user needs to select one of the rain climatic zones, e.g., K. These are the CCIR Rain Climatic Zone for the United States. Clicking the Output button shows $r_{0.01}$ (the reduction factor) and clicking the Step 5 button takes the user to the next step.

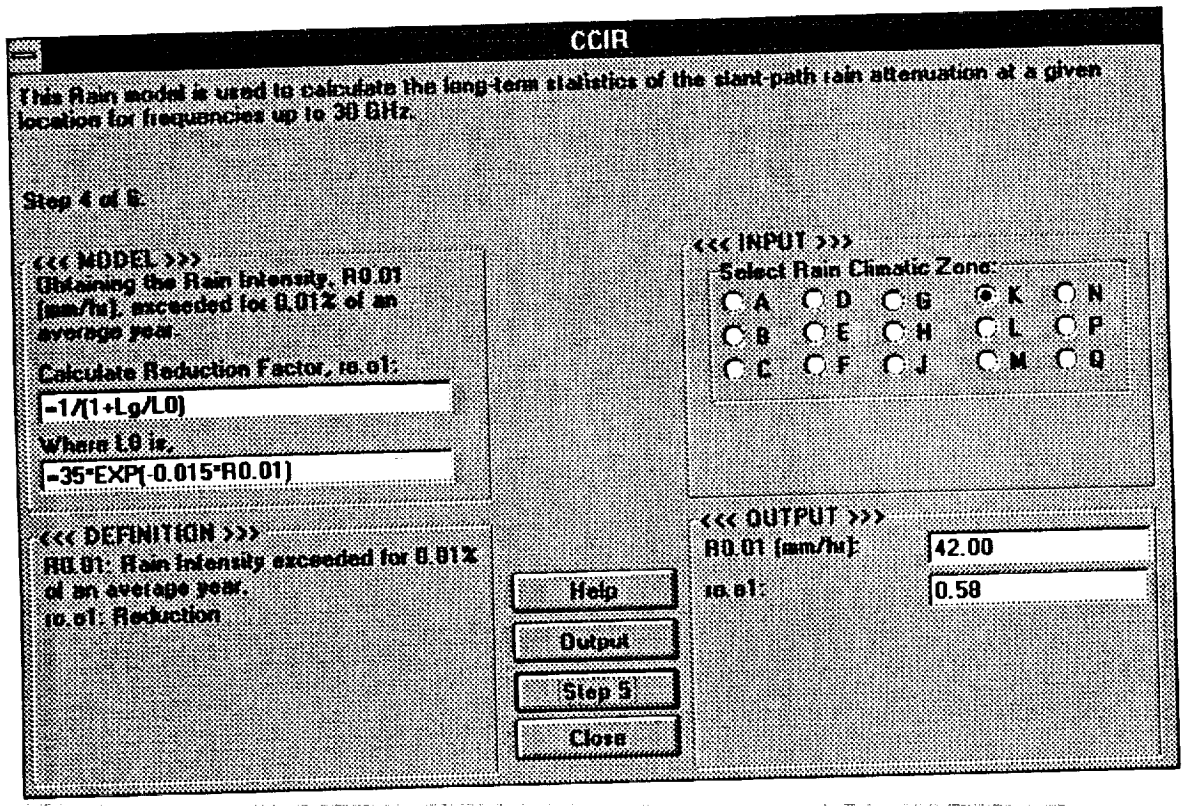

Step 5: Calculates *GammaR*, the specific attenuation using the frequency-dependent coefficient in dB/km. The formula used to calculate *GammaR* is as follows:

$$GammaR = kR_{0.01}^{\alpha},$$

$$k = [k_H + k_V + (k_H - k_V)\cos^2(Theta)\cos(2\,Tau)]/2$$

$$\alpha = [k_H\alpha_H + k_V\alpha_V + (k_V\alpha_H - k_V\alpha_V)\cos^2(Theta)\cos(2\,Tau)]/2k$$

where, *Theta* is the elevation angle in degrees, *Tau* is the polarization tilt angle in degrees. k and α are coefficients taken from Table 1 - Regression coefficients for estimating specific attenuation of Reports of the CCIR, 1990. The user inputs the frequency (e.g., 12.5 GHz), and the *Tau*, (e.g., 45) degrees for circular polarization. Clicking the output button shows *GammaR* and clicking the Step 6 button takes the user to the next step.

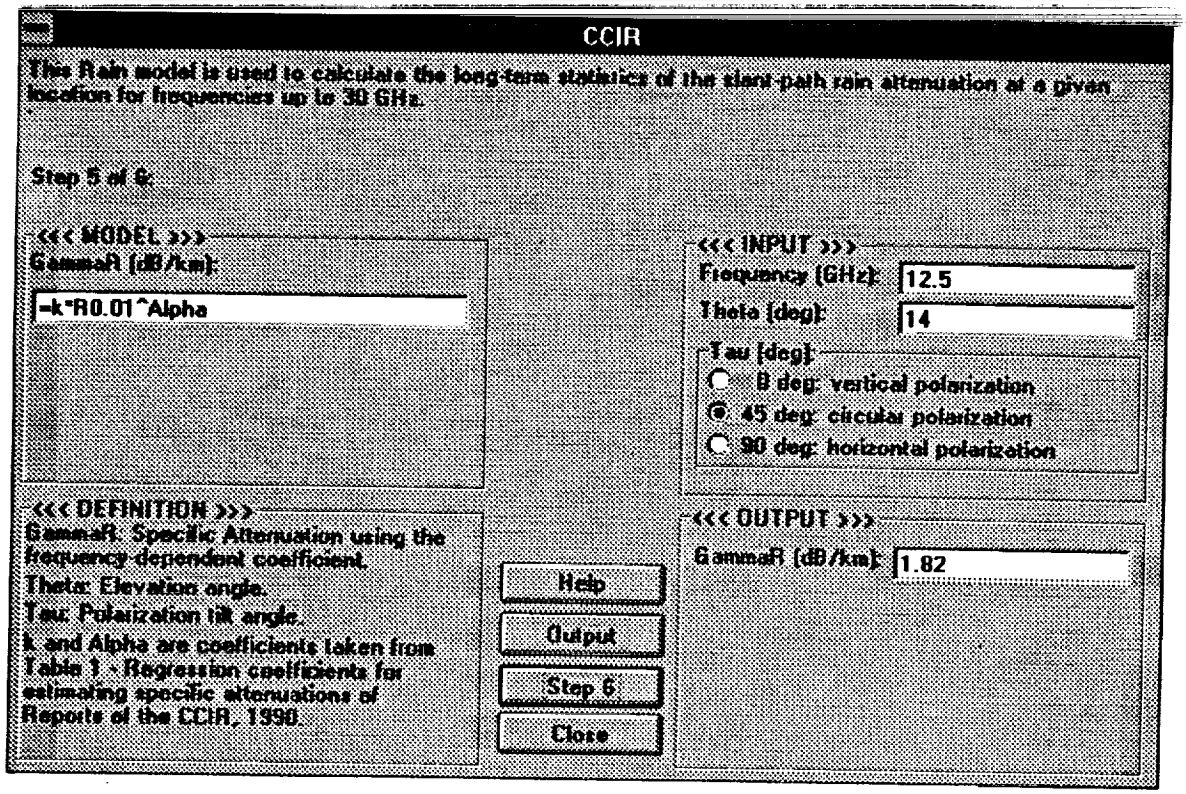

Step 6: Calculates $A_{0.01}$, the attenuation exceeded for 0.01% of an average year in decibels. The formula used for the attenuation exceeded for an average year, $A_{0.01}$ is:

$$A_{0.01} = GammaR * L_s * r_{0.01}$$

where, *GammaR* is the specific attenuation using the frequency-dependent coefficient in dB/km, L_S is the slant-path length below rain height in kilometers and $r_{0.01}$ is the reduction factor. Clicking the Output button shows $A_{0.01}$ (the attenuation exceeded for 0.01% of an average year) and clicking the "Other p (%)" button shows attenuation to be exceeded for other percentages of an average year (0.001 to 1.0 %).

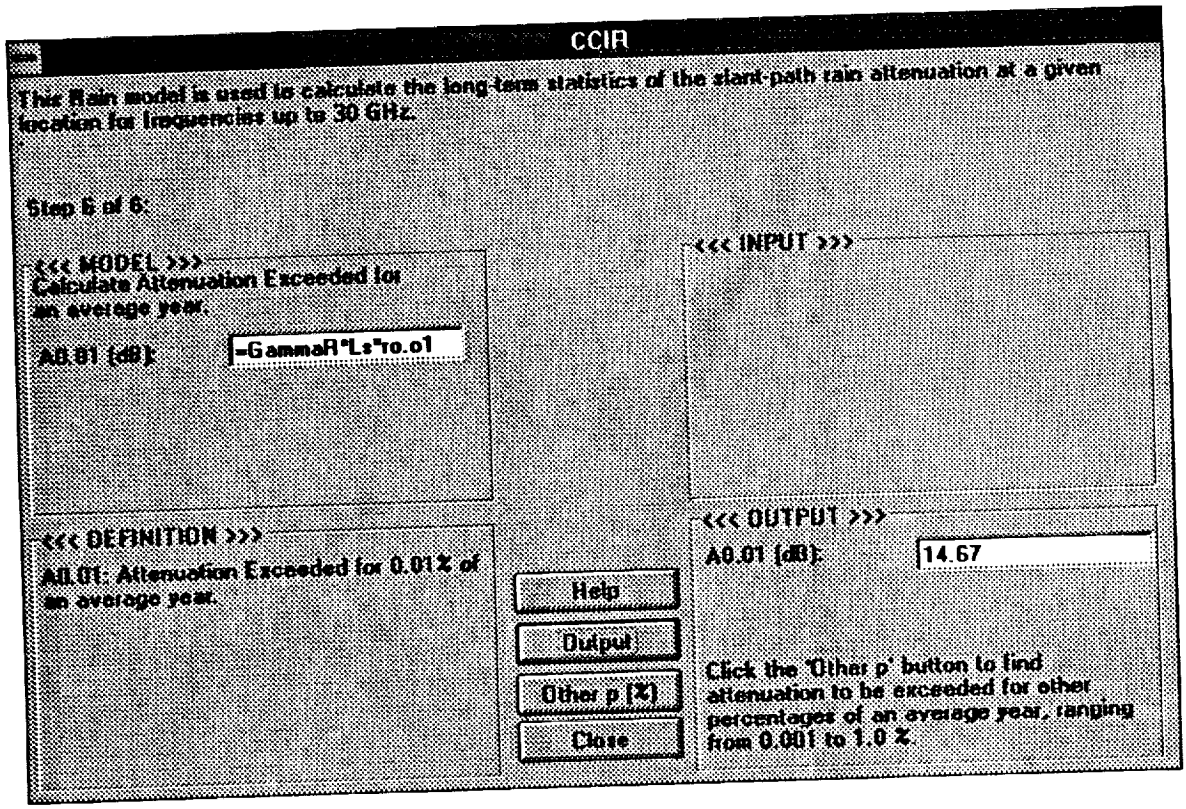

This step also calculates attenuation to be exceeded of an average year for other percentages (0.001 - 1.0 %).

The formula used for p percent of the attenuation exceeded of an average year is as follows:

$$A_p = A_{0.01} * 0.12 * p^{-(0.546+0.043\log(p))}$$

where, p is the percentage of the attenuation exceeded (a user input), Ap is the attenuation exceeded for p percent, and $A_{0.01}$ is the attenuation exceeded for 0.01 percent. Clicking the Output button shows Ap, attenuation of p percentage and ratio of $A_p/A_{0.01}$.

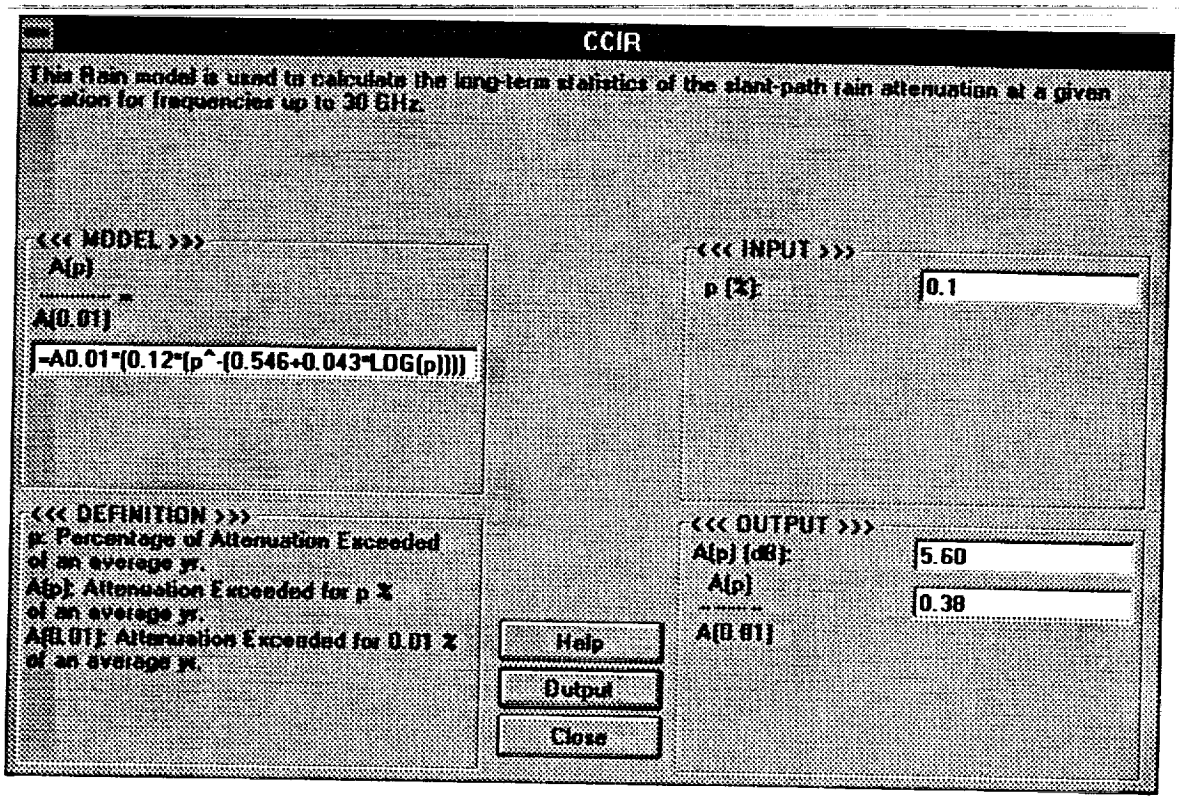

When the Close button is clicked the following dialog box appears:

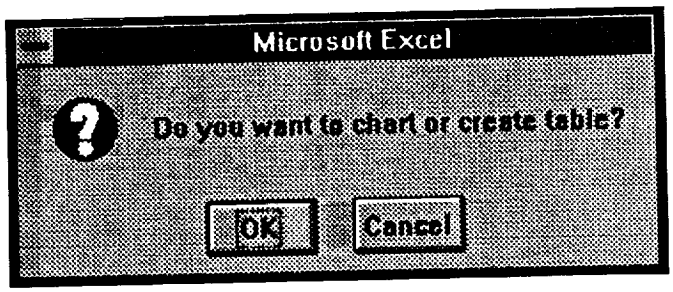

When the OK button is clicked, the following dialog box appears.

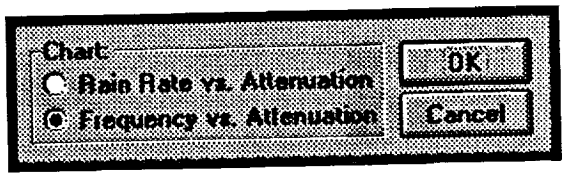

When the user selects a particular option a dialog box appears gathering inputs for that particular option. Here the Frequency versus attenuation button is selected.

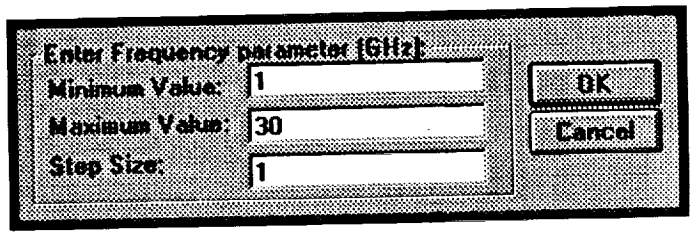

After user inputs the minimum, maximum and step values for the frequency variation and clicks the OK button, a new worksheet will then be invoked to store all of the parameters used, the table, as well as the chart produced. Printing option is available after this step. This concludes the run of the CCIR rain attenuation model.

NAPEX XVII

Session 2

PROPAGATION STUDIES FOR MOBILE/PERSONAL COMMUNICATIONS

Chairman:

John Kiebler

MITRE Corporation

CONTRIBUTION TOWARDS A DRAFT REVISION OF RECOMMENDATION 681: PROPAGATION DATA REQUIRED FOR THE DESIGN OF EARTH-SPACE LAND MOBILE TELECOMMUNICATIONS SYSTEMS

F. Davarian and D. Bishop
Jet Propulsion Laboratory
California Institute of Technology
Pasadena, California

Abstract

Propagation models that can be used for the design of earth-space land mobile-satellite telecommunications systems are presented. These models include: empirical roadside shadowing, attenuation frequency scaling, fade and non-fade duration distribution, multipath in a mountain environment, and multipath in a roadside tree environment. Propagation data from helicopter-mobile and satellite-mobile measurements in Australia and the United States were used to develop the models.

1. Introduction

A simple method for calculating fade depth due to roadside shadowing in typical land mobile satellite environments is presented. A frequency scaling model for signal attenuation is shown. Models for fade and non-fade duration distributions are given. Also, models for clear line-of-sight degradation due to multipath are shown. The models were developed from land mobile satellite measurements.

Working Party 5B examined Recommendation 681 and Report 1009 at its meeting in 1991 in Geneva. At that time, the Working Party decided that Report 1009 did not contain sufficient prediction models to support a revision of Recommendation 681. Recent studies in the United States of America have developed additional propagation prediction models for use in the design and planning of land mobile satellite systems. The models combined with contributions from other administrations should permit the drafting of a revision of Recommendation 681 using Report 1009 as a basis.

2. Empirical Roadside Shadowing Model

Cumulative L-Band fade distributions derived from helicopter-mobile and satellite-mobile measurements in central Maryland, USA have enabled the formulation of an Empirical Roadside Shadowing (ERS) model [Goldhirsh and Vogel, 1992]. The measurements were performed on highways, where the roadside trees were primarily

of the deciduous variety. In order to assess the extent by which the trees populate the roadside, a quantity called percentage of optical shadowing (POS) was defined. This represents the percentage of optical shadowing caused by roadside trees at a path elevation angle of 45° in the direction of the signal source -- the same azimuth as the satellite or the helicopter. A model that is valid for 55% ≤ POS ≤ 75% is given as

$$A(\theta, P) = \alpha(P) + \beta(P)\theta + \gamma(P)\theta^2 \qquad (1)$$

for

$$20° \le \theta \le 60°$$
$$1\% \le P \le 20\%,$$

where A is the fade exceeded in dB, P is the percentage of the distance traveled over which the fade is exceeded, and θ is the path elevation angle to the satellite. The parameters, α(P), β(P), and γ(P) are tabulated in Table 1.

Table 1. Values α(P), β(P), and γ(P) of the ERS Model

Percentage (P)	α(P)	β(P)	γ(P)
20	24.45	-0.7351	5.991×10^{-3}
10	26.84	-0.6775	4.605×10^{-3}
5	29.22	-0.6000	3.219×10^{-3}
2	32.38	-0.5106	1.386×10^{-3}
1	34.76	-0.4430	0.0

The ERS model corresponds to an overall average driving condition encompassing right and left lane driving and opposite directions of travel along highways and rural roads where the overall aspect of the propagation path was, for the most part, orthogonal to the lines of roadside trees and utility poles. The dominant cause of LMSS signal attenuation is canopy shadowing. Figure 1 shows plots of fade exceeded versus the path elevation angle for several constant percentages.

Similar fade measurements were taken in south-eastern Australia. Left-hand circularly polarized continuous-wave transmissions from the Japanese ETS-V satellite at 1545.15 MHz were used. For the 51° elevation angle, the probability of fade exceeded in the Australian data may be described by the following best fit exponential model,

$$P(A) = u \times \exp(-v \times A) \qquad (2)$$

for

$$2\ dB \leq A \leq 15\ dB,$$

where P and A are the same as in Equation 1. The coefficients, u and v, are given in Table 2.

The "moderate" condition in Table 2 corresponds to measurements in which there was 50% to 75% optical shadowing. The "extreme" condition corresponds to measurements in which persistent shadowing occurred. The rms deviations of the measured distributions relative to the best fit curves are included. For small percentages (P = 1% to 2%) and moderate optical shadowing, the model in Equation 2 produces similar results to the model in Equation 1.

Table 2. Best Fit Exponential Cumulative Fade Distribution Parameters for a Path Elevation Angle of 51°

Road Type	u	v	RMS Error (dB)	Fade Range (dB)
Moderate	17.57	0.2184	0.1	2-13
Extreme	95.78	0.1951	0.3	2-15

3. Attenuation Frequency Scaling Model

Mobile fade measurements [Goldhirsh and Vogel, 1992] at L-Band (1.5 GHz) and UHF (870 MHz) have shown that the ratio of fades at equal probability values is approximately consistent with the ratio of the square root of frequencies.

$$A(f_L) = A(f_{UHF})\sqrt{\frac{f_L}{f_{UHF}}} \qquad (3)$$

for

$$1\% \leq P \leq 30\%,$$

where A is the fade exceeded in dB, f_L is the L-Band frequency, and f_{UHF} is the UHF

frequency.

Twenty-four sets of measurements were made driving along tree-lined roads in Central Maryland, USA. The total driving distance was 480 km. Path elevation angles of 30°, 45°, and 60° were used. For frequencies of 1.5 GHz (L-Band) and 870 MHz (UHF), using Equation 3, the predicted ratio of attenuations is 1.31. The ratio of measured attenuations had this mean and an rms deviation of ±0.1 from this value. The scaling applies in the range of P (where P is the percentage of distance traveled over which the fade is exceeded) between 1% and 30%.

An independent validation of Equation 3 is provided by a set of multifrequency measurements [Bundrock and Harvey, 1988] at 893 MHz, 1550 MHz, and 2660 MHz. The average error between these measurements and the model is less than 6%. This validation extends the applicability of Equation 3 to approximately 3 GHz.

4. Fade Duration Distribution Model

Optimal design of land mobile satellite receivers depends on knowledge of the statistics associated with fade durations. Fade duration results at L-Band were obtained from measurements in south-eastern Australia. These measurements were used to develop a model for the cumulative distribution of fade durations [Hase, Vogel, and Goldhirsh, 1991]. The south-eastern Australia measurements were taken with left-hand circularly polarized continuous-wave transmissions radiated from the Japanese ETS-V satellite at 1545.15 MHz. The in- and quadrature-phase detector voltages with noise bandwidths of 500 Hz (one-sided) were recorded at a 1 kHz rate. The output from a power detector with a predetection bandwidth of 200 Hz was recorded at a 1 kHz rate, also. The receiving antenna was of the crossed drooping dipole type with 4 dB gain, an azimuthally omni-directional radiation pattern, and a relatively flat elevation pattern over a beamwidth of 15° to 75°. Fade duration results were obtained by analyzing the average of two consecutive 1 millisecond samples. Fade durations were expressed in units of traveled distance (meters) for which the fades were continuously larger than or equal to thresholds ranging from 1 to 8 dB. Distance duration may be converted to time duration by dividing by the vehicle speed. The fade durations were observed to follow the lognormal distribution. For dd ≥ 0.02 m:

$$P(FD > dd \mid A > A_q) = \frac{1}{2}\left(1 - erf\left[\frac{\ln(dd) - \ln(\alpha)}{\sqrt{2}\,\sigma}\right]\right), \qquad (4)$$

where $P(FD > dd \mid A > A_q)$ represents the probability that the distance fade duration, FD, exceeds the distance, dd, under the condition that the attenuation, A, exceeds A_q.

Also, σ is the standard deviation of ln(dd), and ln(α) is the mean value of ln(dd). The left-hand side of Equation 4 was estimated by computing the percentage number of "duration events" that exceed dd relative to the total number of events for which $A > A_q$. Figure 2 contains a plot of P versus dd (Equation 4) for a 5 dB fade threshold. The best fit regression values are $\alpha = 0.22$ and $\sigma = 1.215$. Table 3 contains the RMS deviations of cumulative distributions of fade durations for various runs relative to the log-normal fit of Equation 4. Equations 2 and 4 may be multiplied to yield the joint probability that FD exceeds dd and A exceeds A_q.

Fade durations, were also derived from measurements at L-Band, taken in central Maryland, USA [Goldhirsh and Vogel, 1989]. A helicopter was used as the transmitter platform with elevation angles of 30°, 45°, and 60°. Smaller elevation angles yielded larger fade durations at fixed percentages. This is consistent with increased shadowing at lower elevation angles.

Table 3. RMS Deviations Relative to Log-Normal Fit (Equation 4) of Cumulative Distributions of Fade Durations for Various Runs Exhibiting Moderate and Extreme Shadowing.

Shadowing Level	% RMS Deviation	Distance (km)
Moderate (Run 1)	16.4	33.0
Moderate (Run 2)	18.0	8.1
Extreme	13.6	2.4

5. Non-Fade Duration Distribution Model

A "non-fade duration" event of distance duration, dd, is defined as the distance over which the fade levels are smaller than a specified fade threshold. The non-fade duration model was developed from the data set that is described in section 4. The measured data fit the following expression:

$$P(NFD > dd \mid A < A_q) = \beta\,(dd)^{-\gamma} \qquad (5)$$

where $P(NFD > dd \mid A < A_q)$ is the percentage probability that a continuous non-fade distance, NFD, exceeds the distance, dd (meters), given that the fade is smaller than the threshold, A_q. Table 4 contains the values of β and γ for roads that exhibit "moderate" and "extreme" shadowing as defined in section 2. A 5 dB fade threshold is used. The

two "moderate" runs in the table were combined to produce a single set of fit coefficients.

Table 4. Non-Fade Duration Regression Values for a 5 dB Fade Threshold at a Path Elevation Angle of 51°

Shadowing Level	β	γ	% RMS Deviation	Distance (km)
Moderate (Run 1)	20.54	0.58	33.3	33.0
Moderate (Run 2)	20.54	0.58	20.5	8.1
Extreme	11.71	0.8371	9.3	2.4

6. Clear Line-of-Sight Degradation Models

In many cases the mobile terminal has a clear line-of-sight to the mobile satellite. Degradation to the signal can still occur under these circumstances. This degradation may be caused by terrain that induces multipath. The mobile terminal receives a phasor summation of the direct line-of-sight signal and several multipath signals. These multipath signals may add constructively or destructively to result in signal enhancement or fade. The multipath signal characteristics depend on the scattering cross-sections of the multipath reflectors, their number, the distances to the receiving antenna, the field polarizations, and receiving antenna gain pattern.

Degradation measurements were made at L-Band and UHF. The receiving antennas were mounted on a van about 2.4 meters above the ground. The antenna patterns were omni-directional in azimuth. Between elevation angles of 15° and 75° the gain varied only 3 dB. Below the horizontal the antenna gain was reduced at least 10 dB.

6.1 Multipath in a Mountain Environment

Experiments were conducted in canyon passes in Colorado, USA [Vogel and Goldhirsh, 1988]. The transmitter was located on a helicopter that flew behind the receiver, which was located on a van. A fixed distance and path depression angle were maintained between the transmitter and receiver. L-Band (1.5 GHz) and UHF (870 MHz) signals were used. The terrain through the canyon was varied. The wall facets were variable in height, orientation, foliage overlay, and distance from the roads. Patches of trees protruded from the canyon walls. The roads contained many twists and turns.

Distributions of fade depth were determined from these experiments. The measured data was modeled with a least square power curve fit.

$$P = a \times A^{-b} \qquad (6)$$

for

$$1\% \leq P \leq 10\%$$

where P is the percentage of distance over which the fade is exceeded, and A is the fade exceeded in dB. The curve fit parameters, a and b, are shown in Table 5.

Figure 3 contains curves of the cumulative fade distributions for path elevation angles of 30° and 45° at L-Band and UHF. Four runs of 87 km total length were taken through two canyon passes (Boulder and Big Thompson Canyons). Each curve on Figure 3 is

Table 5. Parameters for Best Fit Cumulative Fade Distribution for Multipath in Mountainous Terrain

Frequency (GHz)	Elevation = 30°		Elevation = 45°	
	a	b	a	b
0.870	34.52	1.855	31.64	2.464
1.5	33.19	1.710	39.95	2.321

derived from a subset of these four runs. The curve fits agree with the measured cumulative distribution data points to within 0.1 dB rms.

From Figure 3, the fades are 2 to 5 dB for the 45° elevation and 2 to 8 dB for the 30° elevation. The L-Band signals exhibit larger fades than the UHF signals. This could be due to tree fading, or there could have been reflecting facets on the canyon walls that were closer to the L-Band wavelength. The larger fades at 30° elevation angle can, in addition to reasons of scattering geometry, be attributed to the increased propagation path through trees and foliage.

6.2 Multipath in a Roadside Tree Environment

Experiments were conducted along tree lined roads in central Maryland, USA [Goldhirsh and Vogel, 1989]. The transmitter was located on a helicopter flying behind the receiver

carried by a vehicle. Measurement runs were repeated at 30°, 45°, and 60° elevation angles. Signals at UHF and L-Band were received. The measurements were relatively insensitive to path elevation. Therefore, the measurements were combined into a composite distribution for all three elevation angles. The measured data was modeled with an exponential curve fit,

$$P = u \times \exp(-vA) \qquad (7)$$

for

$$1\% \leq P \leq 50\%$$

where P is the percentage of distance over which the fade is exceeded and A is the fade exceeded in dB. The curve fit parameters, u and v, are shown in Table 6.

Figure 4 contains curves of the cumulative fade distributions for L-Band and UHF. The curve fits agree with the measured cumulative distribution data points to within 0.2 dB. Enhanced fading due to multipath would be expected for lower elevation angles (5° to 20°) where forward scattering from relatively smooth rolling terrain may be received from larger distances.

Table 6. Parameters for Best Exponential Fit Cumulative Fade Distributions for Multipath for Tree-Lined Roads

Frequency (GHz)	u	v	Fade Range (dB)
0.870	125.6	1.116	1-4.5
1.5	127.7	0.8573	1-6

REFERENCES

Bundrock, A., and Harvey, R. [1988], Propagation Measurements for an Australian Land Mobile-Satellite System, *Proceedings of Mobile Satellite Conference*, pp. 119-124.

Goldhirsh, J. and Vogel, W.J. [1989], Mobile Satellite System Fade Statistics for Shadowing and Multipath from Roadside Trees at UHF and L-band, *IEEE Transactions on Antennas and Propagation*, Vol. AP-37, No. 4, pp. 489-498, April.

Goldhirsh, J., and Vogel, W.J. [1992], Propagation Effects for Land Mobile Satellite Systems: Overview of Experimental and Modeling Results, NASA Reference Publication 1274, February.

Hase, Y., Vogel, W. J., and Goldhirsh, J. [1991], Fade-Durations Derived from Land-Mobile-Satellite Measurements in Australia, *IEEE Transactions on Communications*, Vol. 39, No. 5, pp. 664-668, May.

Vogel, W.J., and Goldhirsh J. [1988], Fade Measurements at L-band and UHF in Mountainous Terrain for Land Mobile Satellite Systems, *IEEE Transactions on Antennas and Propagation*, Vol. AP-36, No. 1, pp. 104-113, June.

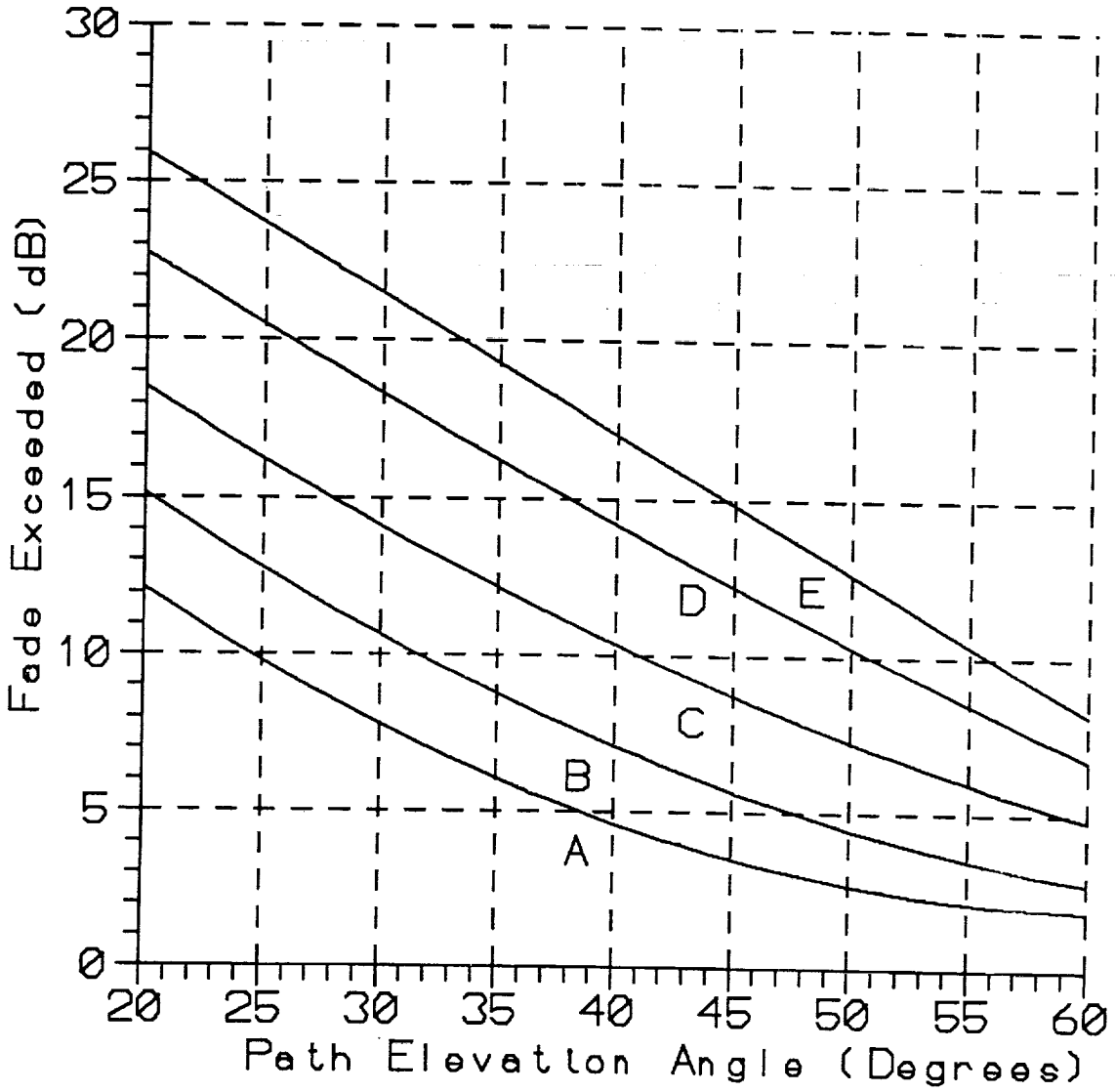

Figure 1. L-Band Fading due to Roadside Shadowing Versus Path Elevation Angle

A: P = 20%
B: P = 10%
C: P = 5%
D: P = 2%
E: P = 1%

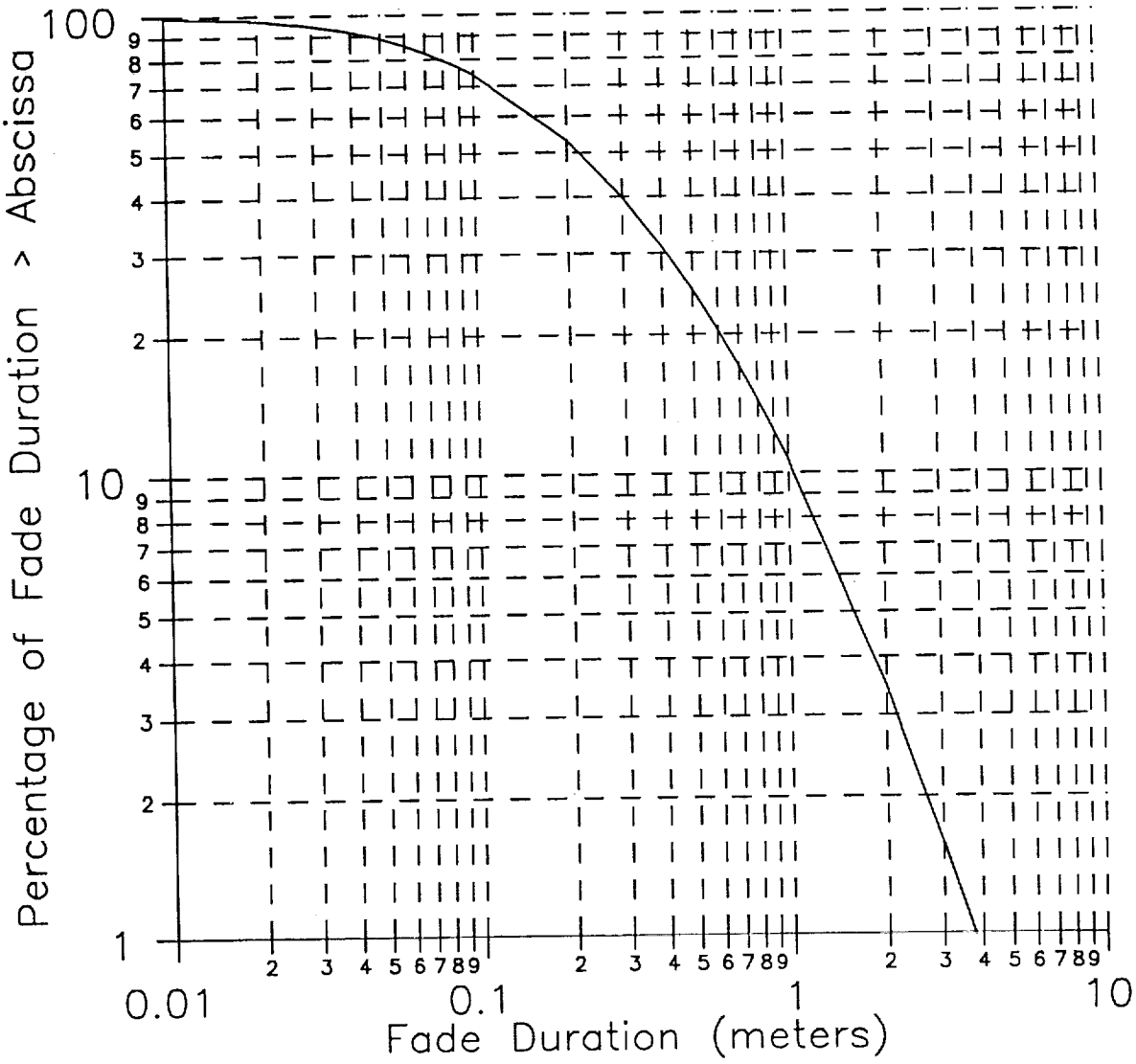

Figure 2. Best Fit Cumulative Fade Distribution for Roadside Tree Shadowing with a 5 dB Threshold

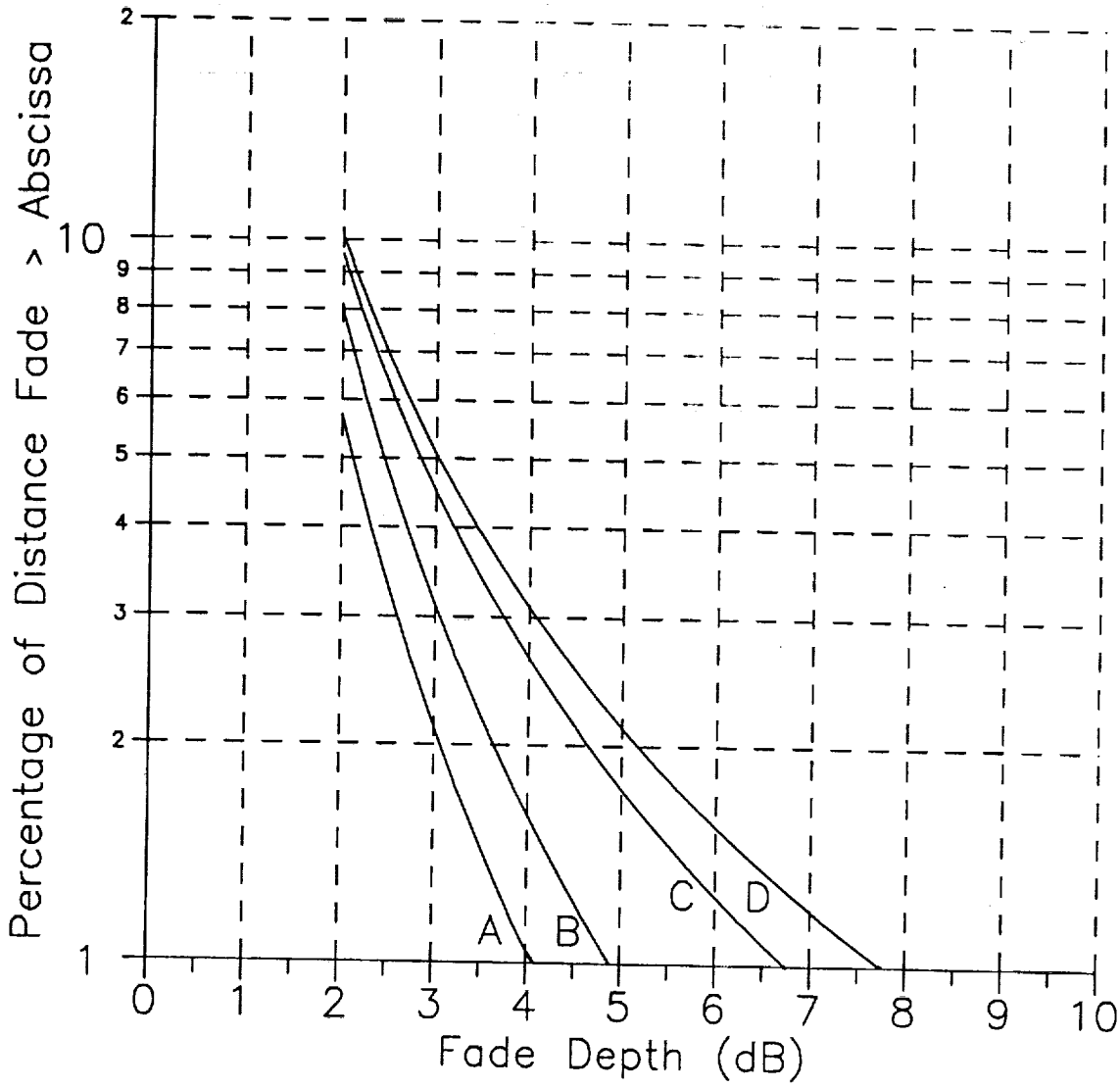

Figure 3. Best Fit Cumulative Fade Distributions for Multipath Fading in Mountainous Terrain

A: 870 MHz, 45 Degrees
B: 1.5 GHz, 45 Degrees
C: 870 MHz, 30 Degrees
D: 1.5 GHz, 30 Degrees

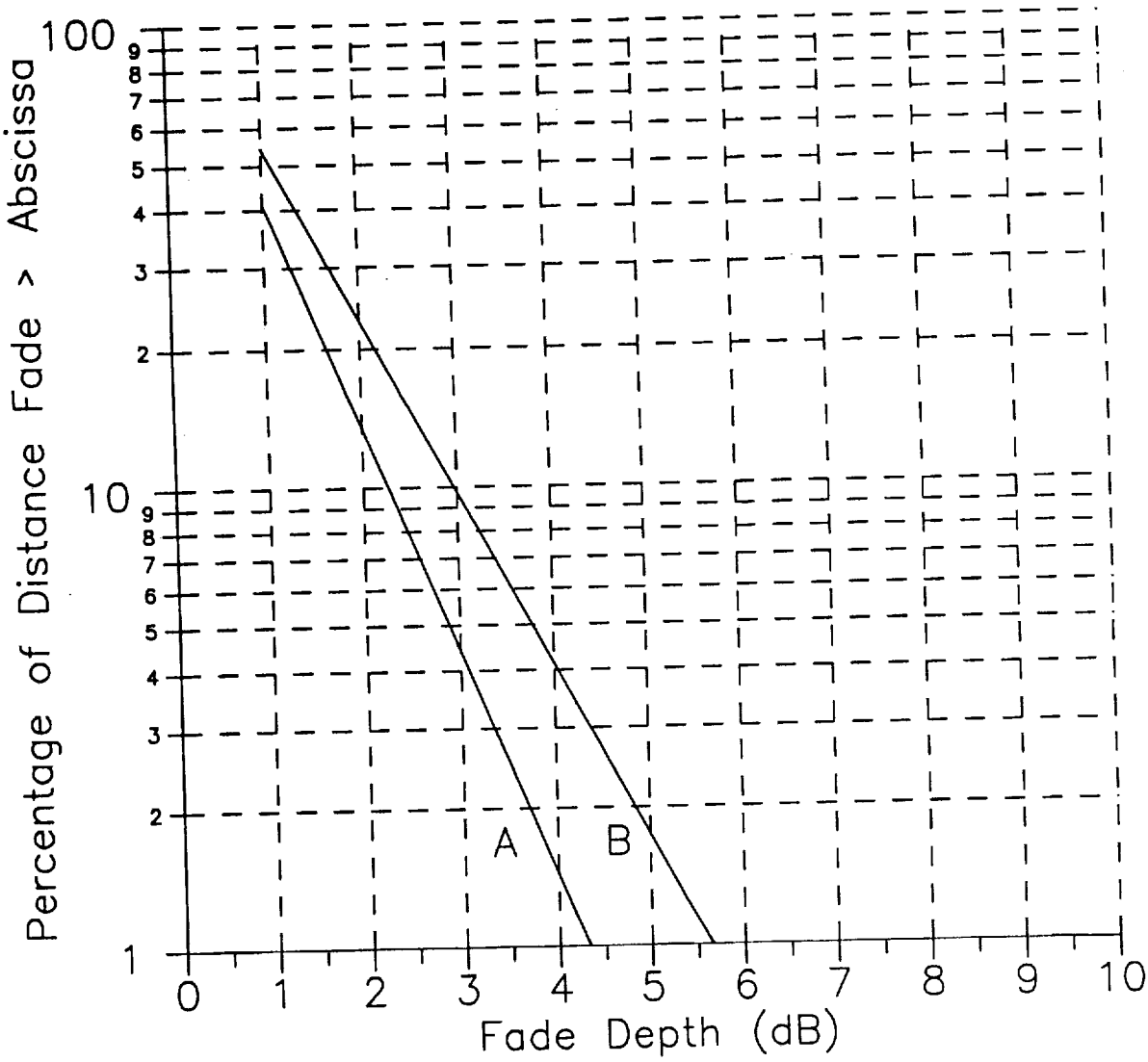

Figure 4. Best Fit Cumulative Fade Distributions for Multipath Fading on Tree-Lined Roads

A: 870 MHz
B: 1.5 GHz

PROPAGATION ISSUES FOR EMERGING MOBILE AND PORTABLE COMMUNICATIONS, A SYSTEMS PERSPECTIVE

Nasser Golshan,
Jet Propulsion Laboratory
California Institute of Technology
Pasadena, California 91109

I. INTRODUCTION

This paper presents the viewpoint of a system engineer regarding the format of propagation information and models suitable for the design of mobile and portable satellite communications systems for the following services: audio broadcast, two way voice, and packet data.

II. PROPAGATION IMPAIRMENTS FOR PORTABLE INDOOR RECEPTION IN SATELLITE COMMUNICATIONS SYSTEMS

The propagation experiments conducted by the University of Texas [1] for the NASA/VOA DBS-R Program have provided critical information on

The overall signal attenuation into buildings and the variation of such attenuation with frequency,

The fine signal structure (spatial and spectral) inside buildings.

However these measurements have the following limitations:

- Measurements were conducted over the 0.75 to 1.8 GHz and the results extrapolated to 3.0 GHz; it would be very useful to extend the measurements to 3.0 GHZ.
- Measurements were conducted using a low gain antenna; corresponding information regarding moderate gain antennas (6-12 dBic) is needed.
- Measurements were conducted using a transmitter atop a mast to simulate the satellite signal; validation using a satellite signal is needed.
- Measurements were conducted inside a few buildings; a larger data-base is required to define the morphological characteristics for indoor satellite reception in various types of buildings around the world.

III. PROPAGATION IMPAIRMENTS AND MITIGATION TECHNIQUES FOR MOBILE SATELLITE COMMUNICATIONS SYSTEMS

The most significant propagation impairment for mobile reception is the intermittent blockage of satellite's line of sight by roadside objects such as trees, buildings, utility poles, highway signs, hills, etc.

Despite the intermittent interruptions of the radio link, a relatively uninterrupted voice circuit has to be maintained for audio broadcast and duplex voice applications. Short interruptions of the RF signal can be mitigated by combination of interleaving and channel coding. Interleaving duration is limited in the order of 30 msec for duplex voice but can be as high as 1 second for audio broadcasts.

Satellite Packet Networks communicate via small data packets. Lost packets due to intermittent signal blockage can be repeated in ARQ systems. Although interleaving is not absolutely necessary for packet data, the channel performance improves if forward error correcting codes with interleaving length equal to packet size are adopted.

IV. CHARACTERIZATION OF MOBILE SATELLITE COMMUNICATIONS CHANNELS IN THE PRESENCE OF ROADSIDE BLOCKAGE WHEN INTERLEAVING AND FEC CODING ARE IMPLEMENTED

The model to be presented here tries to directly describe the performance of mobile satellite communications systems in the presence of roadside blockage when interleaving and FEC are implemented. The model needs to satisfactorily describe both the fine structure of the signal under fading/shadowing conditions, and the morphological aspects of the reception environments. The present paper presents a methodology to model the fine structure of the signal on the scale of the interleaving block. We are also exploring models to present the morphological aspects of the reception environment; this will be reported later.

IV.1 CHARACTERIZATION OF SHORT-TERM MOBILE SATELLITE SIGNAL VARIATIONS

The temporal statistics of the satellite signal received by a mobile receiver during one interleaver block can be best described by the cumulative distribution of the signal recorded during the same period. Since interleaving removes the signal level correlation among adjacent signal samples, the second (and higher) -order statistics of the signal within the interleaver is not needed to determine the performance of the decoder over the interleaver block. The block-by-block performance of the channel decoder can be estimated as described below from the cumulative signal distribution for each block.

Figure 1 shows a typical example of cumulative signal distribution [2] for mobile reception at L-band (1.5 GHz) with heavy signal interruption by foliage. Next we will estimate the required link margin so that a typical block of data with the given cumulative signal distribution can be satisfactorily detected by the combination of interleaving and FEC. The estimation will be performed by approximating the continuous fade distribution as the envelope of a number of step-distributions A1, A2, A3, ... as shown in Figure 1. For example step distribution A1 describes a situation where the signal is suffering from hard blockage 30% of the time and soft blockage of 2.7 dB the remainder 70% of the time. An examination of Figure 1 shows that A1, A2, A3, ..., are conservative estimates of the continuous fade distribution. For each step-distribution we will estimate the required link margin for the proper operation of the decoder. As we can choose any one of the step-functions to approximate the actual signal distribution, the minimum link-margin calculated over the family of step-functions will be chosen as an estimate of the required link margin for the interleaver block in question.

Figure 2 shows an upper bound on the degradation of a Viterbi decoder when the signal is completely blocked during a given percentage of the interleaver block. This figure is based on the ongoing work on DBS-R at JPL [3]. The result is given as a blockage penalty which is defined as the additional link margin compared to the unblocked signal for a Bit Error Rate (BER) performance of 1.0 E-4.0. This figure is based on the assumption of convolutional encoding with constraint length 7 and assumes channel state information is available to the decoder. Figure 3 shows the superposition of the soft-fade and hard-fade penalties from Figures 1 & 2. The sum of the fade-depth for the soft-blockage and the penalty for the hard-blockage provides an upper limit for the link margin required for the satisfactory decoding of this signal distribution (L-band under heavy roadside blockage conditions) by the Viterbi decoder. As discussed in the preceding paragraph the required link margin is the minimum value of the link-margin envelope, namely 6.1 dB for the rate 1/2 convolutional coding and the assumed L-band fade distribution. The link margin requirements presented in Figure 3 for L-band can be extended to S-band by using the experimental finding that the soft fade due to roadside vegetation at one frequency can be scaled to another frequency in proportion to the square root of the frequency [4]; the results are given in Figure 4. Finally the estimated link margin requirements for the four cases under considerations (two code rates of 1/2 & 1/3 and two frequencies L & S-band) are compared in Figure 5.

IV.2 CHARACTERIZATION OF LONG-TERM SIGNAL VARIATIONS

Mobile signal attenuation data for an arbitrary length of roadway can be divided into blocks each corresponding to one interleaver distance (the product of the interleaver duration and the vehicle speed). Typical interleaver distances for mobile voice and packet data satellite communication applications are given in table 1. Then the link margin required for satisfactory reception of each block of signal can be estimated as described in section IV.1. The end result is a time series listing the link margins required for reception of each interleaver block of the data. The results may also be presented in more compact form as a link margin distribution. Link-margin time series and distributions are very useful for trading design link-margin versus system performance. We are also exploring this model to present the morphological aspects of the reception environment. Results will be reported later.

V SUMMARY AND CONCLUSIONS

The propagation experiments conducted by the University of Texas for the NASA/VOA DBS-R Program provided adequate models on the overall signal attenuation into buildings and the fine signal structure (spatial and spectral) inside buildings. These measurements based on the use of a transmitter atop a mast to simulate a satellite signal over the frequency range of 0.75 to 1.8 GHz need to be extended to 3 GHz and also validated using a signal source on a satellite such as TDRS.

While a substantial volume of data exists regarding fade statistics for mobile reception of UHF, L, and S-band signals from satellites, system engineers will greatly benefit if the results are converted into link margin statistics. The link margin statistics will be system specific. A simple procedure for converting fade statistics into link-margin statistics has been worked out for a system using interleaving and convolutional (rates 1/2 and 1/3) error correcting channel coding.

Acknowledgment

The research described in this report was carried out by the Jet Propulsion Laboratory, California Institute of Technology, under a contract with the National Aeronautics and Space Administration.

References

[1] Vogel, W.J. and G.W. Torrence, "Signal Variability Measurements for Satellite Radio Broadcasting into Buildings", Technical Report No. 9101, Electrical Engineering Research Laboratory, The University of Texas at Austin, January, 1991.

[2] Goldhirsh, Julius, and W.J. Vogel, "Mobile Satellite System Fade Statistics for Shadowing and Multipath from Roadside Trees at UHF and L-band", IEEE Transactions on Antennas and Propagation, Vol. AP 37, No. 4, April 1989, pp 489-498.

[3] Simon, M., "Analysis of Channel Performance in a Shadowing Environment for DBS-R Receiver Development", Interoffice Memorandum 3392-92-039, JPL, 1992.

[4] Goldhirsh, Julius, and W.J. Vogel, "Results of 1987 Helicopter Propagation Experiments at UHF and L-band in Central Maryland", Proceedings of NAPEX XII, June 1988, JPL Publication 88-22, pp 18-26.

Figure 1. Cumulative fade distribution for mobile reception on a typical stretch of road with severe blockage of the signal by roadside trees

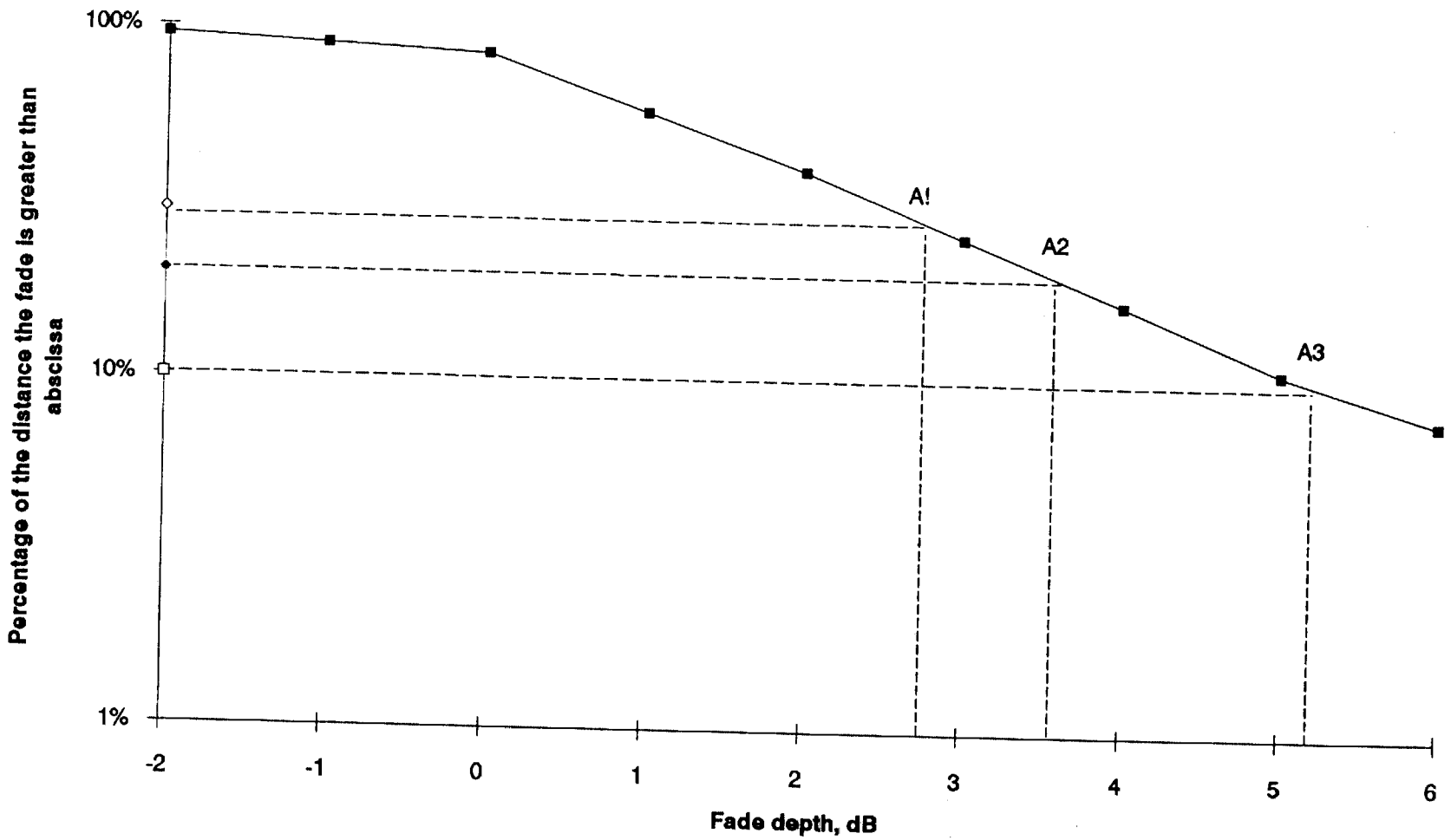

Figure 2. Eb/No penalty for partial hard blockage for BER objective of 1.0 E-4, Gaussian channel with hard blockage, Conv code with k rates 1/2, 1/3, and 1/4

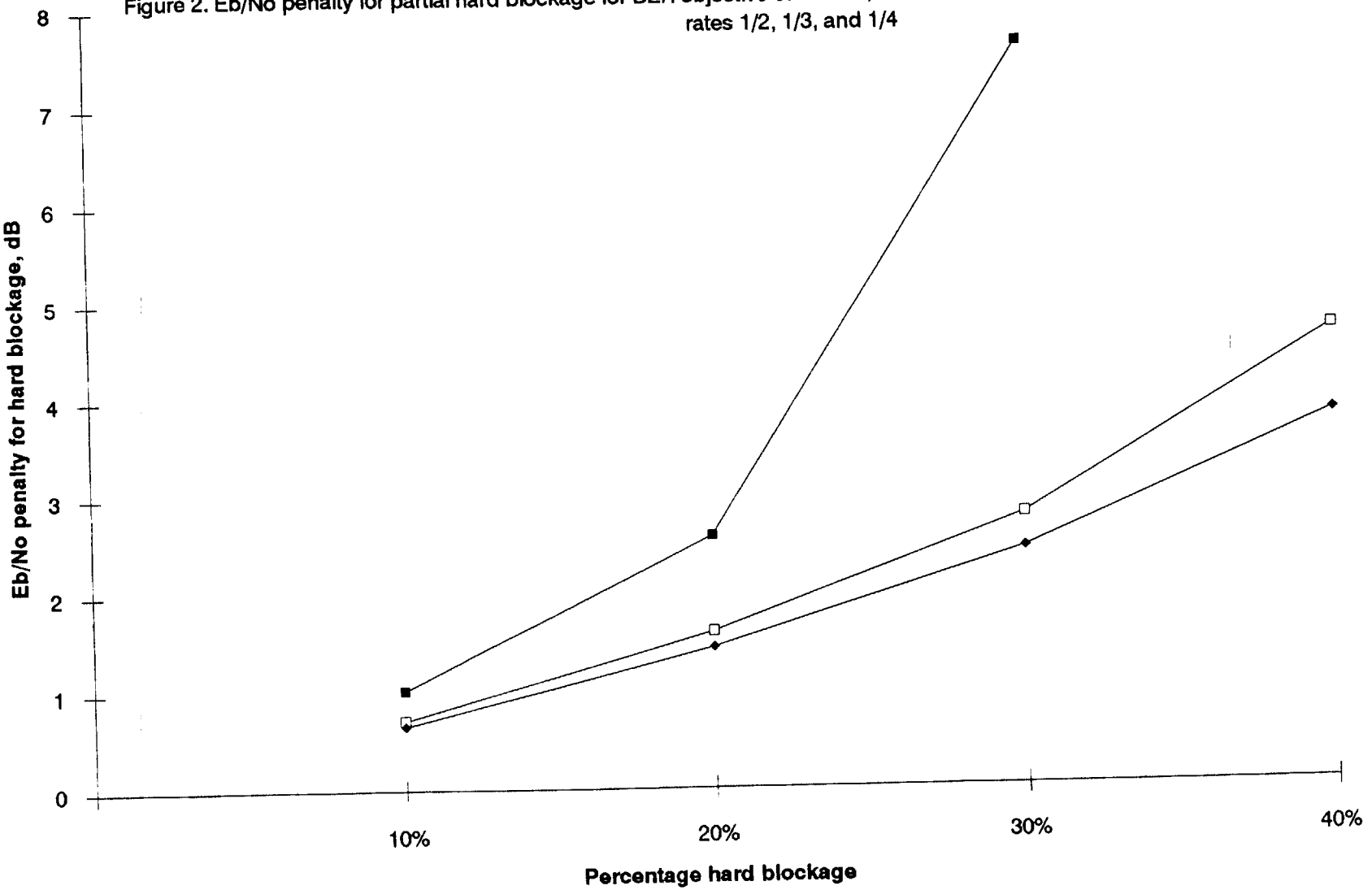

Figure 3 Soft fade-depth and additional penalty due to hard blockage for the typical example of heavy signal blockage

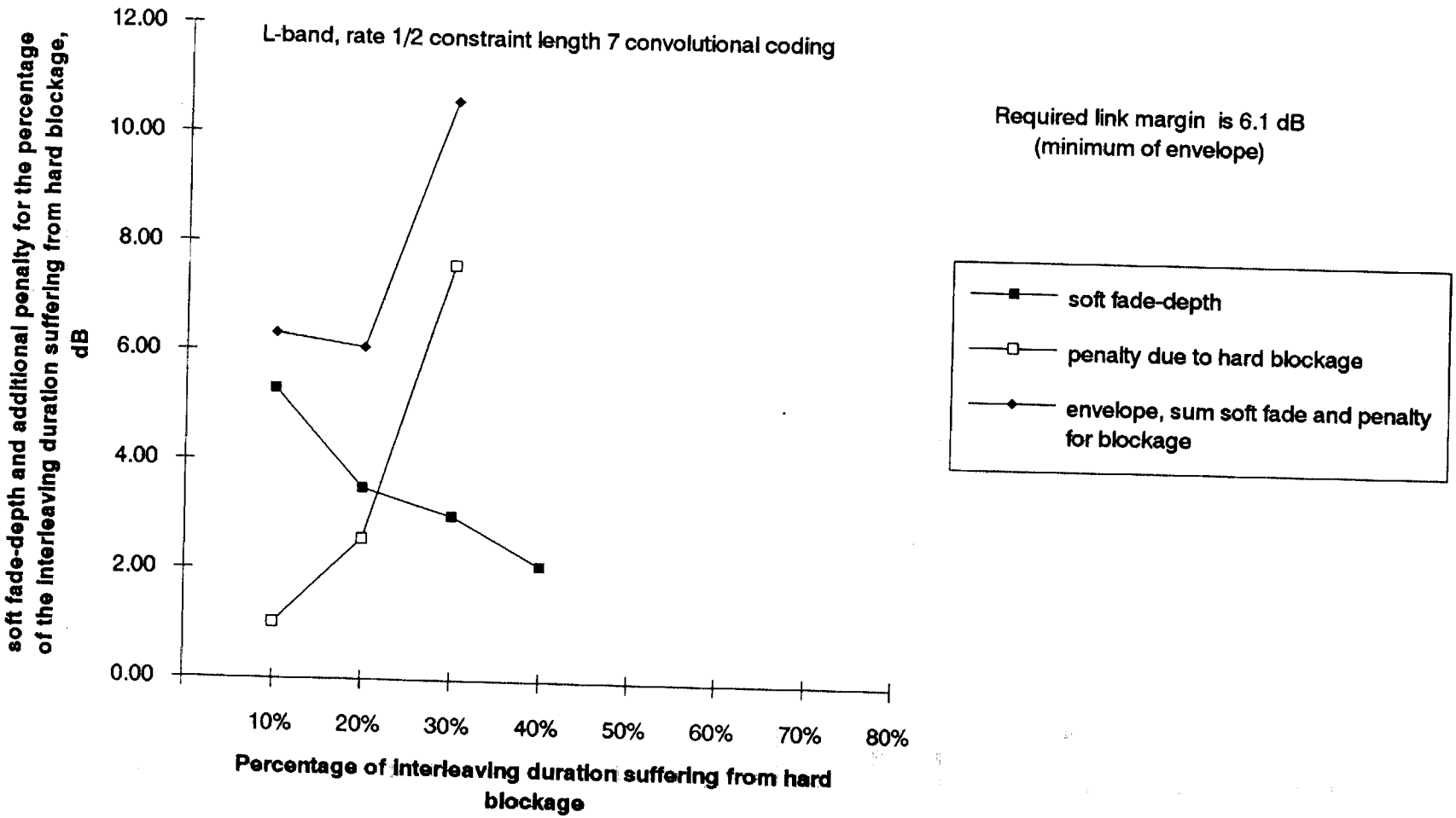

Figure 4 Soft fade-depth and additional penalty due to hard blockage for the typical example of heavy signal blockage

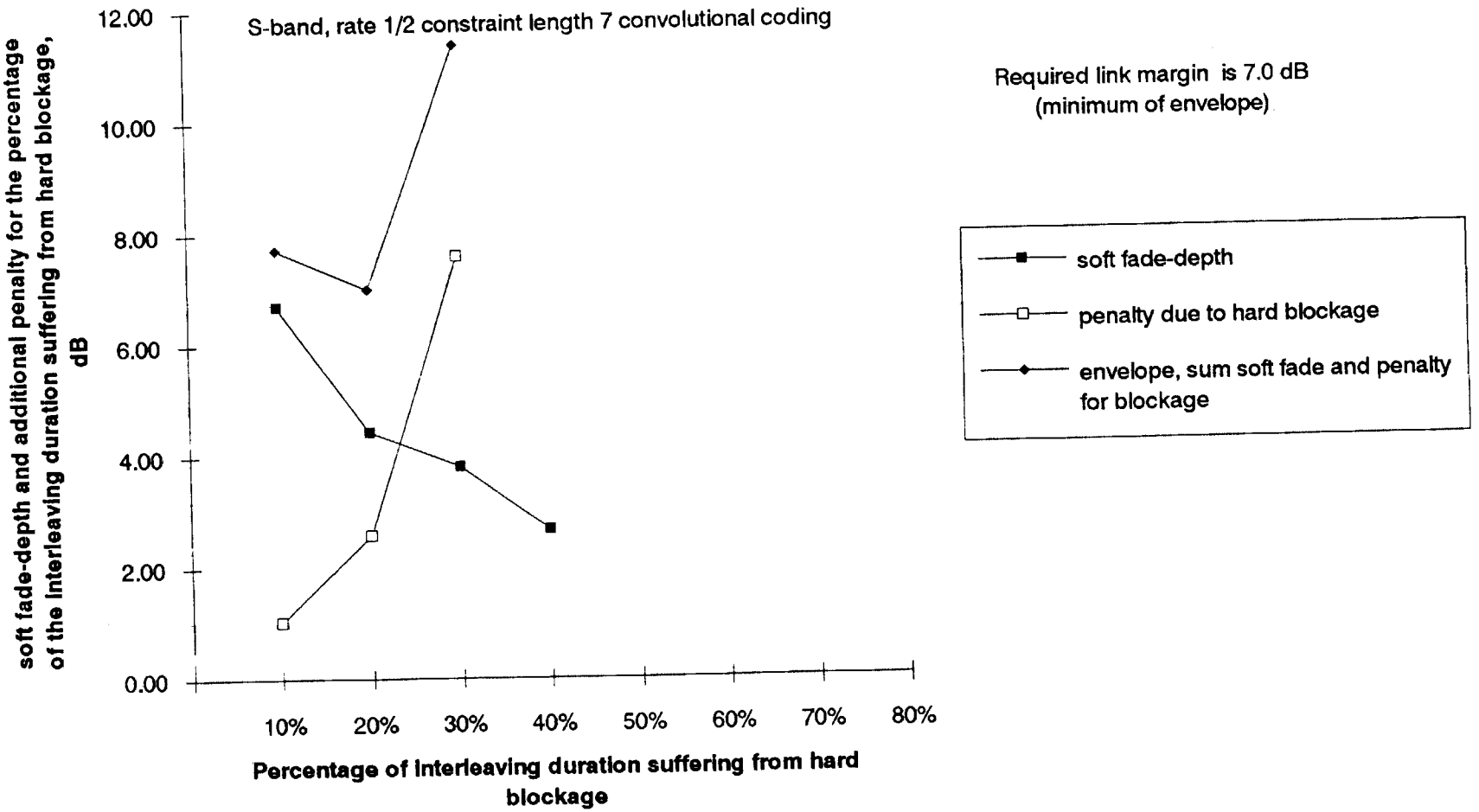

Figure 5. Envelope of estimated link margin for the approximate blockage model for the typical example

required link margin (minimum of the envelope:)

6.1 dB for L-Band, rate 1/2 coding

5.1 dB for L-Band, Rate 1/3 coding

7.0 dB for S-Band, Rate 1/2 coding

6.0 dB for S-Band, Rate 1/3 coding

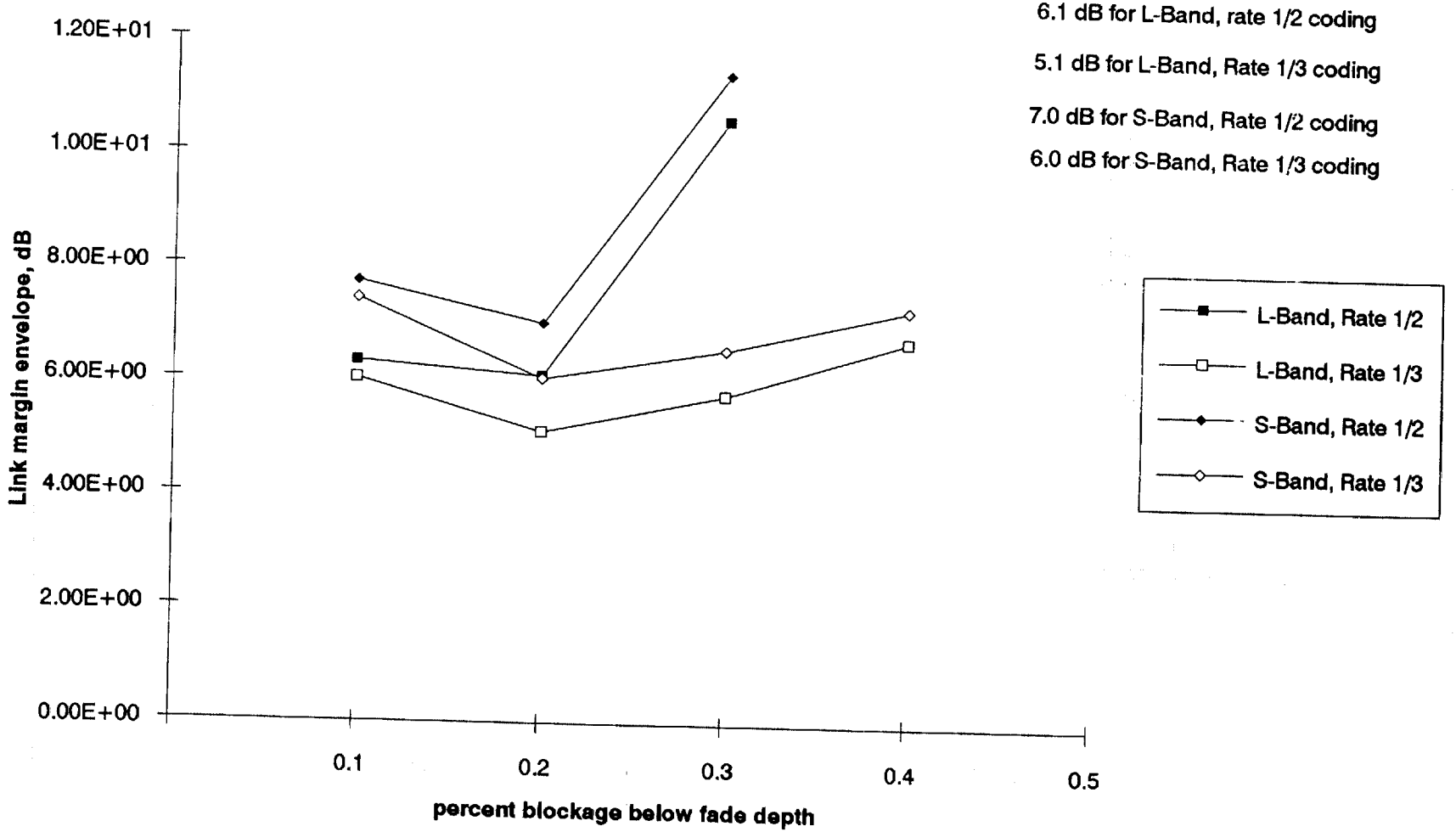

Table 1 Typical interleaving distances for mobile reception of satellite audio broadcast, voice communication and packet data.

SERVICE	SPEED KM/HOUR	INTERLEAVING SIZE DURATION (S)	DISTANCE(M)
DUPLEX VOICE	36	0.03	0.3
DUPLEX VOICE	72	0.03	0.6
DUPLEX VOICE	108	0.03	0.9
AUDIO BROADCAST	36	0.50	5.0
AUDIO BROADCAST	72	0.50	10.0
AUDIO BROADCAST	108	0.50	15.0
PACKET DATA*	36	0.05	0.5
PACKET DATA*	72	0.05	1.0
PACKET DATA*	108	0.05	1.5

* FOR A TYPICAL 264 bit packet-size over a 4.8 kbps channel

PROPAGATION CONSIDERATIONS IN THE AMERICAN MOBILE SATELLITE SYSTEM DESIGN

CHARLES KITTIVER & ED SIGLER
American Mobile Satellite Corporation

ABSTRACT

This paper presents an overview of the AMSC MSS system with special emphasis given to the propagation issues that were considered in the design. The aspects of the voice codec design that effect system performance in a shadowed environment are discussed. The strategies for overcoming Ku-Band rain fades in the uplink and downlink paths of the gateway station are presented. A land mobile propagation study that has both measurement and simulation activities is described.

INTRODUCTION

American Mobile Satellite Corporation (AMSC) is currently in the process of developing a satellite communications system to provide mobile satellite services (MSS) to North America. In 1990 contracts were awarded to Hughes Aircraft Company with SPAR as a major subcontractor for the development of an L-Band satellite to provide MSS services. The satellite will be launched in 1994 with an approximate service start date in late 1994.

Currently the Communications Ground Segment (CGS) of the MSS system is in the process of being developed by Westinghouse Electric Company (WEC). WEC was awarded the contract for the CGS in April 1992. WEC will also be providing production model mobile terminals (MT) for use by system subscribers. Mitsubishi Electric Company (MELCO) is a second supplier of production model MTs.

This paper will first provide an overview of the AMSC MSS system and then discuss details of the propagation issues considered in the design.

SYSTEM OVERVIEW

Figure 1 shows an overview of AMSC's MSS system. The MSAT satellite acts as a "bent pipe" repeater, receiving and transmitting modulated signals to/from the mobile terminals at L-band and relaying them to terrestrial users via Feederlink Earth Stations (FES) at Ku-band. The AMSC network will provide mobile telephony and data services primarily to vehicles like automobiles, trucks, ships, and aircraft. The basic electronics of the MT for each of these mobile applications will be similar with the major differences being

in the antenna and packaging to account for the special environmental conditions encountered. In addition, the aviation applications may require special electronic circuitry to accommodate the greater maneuverability and resulting higher doppler frequency shifts of these mobile platforms.

The MSS system will be designed to provide voice, data and facsimile services. The voice will be digitally encoded using the IMBE (Improved Multi-Band Excitation) algorithm developed by DVSI (Digital Voice Systems, Inc.) which operates at rate of 6.4 KPBS, including FEC. The digital voice signals and/or the data and facsimile signals will modulate a narrow band carrier using QPSK at a rate of 6.75 KBPS, including frame overhead. The modulated signals from the mobile terminals and the FESs will access the satellite using demand assigned SCPC.

There will be two types of FESs in the AMSC system; namely gateway stations and base stations. Gateway stations provide a means for signals from the MTs to be routed via the Public Switched Telephone Network (PSTN) to any terrestrial telephone in the world. Base stations are intended to provide service to a private network user. As such these base stations will allow for limited access to the PSTN.

AMSC will locate its principal gateway FES at a site in Reston, Va. adjacent to our new headquarters building. This FES site will use an 11 meter antenna to provide high availability.

The real time control of the AMSC system is accomplished from a Network Control Center (NCC). The system has been designed to operate with two NCCs, one active and one in a "hot" standby mode ready to take control in the event of a failure of the active station. The backup NCC will be provided and installed at a different location at a future date. The chief function of the NCC is to control the assignment of specific frequencies to the MTs and the FESs to set up a circuit (either voice, data or facsimile) over the satellite. These frequency assignments are made in real time for the duration of each call, so that the power and bandwidth resources of the satellite are available for all systems users on a demand basis.

The function of the Network Operations Center (NOC) is to administer the operation of the system. The NOC collects (from the NCC) and stores call detail records to allow the AMSC billing system to prepare customer bills. It also collects satellite circuit usage records to forward to various engineering and operations personnel for use in analyzing network performance and health. The NOC also contains displays to allow operators to monitor and control the status of the system.

Figure 2 is an artist's conception of the AMSC satellite. The satellite is a three axis stabilized

spacecraft built by Hughes Aircraft Co. with SPAR responsible for the communication subsystem, including antennas. The satellite uses HAC's 601 bus. The spacecraft is being specified to be launched with either an Altlas 2A or Ariane 4 vehicle. The dry mass of the satellite is approximately 2700 lbs with a separation weight of 6425 lbs (Atlas 2A).The solar arrays are capable of providing 3600 watts at end-of-life, equinox.

When the satellite is fully deployed (antennas and solar panels) in-orbit, it will extend to 825 inches (tip-to-tip solar arrays) and 745 inches (antenna edge-to-antenna edge). The design life of the satellite is 15 years with a fuel life of 10 years.

Elliptical unfurlable mesh antennas provide the L-band coverage for the satellite. These antennas are offset feed and are 6 by 5 meters in size. There are separate transmit and receive L-Band antennas. The L-band antennas provide 6 spot beams that cover CONUS and the off-shore points of Alaska, Hawaii, and Puerto Rico.

A single Ku-band antenna, for transmit and receive, is mounted on the earth viewing face, or sub-nadir panel. This antenna is a 30 inch shaped reflector designed to provide coverage for all the land masses of North America including Hawaii and Puerto Rico using two feed horns. The main feed provides nearly uniform coverage over the continental areas plus Puerto Rico while the second feed provides a spot beam over Hawaii.

SERVICE QUALITY CONSIDERATIONS

AMSC will be the one of the first entities to provide MSS services to land mobile platforms. There have been many experiments and field trials of land mobile MSS services throughout the world, that support the viability of these services. However, these experiments and field trials can not be used to accurately predict the quality of the AMSC system throughout our diverse and extensive service area

The remainder of the paper describes those key elements of the AMSC system that determine the overall quality of the system and how these elements have been designed to enhance system performance. These key elements are the voice codec and the RF links or propagation paths between the satellite and the land mobile terminal. In addition, an overview of a propagation study program that will help predict AMSC's service quality, will be provided.

LINK BUDGET OVERVIEW

General

A full presentation of the AMSC link budget and the underlying assumptions is beyond the scope of this presentation, but Table 1 summarizes the results of our link analysis.

In Table 1, the uplink margin is defined as that additional loss that can occur in the uplink path before the received BER into the voice codec exceeds a specified bit error rate (BER), in this case 1×10^{-2}. Similarly, the downlink margin is defined as that additional loss that can occur in the downlink before the specified BER is exceeded. (Note that results of extensive subjective testing on the DVSI IMBE voice codec shows that good voice quality is obtained at a BER of 1×10^{-2}. Actually, acceptable voice quality is obtained with a codec input BER of 4×10^{-2}.

TABLE 1 LINK BUDGET SUMMARY

PARAMETER	FORWARD LINK	RETURN LINK
DOWNLINK MARGIN	≃4.0 dB (K= 10dB) ≃5.5 dB (AWGN) @ L-BAND	≥ 10 dB @ Ku-BAND
UPLINK MARGIN	≃3.0 dB (K= 10dB) ≃4.5 dB (AWGN) @ Ku-BAND	≃5.0 dB (K=10 dB) ≃6.5 dB (AWGN) @ L-BAND
UPLINK POWER CONTROL	≥ 10 dB	NONE

Ku-Band

Since the links from the FES are at Ku-Band, the MSAT link design must account for infrequent periods of severe rainfall induced attenuation. In the forward link uplink, an uplink power control system has been designed into the FES. This power control system will adjust the uplink power transmitted to the satellite based upon the received level of the Uplink Power Control Beacon (UPC) of the satellite. This UPC beacon has been specifically designed to be used as a stable reference for controlling the transmitted power of the FESs in the MSS. The dynamic range of this power control system is in excess of 10 dB.

The return link downlink is also at Ku-Band. With an 9 to 11 meter antenna at our Reston, Va FES site, a downlink margin in excess of 10 dB is obtained on this link. In order to account for periods when the rain attenuation is greater than 10 dB, which occur for about 2 to 4 hours per year total in the Washington, DC area, a diversity RF site will be installed.

Figure 3 is a simplified block diagram of the FES showing the RF diversity site. The RF diversity site will replicate the RF portions (i.e.; antenna, LNA, HPA, & up-down-converters) of the FES at a site about 10 to 15 miles from Reston, Va. An innovative feature of this diversity scheme is the fiber-optic interconnection between the prime and diversity site.

The fiber-optic interconnecting facility will be leased from either TELCO or other private fiber optic providers in the Washington D.C. area. This fiber optic link will carry the IF output of the approximately 2000 channels units located at Reston, Va. Thus the IF signal will be 2000 narrow band QPSK carriers occupying a 200 MHz bandwidth at approximately 1 GHz.

AMSC investigated the state-of-the-art in fiber optic transmission and found a company in California, Ortel, that made several devices that were capable of handling these analog signals. AMSC also found the local Bell operating company quite receptive in exploring the possibility of providing us with a service using these Ortel devices and their extensive fiber facilities.

As far as we know, AMSC's will be the first domestic satellite company to use site diversity to improve service availability. There have been several experiments done to verify and quantify the improvement to be expected through the use of site diversity, but no system has gone operational. AMSC expects that the use of diversity will decrease the downtime due to rainfall attenuation by a factor of 20. Thus resulting in rainfall attenuation induced outages at the two sites of 6 to 12 minutes per year.

L-Band

The L-band uplink and downlink margins vary from 4 dB to about 6 dB, depending on the which link (forward or return) and the link conditions, AWGN or a multipath Ricean K factor of 10 dB. AMSC anticipates that the demodulator in the MT and channel units at the FES will use a form of MSDD (Multi-Symbol Differential Detection) that will perform quite well in a multipath environment without losing much performance over coherent detection.

The margins are limited at L-Band due to the constraints that are placed on the mobile antenna in order to be economical and attractive to AMSC's typical customers. These

margins will not be sufficient to overcome the blockage when the vehicle is fully shadowed by a tree trunk or building. The voice codec selected by AMSC has been designed to overcome outages of short durations, about 100 ms or less, so that when the vehicle is moving past a tree at any typical speed, acceptable voice quality will be obtained in spite of the short blockage.

However, AMSC expects there will be conditions of such dense vegetation and or terrain blockages, that even AMSC's robust codec will experience a temporary outage. AMSC's propagation research effort has been focused on determining to what extent and at what locations these outages will occur. This propagation program will be described later.

CODEC

The DVSI IMBE codec was selected after several rigorous competitive subjective listener tests that were conducted for both INMARSAT and AMSC. A key part of the test was the evaluation of the codec's voice quality when subjected to periodic bursts of high BER. In fact, these high bursty BER conditions were designed to match the road conditions of both heavily and moderately shadowed roads. Actual roadside shadowing data was used to create the burst error patterns.

The DVSI codec scored the best (i.e.; provided the highest voice quality according to the test listeners) among those tested, while experiencing these bursty error conditions. The strategy employed by the decoder is to repeat certain model parameters of the previous good frame of encoded voice (a typical frame is 20 ms) when a frame with high error rate is received. By repeating these model parameters, natural sounding voice is obtained although there may be a slight loss in speech content. This strategy of repeating frames continues for about 5 bad frames or 100 ms, if more bad frames are received after this period, the output of the codec is muted.

Furthermore, in the subjective testing of the codec over simulated roadside shadowing conditions, it was observed that the acceptable voice quality was obtained even if as much as 10% of the voice frames are badly corrupted.

Thus, the purpose of AMSC's propagation research effort is to determine how well the robust strategies of the DVSI codec will perform when exposed to the roadside conditions that exist throughout our service area. To accomplish this task, a two-pronged approach was adopted, measurements and simulations as described in the next section.

PROPAGATION STUDY PROGRAM

Measurement Program

In the summer of 1993, AMSC intends to perform a

propagation experiment using a Standard M terminal and INMARSAT satellites in the Atlantic Ocean region. (Note that the Std M terminal uses nearly the identical codec that AMSC will use.) This test will probably be made over the same Route 295 that was part of Vogel and Goldhirsh's (see Reference) earlier propagation experiments.

In the planned AMSC test a Standard M voice channel will be setup over INMARSAT III satellite at 55° W. Longitude to a terminal that will be specially mounted in a pickup truck. The pickup truck will be equipped with an video camera that will be used to visually record the surrounding landscape while recording the voice quality received by the Std M terminal. In this fashion, AMSC engineers will be able to correlate voice quality with roadside conditions. The test run will be repeated using the AORE INMARSAT III satellite at 15° W. Longitude.

In order to extrapolate the experimental data obtained in the test described above to areas throughout CONUS the simulation program described below was developed for AMSC by CS Communications of Vienna, Va.

Propagation Simulation Program

AMSC will also develop a computer simulation model to estimate communications availability taking into account blockage due to terrain and vegetation.

The foundation of the model is built using dBase III and Clipper 5.0. For terrain information the model uses US Geologic Survey (USGS) electronic topographic data. The model further includes the aggregate effects of vegetation via USGS Land Use/Land Cover (L-series) data. Potential customers are primarily concerned with communications performance along transportation routes: Interstate, primary, secondary, rail line, inland waterways, etc. To provide this feature, US Census Bureau "TIGER" files are used.

The model combines the topographic, land cover, and transportation route information to provide an estimate of satellite visibility at points selected along a user specified route. The points can either be automatically generated based upon on equal spacing between points or selected by hand. At each point, an estimate of link margin is used to determine the communications availability of the point.

The link margin estimate is computed assuming user tolerance of 4 to 6 dB, of codec performance degradation. It was deemed unreliable to make point-wise availability estimates with the level of data detail provided by the topographic and land cover data sources, since L-band propagation is specific to the individual tree limb level. AMSC's intent is to use the estimate path length through any trees and the density of the tree cover to calculate a path

loss due to tree absorption. The calculated path loss is then subtracted from the margin to determine if the point is "available" for communications. In aggregate, the points along the route will converge to the approximate mobile communications availability along the selected route.

Currently, AMSC is using the model to prepare an overall availability estimate for CONUS and on a region by region basis. A matrix of 5 terrain types and 5 vegetation types was created. A matrix applies to an elevation range (30° to 40°,40° to 50°,and 50° to 60°). Geographic areas from the US were selected which met the terrain/vegetation characteristics and the elevation angle ranges. Each geographic area will be simulated with a set of routes chosen such that satellite orientation will not effect the availability estimates. The entire contiguous US has been divided into 0.5° by 0.5° blocks. The blocks are characterized and categorized into the appropriate terrain/land cover type and elevation angle range. The aggregate availability for the US and other geographic divisions can then be calculated.

By comparing the results of the measurement program using the Std M terminal with the model derived availability estimate for the same route, AMSC can establish the validity of the simulation model. Additional measurements versus model comparisons will be performed on routes with varied terrain and vegetation to further validate the propagation model.

SUMMARY

The AMSC MSS system has been designed to provide good quality voice services throughout CONUS and the off-shore regions of Alaska, Hawaii, and Puerto Rico. Uplink power control and site diversity will ensure high availability from the FES or gateway earth station. Characterization of the L-Band land mobile satellite path for the AMSC service areas, is an on-going AMSC activity involving measurements and computer modelling and simulations. A robust voice codec, that has been rigorously tested in several competitive evaluations, has been selected for the AMSC system. These competitive tests included subjective evaluations of the voice codec performance over simulated roadside shadowed environments.

Reference: Vogel, W.J. & J. Goldhirsh, "Mobile Satellite System Propagation Measurements at L-Band Using MARECS-B2" IEEE Trans. Antennas & Propagation, Vol AP-38,no 2, pp 259-264 Feb.1990

MSS System Overview

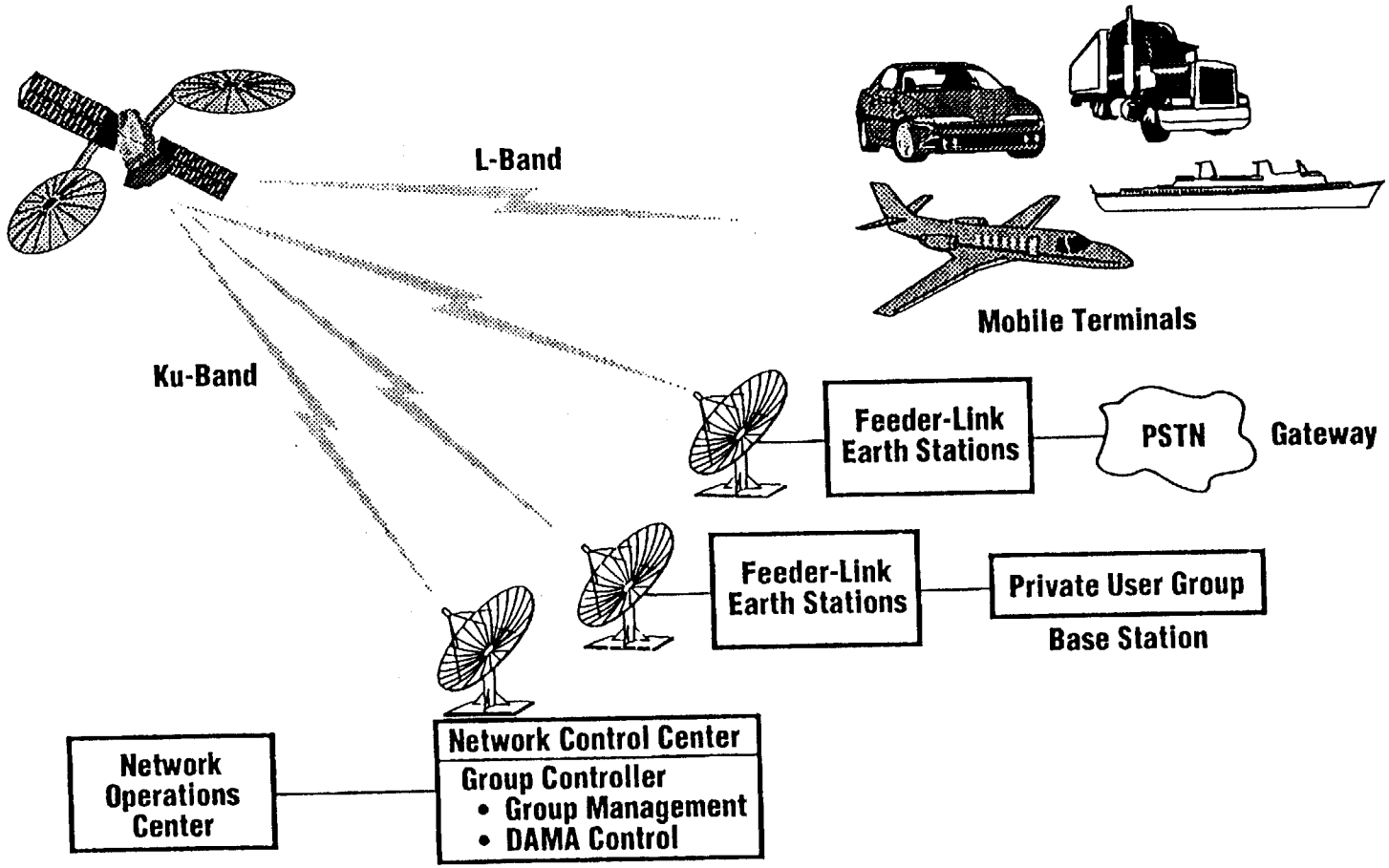

FIGURE 1

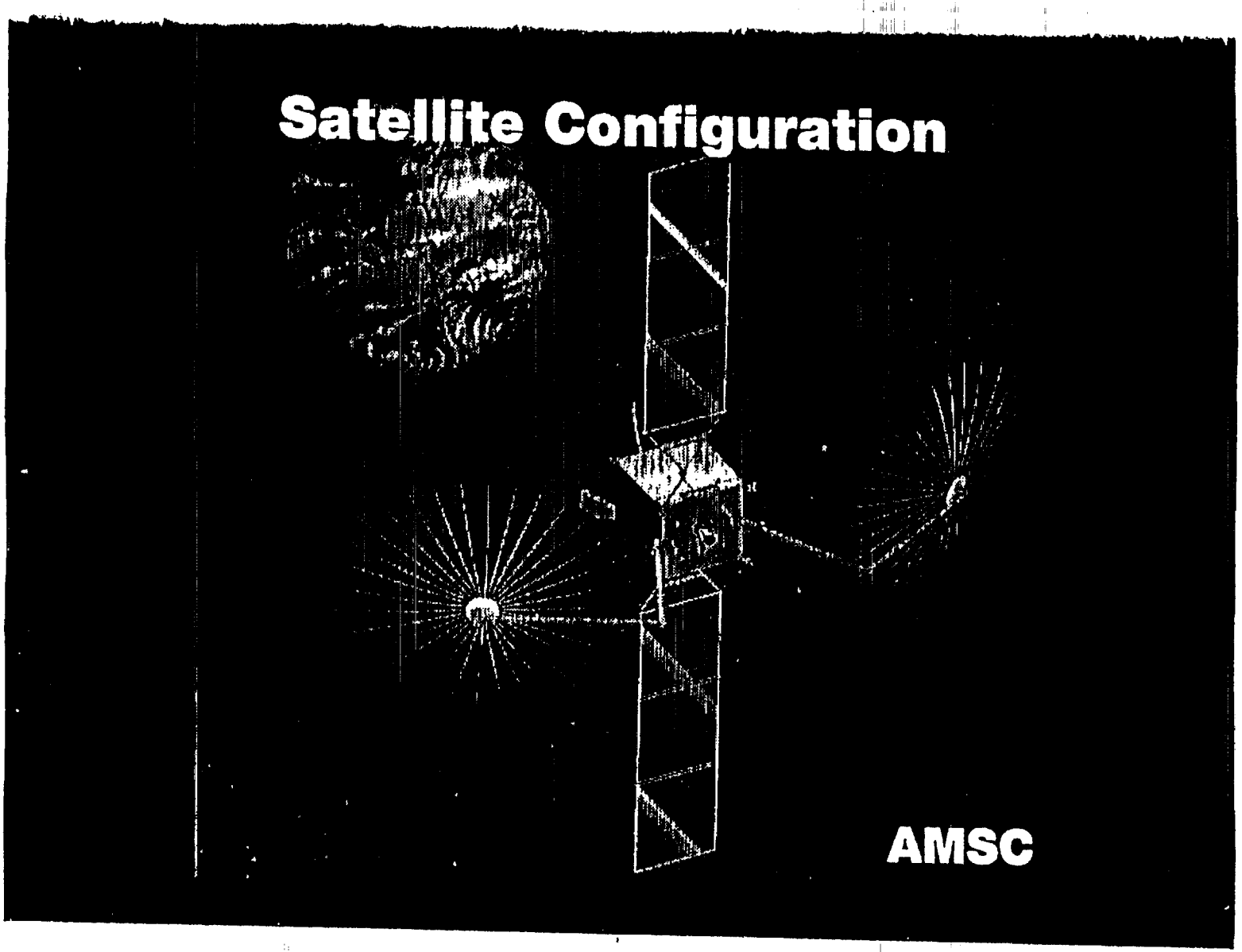

FIGURE 2

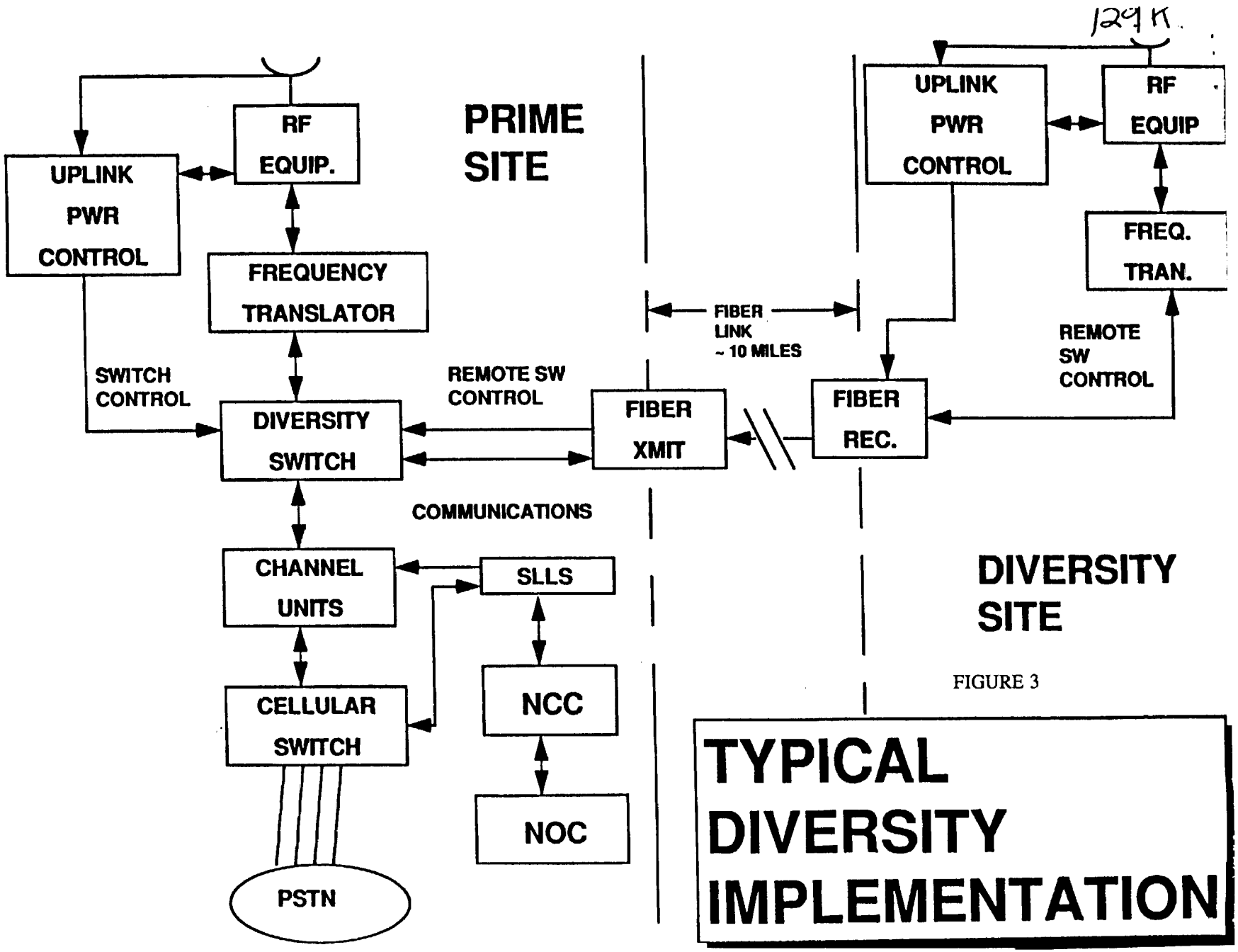
129K
PRIME SITE
RF EQUIP.
UPLINK PWR CONTROL
FREQUENCY TRANSLATOR
SWITCH CONTROL
DIVERSITY SWITCH
REMOTE SW CONTROL
FIBER XMIT
FIBER LINK ~ 10 MILES
FIBER REC.
UPLINK PWR CONTROL
RF EQUIP
FREQ. TRAN.
REMOTE SW CONTROL
COMMUNICATIONS
CHANNEL UNITS
SLLS
CELLULAR SWITCH
NCC
NOC
PSTN
DIVERSITY SITE
TYPICAL DIVERSITY IMPLEMENTATION

FIGURE 3

Characterisation of the LMS Propagation Channel at L- and S-bands: Narrowband Experimental Data and Channel Modelling

Mario Sforza, Sergio Buonomo

The European Space Research and Technology Centre
Keplerlaan 1, 2200 AG Noordwijk, The Netherlands

Abstract

During the period 1983-1992 the European Space Agency (ESA) has carried out several experimental campaigns to investigate the propagation impairments of the Land Mobile Satellite (LMS) communication channel. A substantial amount of data covering quite a large range of elevation angles, environments and frequencies has been obtained. Results from the data analyses are currently used for system planning and design applications within the framework of the future ESA LMS projects. This comprehensive experimental data base is presently utilised also for channel modelling purposes and preliminary results are given in this paper. Cumulative Distribution Functions (PDF) and Duration of Fades (DoF) statistics at different elevation angles and environments have been also included.

1 Introduction

In the design stages of an LMS communication system information regarding the satellite-to-mobile propagation channel is needed to assess link availability objectives, modulation and coding schemes performance, protocols robustness and other system parameters. For conventional geostationary LMS systems, large fade margins are usually required to compensate for signal blockage due to man-made or natural obstacles and for multipath effects. These propagation impairments can be effectively mitigated by means of multisatellite constellations in stable elliptical or circular orbit configurations, in the latter case taking advantage of the in-built

network multivisibility; experimental data or equivalently empirical-statistical channel models are however needed to carry out design studies at system and subsystem levels.

In the field of LMS channel modelling and characterisation, ESA has embarked in a number of research projects involving both experimental and theoretical aspects. In this paper, data on first and second order statistics describing the main narrowband channel propagation features are reported for elevation angles from 20° up to 80°, for several environmental scenarios (open, wooded, suburban and urban) and frequencies (L- and, where possible, S-bands). Empirical models for fade prediction purposes and frequency and elevation scaling laws have been derived for tree-shadowed environments; they are also presented in the following sections.

2 ESA LMS experimental campaigns

The first ESA involvement in LMS experimental measurements dates back to 1983 when the project called PROSAT was first started. The field tests were carried out by using a CW signal up-linked at C-band from an ESA ground station in Villafranca (Spain) to INMARSAT Marecs-A satellite. The frequency of the unmodulated carrier in the down-link channel was of 1.54 GHz. During the first phase of the project, measurements were taken in Belgium and in The Netherlands in open rural, wooded and suburban areas at 27° of elevation angle. The second part of the experimental programme took place in 1987 in Sweden, France and Spain in similar environments, covering a range of elevation angles from 13° to 39°. Specific technical details on the equipment set-ups can be found in [1,2].

One of the problem areas identified by the PROSAT project results was the unrealistic link margin requirement for LMS systems operating at low elevation angles, due to frequent blockage by trees, buildings, bridges and so forth. It was therefore decided to undertake further research activities to address specifically the problem of characterising the LMS propagation channel at elevation angles greater then 40°. Use of highly elliptical orbit configurations, for instance, allows for users in Northern latitudes to be served at mean elevation angles in excess of 50°. In view of these considerations, an airborne experimental campaign was carried out at L- and S-bands (1.3 and 2.6 GHz, respectively) in different locations in North Yorkshire (UK), in cooperation with the British Radiocommunication Agency. Narrowband experimental data were collected in different areas and at elevation angles from 40° up to 80°; further details are given in [3-5].

3 Selected experimental results

A representative sample of first and second order statistics is reported in this section with short descriptions of the environmental characteristics related to the areas under test.

One of the major problem encountered in our work has been the lack of characterisation data

for some specific experimental data files. Furthermore, operational conditions, reference levels, receiver dynamic ranges and antenna radiation patterns were different in the PROSAT project from the airborne campaigns. Finally, the range of elevation angles covered at L-band was larger than at S-band. In order to obtain a more congruent and comprehensive experimental data base it was then decided to carry out additional analyses to establish, at the maximum extent, a unique reference level. The parameters characterising the environments are given as follows:

- Open environment; rural areas with no obstruction along the line-of-sight and occasional passing-by vehicles
- Tree-shadowed environment; rural areas with roadside trees of deciduous variety with Percentage of Optical Shadowing (POS) from 35% to 85% (2-5 meters distant from the road)
- Suburban environment; residential areas with detached two-three storeys houses and scattered trees in low density (10-20 meters distant from the road)
- Urban environment; medium to heavily built-up areas with three to seven storeys buildings and densily distributed utility poles and sign posts (data on urbanisation density were not available)

Taking into account all potential sources of errors, from the experimental set-up down to the data acquisition system, a confidence interval of $\pm 2.5\%$ should be considered for all the experimental data reported in this paper.

3.1 First order statistics

Fade Cumulative Distribution Functions (CDF) are given for elevation angles ranging from 20° up to 80° and for four different environments. Fade depths have been plotted versus elevation angle for each environment and for six different values of percentage of distance (of time, at constant vehicle speed) the fade is exceeded, i.e. link outage from a system engineer viewpoint. Figs. 1 to 4 combine the results of the measurement campaigns previously presented, at L-band (1.3 GHz).

In open rural areas, low implementation fade margins would be needed mostly to counteract residual multipath occurring at low and very low elevation angles; from 40° onward we are consistently within the error of the measurement equipment. The effect of trees shadowing and diffuse incoherent multipath becomes quite evident in wooded areas; on the other hand, these curves are computed on the basis of composite tree-shadowed environments where the POS value fluctuates between 35% and 85%, the latter representing somehow an operational scenario not so likely from the user point of view. In suburban environments, shadowing effects

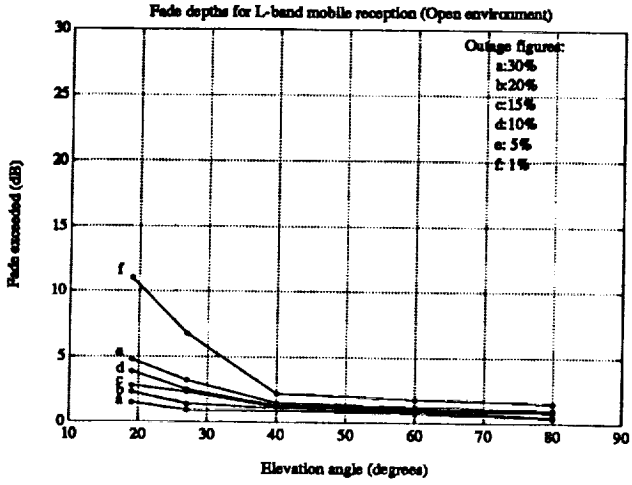

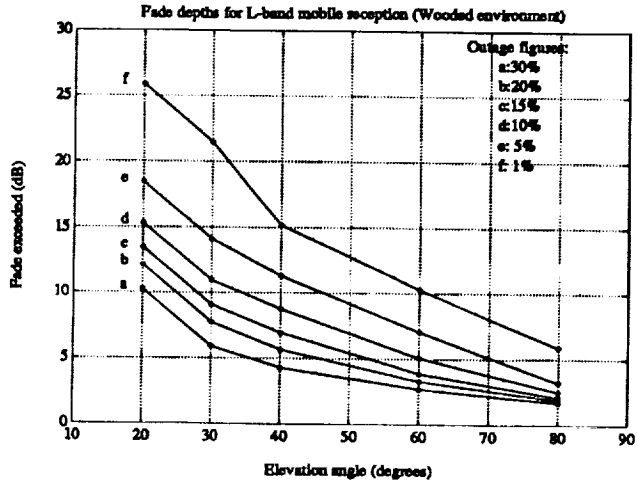

Figs. 1 and 2. Fade depths vs. elevation angle, L-band (open and wooded environments)

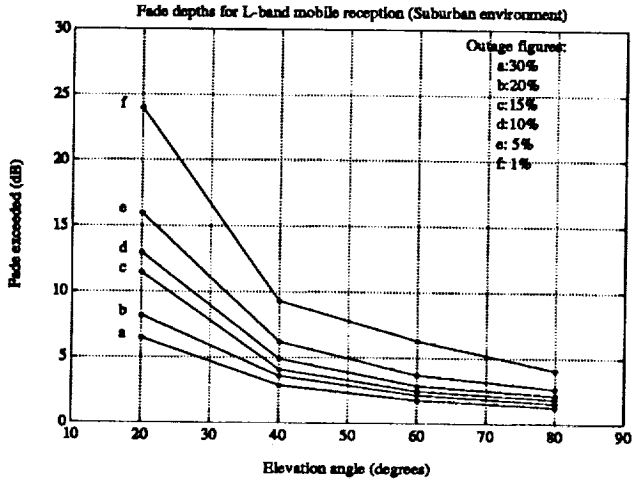

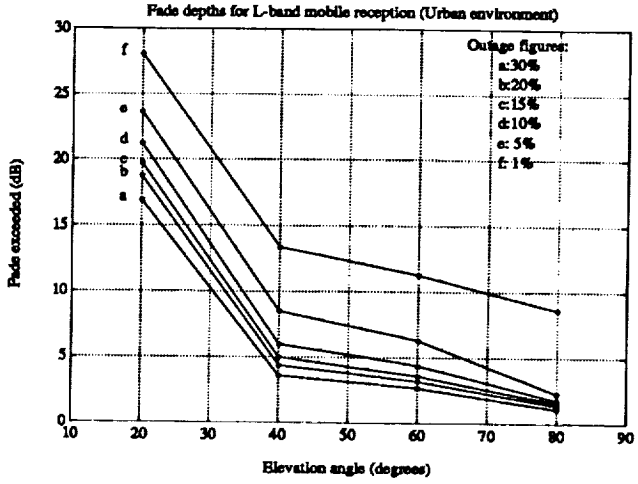

Figs. 3 and 4. Fade depths vs. elevation angle, L-band (suburban and urban environments)

and multipath from nearby houses have a minor impact on the overall fade statistics; this is due, we believe, to the a lower POS figure (the average distance of the obstructing natural or man-made objects from the road is higher). It is however evident the effect of operating the communication LMS service at elevation angles greater than 40-50 degrees, expecially when the satellite-to-mobile link availability requirement is not so stringent (less than 5 dB for 90% of the locations or time). As expected, urban areas present the harshest propagation conditions; at elevation angles lower than 30-40 degrees, the required fade margins are hardly affordable for any economically viable LMS system. The benefit of using high elliptical orbits is again

quite obvious. An additional plot is reported in Fig. 5 to allow for direct comparison between different environmental situations.

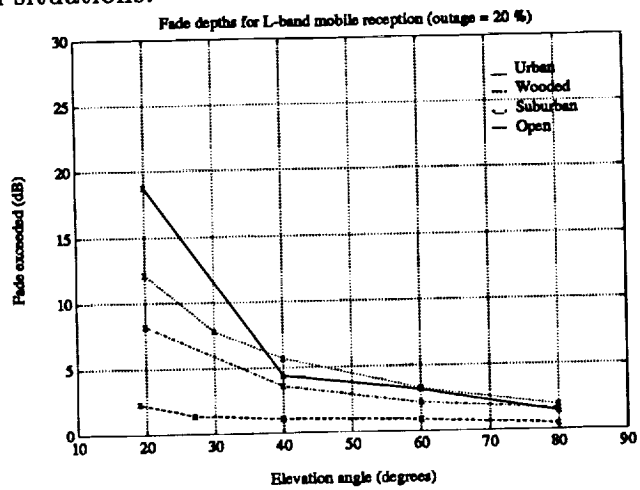

Fig. 5. Fade depths vs. elevation angle, L-band (outage=20%)

Two samples of the CDFs at S-band are also given in Figs. 6 and 7 for tree-shadowed and suburban environments. The S-band airborne experimental campaign was carried out by the University of Bradford in the same locations and roads, using a similar experimental equipment. Though the trees foliage was not exactly in the same conditions of the L-band field tests, interesting considerations can be drawn from the comparison; they are discussed in the modelling section. The curves presented cover of course only a limited range of elevation angles with respect to L-band; an intermediate situation was included at 70° and the results obtained seem to show very little differences, most likely due to a clear line-of-sight already present at 70°.

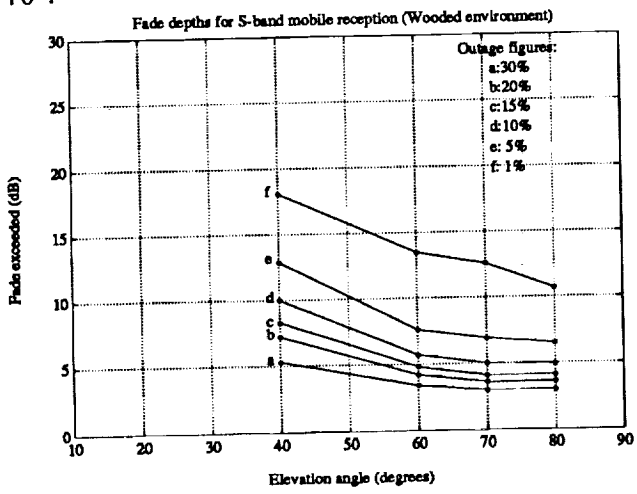

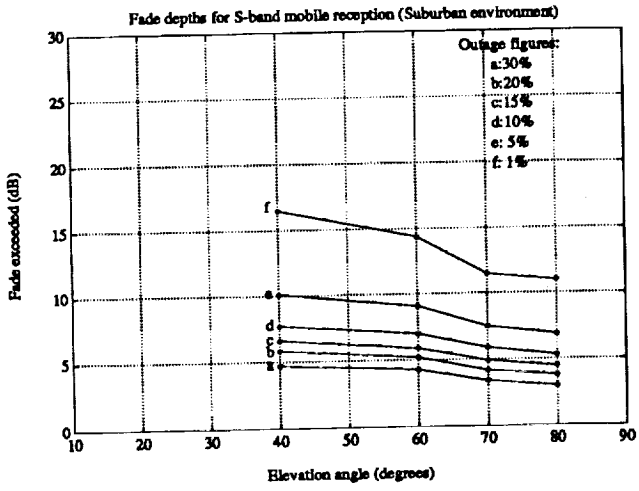

Figs. 6 and 7. Fade depths vs. elevation angle, S-band (wooded and suburban environments)

3.2 Second order statistics

Material related to Average Fade Durations (AFD) and Level Crossing Rates (LCR) statistics for the PROSAT project has been already published [ ]; we will therefore present in this chapter only data related to the airborne campaign. The full list of parameters include AFDs, LCRs, Duration of Fades and Connections, Time Shares of Fades and Connections. Due to the considerable amount of information, covering four elevation angles and four different environments, only Duration of Fades statistics will be shown; these data are currently used in ESTEC for the development of communication protocols and coding schemes for the ARCHIMEDES project.

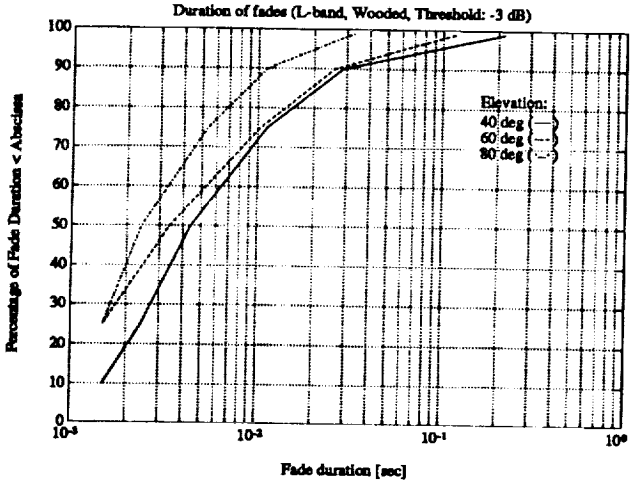

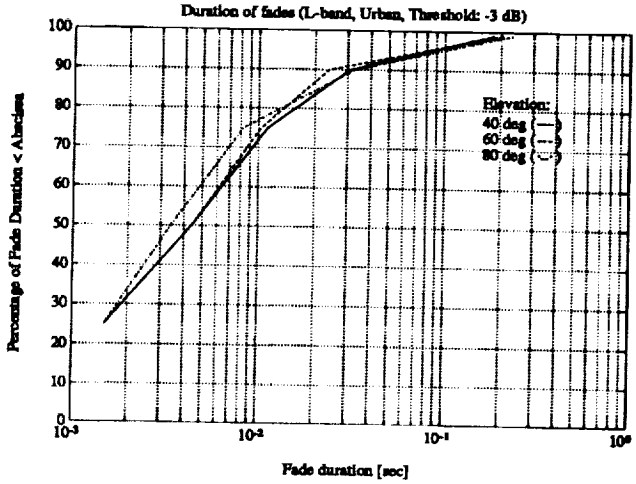

Figs. 8 and 9. Duration of Fades, L-band (wooded and urban environments, thr.=-3 dB)

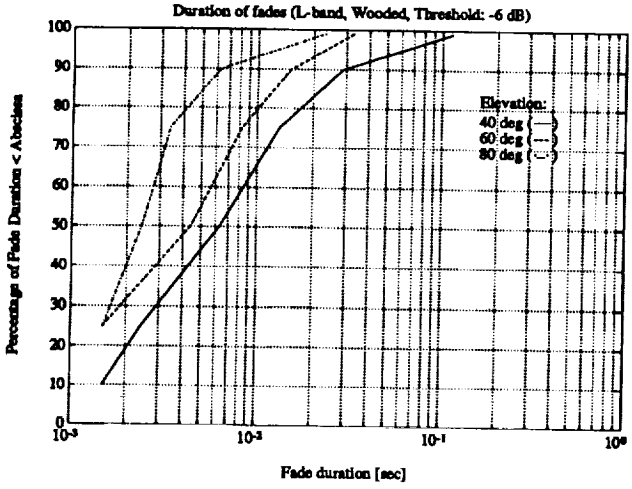

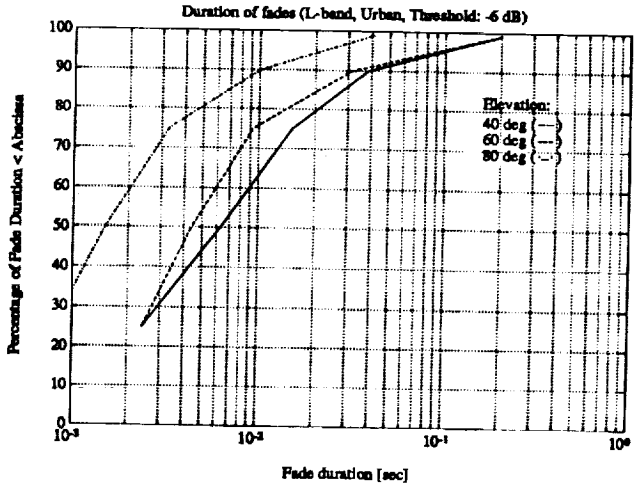

Figs. 10 and 11. Duration of Fades, L-band (wooded and urban environments, thr.=-6 dB)

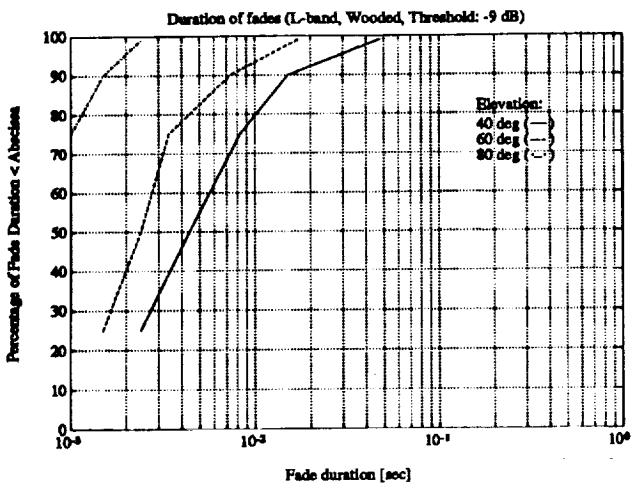

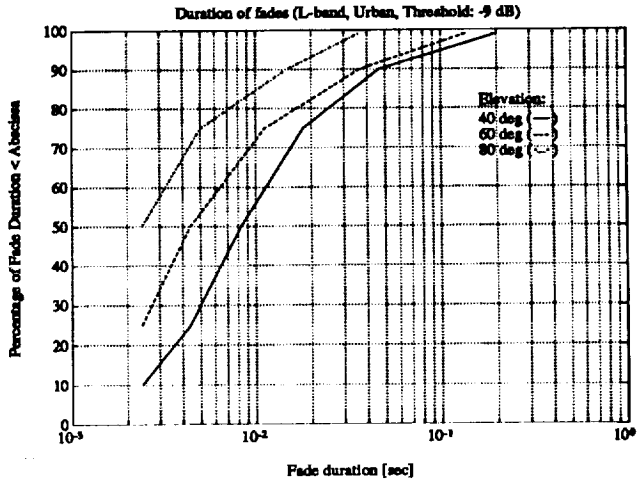

Figs. 12 and 13. Duration of Fades, L-band (wooded and urban environments, thr.=-9 dB)

In Figures 8 to 13, durations of fades statistics relative to tree-shadowed and urban environments are presented for three different threshold levels. The average vehicle speed was of 8.6 and 17.9 m/s for the wooded and urban sections, respectively. Though second order statistical data are presently still to be fully analysed and subject to curve fitting, some preliminary considerations can be drawn from the diagrams given in the figures.

For any given threshold level, the percentage of fades with duration less than a specified value increases with the elevation angle; similarly, for any given percentage of fade events, the average duration decreases with the elevation angle. Finally, the number of fades for a given time duration increase with the threshold level, from -3 down to -9 dB. The rationale supporting these results is related to the fact that the number of natural or man-made objects shadowing the line of sight constantly decreases moving from 40^o up to 80^o.

If to each threshold level reported in the diagrams an equivalent system fade margin is associated, these results can be directly used in the design stages of the LMS main features at system level.

4 Channel modelling

On the basis of the experimental results obtained through numerous measurement campaigns, a consistent amount of in-house studies is currently carried out at ESTEC in the area of LMS channel modelling. Results of least square fitting for cumulative fade distributions and L-/S-band attenuation scaling factor are presented in this section; Duration of Fades curve fitting results will be soon made available.

4.1 The Modified ERS model

A modified version of the Empirical Roadside Shadowing model originally developed by Vogel and Goldhirsh, [6], has been recently elaborated and validated. In our Modified ERS (MERS) empirical model, the range of elevation angles spans from 20° up to 80° and the Percentage of Optical Shadowing (POS) from 35% to 85%; the roadside trees were also of deciduous variety. The model has been validated at L-band frequency only.

The empirical expression, obtained in two different forms by curve fitting the measured cumulative fade distributions, is given, in dB, by:

$$F(Pr,\theta) = -A(\theta)ln(Pr) + B(\theta) \tag{1}$$

$$F(Pr,\theta) = \alpha(Pr)\theta^2 + \beta(Pr)\theta + \gamma(Pr) \tag{2}$$

where Pr is the percentage of the distance (and time, with a vehicle at constant speed) over which the fade is exceeded and θ is the elevation angle. With respect to the ERS model, we have extended and validated equations (1) and (2) for values of Pr up to 30%. In terms more familiar to system engineers, Pr is an indication of the outage experienced in the channel given a certain fade margin on the link. The parameters A and B, in dB, only depend on the elevation angle:

$$A(\theta) = a_1\theta^2 + a_2\theta + a_3 \tag{3}$$

with $a_1 = 1.117 \cdot 10^{-4}, a_2 = -0.0701, a_3 = 6.1304$

$$B(\theta) = b_1\theta^2 + b_2\theta + b_3 \tag{4}$$

with $b_1 = 0.0032, b_2 = -0.6612, b_3 = 37.8581$.

The coefficients α, β and γ in equation (2) depend only on the outage probability Pr; they are reported in Table 1.

Pr (%)	$\alpha(Pr)$	$\beta(Pr)$	$\gamma(Pr)$
1	0.0038	-0.7147	38.7381
5	0.0021	-0.4605	26.4910
10	0.0026	-0.4603	23.1121
15	0.0030	-0.4815	21.4773
20	0.0033	-0.4851	20.0729
30	0.0032	-0.4533	17.4575

Table 1. MERS parameters, as in equation (2).

In Fig. 14, the parametrical curves obtained from the MERS model, equation (1), are plotted with the actual experimental data; the computed rms error is in this case 0.5 dB. For equation (2) the best fit to the experimental data was found to be practically the same.

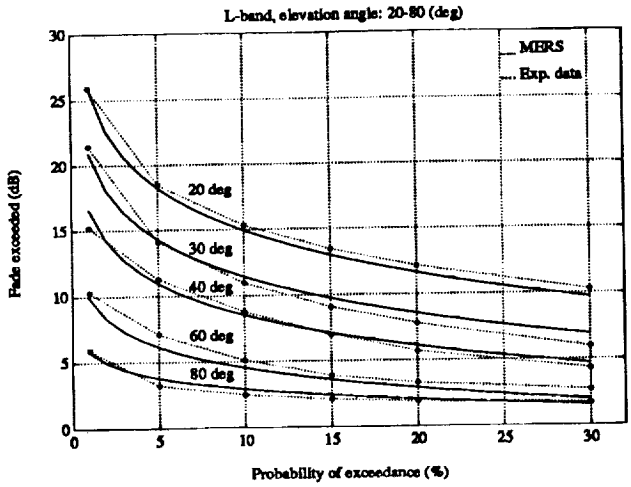

Fig. 14 MERS model vs. experimental data

4.2 S-band versus L-band attenuation scaling factor

From the comparison of the L- and S-band experimental data in tree-shadowed areas, an empirical law relating fade depths at equal probability levels has been derived. Though the measurements were not carried out simultaneously at L- and S-bands, the scaling factor was found to be approximately consistent with the square root of the frequencies ratio and with similar results obtained by Vogel, Goldhirsh and Hong, [7,8]:

$$F(f_{S-band}) \approx 1.41 F(f_{L-band}) \tag{5}$$

with f_{S-band}=2.6 GHz, f_{L-band}=1.3 GHz and where the coefficient 1.41 has an rms error of $\pm$0.5 dB over a fade exceedance range from 1% to 30 %.

5 Conclusions

In this paper, a comprehensive set of experimental results from LMS measurement campaigns at L- and S-bands has been presented. Cumulative fade distributions have been given for a wide range of operational scenarios, environments and elevation angles. Representative samples of duration of fades statistics have been also reported and discussed. Based on the experience gathered in the analyses of the experimental data, empirical fade prediction models have been developed and they are presently used in the preliminary design stages for future ESA LMS systems.

References

[1] *PROSAT, Phase I Report*, ESA STR-216, May 1986

[2] *Study of propagation factors applicable to Land Mobile Satellite Missions*, Final Report of ESA contract 6757, D.C.G. Ingenieros, December 1986, Madrid

[3] M. Sforza, B. Arbesser-Rastburg, J.P.V.P. Baptista, *Propagation aspects for the planning of Land Mobile Satellite Systems*, Proceed. 14th Int. Comms. Satellite Systems Conf., March 22-24 1992, Washington, DC

[4] H. Smith, M. Sforza, B. Arbesser-Rastburg, J.P.V.P. Baptista, *Propagation measurements for Land Mobile Satellite systems using high elliptical orbits*, Proceed. 2dn European Conf. Satellite Comms, October 22-24 1991, Liege

[5] *Characterisation of the Land Mobile Satellite channel at L and S bands: narrowband measurements*, Final Report of ESA POs 104433/114473, University of Bradford, February 1993

[6] W.J. Vogel, J. Goldhirsh, *Mobile Satellite System propagation measurements at L-band using MARECS-B2*, IEEE Trans. AP, vol. 38, pp. 259-264, Feb. 1990

[7] W.J. Vogel, U.S. Hong, *Measurement and modeling of Land Mobile Satellite propagation at UHF and L-band*, IEEE Trans. AP, vol. 36, pp. 707-719, May 1988

[8] J. Goldhirsh, W.J. Vogel, *Mobile Satellite System fade statistics for shadowing and multipath from roadside trees at UHF and L-band*, IEEE Trans. AP, vol. 37, pp. 489-498, Apr. 1989

Results of Multiband (L, S, Ku Band) Propagation Measurements and Model for High Elevation Angle Land Mobile Satellite Channel

M.A.N. Parks, G.Butt, B.G.Evans
Centre for Satellite Engineering Research
University of Surrey
Guildford, Surrey, England

M.Richharia
INMARSAT, London, England

1.0 Introduction

Signal propagation in the land mobile satellite (LMS) service is an important consideration due to its critical impact on the overall economic and commercial viability of the system. At frequencies allocated for LMS systems, shadowing of the line-of-sight (LOS) signal as well as multipath propagation phenomena can severely impair the link availability. In particular, as most of the studies have shown, the shadowing of LOS signal causes long and deep fades in a variety of mobile environments due to the inherent nature of the channel between the satellite and a mobile. Roadside obstacles, such as buildings, trees, utility poles etc., in the immediate vicinity of a mobile and the surrounding terrain are major sources of signal shadowing in LMS links. Therefore, a proper knowledge of link degradation is essential for cost-effective planning of a satellite based mobile communication system.

This paper reports on the results of a propagation campaign undertaken to characterise the fading nature of LMS channel at high elevation angles. It was envisaged that one of the most important physical variable contributing to the amount of LOS signal shadowing is the elevation angle of the satellite [1]. At higher elevation angles to the satellite, less obstructions in the direct satellite-to-mobile path would therefore amount to statistically better link availability. Narrowband channel measurements were carried out at three RF frequencies corresponding to L (1.3 GHz), S (2.32/2.45 GHz) and Ku (10.4 GHz) bands. The campaign itself was divided into two phases to observe the effects of seasonal variation of foliage on the roadside trees. First phase measurements were carried out in September 1991 when trees were in full foliage. The second phase

measurements were made during the early spring of 1992 (April 1992); during the time of year when leaves on the deciduous trees were beginning to reappear. Details of the experiment design and procedures adopted for the measurements are contained in [2] for interested readers. In the following sections some important aspects from the statistical analysis of the propagation data are presented.

2.0 Channel Characteristics:

The narrowband measurements of the LMS channel at L, S and Ku-band were analysed off-line to evaluate the first and second order statistics. These statistics provide useful information on channel behaviour as a function of frequency, elevation angle and mobile environment. The relative effect of foliage density on signal fading for the above mentioned variables is obtained by comparing the statistics from the two measurement phases.

2.1 First Order Statistics:

CDF's of Phase-I Measurements: Figure 1 shows the cumulative distribution functions (CDFs) based on the statistical analysis of the channel recordings, made in the environment considered as suburban for this study, during the first phase of measurement campaign in September 1991. CDF curves corresponding to the 60° and 80° elevation angles for all three frequencies are included. It is clear from the curves that as the elevation angle increases fade depth reduces for equiprobable link availability. For example, link margins of the order of 16.5, 18.5 and 27.5 dB are required to provide reliable communication for 99% of the time at L, S and Ku band frequencies, respectively, at 60° elevation angle. When elevation angle to the transmitting source is 80°, the corresponding margins reduce to 12, 16 and 26 dB respectively. The improvement in the required link margins as a result of the increase in the elevation angle stands at 27% for L-band, 13.5% for S-band and 5.5% for Ku-band, demonstrating maximum advantage to be gained at L-band.

Analysis of measurements made in another environment with heavy tree shadowing, considered as wooded for this study, show that signals suffer higher attenuations as compared to those in the suburban environment at 60°, but there is marked improvement at 80°. The L-band attenuation for 99% availability in the wooded environment

was found to be 18.5 dB at 60° which reduced to about 8 dB at 80° elevation angle, an improvement of 57%. At Ku-band, the attenuation levels for the same link probability were 28 and 24 dB corresponding to elevation angles of 60° and 80° respectively, the improvement in this case was only 14%. Less signal degradation at higher elevation angle for the wooded environment may be explained in terms of the nature of trees in the wooded environment that constituted the major shadowing source. Non-deciduous coniferous trees dominated the tree population in the wooded environment which are believed to have contributed less to the signal shadowing at 80°.

In the mobile environment considered as open for this study, signal degradation was found to be limited compared to the attenuations experienced in the other two environments. The analysis results confirmed that in the absence of any major shadowing or scattering sources (apart from occasional overhead bridges) signals generally did not experience long or deep fades. At 1% outage probability, fades in the range of 2-4 dB were observed for L, S and Ku-band signals.

CDF's of Phase-II Measurements: Figure 2 contains the measurement results for the suburban environment obtained during the second phase. Sharp reductions in attenuations result when elevation angle is increased from 60° to 80°. It is interesting to note, however, that 60° curves at all frequencies are very similar to those obtained during the first phase. The sharp reduction in fades at 80° may be attributed to the reduced foliation of deciduous trees, which dominated the tree population in the suburban environment, during the early spring time. At 1% link outage probability, the improvement in link margins was 79% at L-band, 62% at S-band and 69% at Ku-band when the elevation angle increased from 60° to 80°. The results show the extent of influence of foliage on the fade depth especially at higher elevation angles, and highlight the significance of physical conditions in a mobile channel influencing link margin requirements.

Since the tree population in the wooded environment was predominantly non-deciduous, there was minimal seasonal effect as far as defoliation was concerned. This was reflected in the marginal difference in attenuation levels at all frequencies when compared to respective phase-I wooded

environment results. The maximum difference was observed at Ku-band where an almost uniform difference of 4 dB was observed at all significant link availability levels. The difference at S and L-band reduced as the frequency decreased. Such an observation implies that mobile channel behaviour is sensitive to the radio-frequency.

2.2 Second Order Statistics:

Second order statistics evaluated from the channel measurements and presented here include signal level crossing rate and average fade durations. Such information, particularly average fade durations, are useful in determining optimum parameters of communication sub-systems such as modulation, coding and transmission data rates for digital systems etc. [3].

Figures 3 and 4 illustrate level crossing rates (LCR) for the suburban environment derived from phase I and II measurements. The level crossing rate has been normalised to signal wavelength. In all cases the rate of level crossing in a positive direction peaks around the 0 dB level, indicating the presence of LOS signal for most of the time. Rapid fluctuations near LOS level imply the presence of weak diffusely scattered signals and hence received signal may reasonably be assumed to be Rician distributed, although this has not been confirmed analytically. As the frequency increases, the level crossing rates drop indicating deeper signal attenuation. The effect of reduced shadowing of LOS at higher elevation angles is evident from peaks of LCR curves near 0 dB level. Figures 5 and 6 show average fade duration (AFD) curves for the suburban environment from phase-I and II. Similar observations can be made from these curves. The availability of unshadowed LOS signal is clear from reduced fade durations near 0 dB level in all cases. It is worth mentioning at this point that the second order statistics are sensitive to sampling rates at which the analog signals are digitised for computer analysis. The vertical dotted lines in all second order plots indicate the attenuation level beyond which there could be little statistical confidence in the second order statistics. Therefore, care must be exercised in interpreting results above the fade level indicated.

3.0 Models

The results from the Multiband Campaign have been further analysed using statistical distributions and the model proposed by Lutz, et al,[6]. As shown by Table 1. the analysed results compare favourably with the statistics presented by Lutz in the suburban and wooded categories for the higher elevation angles considered.
An example of Shadow Factor verses Elevation Angle for the suburban category is shown by Figure 7. This shows the general trend that the shadow factor reduces as the elevation angle increases, thus providing a more reliable communication channel.

An empirical model has been developed to predict the required system margin for the specified link availability as a function of RF frequency ($1.3 < f < 10.4$ GHz) and elevation angle ($60^o < \phi < 80^o$) for average shadowing conditions. The model, Empirical Fading Model (EFM), is given by :-

$$M\ (\text{dB}) = A.\text{Ln}(p) + C$$

Where : M corresponds to the required link margin for the specified outage probability, p (%), in the range of 1 to 20, and f is frequency in GHz. The constants A and C are determined as follows:-

$$A = 0.029\phi - 0.182f - 6.315$$

$$C = -0.129\phi + 1.483f + 21.374$$

Further work comparing the above model with that of the Empirical Roadside Shadowing Model, (ERS),[7] and CCIR Model [8] has been carried out in order to enhance the range of elevation angles of these models. A combined model for L-Band has been derived in a similar form to that given above and in [7]. A typical comparison of the models for 10% fade exceedance level is shown by Figure 8, as well as the combined model. The model Suburban/Rural Empirical Fading Model (S/REFM), is given by :-

$$M\ (\text{dB}) = B.\text{Ln}(p) + D$$

Where :-

$$B = 23.5f - 0.108\phi + 0.0018\phi\text{^}2 - 38.5$$

$$D = -58.5f - 0.375\phi + 121.5$$

And

M and f are defined as above and p (%) is in the range of 5 to 20.

4.0 Conclusion

The LMS channel behaviour may be summarised as:

* As the path elevation angle to the satellite increases, the attenuation due to shadowing and multipath the channel conditions reduce.

* In general, signal attenuation increases as a function of increasing radio-frequency.

* The effect of foliage density on the attenuation level has been found to be significant, particularly at higher elevation angles.

* The fading character of the LMS channel is significantly dependent upon the type of surrounding environment.

These conclusions tend to substantiate the general trend of various findings from other propagation studies carried out under different terrain types, and in most cases in different geographical locations i.e., Europe, the United States and Australia, and at various RF frequencies. Limited data exist at frequencies and elevation angles considered during this study. However, results from propagation studies elsewhere [4], [5] at comparable elevation angles, RF frequencies and mobile environments are in reasonably good agreement with the statistical results presented here. This experiment is believed to be the first ever attempt to cover such a wide range of frequencies and high elevation angles simultaneously. The results presented in Section 2. provide indications on the link margin requirements for frequencies in L, S and Ku bands at elevation angles above 60°.

The Centre for Satellite Engineering Research (CSER) is further pursuing the propagation issues of mobile-satellite channel by planning a wideband channel measurement campaign at L and S bands. The results of the wideband sounding are expected to provide useful information, particularly on the coherence bandwidth and delay spread of the channel, and the effect of RF frequency, elevation

angle and mobile environment on such parameters. These parameters are believed to be important in determining the optimum signalling format, signal modulation and channel coding schemes for future mobile/personal satellite communication systems.

References:

[1] University of Surrey: *'A Study on the Feasibility of High Elevation Angle Propagation Experiment Applicable to Land Mobile Satellite Services'*, ESA contract 8084/88/NI/PB, 1989

[2] Butt, G., Evans, B.G., Richharia, M.: *'Narrowband Channel Statistics from Multiband Propagation Measurements Applicable to High Elevation Angle Land Mobile Satellite Systems'*, IEEE Journal on Selected Areas in Communications, vol. 10, no. 8, October 1992, pp.1219-1226

[3] Parsons, J.D.: *'The Mobile Radio Propagation Channel'*, Pentech Press, London, 1992

[4] Goldhrish, J., Vogel, W.J.: *'Mobile Satellite System Fade Statistics for Shadowing and Multipath from Roadside Trees at UHF and L-band'*, IEEE Transactions on Antennas & Propagation, vol.37, no.4, April 1989, pp.489-498

[5] Smith, H., Sforza, M., Arbesser-Rastburg, B., Baptista, J.P.V., Barton, S.K.: *'Propagation Measurements for S-band Land Mobile Satellite Systems using Highly Elliptical Orbits'*, Proceedings of Second European Conf. on Satellite Communications, Liege Belgium, 22-24 October 1991, pp.517-520

[6] Lutz, E., et al.,*'The Land Mobile Satellite Communication Channel - Recording, Statistics, and Channel Model'*, IEEE Transactions on Vehicular Technology, Vol 40, No.2, May 1991

[7] Goldhirsh, J., Vogel, W.J.: *'Propagation Effects for Land Mobile Satellite Systems: Overview of Experimental and Modeling Results'*, NASA Reference Publication 1274, February 1992

[8] CCIR XVIth Plenary Assembly, Geneva, *'Factors Affecting the Choice of Antennas for Mobile Stations of the Land Mobile-Satellite Service'*, Report 925-1 1986

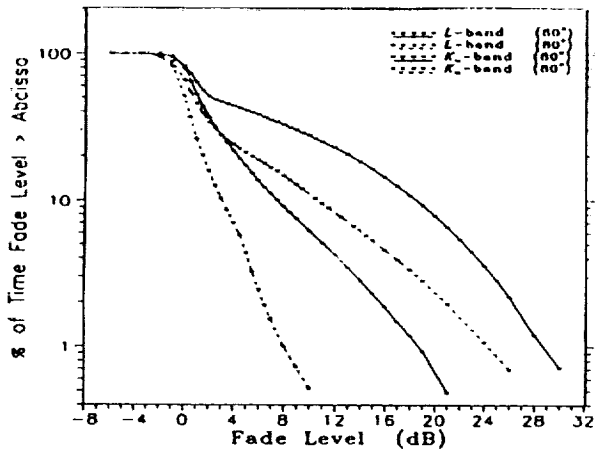

Figure 1: CDFs for the Suburban environment (*Phase-I*)

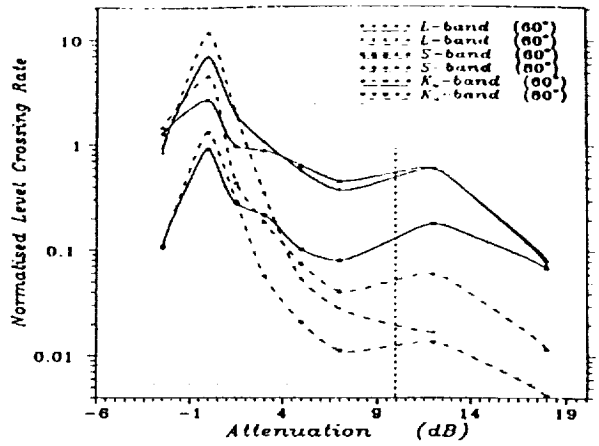

Figure 4: Normalised LCR for the Suburban environment (*Phase-II*)

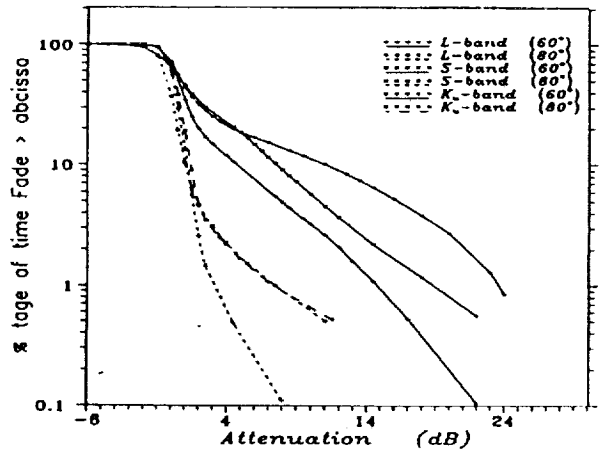

Figure 2: CDFs for the Suburban environment (*Phase-II*)

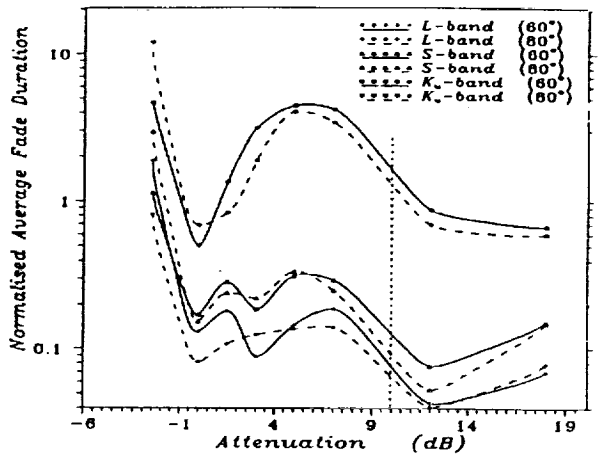

Figure 5: Normalised AFD for the Suburban environment (*Phase-I*)

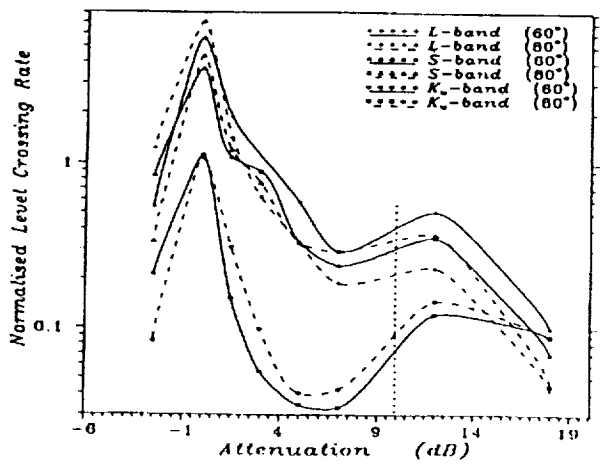

Figure 3: Normalised LCR for the Suburban environment (*Phase-I*)

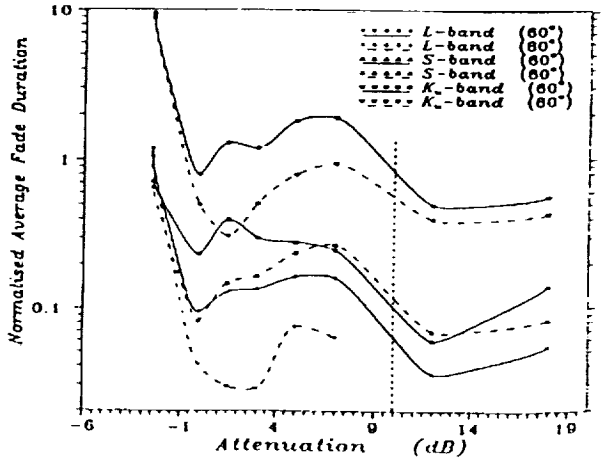

Figure 6: Normalised AFD for the Suburban environment (*Phase-II*)

Table 1: ***Comparison of Parameters of the Analog Channel Model as proposed by Lutz et al***

Elevation Angle	Environmental Category	Time-Share Factor (A)	10Log(c)	Mean Value (μ)	Standard Dev. (Δ)	Antenna Gain dBi
13	City	0.89	3.9	-11.5	2.0	3.0
18	City	0.80	6.4	-11.8	4.0	3.0
21	City	0.57	10.6	-12.3	5.0	5.0
24	City	0.66	6.0	-10.8	2.8	3.0
34	City	0.58	6.0	-10.6	2.6	3.0
43	City	0.54	5.5	-13.6	3.8	3.0
60	**Suburban**	**0.224**	**13.23**	**-6.1**	**2.8**	**4.0**
70	**Suburban**	**0.03**	**14.68**	**-6.1**	**2.2**	**4.0**
80	**Suburban**	**0.007**	**17.70**	**-6.4**	**3.2**	**4.0**
13	Highway	0.24	10.2	-8.9	5.1	3.0
24	Highway	0.25	11.9	-7.1	6.0	3.0
34	Highway	0.008	11.7	-8.8	3.8	3.0
43	Highway	0.002	14.8	-12.0	2.9	3.0
24	Wooded	0.59	9.9	-9.3	2.8	3.0
24	Wooded	0.54	10.7	-5.3	1.3	5.0
60	**Wooded**	**0.655**	**10.58**	**-6.3**	**2.5**	**4.0**
70	**Wooded**	**0.378**	**13.95**	**-6.9**	**5.1**	**4.0**
80	**Wooded**	**0.077**	**10.84**	**-5.1**	**3.1**	**4.0**

Where :-

c = The direct-to-multipath signal power ratio in dB

μ = The mean power level decrease in dB

Δ = The standard deviation of the power level due to shadowing in dB

Fig 7: Shadow Factor vs Elevation Angle for Sub-urban Category

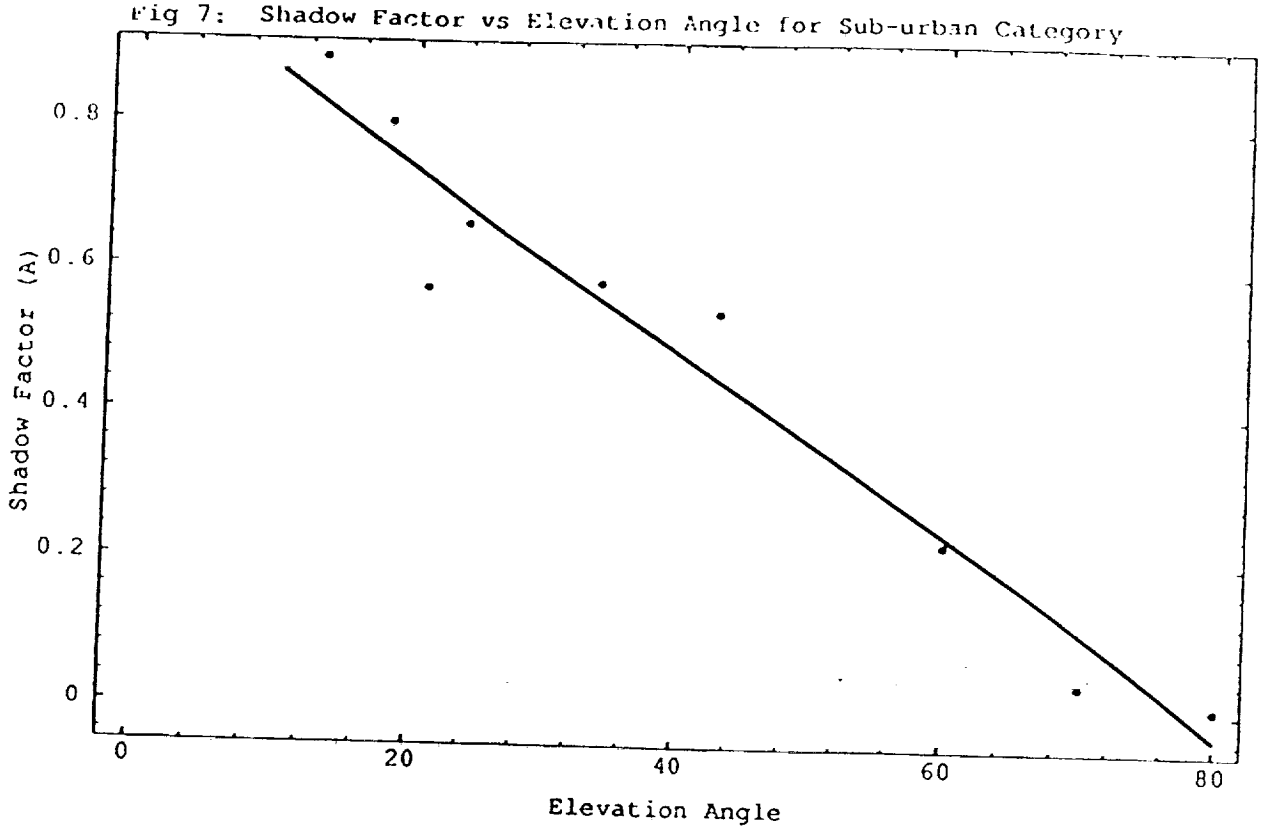

Fig 8: Comparison of CCIR, ERS, and EFM Models at L-Band.

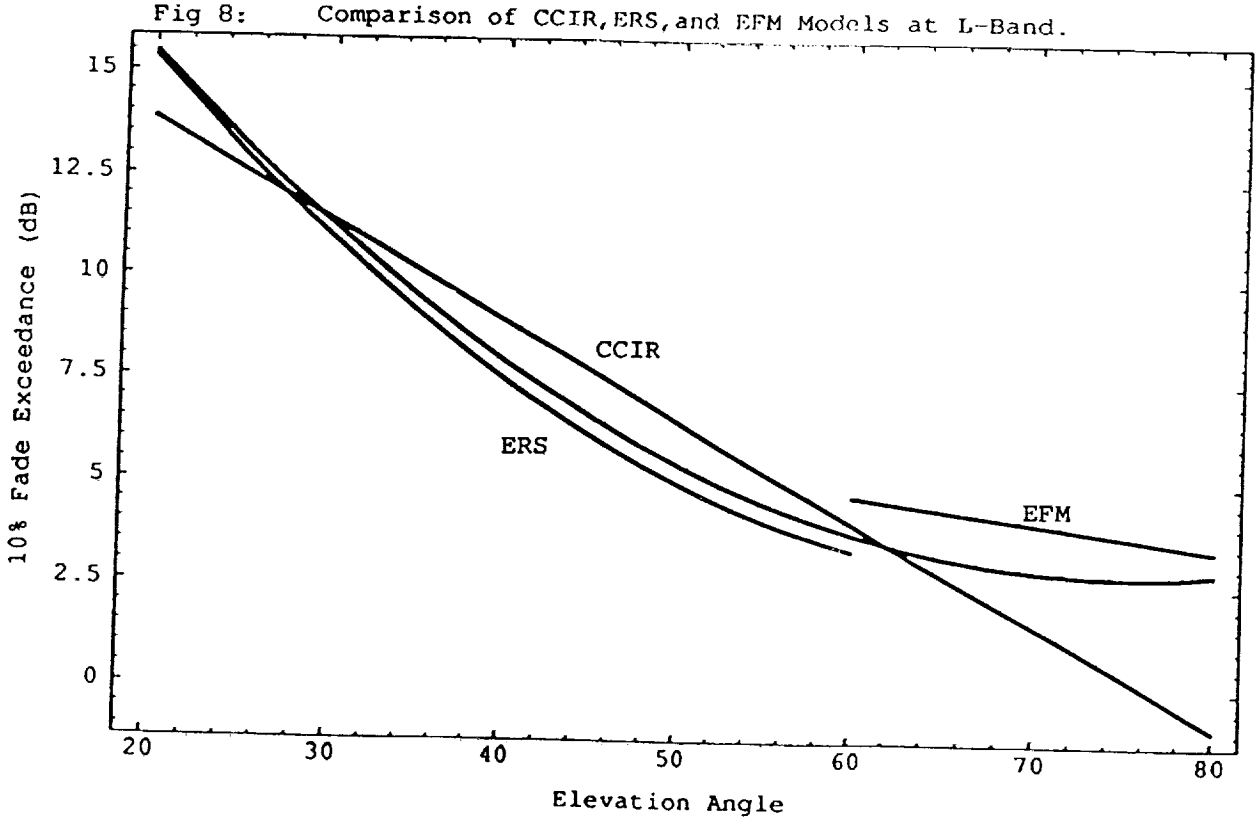

EFFECTS OF THE EQUATORIAL IONOSPHERE ON L-BAND EARTH-SPACE TRANSMISSIONS

by
Ernest K. Smith and Warren L. Flock
NASA Propagation Information Center
ECE Department, University of Colorado
Boulder, Colorado, 80309

Abstract
Ionosphere scintillation can effect satellite telecommunication up to Ku-band. Nighttime scintillation can be attributed to large-scale inhomogeneity in the F-region of the ionosphere predominantly between heights of 200 and 600 km. Daytime scintillation has been attributed to sporadic E. It can be thought of as occurring in three belts: equatorial, high-latitude, and mid-latitude, in order of severity. Equatorial scintillation occurs between magnetic latitudes ± 25 degrees, peaking near ± 10 degrees. It commonly starts abruptly near 2000 local time and dies out shortly after midnight. There is a strong solar cycle dependence and a seasonal preference for the equinoxes, particularly the vernal one. Equatorial scintillation occurs more frequently on magnetically quiet than on magnetically disturbed days in most longitudes. At the peak of the sunspot cycle scintillation depths as great as 20 dB have been observed at L-band.

1. Introduction.

This paper is designed to respond to the question "What additional problems does one have due to equatorial scintillation when operating satellite systems with equatorial earth stations at L-band". With this objective in mind we review the intensity, geomorphology and temporal characteristics of equatorial scintillations, discuss the indices which experimenters use to measure ionosphere scintillation, and look at currently available models. As the paper is aimed at non-ionosphericists, an effort is made to keep it as simple and applications-oriented as possible.

1.1 Background.

Ionospheric scintillation was first recognized in the mid-forties (Flock 1987). Interestingly enough, the early observations of scintillation were of signals from radio stars - direct analogs of the earth-space transmissions of interest now. During the IGY there was special attention paid to the equatorial ionosphere and a host of strange effects were discovered which had the same temporal characteristics which we now associate with equatorial scintillation. One of these was named the "Far Eastern Anomaly" (Bateman, et al. 1959) and is illustrated in the beautiful range-time record shown in Figure 1, taken by Jim Watts on a low-latitude ionospheric scatter circuit. Note the sudden commencement of the broadened trace shortly after sundown which gradually decreases after midnight. Equatorial "bubbles" (regions of plasma deficiency) were observed at Jicamarca, Peru to follow the same temporal characteristics and were observed to rise to elevations of over a thousand km (Kelley et al. 1981, Kelley 1989). These plasma depletions are believed to be aligned along the Earth's magnetic field, have dimensions of 100-200 km east-west and several thousand km north-south, and to move eastward with velocities of 50-200 m/s. These depletion regions are then the seat of irregularities with scale sizes of meters to tens of kilometers (Johnson 1988).

Persons interested in high-latitude scintillation are referred to an excellent paper by Kersley et al. (1988) on the subject.

1.2 Geographic and Temporal Characteristics.

The oft-reproduced diagram shown in Figure 2 (Basu et al. 1988) contains a wealth of information. Solar cycle dependence is illustrated by the different depths of fading indicated for the solar maximum (up to 20 dB), and solar minimum (as low as 1 dB). The geographic extent is shown to be at least 20 degrees north and south of the equator at solar maximum, with peaks on either side of the equator. The diurnal behavior is in this figure. Scintillations start shortly after 2000 local time and decay shortly after midnight.

An ambiguity in Figure 2, as in similar earlier representations (e.g. CCIR 1986), is that the identity (geographic, geomagnetic or magnetic) of the equator is left vague. The reason for this is presumably that as worldwide measurements are not available it is difficult to generalize one's data to apply worldwide.

By geomagnetic coordinates one refers to the Earth's dipole field, as represented by a magnet placed at the center of the Earth. The total intensity F of the Earth's dipole field in gauss is given by

$$F = (0.3\ R^3/r^3)[1 + 3\ \sin^2 \Theta]^{1/2} \qquad (1)$$

where R is the Earth's radius (6371 km), r is the distance from the center of the Earth, in the same units as R, and θ is geomagnetic latitude. The axis (slightly time variant) is given for January 1988 as passing through 79.1 degrees N geographic latitude and 289.1 degrees East geographic longitude (Davies 1989). Geomagnetic latitude for the Earth is given in Figure 3. The dip I in the geomagnetic coordinate system is simply related to the geomagnetic latitude L by

$$\tan L = 0.5 \tan I \qquad (2)$$

By magnetic or dip latitude L' (Smith 1957) is meant the latitude one would obtain from the analogous expression to (2) if the true ionospheric dip I' is substituted in (2),

$$L' = \tan^{-1}(0.5 \tan I') \qquad (3)$$

Magnetic latitude for the Earth is given in Figure 4. The normal procedure for obtaining magnetic latitude is to use the smoothed value of the surface dip and enter that in equation (3). As one goes up in altitude the direction of the Earth's field will gradually approach the dipole value given by expressions (1) and (2). How rapidly that value is approached is illustrated in Figure 5. For altitudes below 3000 km the true dip is seen to be better represented by magnetic latitude.

2. Observations.

The most applicable observations are the extensive ones made at C-band (primarily at 4 GHz) at Intelsat stations and those at L-band on the 1.5 GHz signal from Marisat. There is also a limited number of recordings taken in August 1980 of L1 and L2 GPS signals (Rino et al. 1981).

2.1 Amplitude Scintillation.

Shown in Figure 6 (Fang 1988) are recordings made at Stanley, the Hong Kong Intelsat station, on March 3-4, 1988 (at the peak of the solar cycle) of two satellites: the Pacific Ocean Regional (POR) at 174 degrees E and the Indian Ocean Regional at 63 degrees E. Hong Kong was the only receiver location. It could receive POR and IOR directly at 3950 MHz and it could receive the signal uplinked to POR and IOR from Sentosa, Singapore and

Si Racha, Thailand at 6 GHz and down-linked at 4 GHz. If one assumes (as does the author) that the main effect is on the down-link (at the lower frequency) then one is faced with an eastward movement of the disturbance at the time when the sub-solar point is moving westward. This result is in agreement with spaced-antenna measurements of smaller scale inhomogeneity (Johnson 1988) but the rate of travel exceeds the 200 m/s found to be maximum in that experiment.

2.2 Phase Scintillation.

Figure 7, taken from Rino et al. (1981), is an example of data recorded during twelve consecutive evenings starting August 21, 1980 at Kwajalein Atoll. (Note that this was not a seasonal peak.) Measurements of amplitude and phase were made during scintillation periods on both the L1 (1575.42 MHz) and L2 (1227.6 MHz) signal. During periods of moderate scintillation the phase deviations on L1 exceeded 50 radians while those on L2 exceeded 75 radians. In the example shown in Figure 7 the satellite (GPS 8) rose from the southeast around 2250 local time and achieved its maximum elevation of 70 to 75 degrees around 0330.

To quote from page 256 of the article "During seven of these evening data runs, the scintillation was severe enough that the GPS 5010 receiver could not maintain lock on the signal during the early portion of the pass. When the satellite was above about 30 degrees, however, the scintillation was not severe enough to cause the receiver to break lock..."

2.3 Frequency spectrum.

By frequency spectrum is meant the prevalence of frequency components in the oscillations of the received signal under scintillation conditions. An example of this is shown in Figure 8 where it can be seen that the most dominant frequency is around 10 seconds (O.1 Hz). The prevalence of higher frequencies decays roughly as f^{-3} (CCIR 1990).

3. Dependencies.

The term "correlations" might be used here, but "dependency" seems to reflect a peak at a certain time of day or season somewhat better.

3.1 Solar Cycle.

There is a clear correlation of strong scintillation with sunspot cycle as reflected in Figure 9 (CCIR 1990). However, as pointed out by Aarons (1981) this does not mean for all months or all times of day. Aarons relates the maximum scintillation regions to the Appleton anomaly, i.e. the fact that the maximum ionization in the F-region of the ionosphere is not located at the equator but in low-latitude peaks on either side of it as is illustrated in Figure 2.

3.2 Season.

The strongest scintillation at periods of high sunspot number for stations located near the two geographical maxima in Figure 2 are in equinoctial months with the vernal equinox preferred over the autumnal (Fang 1981, Basu et al. 1998).

3.3 Diurnal.

The diurnal variation of equatorial scintillation shows a strong preference for the hours of 2000 to 0100 local time as is well illustrated by Figures 1 and 2.

3.4. Magnetic.

There are two aspects to the magnetic dependence. That concerning the dependence on geographic, dipole or dip latitude has been discussed under 1.2. The suggestion is that dip

or magnetic latitude is the better choice of the three. The other aspect is whether times of magnetic quiet or disturbance are preferred. As shown by Aarons (1981) and others there is a preference for quiet days for strong scintillation.

4. Scintillation Indices.

The quantification of scintillation indices can be attributed to Briggs and Parkin (1963). Their treatment was restricted to amplitude scintillation. They reasoned that, inasmuch as what is actually observed in recordings of satellite signals is a recorder deflection proportional to the amplitude of the received wave, measures related to the mean deviation and root-mean-square deviation were logical. These measures they denoted by S_1 and S_2 defined as follows:

$$S_1 = \frac{1}{\overline{R}} \overline{|R - \overline{R}|} \qquad \text{normalized mean deviation} \qquad (4)$$

$$S_2 = \frac{1}{\overline{R}} \left\{ \overline{(R - \overline{R}^2)} \right\}^{1/2} \qquad \text{normalized RMS deviation} \qquad (5)$$

where R is the received amplitude, $\overline{R}$ is the mean value and $\overline{R - \overline{R}}$ is the mean deviation of the sample record. The values are then normalized. Hence, S_1 is the normalized mean deviation, and S_2 is a normalized standard deviation.

The authors reasoned further that, inasmuch as satellite scintillation recordings measure power, R^2 , rather than amplitude, R, two parallel indices, S_3 and S_4 , should be defined:

$$S_3 = \frac{1}{\overline{R^2}} \overline{|R^2 - \overline{R^2}|} \qquad (6)$$

$$S_4 = \frac{1}{\overline{R^2}} \left\{ \overline{(R^2 - \overline{R^2})^2} \right\}^{1/2} \qquad (7)$$

In their discussion Briggs and Parkin (1963) use an index S as a measure of scintillation depth defined as:

$$S^2 = \frac{\overline{R^4} - (\overline{R^2})^2}{(\overline{R^2})^2} \qquad (8)$$

For a Rayleigh distribution, applying to the limiting case where phase deviations are large, the relationships between the indices are:

$$S_1 = 0.42\, S_4 \qquad (9)$$

$$S_2 = 0.52\, S_4 \qquad (10)$$

$$S_3 = 0.73\, S_4 \qquad (11)$$

$$S \equiv S_4 \qquad (12)$$

Whitney (1969) proposed a scintillation index, S.I., defined as:

$$S.I. = \frac{P_{max} - P_{min}}{P_{max} + P_{min}} \quad (13)$$

where P_{max} is the power amplitude of the third peak down from the maximum measured, and P_{min} is the third peak up from the minimum excursion in a 15 minute period of recording. Later usage (Yeh et al. 1981) takes the highest peak and minimum excursion instead of the third up and third down.

5. Models.

Computer modeling of equatorial scintillation was initially based on two data sets (Secan et al. 1993). The first was data collected from the Wideband satellite in the 1970s at Ancon, Peru, and Kwajalein Atoll (VHF, UHF, and L-band). The second was data collected from the Marisat satellite from Ascension Island (L-band) and Huancayo, Peru (VHF), and from the Fleetsat satellite from Manila (VHF). The Wideband satellite data included both intensity and phase (WBMOD) and has been gradually enhanced over the years (Secan et al. 1987) to its latest version (Secan et al. 1993): "The WBMOD uses a collection of empirically derived models to describe the global distribution and behavior of naturally occurring ionospheric irregularities, and a power-law phase-screen propagation model to calculate estimates of the level of intensity and phase scintillation that these irregularities would impose on a user-defined system and geometry." Details of this code can be obtained from James A. Secan, Northwest Research Associates, Inc. P.O. Box 3027, Belleview, Washington 98009.

6. References

Aarons, J. (1981) Microwave equatorial scintillation intensity during solar maximum. 193-201, **Proceedings of the Ionosphere Effects Symposium 1981**, U.S. Gov't Printing Office.

Basu, Sa., E. MacKenzie, and Basu, Su. (1988). Ionospheric constraints on VHF/UHF communications links during solar maximum and minimum periods, **Radio Sci., 23**, 363-378, May-June.

Bateman, R., J.W. Finney, E.K. Smith, L.H. Tveten, and J.M. Watts (1959). IGY observations of F-layer scatter in the Far East, **J. Geophys. Res., 64**, 403-405.

Briggs, B.H., and I.A. Parkin (1963). On the variation of radio star and satellite scintillation with zenith angle. **J. Atmos. Terr. Phys. 26**, 1-23.

CCIR (1986). Ionosphere effects upon earth-space propagation, Report 263-6, **vol. 6: Propagation in Ionized Media of CCIR XXVIth Plenary Assembly**, ITU Geneva.

CCIR (1990) Ionosphere effects upon earth-space propagation, Report 263-7, **Annex to vol. 6: Propagation in Ionized Media of CCIR XXVIIth Plenary Assembly**, ITU Geneva.

Davies, K. (1989). **Ionospheric Radio**, Peter Peregrinus, Ltd. on behalf of the IEE.

Fang, D.J. (1981). C-band ionospheric scintillation measurements at Hong Kong Earth station during the peak of solar activity in sunspot cycle 21, 181-192, **Proceedings of the Ionosphere Effects Symposium 1981**, U.S. Gov't Printing Office.

Fang, D.J. and M.S. Pontes (1981). 4/6 Ghz ionospheric scintillation measurements during the peak of sunspot cycle 21, **COMSAT Tech. Rev. 11**, No. 2, 293-320.

Flock, W.L. (1987). **Propagation Effects on Satellite Systems at Frequencies Below 10 GHz - A Handbook for Satellite System Design**. NASA Reference Publication 1108(02).

Kelley, M.C. (1989). **The Earth's Ionosphere - Plasma Physics and Electrodynamics**. Academic Press

Kelley, M.C., M.F. Larson, C.A. LaHoz, and J.P. McClure (1981). Gravity wave initiation of equatorial spread F. **J. Geophys. Res. 86**, 9087.

Kersley, L., S.E. Pryse, and N.S. Wheadon (1988). Amplitude and phase scintillation at high latitudes over Europe, **Radio Sci. 23**, 320-330 (May-June)

Johnson, A.L. (1988). Short-term magnetic field alignment variations of equatorial ionospheric irregularities, **Radio Sci. 23**, 331-336, May-June.

Johnson, F.S. (1961). **Satellite Environment Handbook**, Stanford University Press.

Mollen, T.A., C.H. Liu and D.J. Fang (1988). A study of C-band equatorial scintillation in the Asian sector, **Radio Sci. 23**, 337-345, May-June.

Rino, C.L., M.D. Cousins, and J.A. Klobuchar (1981). Amplitude and phase scintillation measurements using the Global Positioning System, 253-261 of **Proceedings of the Ionosphere Effects Symposium 1981**, U.S. Gov't Printing Office.

Secan, J.A., E.J. Fremouw, and R.E. Robins (1987). A review of recent improvements to the WBMOD ionospheric scintillation model. 607-616, **Effect of the Ionosphere on Communications, Navigation, and Surveillance Systems**, J. Goodman, Ed., U.S. Gov't Printing Office.

Secan, J.A., R.M. Bussey, E.J. Fremouw, and Sa. Basu (1993). An improved model of equatorial scintillation, **Proceedings of the Ionosphere Effects Symposium 1993**, U.S. Gov't Printing Office.

Smith, E.K. (1957). Magnetic latitude derived from the dip angle, Appendix III of **Worldwide Occurrence of Sporadic E**, NBS Circular 582, U.S. Gov't Printing Office.

Smith, E.K. (1974). ***A Study of Ionospheric Scintillation As It Affects Satellite Communication***. OT Technical Memorandum 74-186, U.S. Department of Commerce.

Whitney, H.E. (1969). The definition of scintillation index and its use for characterizing ionospheric effects, 3-5, **AGARD Report 571**, Jules Aarons, Ed.

Yeh, K.C., J.P. Mullen, J.R. Medeiros, R.F. da Silva and R.T. Medeiros (1981). Ionospheric scintillation observations at Natal, 202-209, **Proceedings of the Ionosphere Effects Symposium 1981**, U.S. Gov't Printing Office.

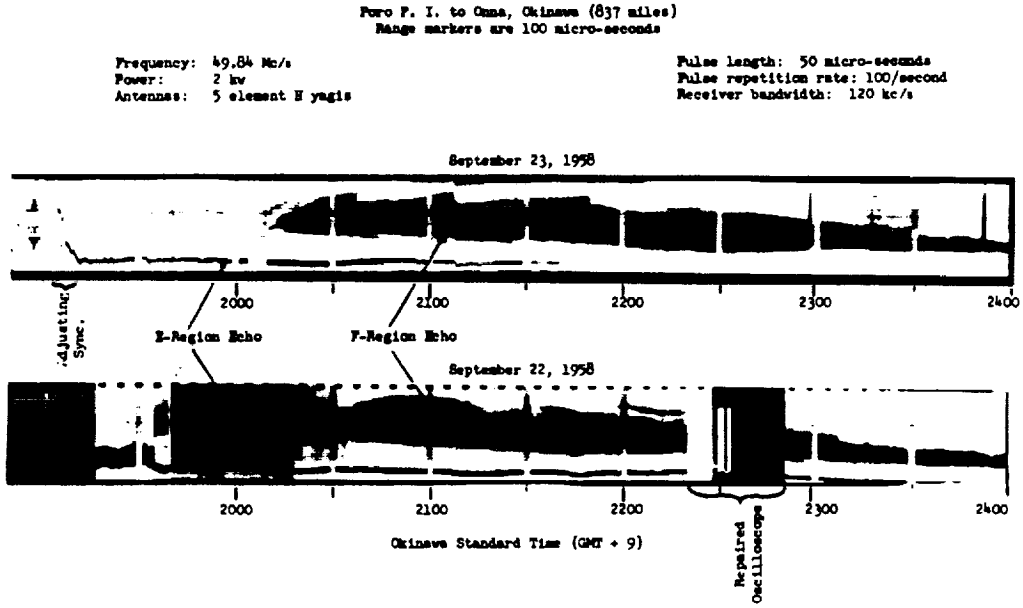

Figure 1. The "Far Eastern" or evening signal anomaly; after Bateman et. al., 1959)

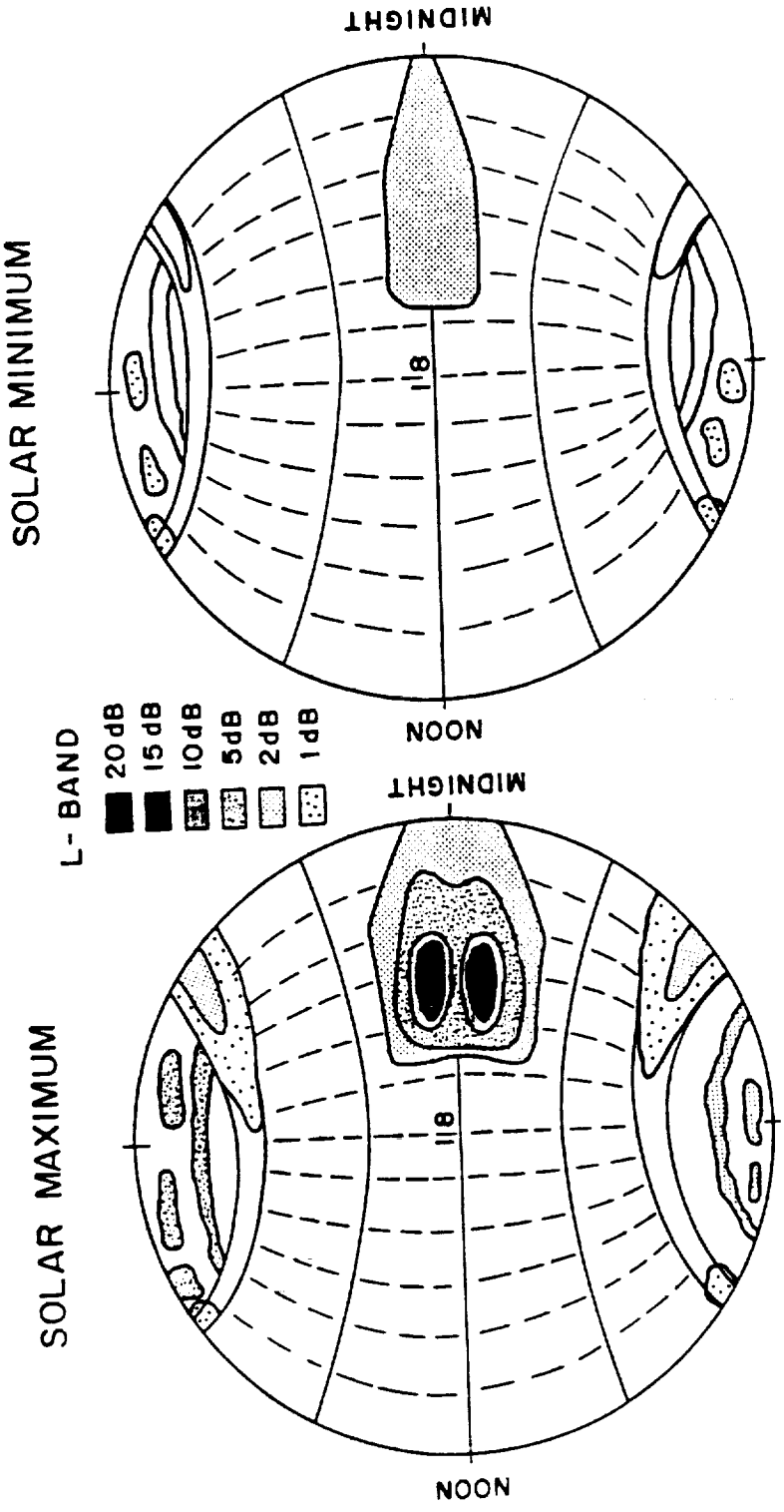

Figure 2. Illustrative picture of scintillation occurrence based on observations at L-band (1.6 GHz); after Basu et al. 1988.

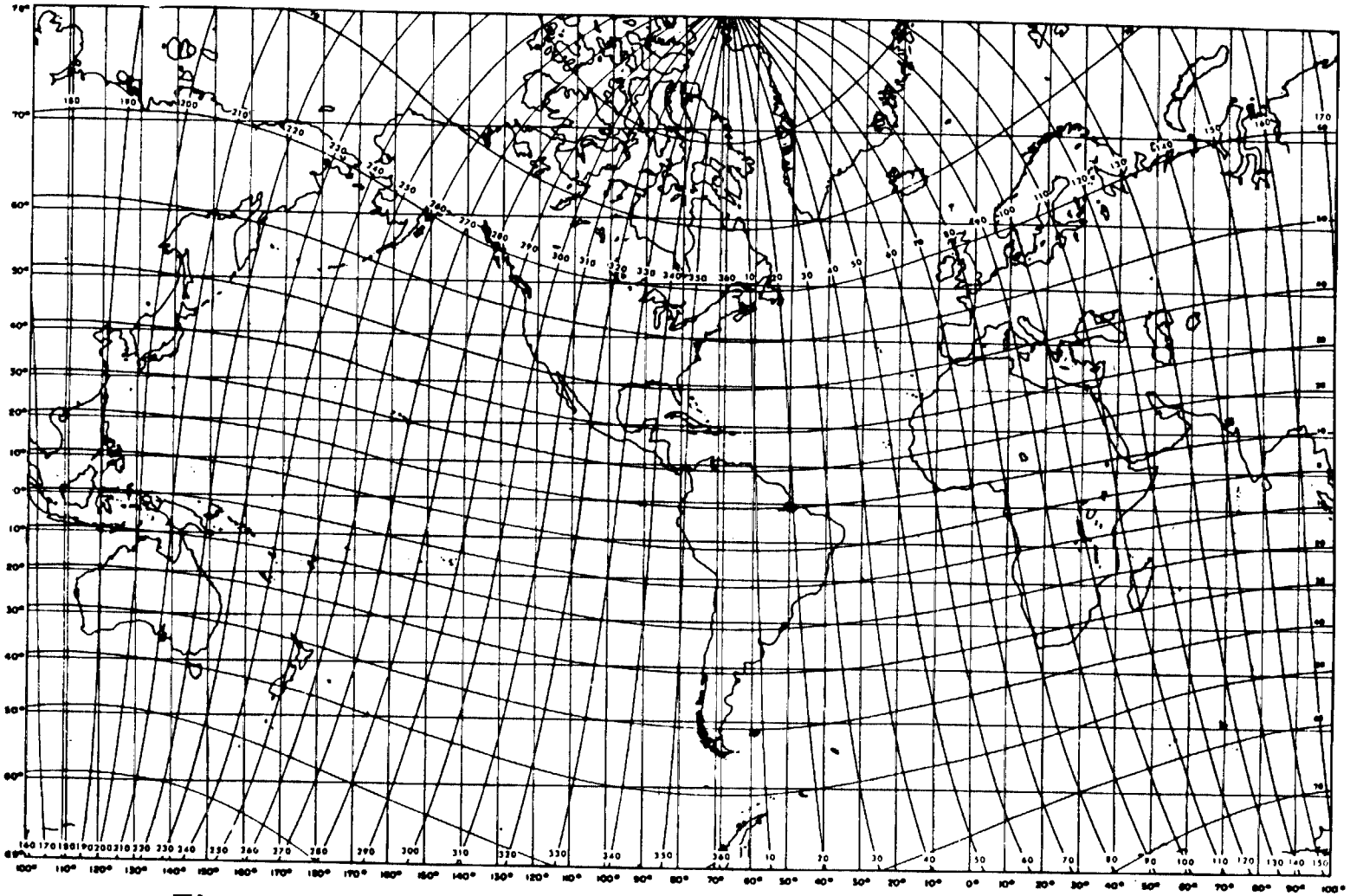

Figure 3. Geomagnetic dipole field coordinate grid superimposed on a Mercator projection of the world; after Johnson 1961.

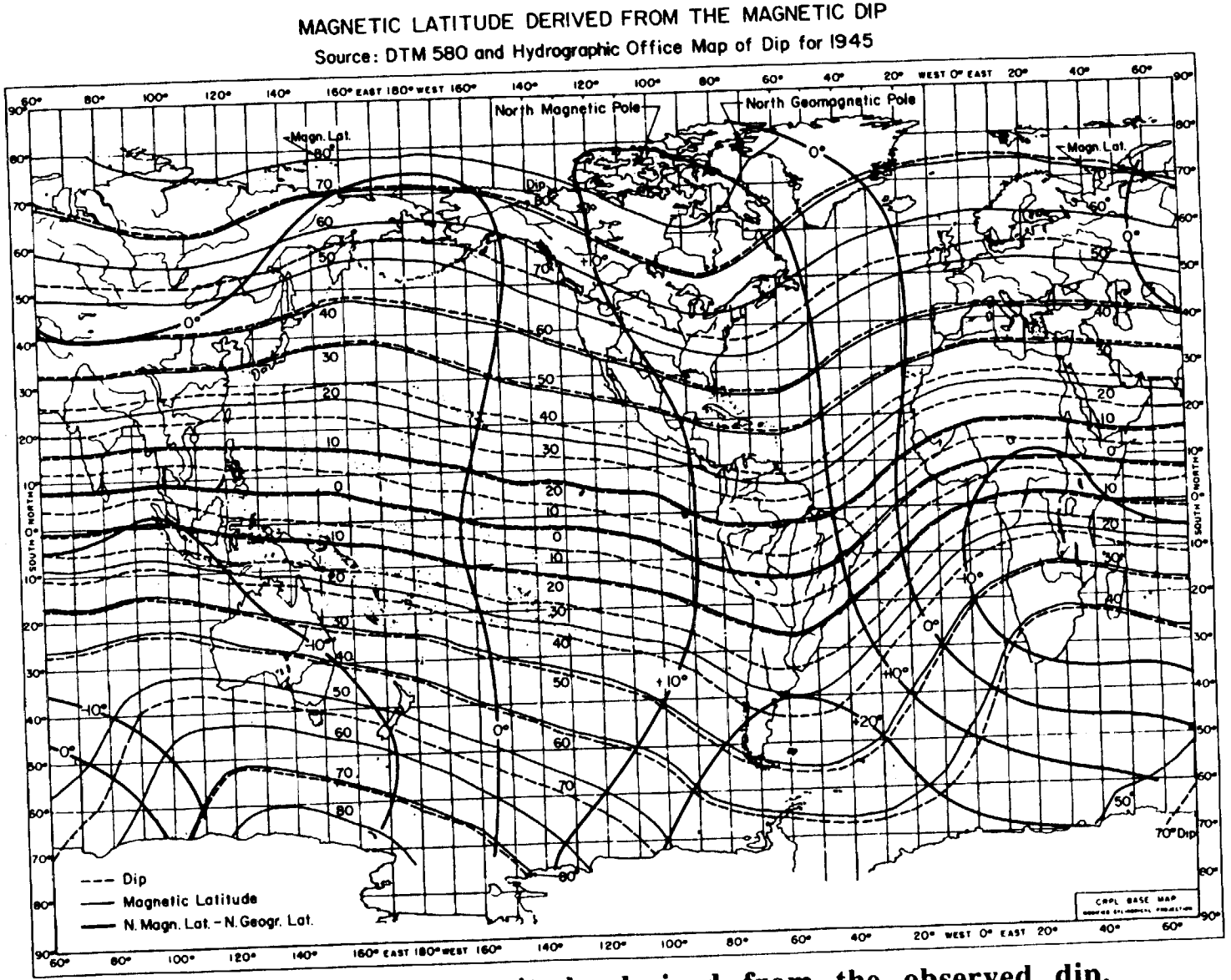

Figure 4. Magnetic latitude derived from the observed dip, epoch 1955; after Smith 1957.

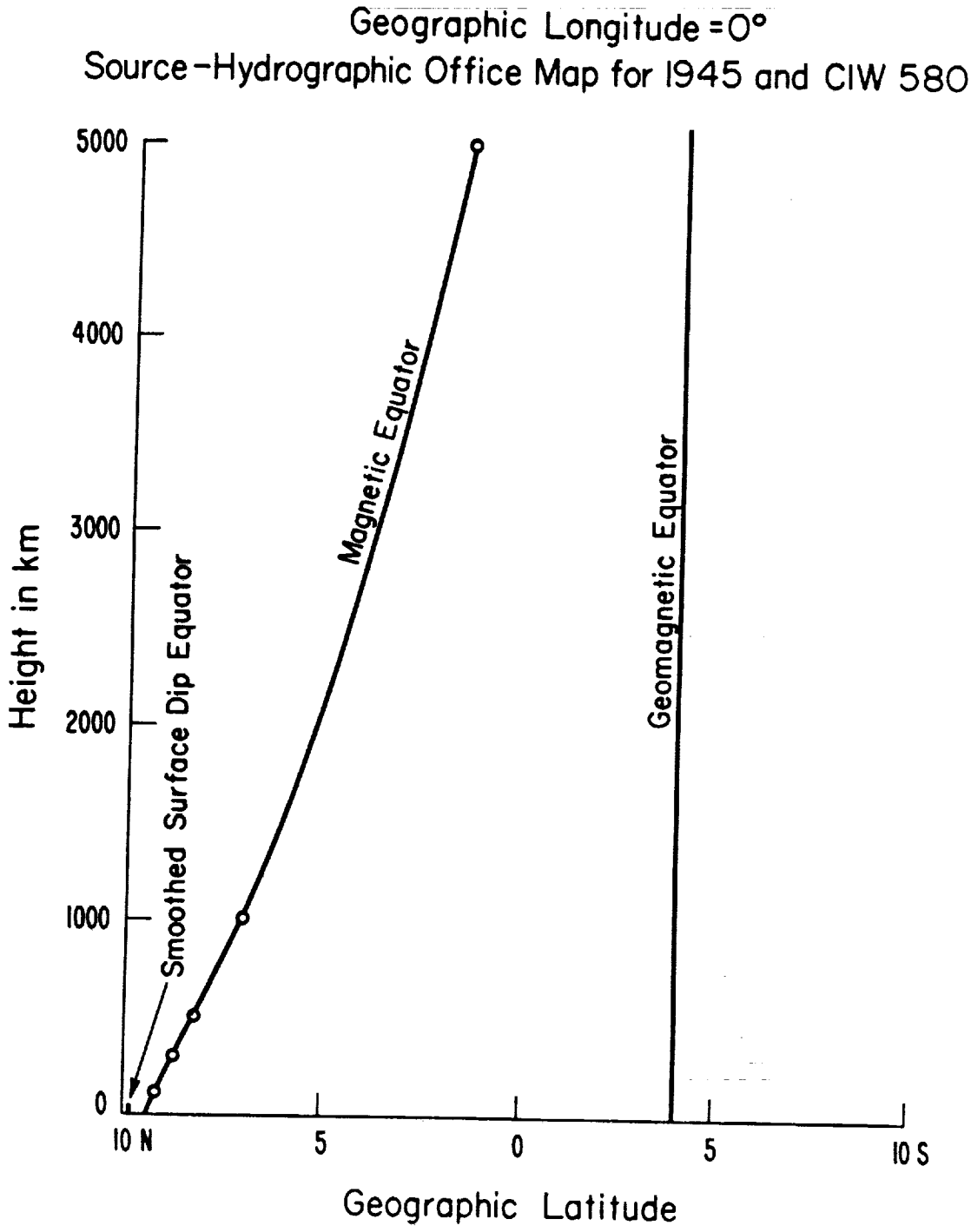

Figure 5. Comparison of the surface magnetic equator with the geomagnetic equator as a function of altitude above the earth; after Smith 1957.

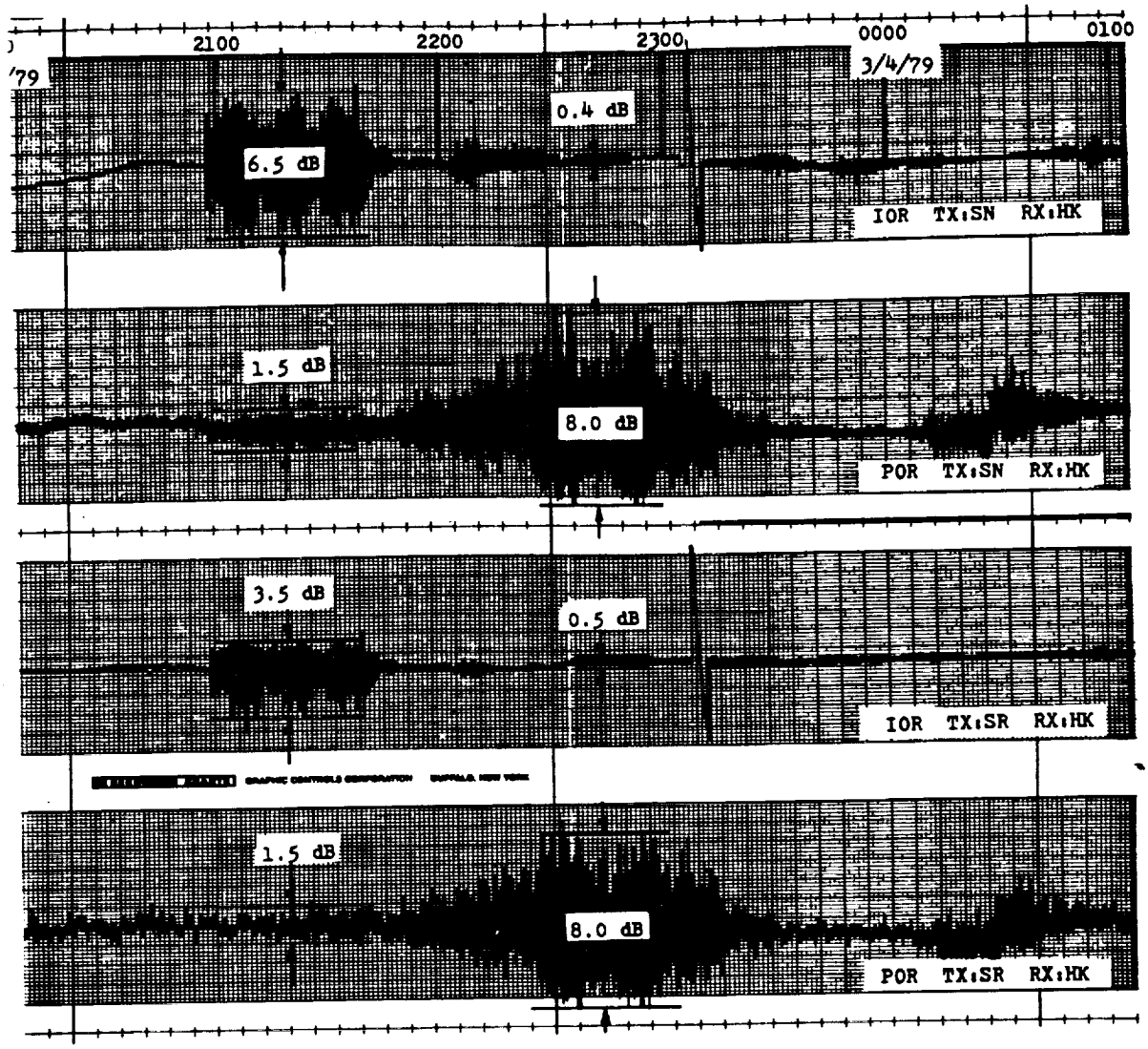

Figure 6. Records of C-band ionospheric scintillation on March 3-4, 1979 from Hong Kong; after Fang 1981.

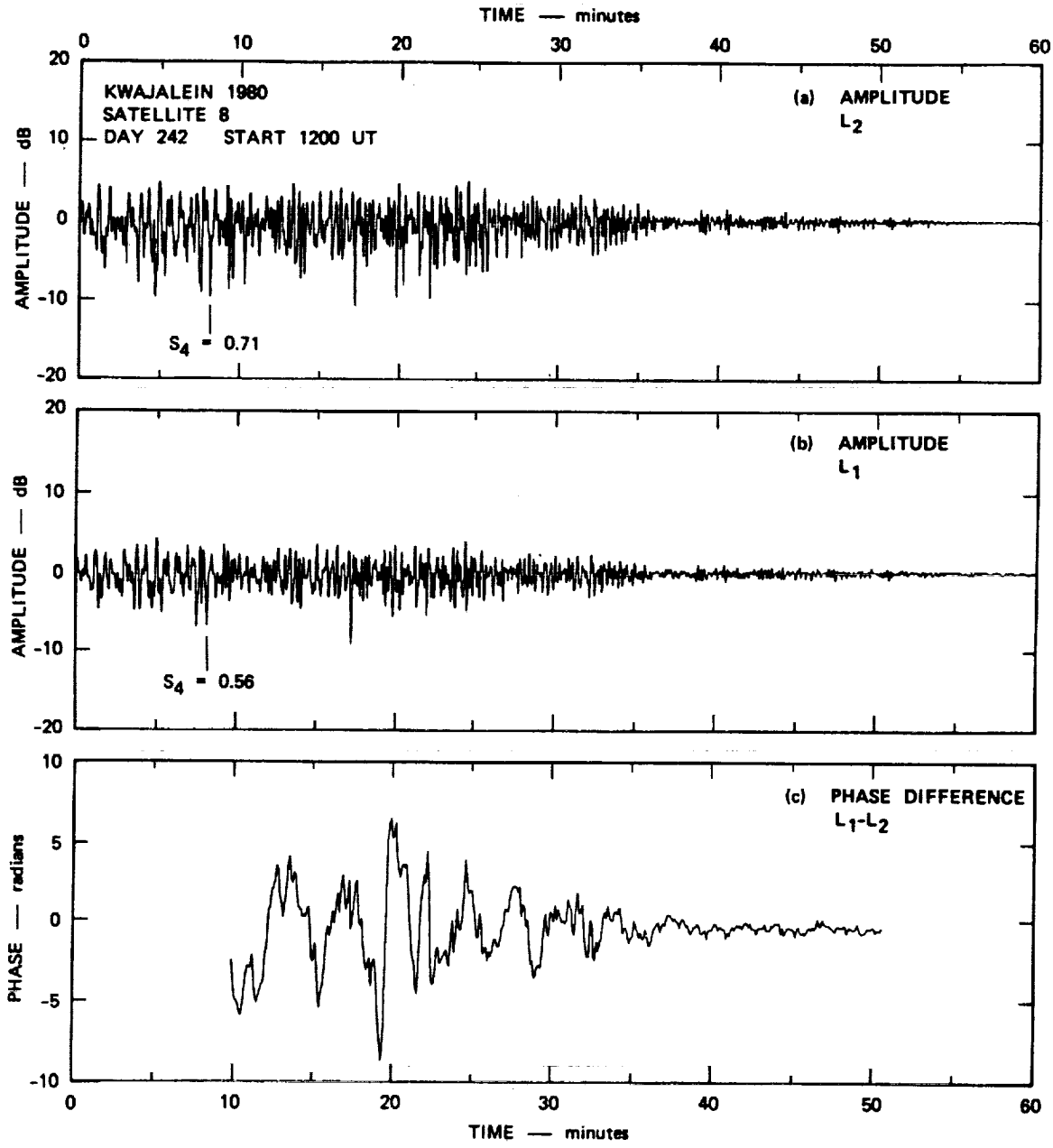

Figure 7. Example of strong L-band scintillation and decay on GPS signals; after Rino et al. 1981.

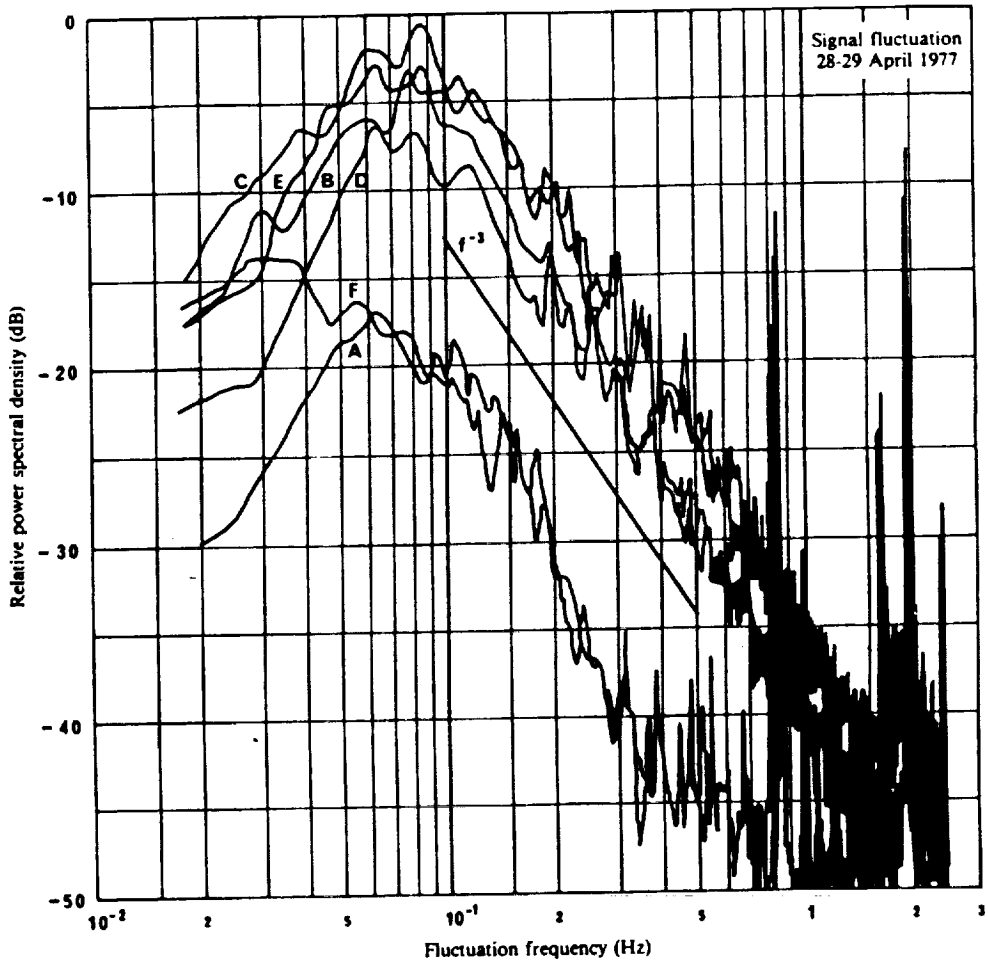

Figure 8. Power spectral density estimates for a geostationary satellite (Intelsat 4) at 4 GHz.; after CCIR 1990.

The scintillation event was observed during the evenings of 28-29 April 1977 at Taipei Earth Station

A: 30 minutes before event onset
B: at the beginning
C: 1 hour after
D: 2 hours after
E: 3 hours after
F: 4 hours after

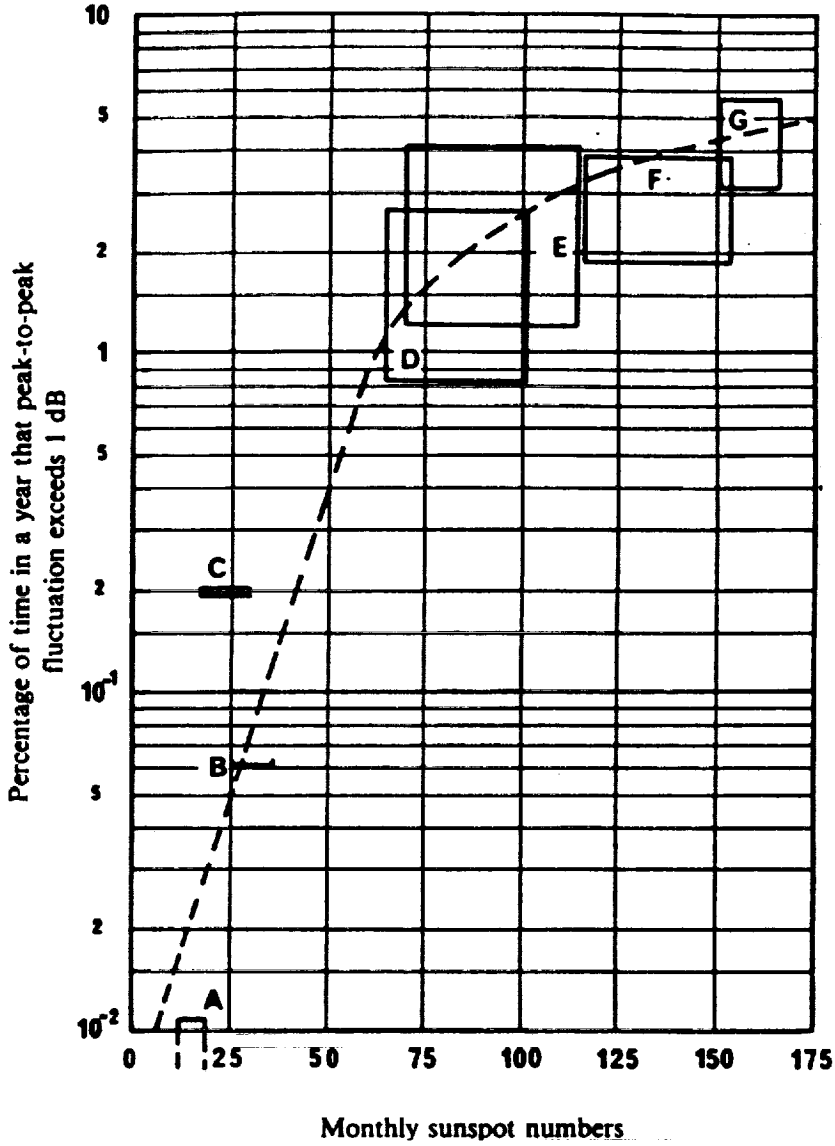

Figure 9. Dependence of 4 GHz equatorial scintillation on sunspot number; after Fang 1980, Fang and Pontes 1981

The bars and squares are the ranges of variations over a year for different carriers.

A: 1975-1976, Hong-Kong and Bahrein, 15 carriers
B: 1974, Longovilo, 1 carrier
C: 1976-1977, Taipei, 2 carriers
D: 1970-1971, 12 stations, > 50 carriers
E: 1977-1978, Hong-Kong, 12 carriers
F: 1978-1979, Hong-Kong, 10 carriers
G: 1979-1980, Hong-Kong, 6 carriers

TREE ATTENUATION AT 20 GHZ: FOLIAGE EFFECTS

W. J. Vogel, EERL, The University of Texas at Austin

J. Goldhirsh, APL, The Johns Hopkins University

Abstract - Static tree attenuation measurements at 20 GHz (K-Band) on a 30° slant path through a mature Pecan tree *with* and *without* leaves have shown median fades exceeding approximately 23 dB and 7 dB, respectively. The corresponding 1% probability fades were 43 dB and 25 dB. Previous 1.6 GHz (L-Band) measurements for the bare tree case showed fades *larger* than those at K-Band by 3.4 dB for the median and *smaller* by approximately 7 dB at the 1% probability. While the presence of foliage had only a small effect on fading at L-Band (approximately 1 dB additional for the median to 1% probability range), the attenuation increase was significant at K-Band, where it increased by about 17 dB over the same probability range.

Introduction

First generation personal and mobile satellite communication systems will soon become operational at frequencies near 1.6 and 2.5 GHz (L- and S-Band). To ensure that these systems provide dependable services in the presence of fading caused by multipath or shadowing, their designers rely upon propagation results obtained by many researchers over the last decade [1]. The limited spectrum allocated to mobile satellite services at L- and S-band, however, has proponents of follow-on systems looking towards the 20/30 GHz region, where much more bandwidth is available, but where mobile propagation effects have not yet been characterized. It is anticipated that, at K-Band, the major causes of signal attenuation on mobile links will be blockage due to buildings, tree shadowing, and rain attenuation. This contribution describes a preliminary experiment performed to characterize what will probably be the most pervasive cause of mobile K-Band fading, namely tree shadowing, as suggested by horizontal path measurements at 29 GHz through single Pecan trees, which reported average attenuations of 32 dB to 18 dB for trees with and without leaves [2]. The results described here were derived from a configuration simulating a satellite-to-earth path. They revealed considerable fading at K-Band and significant difference between L- and K-Band in the seasonal variability of tree shadowing, i.e., the effect of foliage. The difference has implications on the success of fade mitigation techniques, such as error correction coding.

Measurement of Tree Attenuation

At the present time, options for performing mobile K-Band tree attenuation measurements on an elevated path in the U.S. are limited to observing the Olympus satellite beacon. While the Olympus beacon illuminates the eastern U.S. with an elevation angle of 16°, its low power requires at least a 60 cm diameter antenna to achieve a signal to noise ratio (SNR) of approximately 20 dB in a narrow-band receiver. There are several disadvantages to using such a large antenna. First, the narrow beamwidth (1.7°) makes a mobile platform from which to observe Olympus extremely difficult and expensive. Second, the tower measurements described here have demonstrated that a significantly higher fade margin is required than is realistically achievable for mobile scenarios using Olympus. Furthermore, aperture averaging of tree shadowing and multipath suppression may make results obtained with a large antenna not

representative of mobile performance when using planned smaller antennas. Efforts are underway to execute an extensive land mobile satellite propagation campaign in Central Maryland and Alaska using the Advanced Communications Technology Satellite (ACTS) in its high gain mode, where a 50 dB SNR will be achieved with just an 8 cm diameter tracking antenna [3].

Experimental Details

In order to provide an estimate of the 20 GHz slant path attenuation expected from roadside trees for the planned mobile ACTS fade measurement experiment, a campaign was undertaken to measure the slant path stationary attenuation caused by trees at 19.6 GHz and to compare these results with earlier measurements at 1.6 GHz. Both sets of measurements were repeated for a Pecan tree *with* and *without* leaves to establish the seasonal variability of attenuation. An evergreen Magnolia tree was also tested at K-Band using a similar geometry. Table 1 summarizes the pertinent experimental parameters.

Table 1 EXPERIMENTAL PARAMETERS

	L-Band	K-Band
Frequency	1.6 GHz	19.6 GHz
Polarization	RHCP	Vertical
Transmitter Power	100 mW	1mW
Transmitter Beamwidth	90°	66°
Transmitter Height	20 m	18 m
Elevation Angle (Pecan/Magnolia*)	30°/NA	26°/61°
Range (Pecan/Magnolia*)	36/NA m	36/21 m
Receiver Beamwidth	90°	32°
Receiver Noise Temperature	< 400 K	< 400 K
Receiver Noise Bandwidth	1000 Hz	1000 Hz
Receiver Height	1.5 m	1.5 m
Dynamic Range	> 50 dB	> 50 dB

* NA denotes Not Available

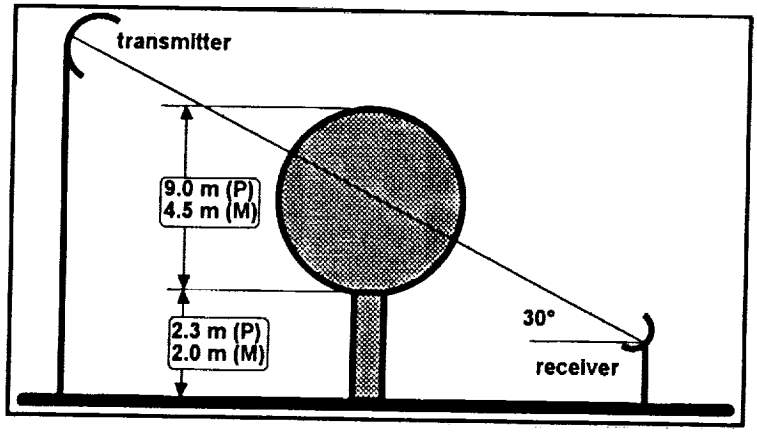

Fig. 1 Experimental Configuration for Pecan (P) and Magnolia (M) Trees with Foliage

The measurements at L-Band were performed on 13 December 1990 and 12 July 1991. The receiving antenna was mounted on a motorized positioner placed within the geometric shadow zone of a pecan tree (Figure 1). The antenna was moved slowly over a horizontal distance of several m, while the received power was sampled every 0.1 s for the duration of about 100 s. At K-Band, measurements were performed on 10 March 1993 and 11 May 1993 employing the same approximate geometry. The receiving antenna was hand-held and moved horizontally over a distance of several m, first in the shadow of the same Pecan tree, and then in the shadow of a

nearby evergreen Magnolia tree (Figure 1). Quadrature detector receiver voltages were sampled at a 1000 Hz rate for several minutes. The path length within the crown was, on average, 9 m for the Pecan tree and 4.5 m for the Magnolia tree. The clear line-of-sight (LOS) level at both frequencies and each tree was determined by moving the receiver axially to a point where the signal path was unobstructed.

Results

Time series examples at the two measurement frequencies are plotted in Figure 2. The 1 s sample of the K-Band clear LOS signal (upper curve) shows the effect of multipath reflections. Even though the path from transmitter to receiver was unobstructed, the Pecan tree was within the field of view of both antennas. Forward- scatter from the Pecan tree causes constructive and destructive interference with the direct signal as relative phases change. The upper frequency of this variation equals the ratio of the relative speed of the receiver to the wavelength. Here it is below 10 Hz, indicating that relative motion between observer and the tree was below about 0.15 m/s. For the 1 s segment of data shown, the attenuation by the bare Pecan (second curve from top) was in the 2 to 7 dB range, compared to 8 dB and 20 dB for the 45 s data of L-Band attenuation (third curve from top on left). When the Pecan was in full foliage, the L-Band signal level decreased slightly below the bare case. On the other hand, the K-Band signal level decreased dramatically, showing fades in the 20 to 40 dB range (fourth curve from top on right). Similar fades were observed through an evergreen Magnolia tree with big, waxy leaves (fourth curve from top on left). We conclude from these results that foliage is a major contributor to signal attenuation at K-Band but not at L-Band, and that the wood part of the tree is predominantly responsible for attenuation in the lower frequency range.

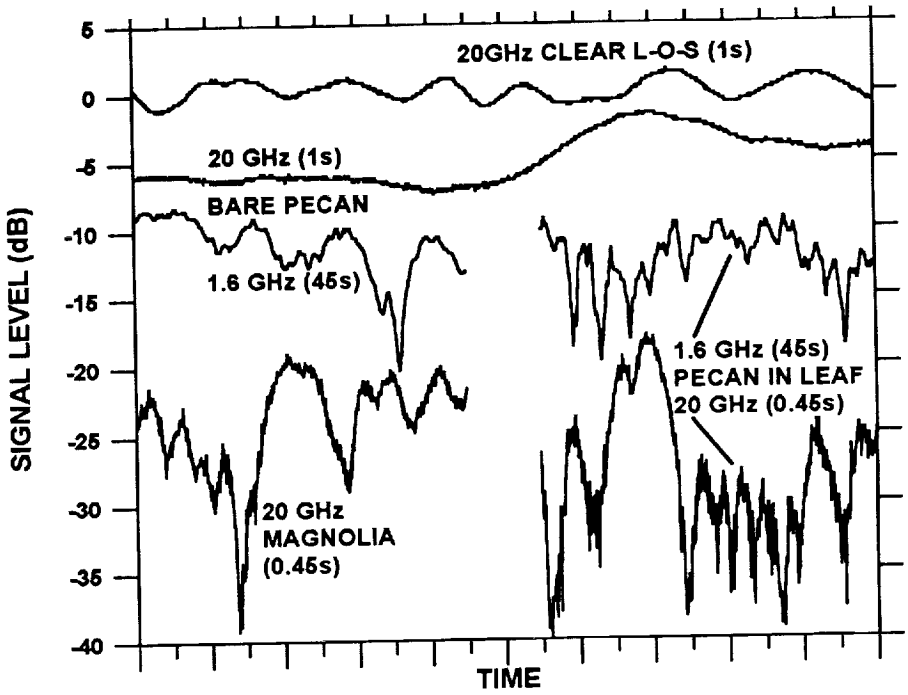

Fig. 2 Time Series Examples of Tree Shadowing Effects When the Receiver is in Motion

The cumulative distribution functions (CDFs) in Figure 3 give the fraction of locations at which fade levels were exceeded for cases in which the path was either entirely unobstructed (clear LOS) or entirely obstructed (tree shadowed). These distri-butions demonstrate that the presence of foliage increases the median L- and K-Band fading by approximately 1 and 17 dB vis-à-vis the bare tree case, respectively. Also apparent is that at L-Band fading can be higher than at K-Band for the bare tree case. This may be explained by noting that for the given geometry, the L-Band Fresnel zone diameter is about 2.7 m compared to 0.7 m at K-Band. Assuming the branches of a bare tree act similar to a conducting mesh, the L-Band Fresnel zone size is larger than the mesh scale at all receiver positions and the signal is always attenuated. In contrast, at K-Band there are many positions where the branch spacing is comparable to or larger than the K-Band Fresnel dimension. Hence, smaller attenuations are experienced for these geometries. On the other hand, at some locations (e.g., at the 1% probability), the openings between branches are smaller than the K-Band Fresnel dimension and significantly deeper fading occurs than at L-Band (e.g., 25 dB versus 18 dB). The measured median and 1% fades are summarized in Table 2 for the bare Pecan, Pecan with leaf, and Magnolia with leaf along with the estimated corresponding attenuation coefficients.

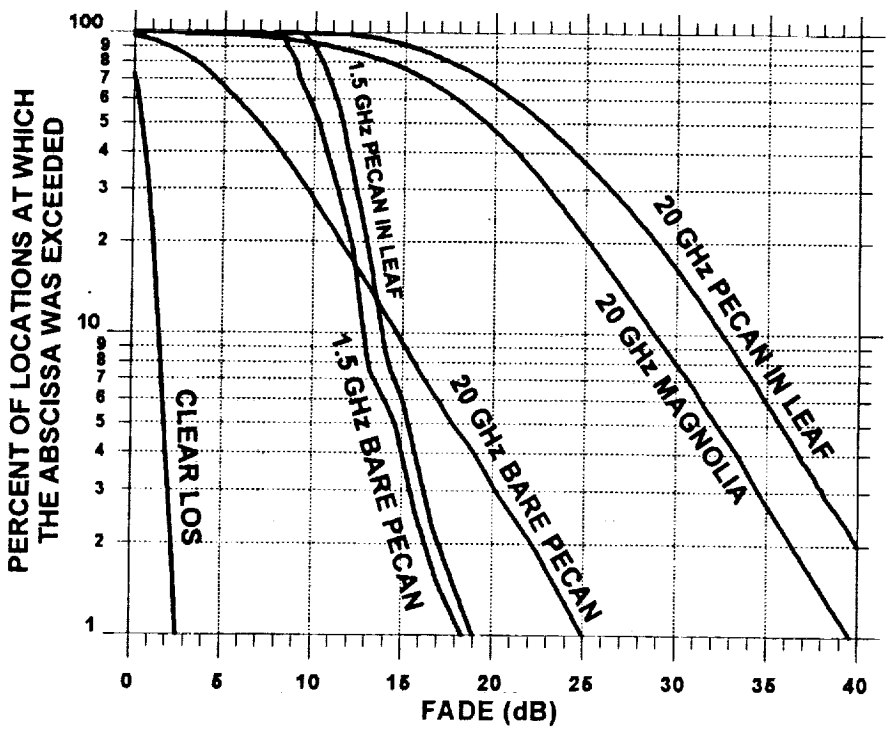

Fig. 3 The Cumulative Distribution Functions for the Clear LOS, as well as Pecan and Magnolia Trees *With* and *Without* Foliage

Table 2 MEDIAN AND 1% FADES AT L- AND K-BAND

		Total Fade (dB)		Attenuation Coefficient (dB/m)	
		L-Band	K-Band	L-Band	K-Band
Clear L-O-S	Median		0.5		
	1%		2.6		
Bare Pecan	Median	10.3	6.9	1.1	0.75
	1%	18.4	25.0	2.0	2.8
Pecan in Leaf	Median	11.6	22.7	1.3	2.5
	1%	18.6	43	2.1	4.8
Magnolia	Median		19.6		4.4
	1%		39.6		8.8

Summary and Conclusions

In preparation for planned mobile propagation measurements with ACTS, an experimental campaign was undertaken to establish the expected attenuation from tree canopies at 20 GHz. Median and 1% probability fades for the full foliage case were noted to be approximately 23 dB and 43 dB, respectively, for the Pecan tree. Attenuations of 20 dB (median) and 40 dB (1%) were experienced for the Magnolia tree.

An unexpected result was that the 20 GHz median attenuation for the Pecan tree without foliage was found to be approximately 3 dB smaller than the median attenuation at 1.6 GHz. This difference may be explained in terms of the relative dimensions of the spacing between branches and the relative Fresnel dimensions for the two frequencies at the tree location. The openings between branches for many receiver LOS aspects were comparable to or larger than the K-Band Fresnel dimension (0.7 m), whereas the branch spacing was always within the L-Band Fresnel dimension (2.7 m). There were, however, some receiver geometries for which the LOS aspect was such that the branch spacing was smaller than the K-Band Fresnel dimension, and significantly larger fading was measured for these cases (e.g., 8 dB larger at 1% probability). The attenuation scaling formulation relating the ratio of fades to the square root of the ratio of the frequencies, previously validated in the range between UHF (870 MHz) and S-Band (3 GHz) [1], was tested at K-Band. It was found not to be applicable between 1.6 GHz and 19.6 GHz for the Pecan tree case.

Acknowledgments: This effort was supported by the NASA Propagation Program sponsored by the Office of Commercial Programs under JPL Contract 956520 for The University of Texas and N0039-91-C-001 for The Johns Hopkins University.

References

1. J. Goldhirsh and W. J. Vogel, "Propagation Effects for Land Mobile Satellite Systems: Overview of Experimental and Modeling Results," NASA Reference Publication 1274, February 1992

2. E. J. Violette, R. H. Espeland, and F. Schwering, "Vegetation Loss Measurements at 9.6, 28.8, and 57.6 GHz Through a Pecan Orchard in Texas," CECOM Report 83-2, US Army Communications-Electronics Command, Fort Monmouth, New Jersey, March 1983

3. J. Goldhirsh, W. J. Vogel, and G. W. Torrence, "K-Band Mobile Propagation Measurements Using ACTS," *Proceedings of the International Mobile Satellite Conference, IMSC '93,* Pasadena, California, June 16-18, 1993.

ACTS MINIWORKSHOP

Session 1

PROGRAM STATUS AND UPDATE

Chairman:

Faramaz Davarian

Jet Propulsion Laboratory

ADVANCED COMMUNICATIONS TECHNOLOGY SATELLITE (ACTS) PROGRAM

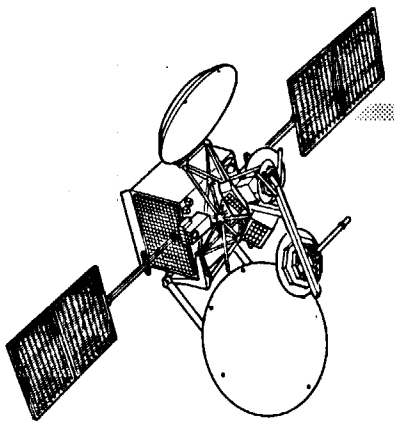

ROBERT BAUER
NASA LEWIS RESEARCH CENTER

ACTS PROJECT UPDATE

ACTS MINI WORKSHOP/NAPEX XVII
PASADENA, CA
06/14-15/93

ACTS

NASA

PROJECT STATUS

LAUNCH PREPARATIONS

- SPACECRAFT MATED TO TOS; VERTICAL PROCESSING FACILITY (VPF) COMPLETE; MOVE TO PAD BY 06/24 FOR INTEGRATION WITH DISCOVERY.

- TARGET LAUNCH DATE: JULY 15, 1993

- ACTS LAUNCH DATE DEPENDENT ON ENDEAVOR LAUNCH (JUNE 20)

ON ORBIT CHECKOUT

- TRANSFER/DRIFT ORBIT: COMPLETE AT ABOUT L + 11 DAYS

- MCP TURN-ON: ABOUT 8 DAYS AFTER DRIFT ORBIT WHEN S/C IS 3-AXIS STABILIZED. (KBT, UFB TURN-ON SHORTLY AFTERWARDS)

- FINISH SPACECRAFT (BUS/PAYLOAD) TESTING: ~30 DAYS AFTER LAUNCH (08/13).

- SYSTEM CHECKOUT FOLLOWS S/C TESTING: DURATION = 50 DAYS. COMPLETED 10/02.

ALL LEWIS READINESS REVIEWS COMPLETED. STS REVIEWS THROUGH JULY.

EXPERIMENTS PROGRAM STATUS

EXPERIMENTS PERIOD STILL BEGINS 10/04/93!

PROPAGATION EXPERIMENTS

- ALTHOUGH INITIAL KBT, UFB TURN-ON APPROXIMATELY AUG. 7, NO REQUIREMENT TO MMAS TO MAINTAIN SIGNALS UNTIL REFERENCE TERMINAL EQUIPMENT (RTE, PART OF MASTER CONTROL STATION) IS BROUGHT ON-LINE AUG. 13.

- USE AUG. 13 FOR APT ANTENNA ALIGNMENT BEGIN.

- FOR CLASS II AND USERS OF THE MULTIBEAM COMM. PACKAGE, USE EXPERIMENTS BEGIN DATE OF OCT. 4.

EOA EXPERIMENTS

- TOTAL OF 72 APPROVED EXPERIMENTS (INCLUDES PROPAGATION).

- 86 ORGANIZATIONS PARTICIPATING

- SPACECRAFT ALLOCATION FOR 1ST 6 MOS.- 98.9% OF PRIME HOURS
  78.2% OF OFF PRIME HRS

ACTS

NASA

EARTH STATION STATUS

NGS/MCS

- TERMINAL INSTALLATION AT LEWIS COMPLETED. READY TO SUPPORT TRAINING AND FLIGHT SIMULATIONS.

- COMSAT OPERATORS HIRED AND ON-BOARD.

T1 VSAT

- PROBLEMS ENCOUNTERED WITH HPFD'S. M/A-COM AND STEINBRECHER UNITS BEING CORRECTED AND TESTED.

- ENHANCEMENTS BEING WORKED INCLUDE: S/W MOD's, ECHO CANCELLERS, CABLE LENGTH, UPLINK POWER LEVELING, AND UPLINK/DOWNLINK ATTENUATORS.

HIGH DATA RATE

- MOTOROLA/BBN CONTRACTED TO DEVELOP (622 MBPS MAX THROUGHPUT).

- CDR HELD 04/28-29/93 AT BBN.

- DELIVERY OF OPERATIONAL TERMINALS IS 08/94 (QUANTITY = 5).

EARTH STATION STATUS, cont.

USAT

- DELIVERY OF OPERATIONAL TERMINALS IS 08/94 (QUANTITY = 5).
- PRODELIN SELECTED AS ANTENNA SUPPLIER.
- ALL CRITICAL H/W ORDERED; PROJECT ON SCHEDULE & WITHIN BUDGET.

AMT/AERO

- AMT ON SCHEDULE TO BEGIN EXPTS. IN 10/93.
- AERO EXPT. TO BEGIN 03/94

ACTS

NASA

ACTS
LeRC Current Assessment

BASELINE: TBD

STATUS : 6/08/93

PREPARED BY: COOK/BEZNOSKA

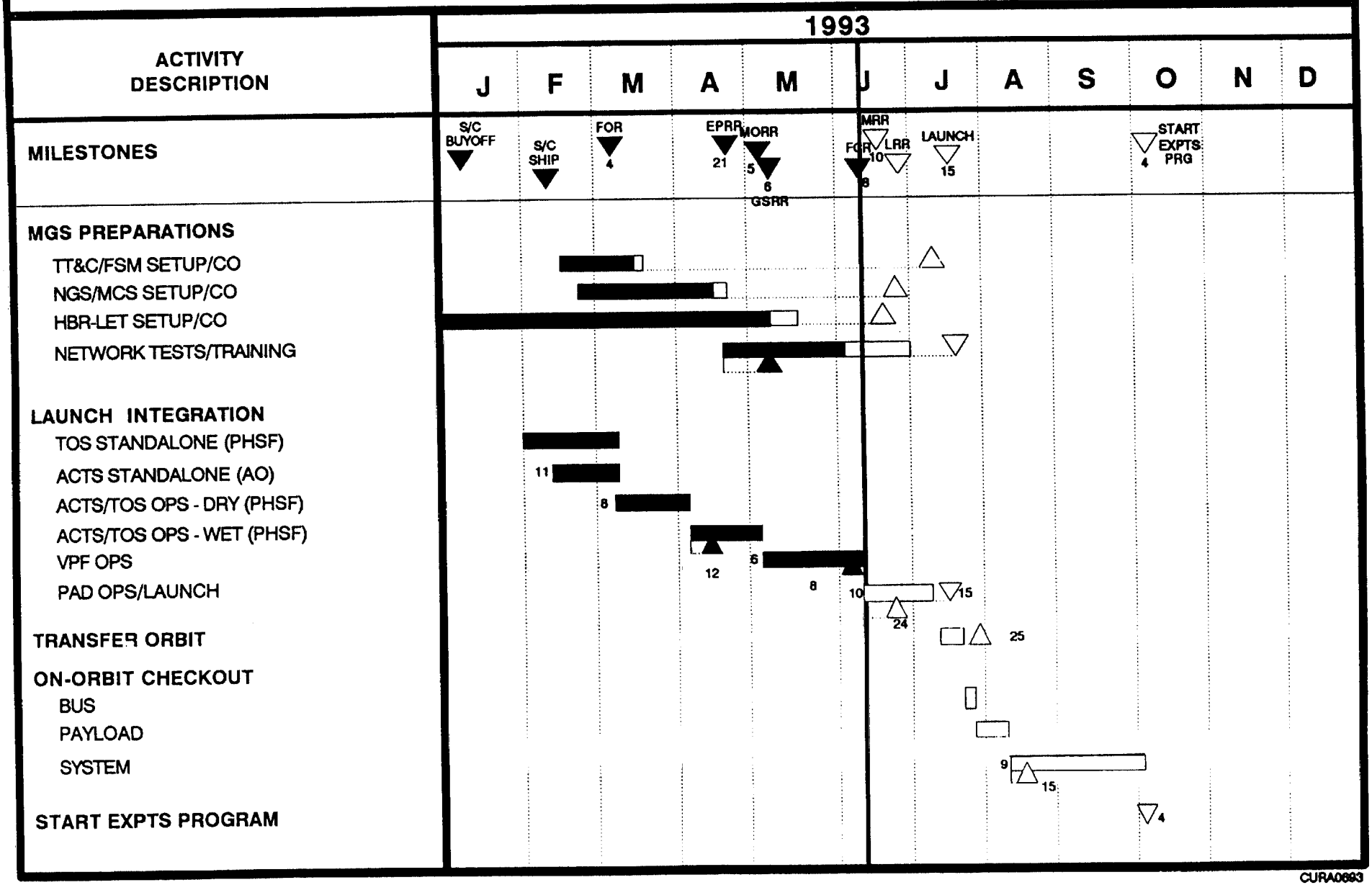

CURA0693

July 1993

ACTS On-Orbit Checkout Plan

SUNDAY	MONDAY	TUESDAY	WEDNESDAY	THURSDAY	FRIDAY	SATURDAY
				1	2	3
4	5	6	7	8	9	10
11	12	13	14	15 ACTS LAUNCH	16	17 TRANSFER ORBIT INJECTION
18	19	20	21	22	23	24
25	26	27	28 3 AXIS STABILIZED	29	30	31

DRIFT ORBIT

DRIFT ORBIT

S/C BUS TESTS

August 1993

ACTS On-Orbit Checkout Plan

SUNDAY	MONDAY	TUESDAY	WEDNESDAY	THURSDAY	FRIDAY	SATURDAY
1	2	3	4 PAYLOAD CHECKOUT (MCP TURN-ON)	5	6	7 **KBT, UFB TURN-ON (ESTIMATE)**
			PAYLOAD CHECKOUT			
S/C BUS TESTS						
8	9	10	11	12	13 BEGIN SYSTEM CHECKOUT (RTE turn-on)	14
PAYLOAD CHECKOUT						
S/C BUS TESTS						
15	16	17	18	19	20	21
	SYSTEM CHECKOUT					
22	23	24	25	26	27	28
	SYSTEM CHECKOUT					
29	30	31				
	SYSTEM CHECKOUT					

September 1993

ACTS On-Orbit Checkout Plan

SUNDAY	MONDAY	TUESDAY	WEDNESDAY	THURSDAY	FRIDAY	SATURDAY
			1	2	3	4
5	6	7	8	9	10	11
12	13	14	15	16	17	18
19	20	21	22	23	24	25
26	27	28	29	30		

SYSTEM CHECKOUT

October 1993

ACTS On-Orbit Checkout Plan

SUNDAY	MONDAY	TUESDAY	WEDNESDAY	THURSDAY	FRIDAY	SATURDAY
					1 SYSTEM CHECKOUT	2
3	4 EXPERIMENTS PERIOD BEGINS	5	6	7	8	9
10	11	12	13	14	15	16
17	18	19	20	21	22	23
24	25	26	27	28	29	30
31						

ACTION ITEM RESPONSE

TOPIC: NASA's PLANS TO DISSEMINATE SATELLITE MANEUVERS, EPHEMERIS, AND UNUSUAL EVENTS (ACTS BULLETINS)

ASSIGNED TO: ROBERT BAUER, NASA LEWIS

ACTION TAKEN:

- Topic was discussed at ACTS Operations Working Group session based on example provided by T. Pratt from Olympus program to determine what information MMAS can provide and how often.
  - Description of S/C maneuvers and list of S/C position information that is to be provided is enclosed.
  - S/C position information updated after each maneuver (~ 1/wk) with refined post-maneuver data.
  - All unusual events and events impacting experiments will be posted.
  - *NOT PROVIDED* - Antenna pointing data for each site.

- Bulletin Board Status
  - System to be implemented by Computer Services Division at Lewis; ACTS Experiments Office to be system administrator.
  - INTERNET access.
  - Will have interactive and read-only applications.
  - To be used as primary communication tool for routine information to all experimenters.
  - Requirements drafted; estimate is to have e-mail list on-line by July 9.
  - Back-up position: If system unavailable by beginning of ACTS beacon turn-on, information will be fax'd to experimenters.

PROPOSE: S/C information be E-mailed directly to all propagation experimenters (or to one name/site).
Create a propagation distribution list.
NEED: INTERNET addresses and FAX numbers for all propagation experimenters.

ACTS ORBIT & ATTITUDE CONTROL OPERATIONS

Procedures

Contained in S/C Operating Instruction SOI-ACTS-A-01, Attitude Control Operations.

ACTS S/C Analyst generates maneuver schedules and maneuver parameters.

ASOC off-line computer supports all operations.

- Stationkeeping
- Ranging
- Momentum Unloading
- Yaw Control
- S/C Offset Pointing

Stationkeeping

Goal is to do N/S maneuver on weekends for minimum experiment impact but E/W maneuver may be necessary during week.

Notify experimenters of possible pointing degradation due to attitude disturbances during maneuver.

North/South

Maintains inclination within +/-0.05° box.
Expect 3 to 4 week intervals with 0.01° margin.

Execute near ascending node per orbit determination for minimum fuel usage.

Plan primary and alternate day (Sat & Sun).

Maneuver duration expected to be < 2 hours.

N/S Coupling to E/W

E/W drift correction (if necessary) at least two days after N/S.

East/West

Drift correction maintains longitude within +/-0.05° box.

Expected at 11 to 14 day intervals for 0.01° margin.

Execution time (~apogee/perigee) depends on eccentricity.

Maneuver duration expected < 1/2 hour (small disturbance).

Eccentricity Control

Second half of E/W, 12 hours later (apogee/perigee) if required.

Ranging

Done before and after maneuvers for orbit determination.

Done hourly from 5-15 minutes past hour over 24-48 hours.

Transparent to experiment operations.

Typical Stationkeeping Timeline (ASOC activities)

M- 21 days	Distribute schedule with approx. S/K times
M- 3 days	Activate Ranging to update ephemeris
M- 1 day	S/C Analyst generates final N/S maneuver parameters based on most recent OD
M- 1 hr	Turn-on RMAs to warm up Enable thrusters to warm up cat bed heaters Upload parameters to ASP 1 Enable S/K APEMAC Request NGS load CRG for abort cmds
M- 5 min	Activate Gyro Bias Estimator
M- 0	Activate maneuver (~1/2 hr before asc. node) N/S Coarse Mode Send maneuver run cmds to reset backup timer
M+ 1 hr	Switch to N/S Fine Mode to reduce disturbances
M+ 90 min	Terminate maneuver Disable thrusters and RMAs
M+ 2 hrs	Activate Ranging to confirm maneuver performance
M+ 2 days	S/C Analyst determines day/time for next E/W maneuver and generates final maneuver parameters based on orbit determination

E/W maneuver and subsequent stationkeeping operations over life of mission follow similar two day timeline.

Optimization of maneuvers and evaluation of orbit and attitude disturbances expected to improve as S/C Analyst gains familiarity with S/C characteristics.

Momentum Unloading

Required every 5-7 days to control MWA speed.

Expected Wednesday night and/or weekends to maintain margin on wheel speed. Can be combined with stationkeeping.

APEMAC enabled/disabled by command.
Manual mode is backup.

Expected to be transparent to experiments due to small thruster pulses.

Yaw Control

Ephemeris upload required at least weekly to ASP RAM.

Planned for Sunday (after S/K).
Transparent to experiment but prudent to avoid LET-MSM configuration periods or BFN/MSM initialization.

S/C Analyst generates ephemeris in ASOC Off-line computer with output reformatted for hex commands.

S/C Analyst checks coefficients for continuity.

Operator uploads files to ASP 1 (approx. 1 hr) before first new window.

ASP upload verified by dump of ASP 1 before first new window.

Modifications to Estimator Table handled same way if required based on On-orbit Checkout evaluation.

S/C Pointing (for MBA optimization and characterization)

Commands provide static pitch or roll offset to Autotrack or ESA by biasing the zero attitude reference in 0.005° steps.

Pitch offset (ATR/ESA bias) commands sent at approx. one minute intervals for immediate stable offset.

Roll offset requires MTA or MWA pivot and ATR/ESA bias and will cause nutation. MBA requirements needed to define details.

Variable offsets can be loaded into 24 hour ASP table with six minute intervals.

Temporary pitch/roll offset may require yaw ephemeris correction for one or both windows.

print:all notebookRUNNING VTVM1.....RUNNING VTVM1Resent-
From: OPEX@ESTEC
To: FUBDPT1@ITCASPUR,
JBELSHAW@ESTEC
Subject: NO SUBJECT
Date: Thu, 10 16 11:46 EDT ← October 16, 1992
Comment: Converted PROFS message

From: OPEX Coordinator (XEP)
----------Original Message----------
To: BARBESSE--ESTEC JBELSHAW--ESTEC
OPEX --ESTEC

FROM: M LOMBARDO - OLYMPUS MOM / F D'AMORE - OLYMPUS OOM
TO : J BELSHAW, B ARBESSER-RASTBURG, XEP ESTEC(OPEX) ← Olympus Propagation Experiment
INFO:

SUBJECT: OPEX; OLYMPUS EXPERIMENTERS ANTENNA POINTING FIT

ORBITAL PARAMETERS

ORBITAL ELEMENTS IN PEPSOC SYSTEM
SEMI MAJOR AXIS (KM) = 42165.401077
ECCENTRICITY = .000214
DECLINATION (DEG) = .451978
ASCENDING NODE (DEG) = 84.056627
ARG. OF PERIGEE (DEG) = 54.240946
TRUE ANOMALY (DEG) = 226.471957

STATE VECTOR IN PEPSOC SYSTEM
X - COMPONENT (KM) = 42024.301143
Y - COMPONENT (KM) = 3506.614390
Z - COMPONENT (KM) = -326.869435
X - COMPONENT (KM/SEC) = -.256068
Y - COMPONENT (KM/SEC) = 3.063475
Z - COMPONENT (KM/SEC) = .004512

SUBSATELLITE POINT
LONGITUDE (EAST,DEG) = -19.002
LATITUDE (NORTH,DEG) = -.444

EPOCH (UT) = 1992/10/15 AT 0: 0: 0

This information to be provided by GE ~ weekly.

ANTENNA POINTING DATA

START DATE (=REF. TIME) 1992/10/15 AT 0
END DATE 1992/10/20 AT 23

STATION		CONSTANT	LINEAR	SINUS	COSINUS
RAZ	AZ	223.1934	-.0078	.0704	-.2430
	EL	26.3918	.0038	.0740	-.4351
LESSIVE	AZ	210.3816	-.0085	.0575	-.1670
	EL	28.0500	.0027	.0832	-.4652
LOUVAIN	AZ	209.4821	-.0035	.0562	-.1600

Drift SINE COSINE

ACTS Propagation Experiments: Status

- Class I experiment contracts in place
  - University of Alaska
  - Colorado State University
  - COMSAT Laboratories
  - University of Oklahoma
  - University of South Florida
  - Stanford Telecommunications
- Class I experiment contracts pending
  - Florida Atlantic University
- Class I experiment agreement
  - University of British Columbia
  - Agreement signed by NASA; Awaiting concurrence by Canadian Department of Communications

ACTS Propagation Experiments: Status (Cont.)

- Class II experiment contracts in place
  - COMSAT Laboratories
  - Johns Hopkins University
  - University of Texas
- Class II experiment contracts pending
  - Georgia Tech Research Institute
- Other propagation experiments
  - Agreement to formalize Teleglobe Canada experiment being drafted by DOC

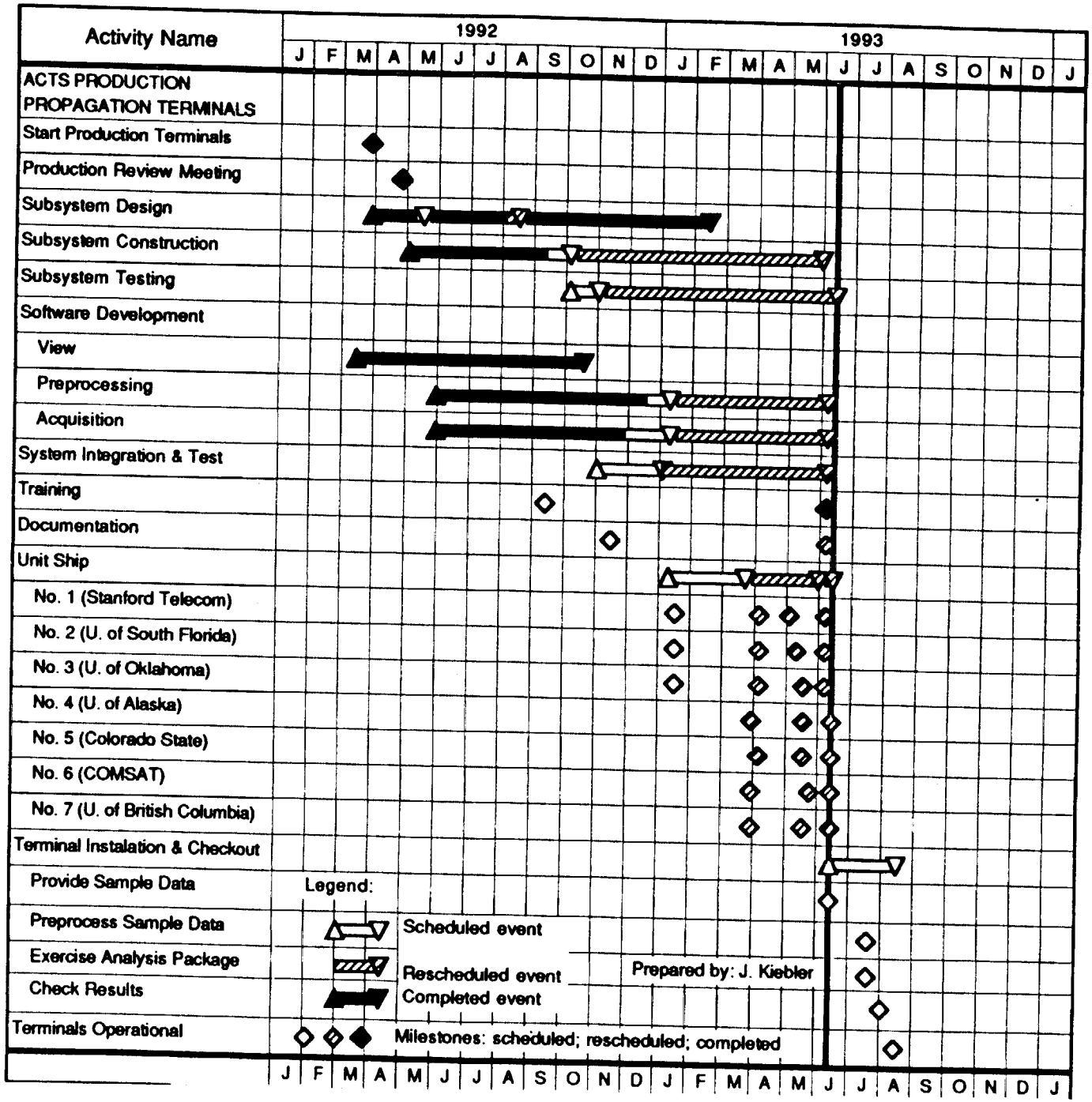
Activity Name
1992
1993
J F M A M J J A S O N D J F M A M J J A S O N D J
ACTS PRODUCTION PROPAGATION TERMINALS
Start Production Terminals
Production Review Meeting
Subsystem Design
Subsystem Construction
Subsystem Testing
Software Development
View
Preprocessing
Acquisition
System Integration & Test
Training
Documentation
Unit Ship
No. 1 (Stanford Telecom)
No. 2 (U. of South Florida)
No. 3 (U. of Oklahoma)
No. 4 (U. of Alaska)
No. 5 (Colorado State)
No. 6 (COMSAT)
No. 7 (U. of British Columbia)
Terminal Instalation & Checkout
Provide Sample Data
Preprocess Sample Data
Exercise Analysis Package
Check Results
Terminals Operational
Legend:
Scheduled event
Rescheduled event
Completed event
Milestones: scheduled; rescheduled; completed
Prepared by: J. Kiebler

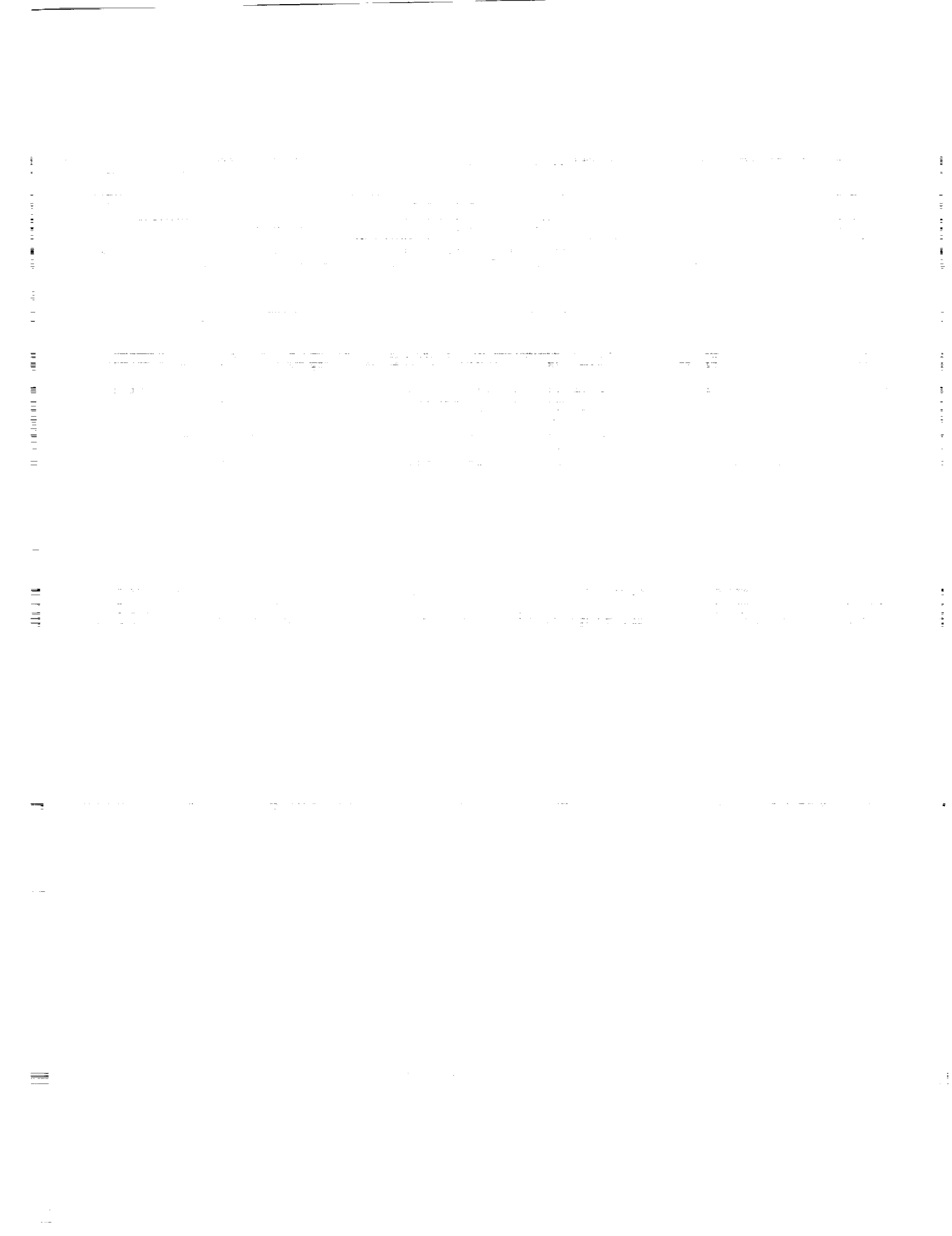

THE ACTS PROPAGATION TERMINAL DELIVERY AND SUPPORT

Warren Stutzman

Virginia Polytechnic Institute & State University
Bradley Department of Electrical Engineering
Satellite Communications Group
Blacksburg, Virginia 24061-0111

ACTS MINI-WORKSHOP
PASADENA, CA

June 14, 1993

VIRGINIA TECH
Satellite
Communications
Group

aptdel.drw
05/17/93

OUTLINE

- APT Program Overview
- Terminal Overview
- Physical units
- Test results
- Status of terminals and schedule
- Shipping cartons
- Site Support

a:outline.drw
06/09/93

ACTS PROPAGATION TERMINAL (APT) DEVELOPMENT PROGRAM OVERVIEW

OLYMPUS Measurement Campaign
- 12, 20, 30 GHz beacons
- Tested shared beacon receiver/total power radiometer design
- Determined that 1 Hz sample rate is sufficient
- Developed data collection software

Goals for APT
- Developed by user community

APT Prototype (1991-92)
- PDR: May 30, 1991
- CDR: July 7, 1992
- System tests with Olympus and ACTS: Summer 1992

APT Production (March 1992 - June 1993)
- Produce 7 terminals for experimenters
- Maintain prototype
- ACTSVIEW software
- Preprocessing software

Experiment Support (July 1993 -)

dev1.drw
05/25/93

APT CHARACTERISTICS

ACTS Spacecraft Beacons

Frequency

Primary	20.185 GHz (V)	27.505 GHz (V)
Backup	20.195 GHz (H)	27.505 GHz (V)

Antenna

1.22 m offset	HP: 0.85° @ 20.2 GHz	0.61° @ 27.5 GHz

Beacon Receivers

RF: Direct downconversion to 70 MHz

IF: 5 MHz intermediate, 455 kHz output

Sampling: 606 kHz (303 I, Q) at 455 kHz

DRX: Acquisition

Bandwidth: 180 kHz

Algorithm: 6 - 32k FFTs

Time to acquire: 3 s in fades up to 25 dB

Tracking

Bandwidth: 10 kHz

Algorithm: FFT and filtering to determine frequency and power

Lock: 31 dB fade

Radiometers

Input: 70 MHz from RF

Type: Total power

Detection bandwidth: 50 MHz

dev2.drw
06/07/93

APT FUNCTIONAL SUBSYSTEMS

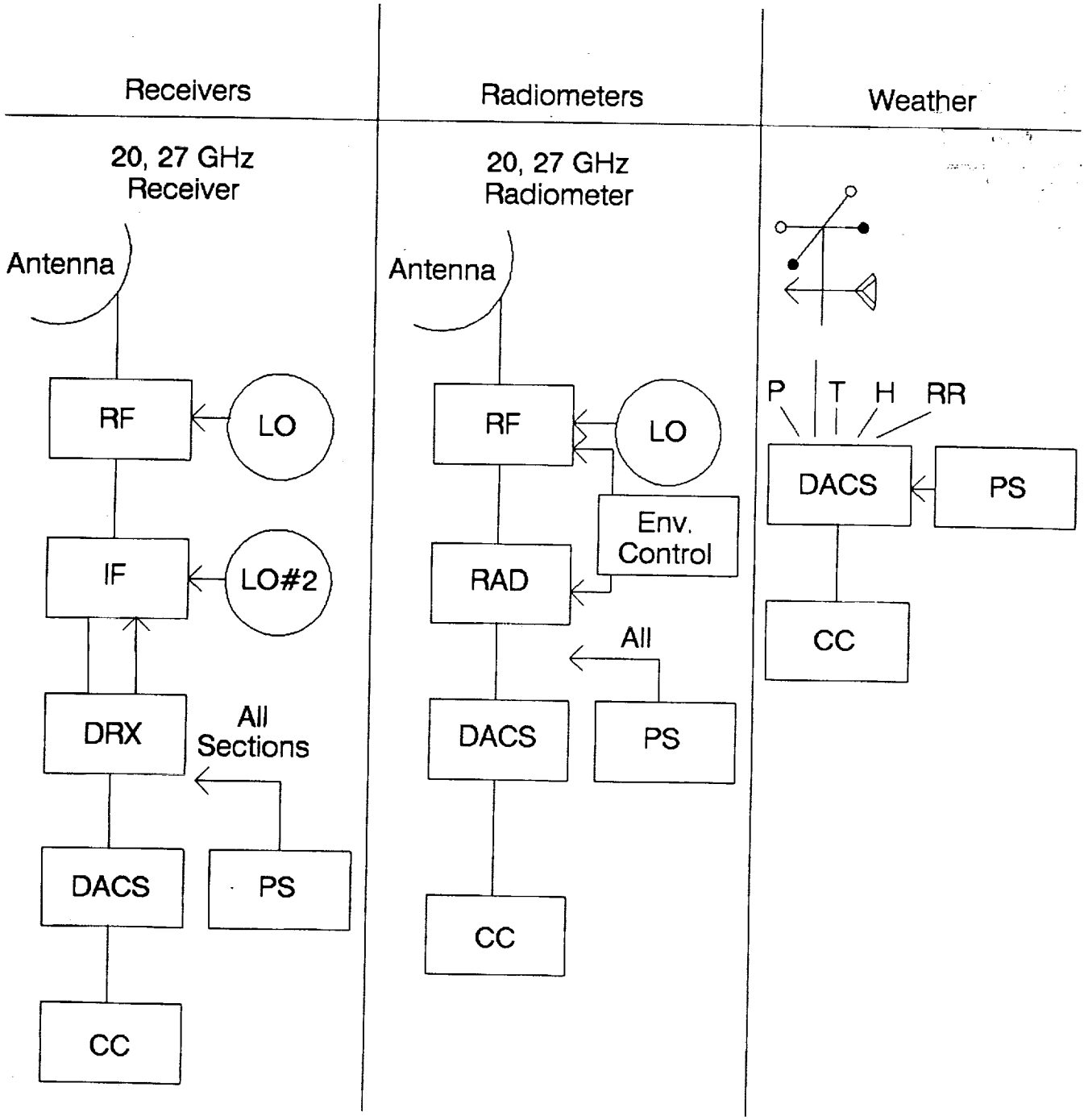

func1.drw
04/09/93

ACTS Propagation Terminal Physical Diagram

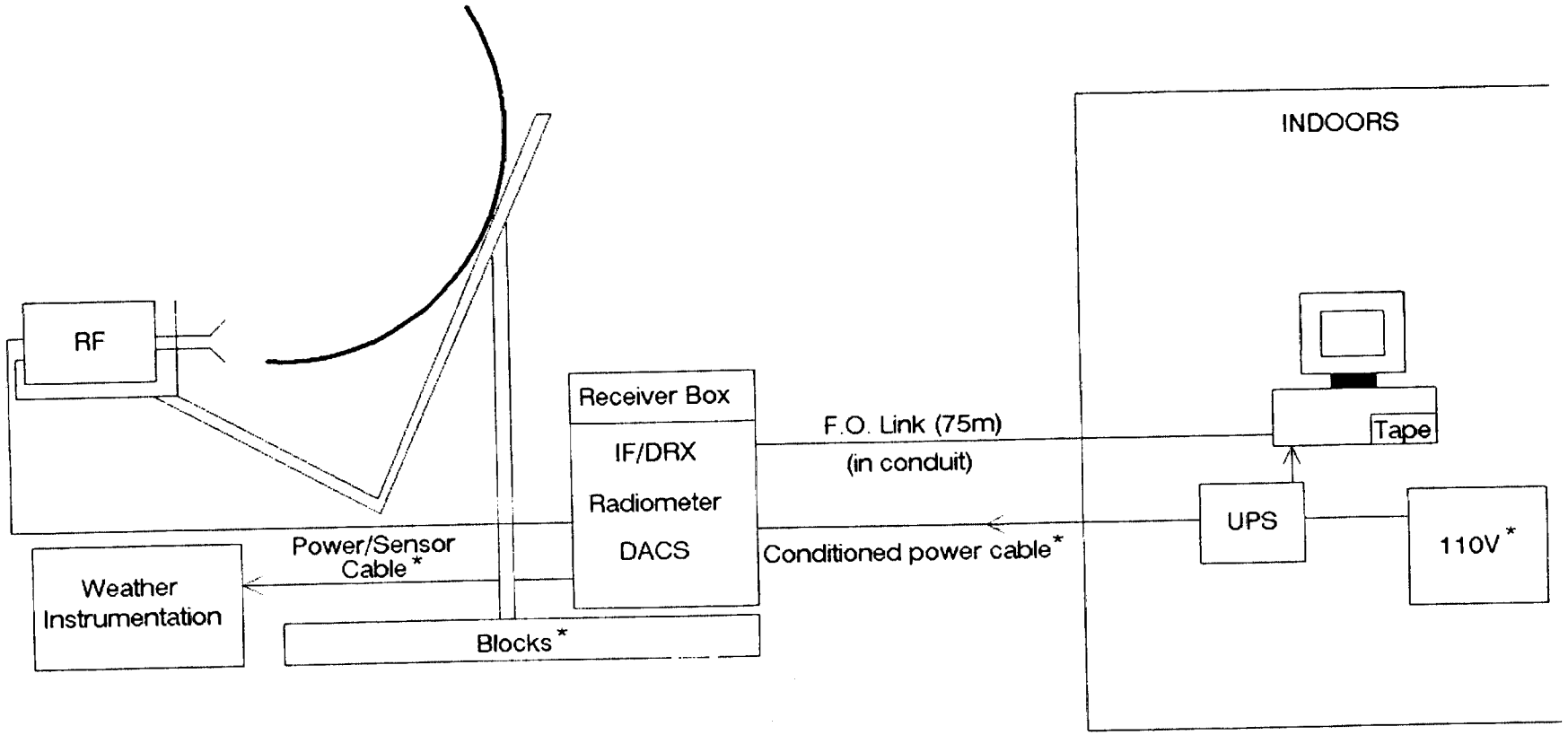

* User supplied

physical.drw
06/09/92

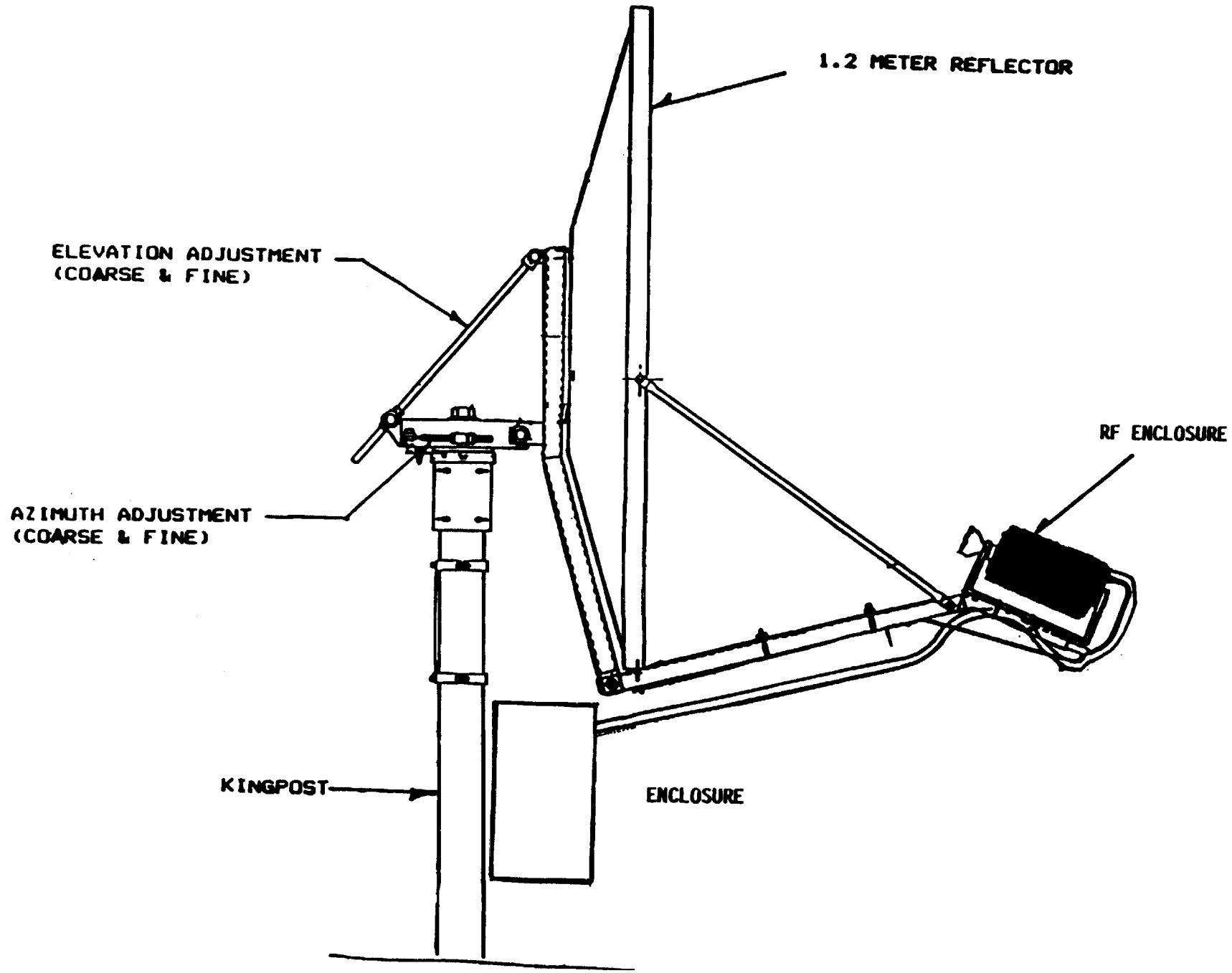
1.2 METER REFLECTOR
ELEVATION ADJUSTMENT
(COARSE & FINE)
RF ENCLOSURE
AZIMUTH ADJUSTMENT
(COARSE & FINE)
KINGPOST
ENCLOSURE

ACTS Receiver Enclosure Layout

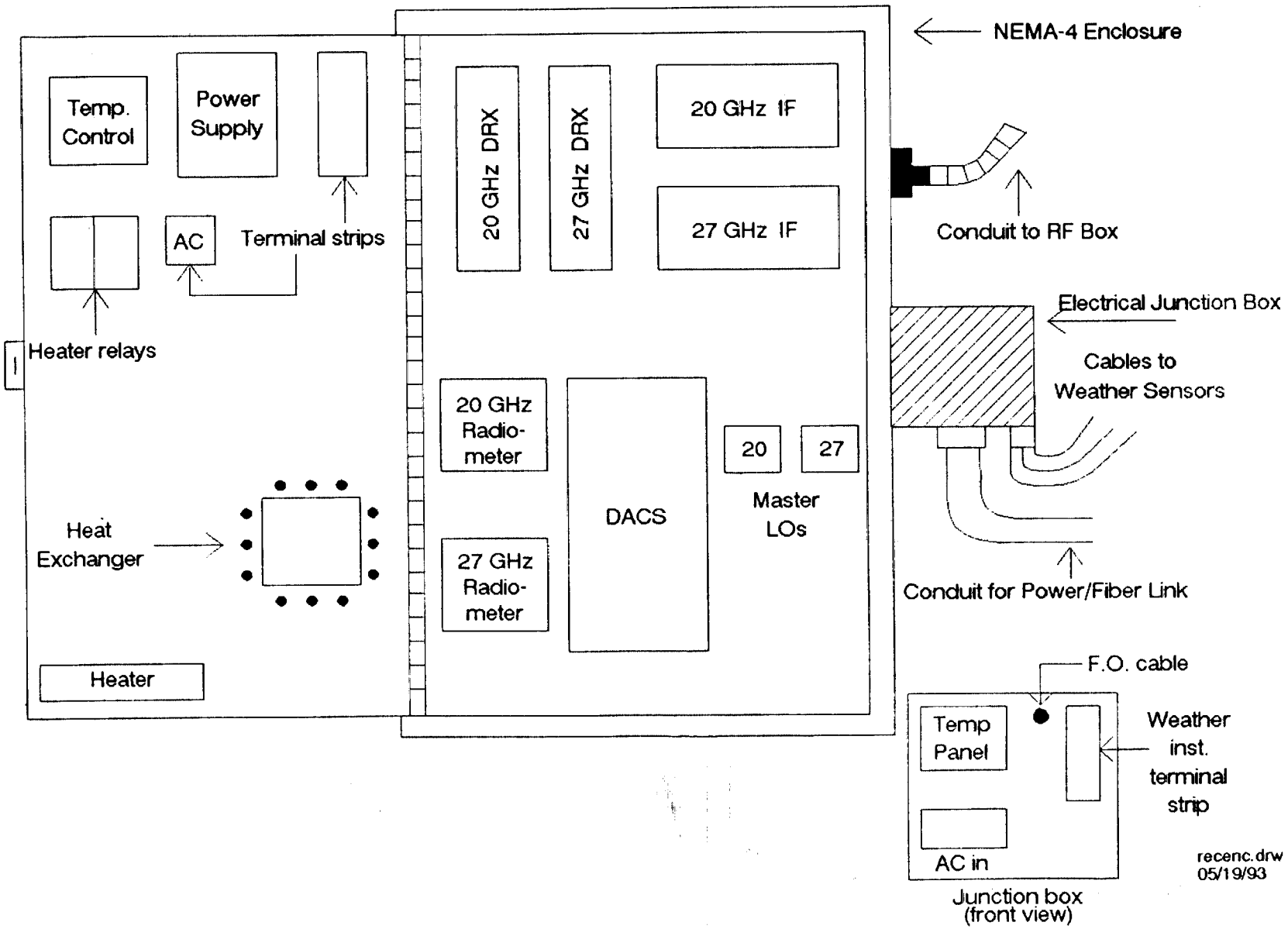

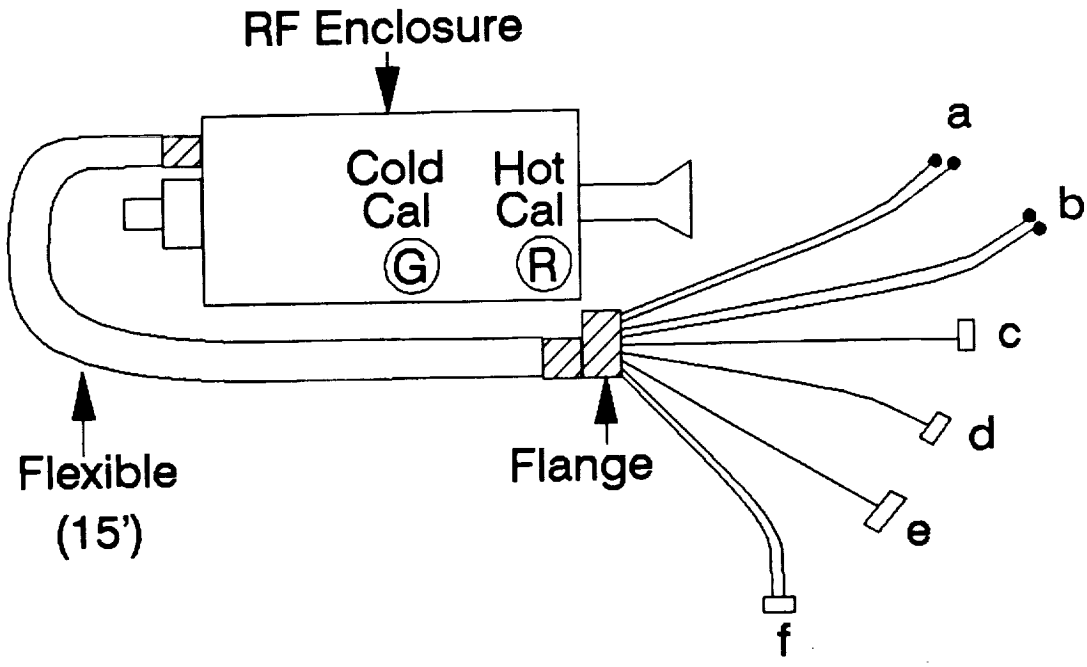

a) LO drive (20, 27) RG58 w/SMA-male.

b) 70 MHz IF (20, 27) Microflex 150 w/SMA-male.

c) RF power cable, 3 conductor twisted w/4 pin molex.

d) RF control cable w/DB25 male connector.

e) RF control cable w/DB9 male connector.

f) RF temperature control cable assy (two cables) w/DB-15 profile hybrid connector.

conduit.drw
06/01/93

Figure 3.1-2. Conduit/Cable assembly between RF and Receiver Enclosures.

ACTS PROPAGATION TERMINAL

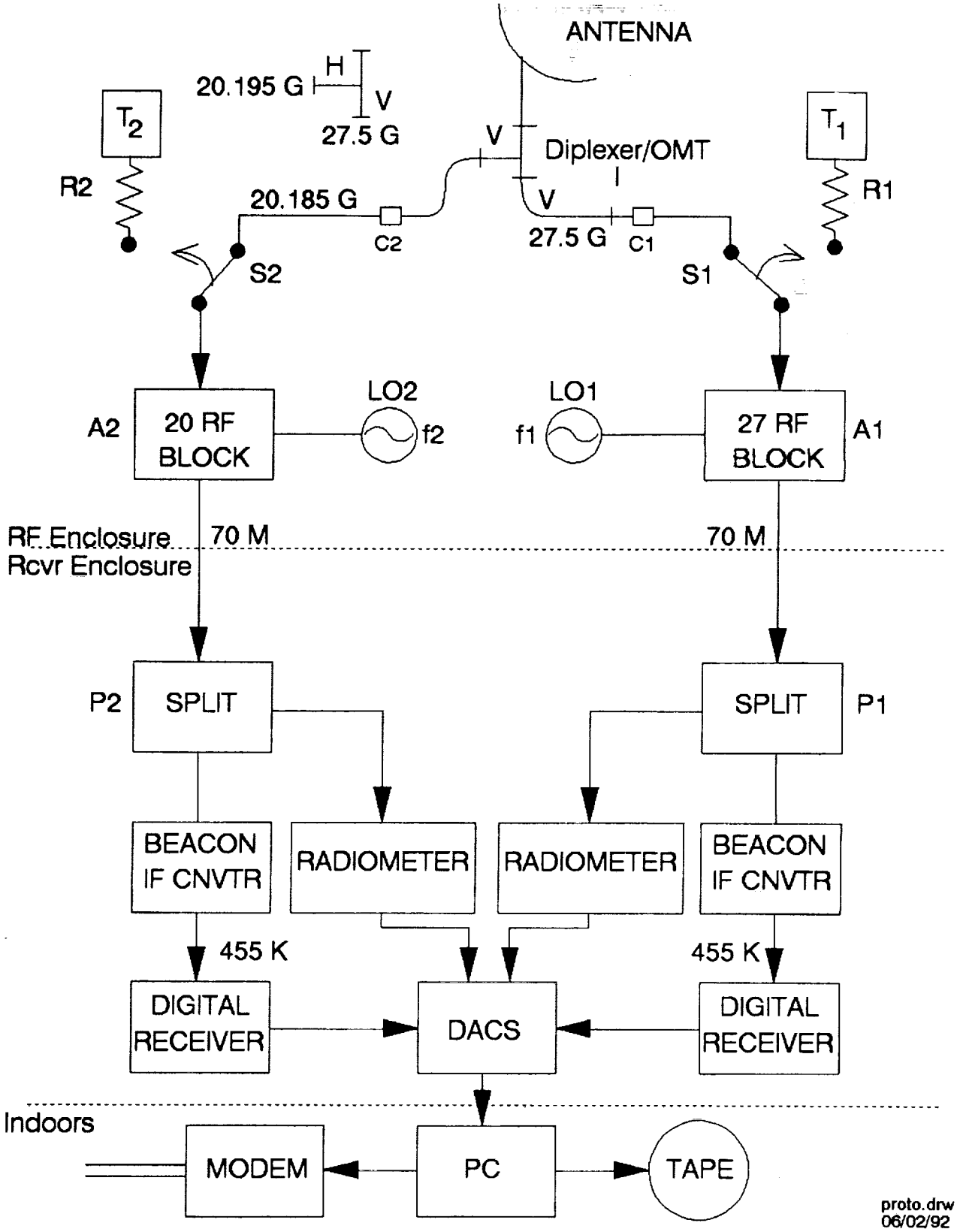

TEST RESULTS

- IF/Digital Receiver (Prototype)
  - Signal injection - linear response
  - Olympus 20 GHz beacon during a rain storm -
    - Reproduced Olympus analog receiver exactly
- Full Prototype system
  - ACTS spacecraft in NJ - acquired and measured spectra
- Beacon tests - Production
  - RF signal injection
  - Stable with time tests
- Radiometer tests - Production
  - Hot/Cold calibrations
  - Stable with time tests
  - Rain Measurements with system outside

a:test1.drw
06/10/93

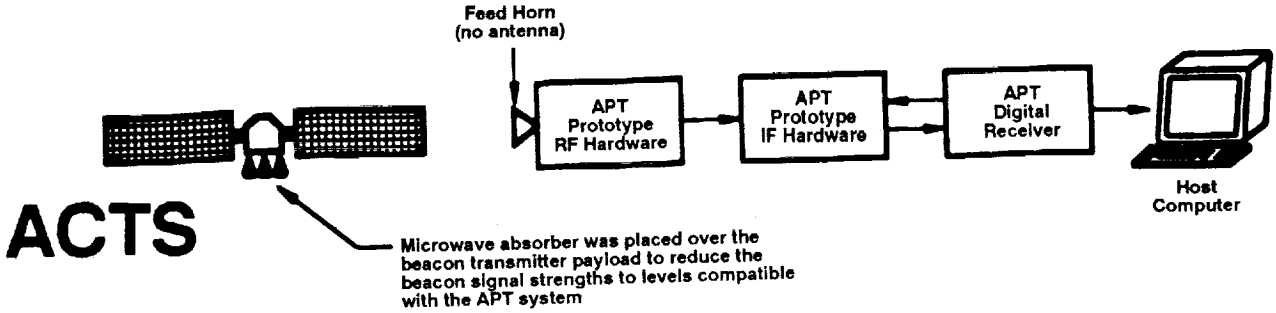

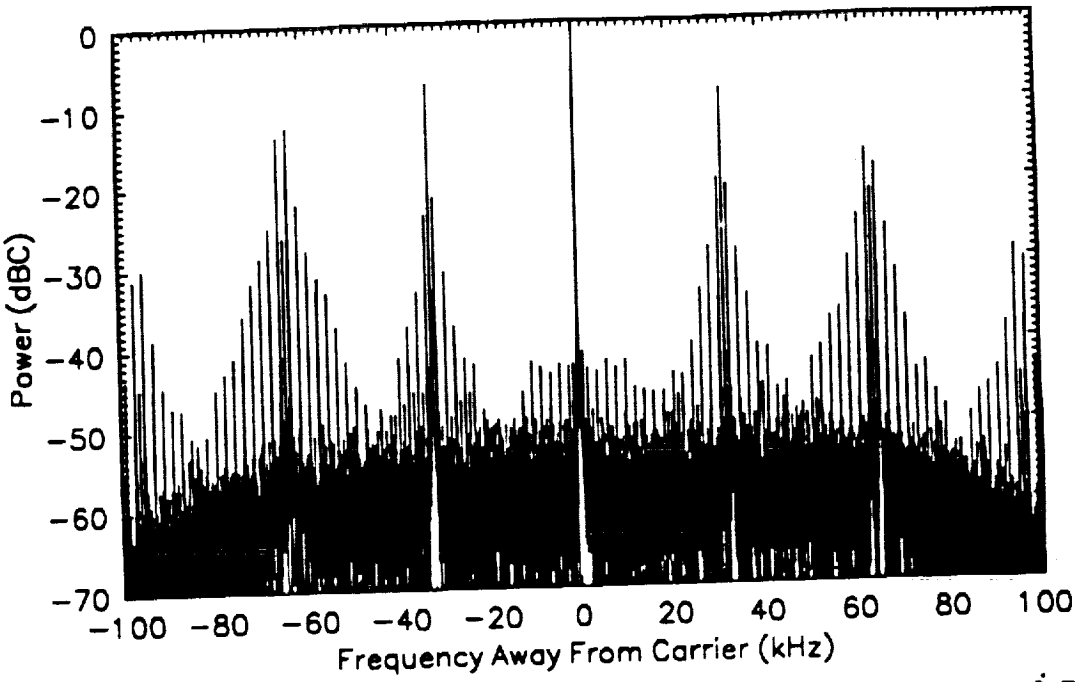

32768-point spectrum of the ACTS 20 GHz beacon in *Digital PCM Telemetry Mode*.

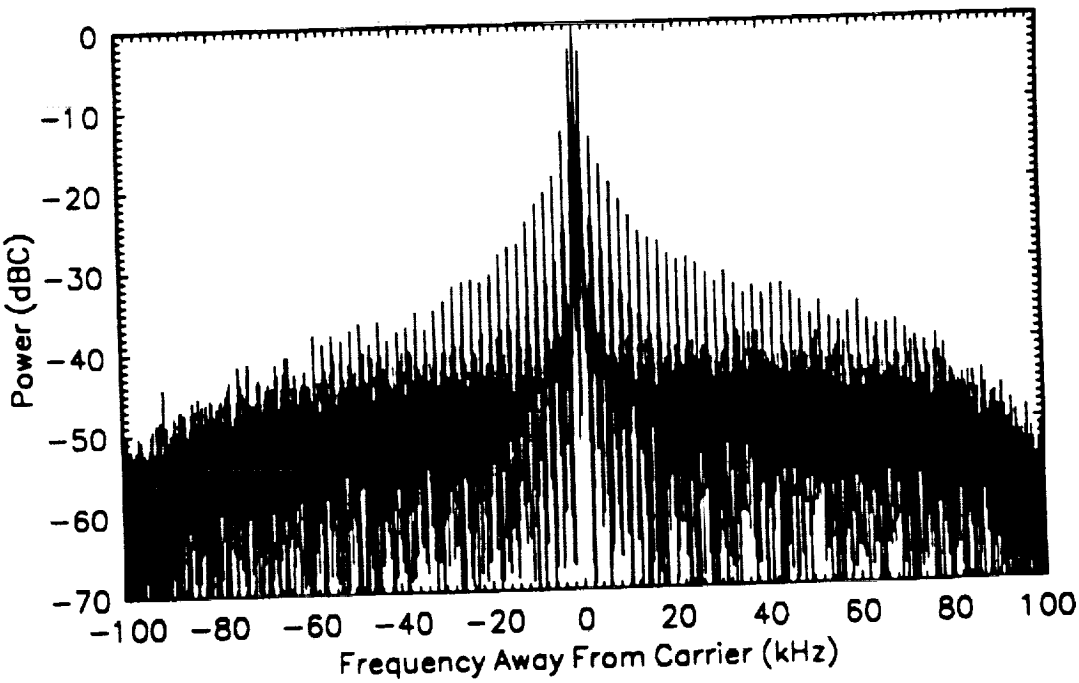

32768-point spectrum of the ACTS 20 GHz beacon in *PCM Direct Mode*.

ACTS Digital Receiver Power Measurement

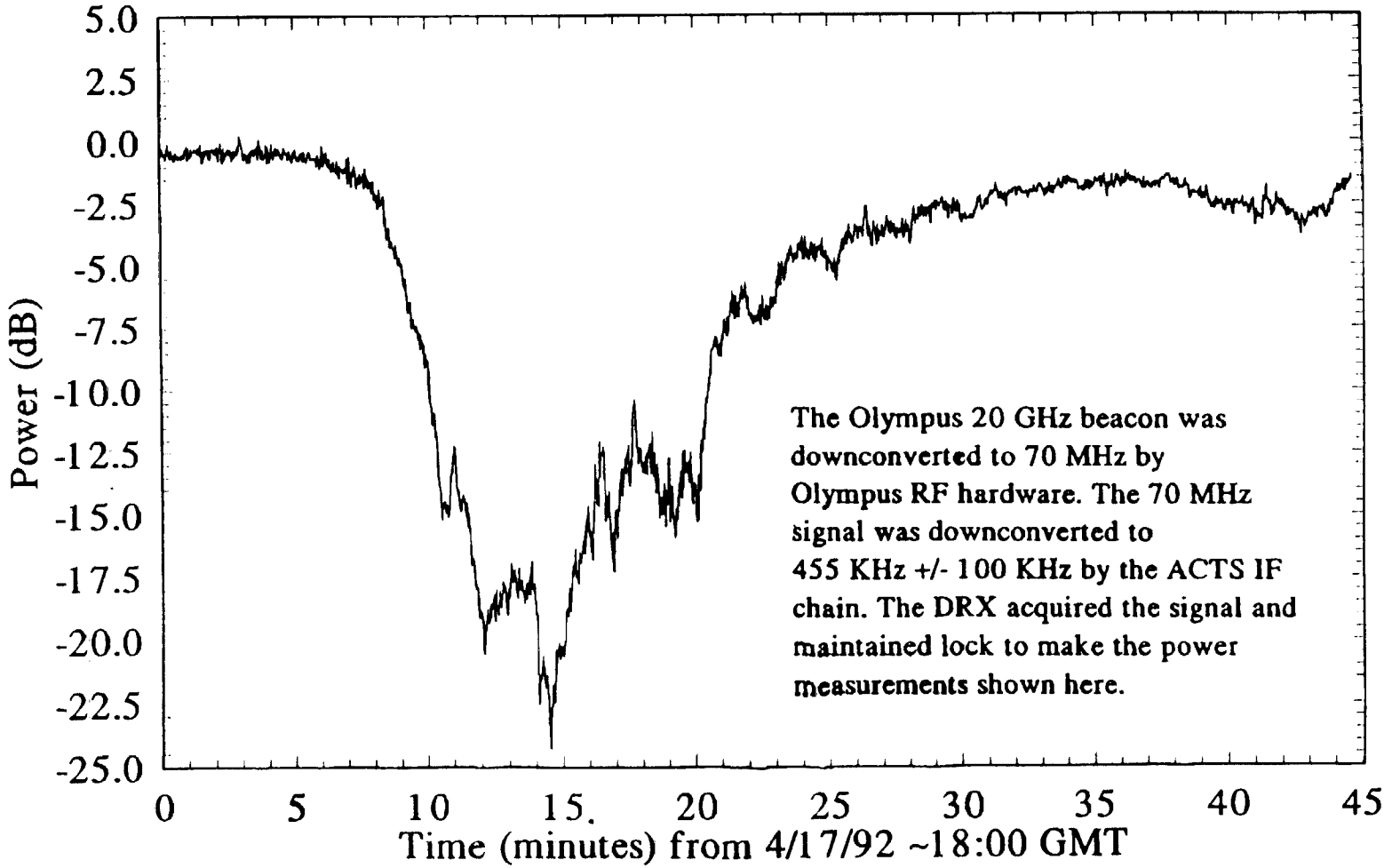

OLYMPUS Analog Receiver Power Measurement

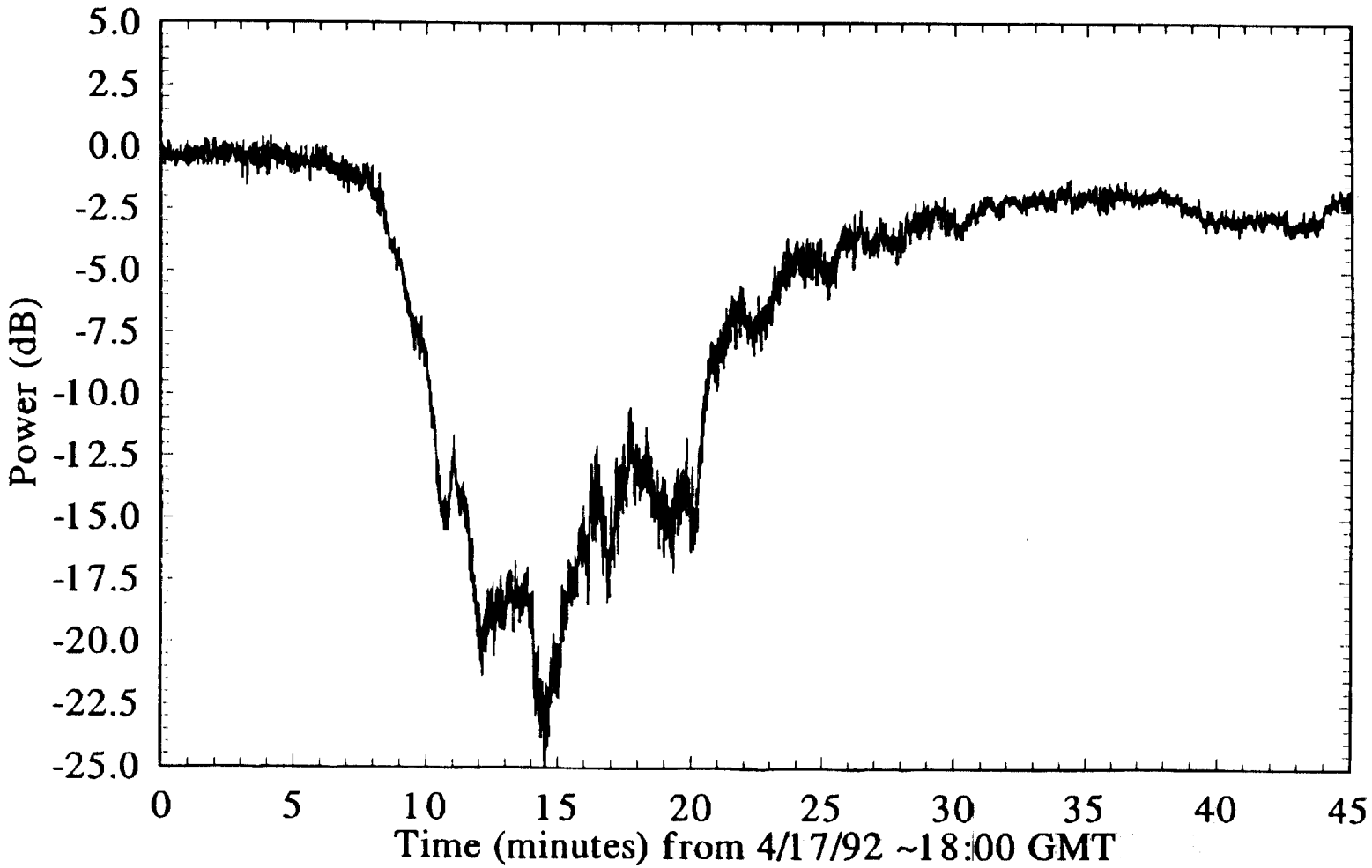

Radiometer Operation during a Thunderstorm

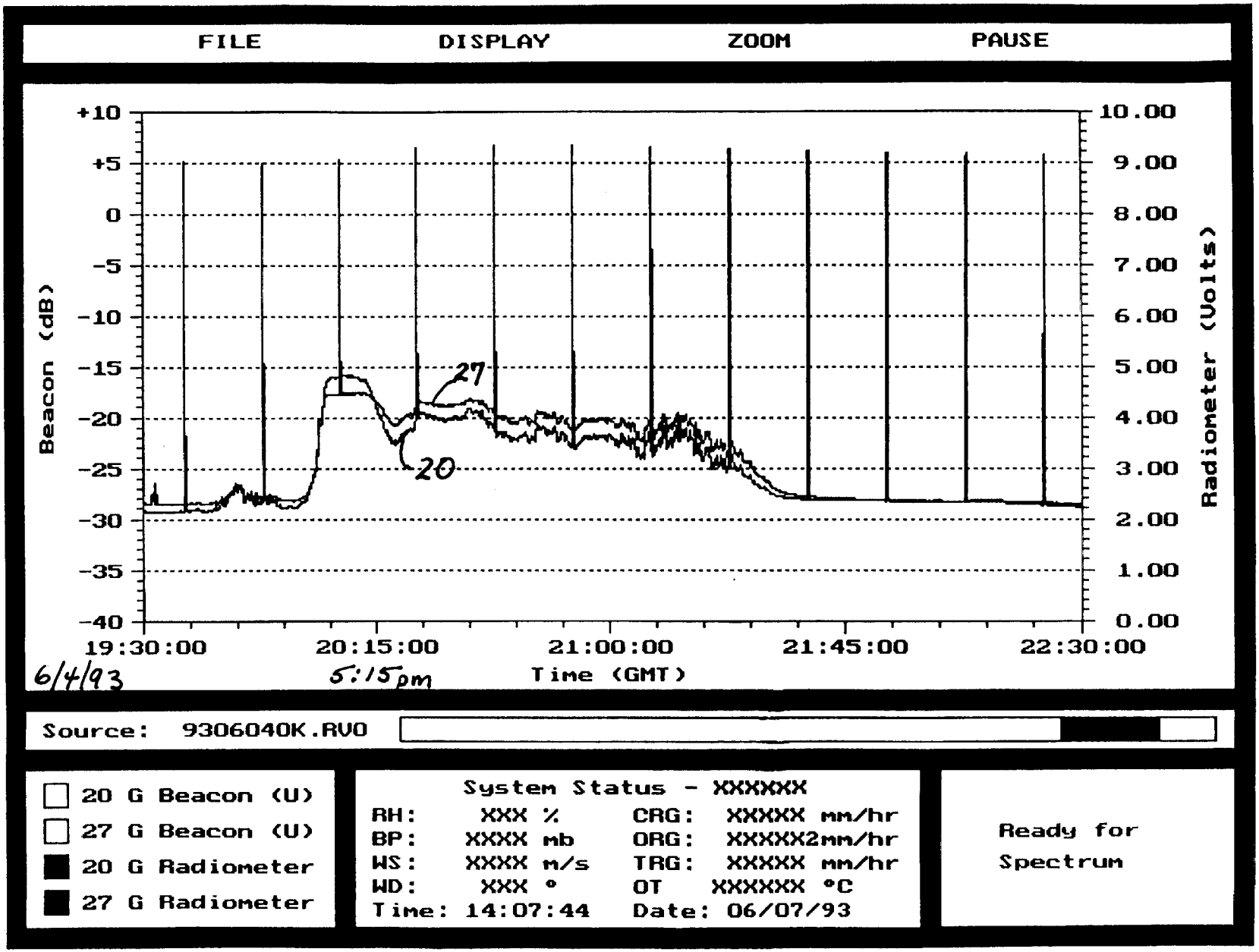

APT SHIPPING CARTONS

- Units shipped from Blacksburg, Virginia

Box No.	Description
1	Receiver Enclosure
2	RF Enclosure
3	Computer CPU
4	Computer Monitor
5	Miscellaneous

- Units shipped directly from manufacturers

  Antenna pedestal
  Antenna
  Wind gauge
  Capacitive rain gauge
  Uninterruptable power supply

a:units.drw
06/09/93

ACTS Propagation Terminal Production Schedule

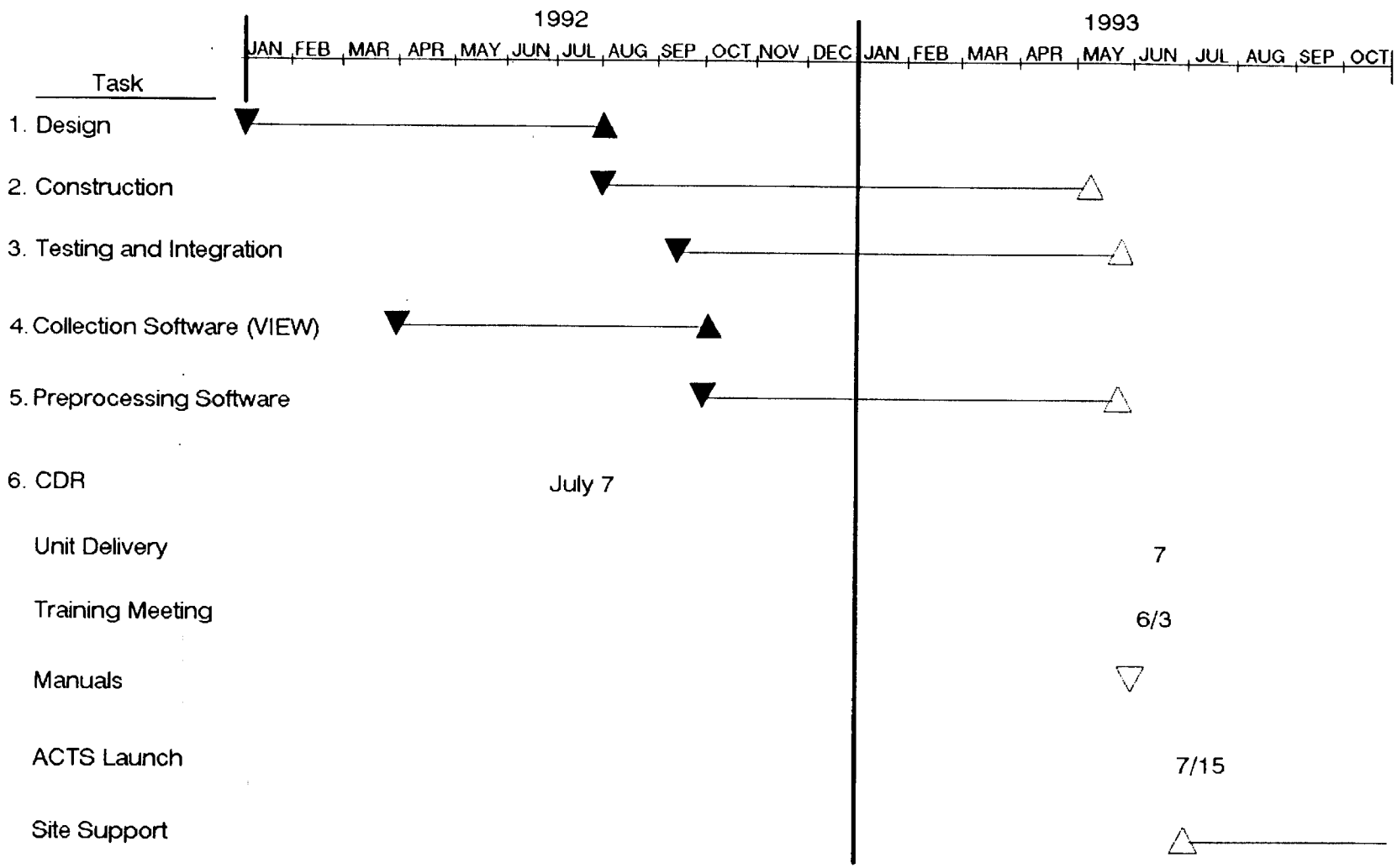

sched.drw
05/14/93

TERMINAL STATUS SUMMARY

Hardware

- LNB problems solved by adding an isolator to 20 G channels
- Shipping schedule
  - Week of 6/7: 2 6/14: 2 6/21: 2 6/28: 1
- Shipping order
  - NM, FL, OK, AK, CO, MD, BC

Software

- DACS code - complete
- ACTSVIEW - complete
- 20 Hz-rate data development in progress

Documentation

- Training Session - Held on 6/3 with full site representation
- Hardware Manuals - distributed
- ACTSVIEW Code and Manual - distributed
- Preprocessing Code and Manual - nearly complete

a:term1.drw
06/09/93

ACTS Propagation Site Support at Virginia Tech

Hardware

- Maintain operational spares for a subassembly swap
- Maintain documentation including calibration procedures
- Send updates to experimenters

Software

- Maintain DRX software, DACS software, VIEW, Preprocessing
- Send software updates to experimenters by E-mail

Site Visits

- As necessary for troubleshooting/calibration

Data Collection/Reduction

- Advise experimenters of S/C changes
- Process data in same fashion as experimenters

site1.drw
06/07/93

DATA COLLECTION WITH THE ACTS PROPAGATION TERMINAL

Will Remaklus

Virginia Polytechnic Institute & State University
Bradley Department of Electrical Engineering
Satellite Communications Group
Blacksburg, Virginia 24061-0111

ACTS MINI-WORKSHOP
PASADENA, CA

June 14, 1993

VIRGINIA TECH
Satellite
Communications
Group

data2.drw
05/17/93

DACS SYSTEM OVERVIEW

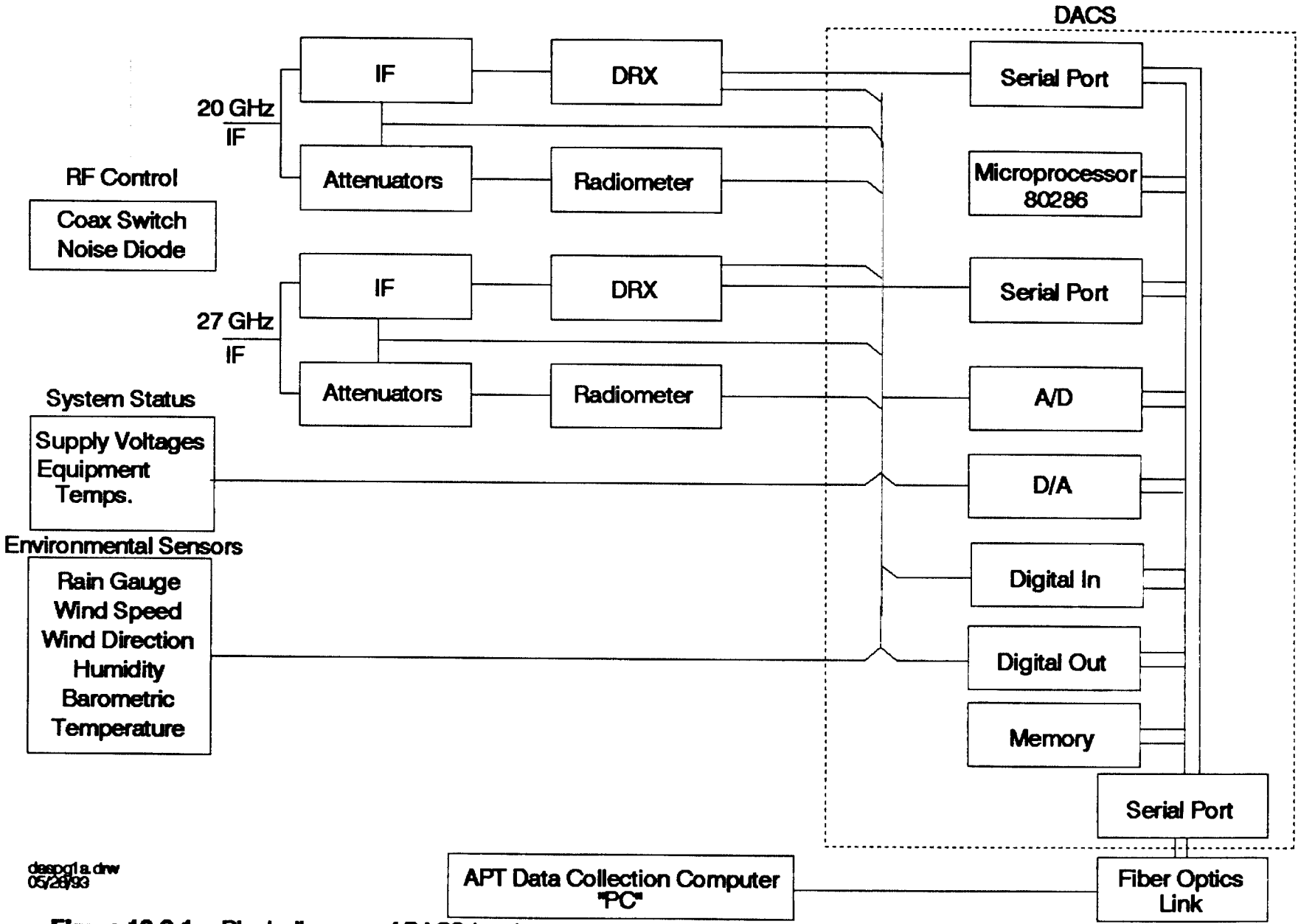

Figure 13.2-1. Block diagram of DACS hardware.

DACS BOARD

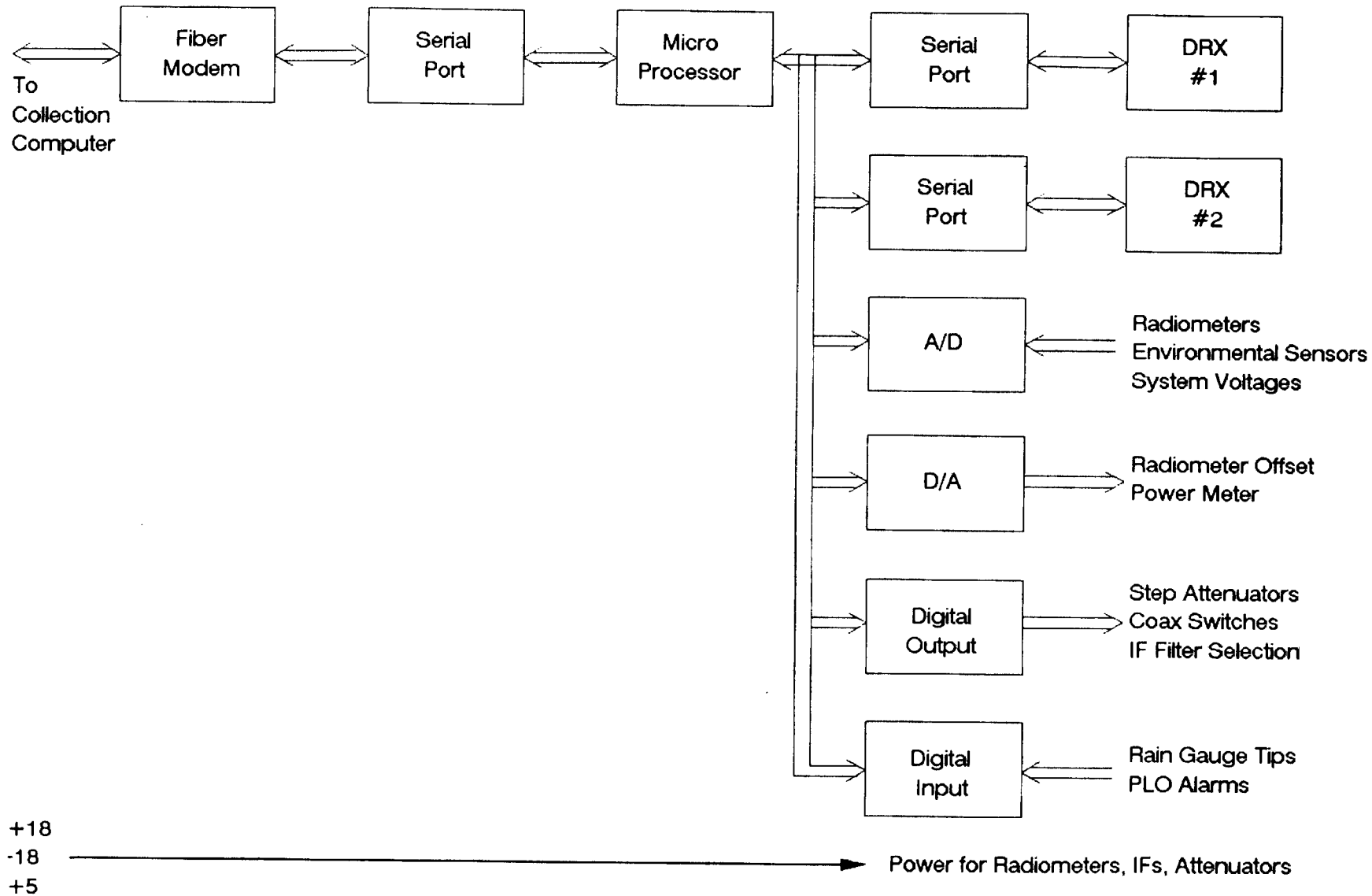

dacs.drw
03/17/92

APT Data Collection Computer

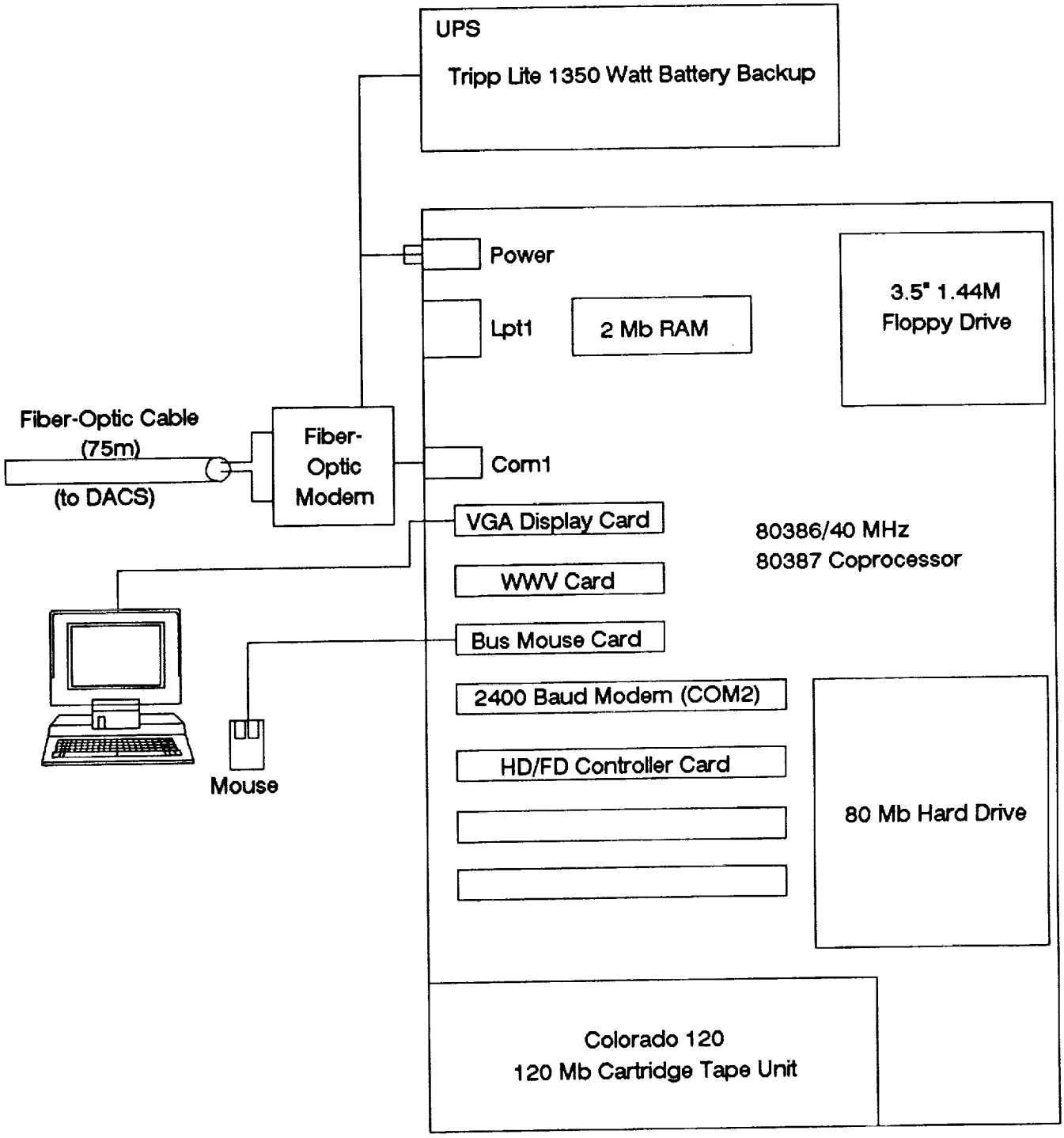

collect.drw
05/28/93

Figure 13.2-2. Configuration of the data collection computer hardware.

APT Software Downloading

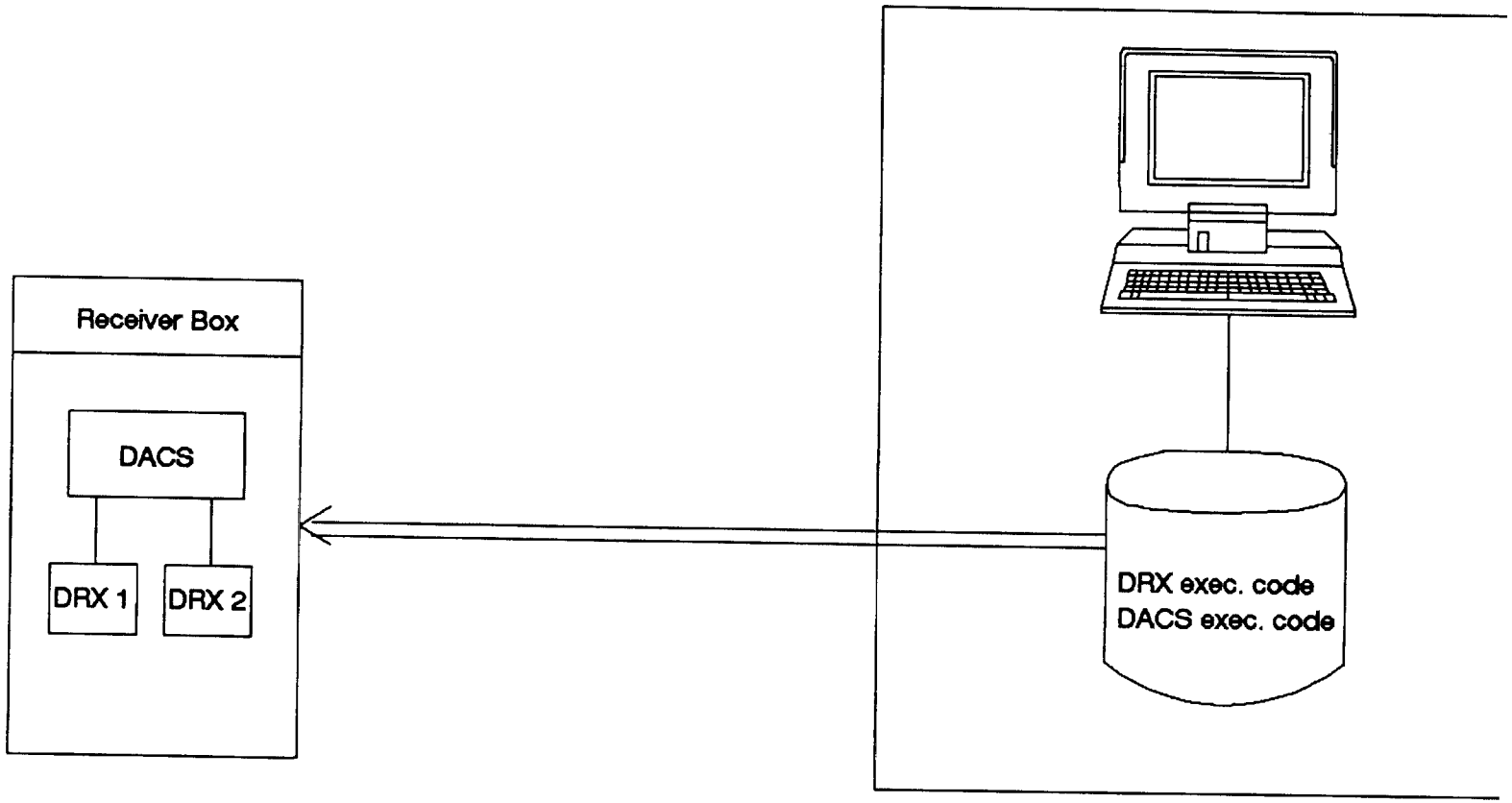

Digital Receiver and DACS executable code can be (re)loaded from the collection computer hard disk either under operator command or automatically at power up/reset.

apts.drw
05/27/93

Figure 13.4-1. Block diagram of the downloading process.

271
A-4

Table 7.2-1

Configuration of Terminal Strip for The Receiver Enclosure

Tipping bucket rain gauge sensor	1	□	Green terminal case ground
Outside air temperature sensor	2	14	Tipping bucket rain gauge GND
Wind direction sensor	3	15	Outside air temperature GND
Wind speed sensor	4	16	Wind direction GND
Barometric pressure sensor	5	17	Wind speed GND
Relative humidity sensor	6	18	Barometric Pressure GND
Capacitive rain gauge sensor	7	19	Relative humidity GND
Optical rain gauge sensor	8	20	Capacitive rain gauge GND
Test align output	9	21	Optical rain gauge GND
Wind direction, +15 V	10	22	GND
Barometric pressure, +15 V	11	23	GND
Relative humidity, +15 V	12	24	GND
Capacitive rain gauge, +15 V Optical rain gauge, +15 V	13	25	GND

DATA STORAGE FOR APT

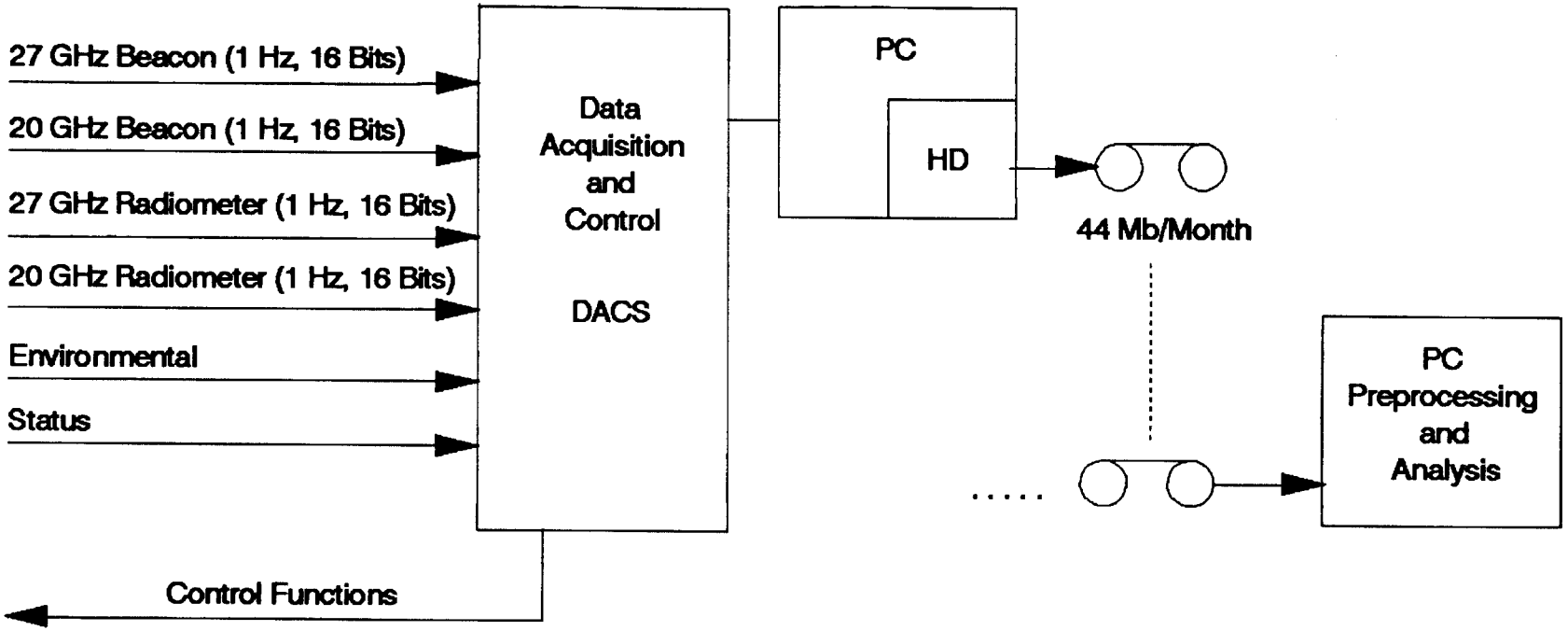

Data file (one second data rate):

| Time (4) | 20 GHz Beacon (2) | 27 GHz Beacon (2) | 20 GHz Rad (2) | 27 GHz Rad (2) | Status 1 (2) | Status 2 (2) |

Field ↓ (# of Bytes) ↓

Time multiplexed fields include:
- Environment
- Monitors
- ID
- Calib. on/off

Beacon data are signal power in 0.01 dB;

Radiometer data are voltage in 0.001 V.

Storage Requirements: $\left(16 \frac{\text{Bytes}}{\text{Sec}}\right)\left(60 \frac{\text{Sec}}{\text{Min}}\right)\left(60 \frac{\text{Min}}{\text{Hr}}\right)\left(24 \frac{\text{Hours}}{\text{Day}}\right) = 1.32 \frac{\text{Mb}}{\text{Day}}$

apdr9.drw
apdr.pif
06/09/93

Figure 13.8-1. Data storage format.

ACTS Propagation Experiment Data Flow

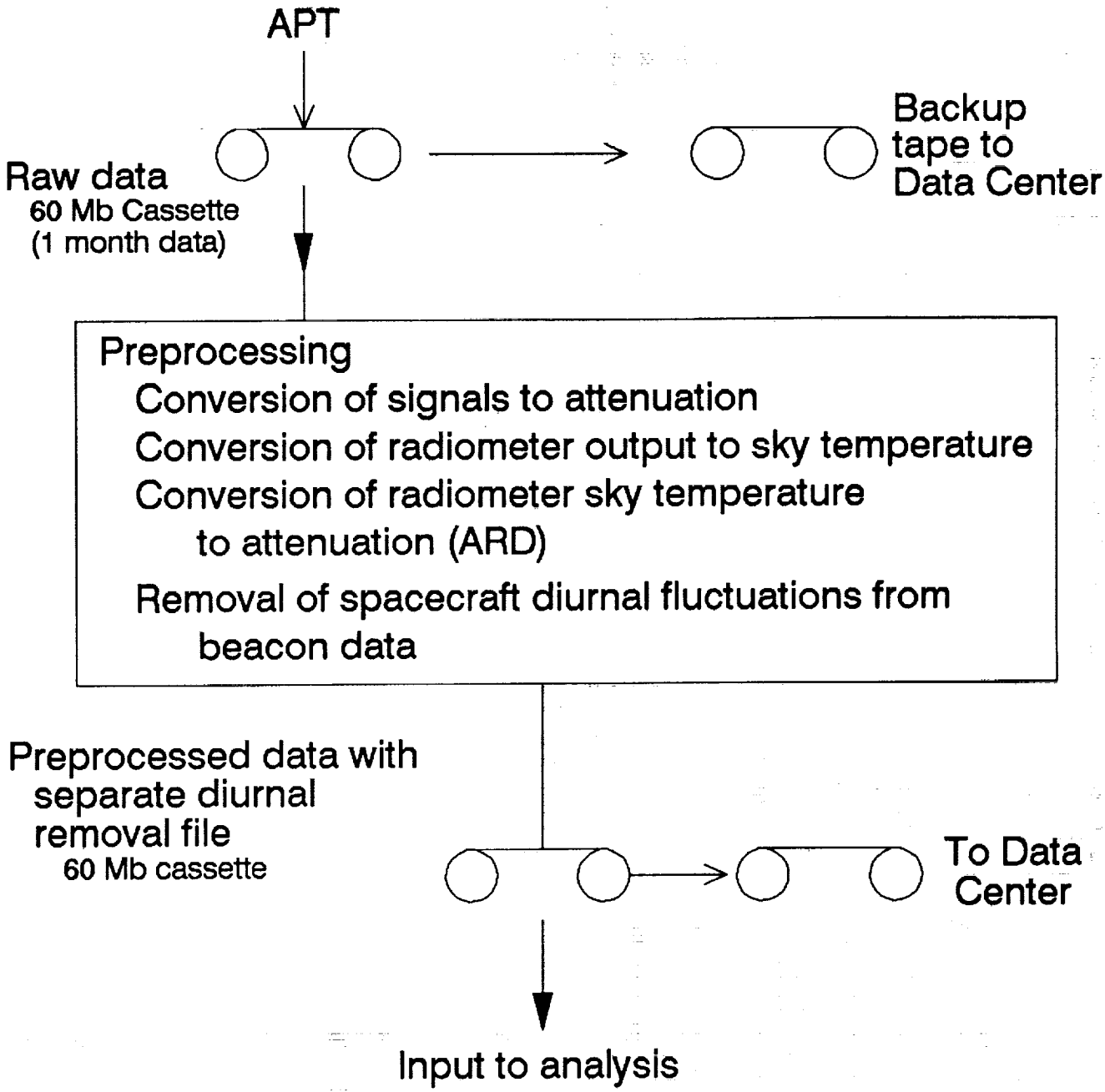

flow.drw
06/11/93

PREPROCESSING DATA COLLECTED WITH THE ACTS PROPAGATION TERMINAL

Doug Gaff

Virginia Polytechnic Institute & State University
Bradley Department of Electrical Engineering
Satellite Communications Group
Blacksburg, Virginia 24061-0111

ACTS MINI-WORKSHOP
PASADENA, CA

June 14, 1993

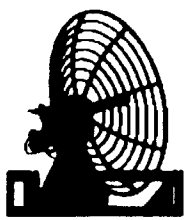

VIRGINIA TECH
Satellite
Communications
Group

Steps in ACTS Data Preprocessing

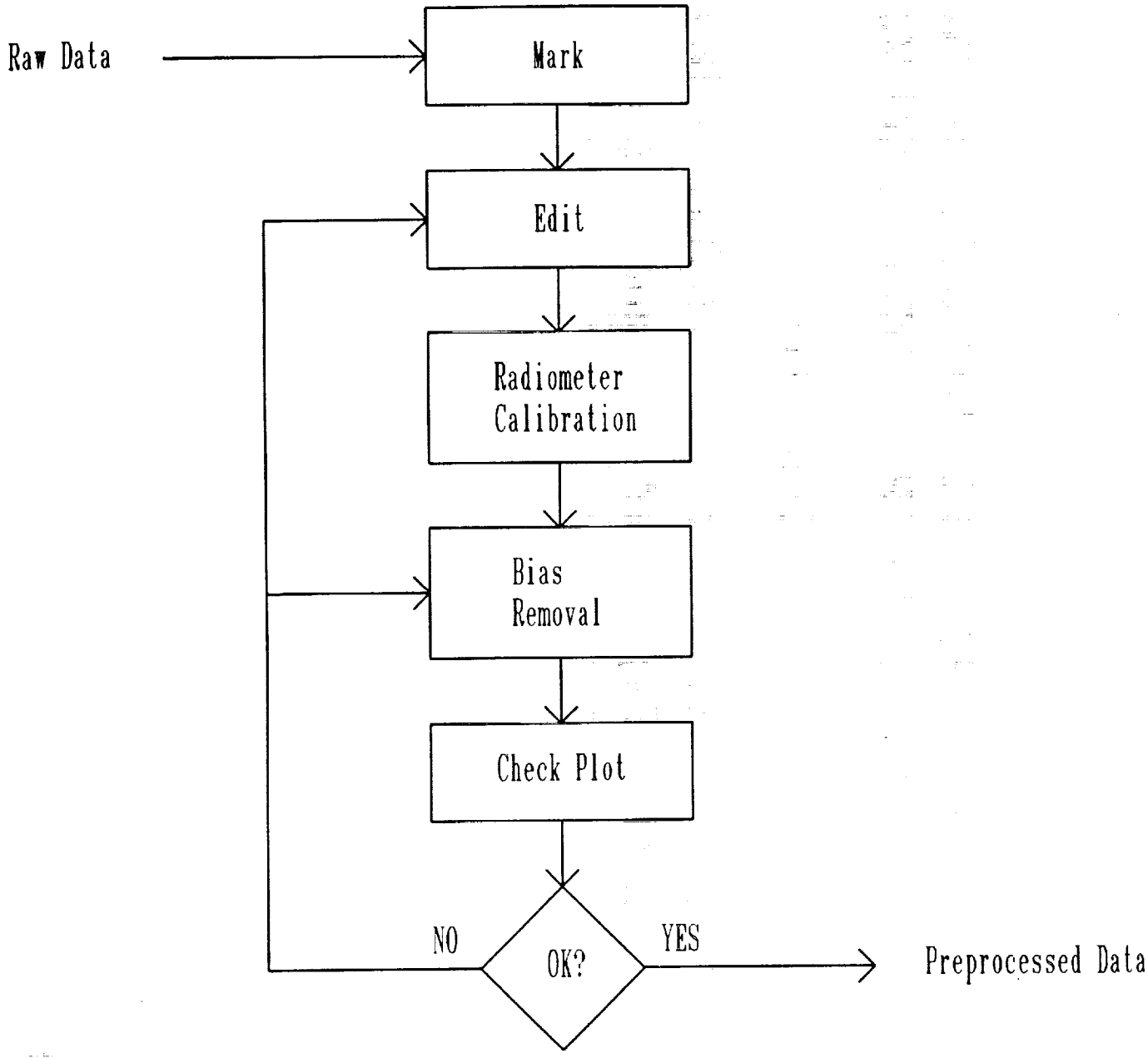

MARK Step

- *Automatic* Procedure

- Functions
  - Fills holes in data
  - Transfers status information for beacon and radiometer signals
  - Checks beacon and radiometer data for large slope changes
  - Checks system voltages and temperatures to ensure that they're in range

- Types of Marks put on data
  - Beacon Acquisition Mode
  - Tracking Disabled
  - Bad DRX data
  - Low SNR on Beacon
  - Radiometer Calibration
  - Radiometer in Setup
  - Data Missing
  - Statistical Failure
  - Equipment Failure

ACTS BEACON EXPERIMENT OPERATIONS FAULT LOG

STATION NAME:	PERIOD (MONTH/YEAR):

#	UTC DAY	UTC TIME START	UTC TIME STOP	CATE-GORY 0	1	2	CAUSE & ACTION	CHANNELS AFFECTED B 2 0	R 2 0	B 3 0	R 3 0	M E T	INIT

CIRCLE DAYS WITHOUT FAULT

1	2	3	4	5	6	7	8	9	10	11	12	13	14	15	16
17	18	19	20	21	22	23	24	25	26	27	28	29	30	31	

CIRCLE DAYS WHEN DATA WERE ARCHIVED TO TAPE

1	2	3	4	5	6	7	8	9	10	11	12	13	14	15	16
17	18	19	20	21	22	23	24	25	26	27	28	29	30	31	

Category definitions:

0 = No effect on collected data. Data were collected, but something notable happened.

1 = Clear air downtime. Contributes to rain time base, but not scintillation time base.

2 = Non-clear air down-time. Potentially missed rain event data.

ACTS BEACON EXPERIMENT EVENT LOG

STATION NAME: | **PERIOD (MONTH/YEAR):**

#	UTC DAY	UTC TIME START	UTC TIME STOP	EVENT TYPE				PRECIPITATION		COMMENTS	INIT
				SCIN	RAIN	LTNG	SNOW	TIP COUNT (.01")	MAX. RATE (MM/HR)		

CIRCLE DAYS WITHOUT EVENT

1	2	3	4	5	6	7	8	9	10	11	12	13	14	15	16
17	18	19	20	21	22	23	24	25	26	27	28	29	30	31	

EDIT Step

- *User - Controlled* Procedure

- Functions
  - User checks "Low SNR," "Statistical Failure," and "Equipment Failure" status tags for possible bad data
  - User marks portions of data bad if necessary
  - All data is "tagged" good or bad upon exit from this step

RADIOMETER CALIBRATION Step

- *Automatic* Procedure

- Functions
  - Convert radiometer voltages to sky temperature in Kelvin and then to ARD in dB
  - Hot and Cold Load calibrations applied
  - Noise Diode and Reference Load calibrations applied

BIAS REMOVAL Step

- *User - Controlled* Procedure

- Function
  - User removes signal fluctuations due to diurnal variation, front end heating, ice on the feed, etc.

CHECK PLOT Step

- *Automatic* Procedure

- Functions
  - Generates a plot similar to the daily plot which displays AFS and ARD
  - All data "tagged" bad is excluded from plot
  - User checks this plot to ensure that all bad data and all signal fluctuations were removed in the EDIT and BIAS REMOVAL steps

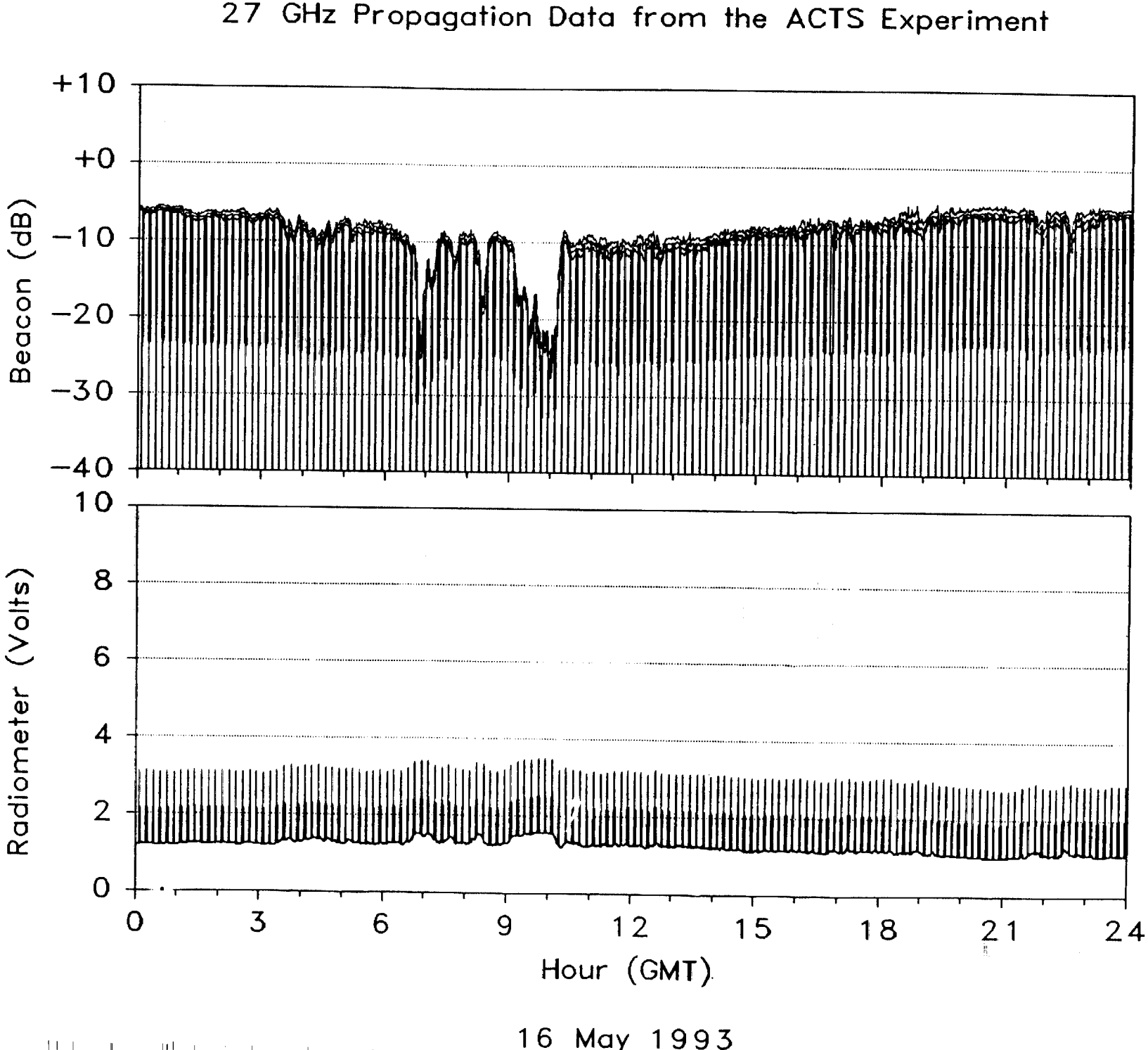
27 GHz Propagation Data from the ACTS Experiment
+10
+0
−10
−20
−30
−40
Beacon (dB)
10
8
6
4
2
0
Radiometer (Volts)
0
3
6
9
12
15
18
21
24
Hour (GMT)
16 May 1993

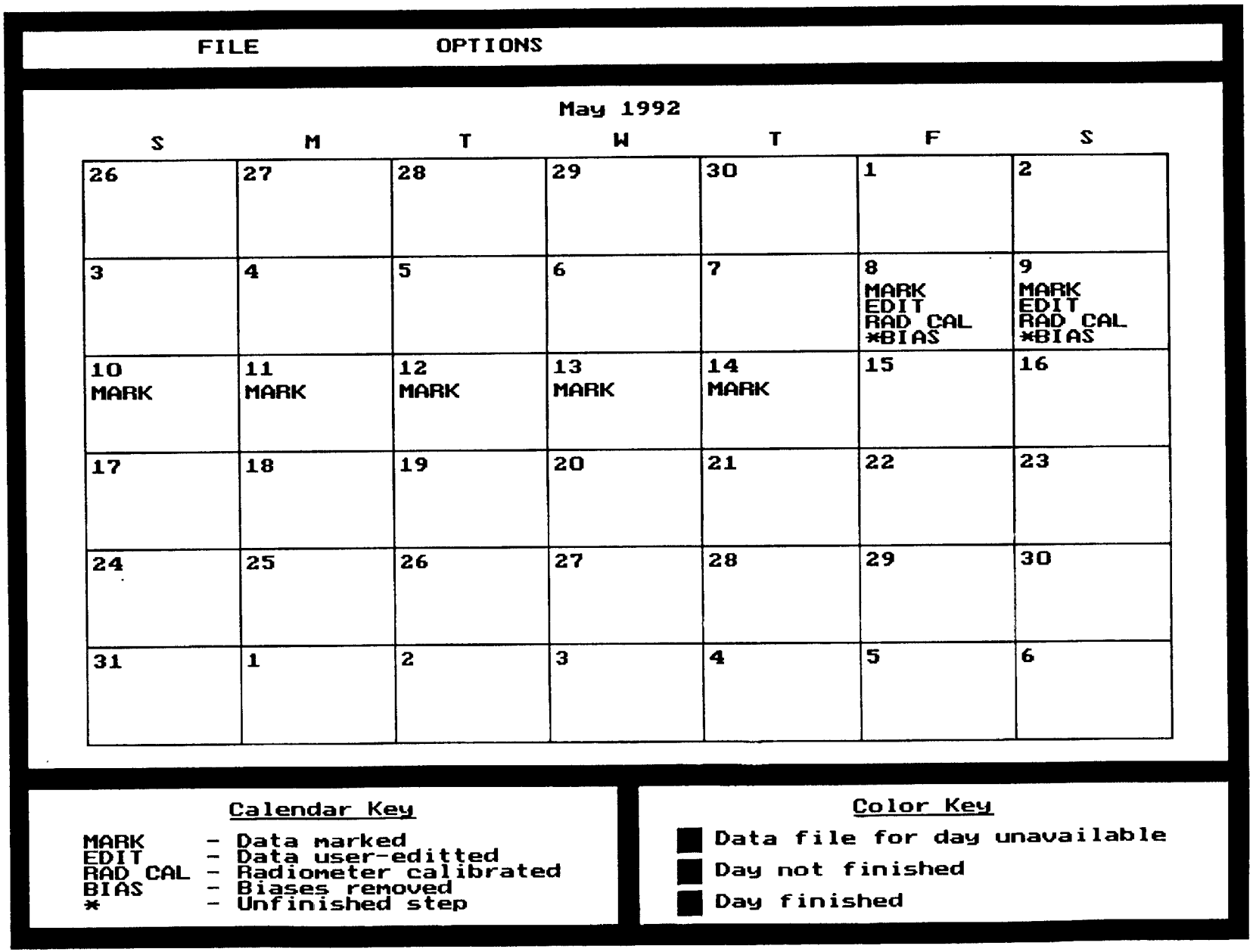
FILE
OPTIONS
May 1992
S M T W T F S
26 27 28 29 30 1 2
3 4 5 6 7 8 MARK EDIT RAD CAL *BIAS 9 MARK EDIT RAD CAL *BIAS
10 MARK 11 MARK 12 MARK 13 MARK 14 MARK 15 16
17 18 19 20 21 22 23
24 25 26 27 28 29 30
31 1 2 3 4 5 6
Calendar Key
MARK - Data marked
EDIT - Data user-editted
RAD CAL - Radiometer calibrated
BIAS - Biases removed
* - Unfinished step
Color Key
Data file for day unavailable
Day not finished
Day finished

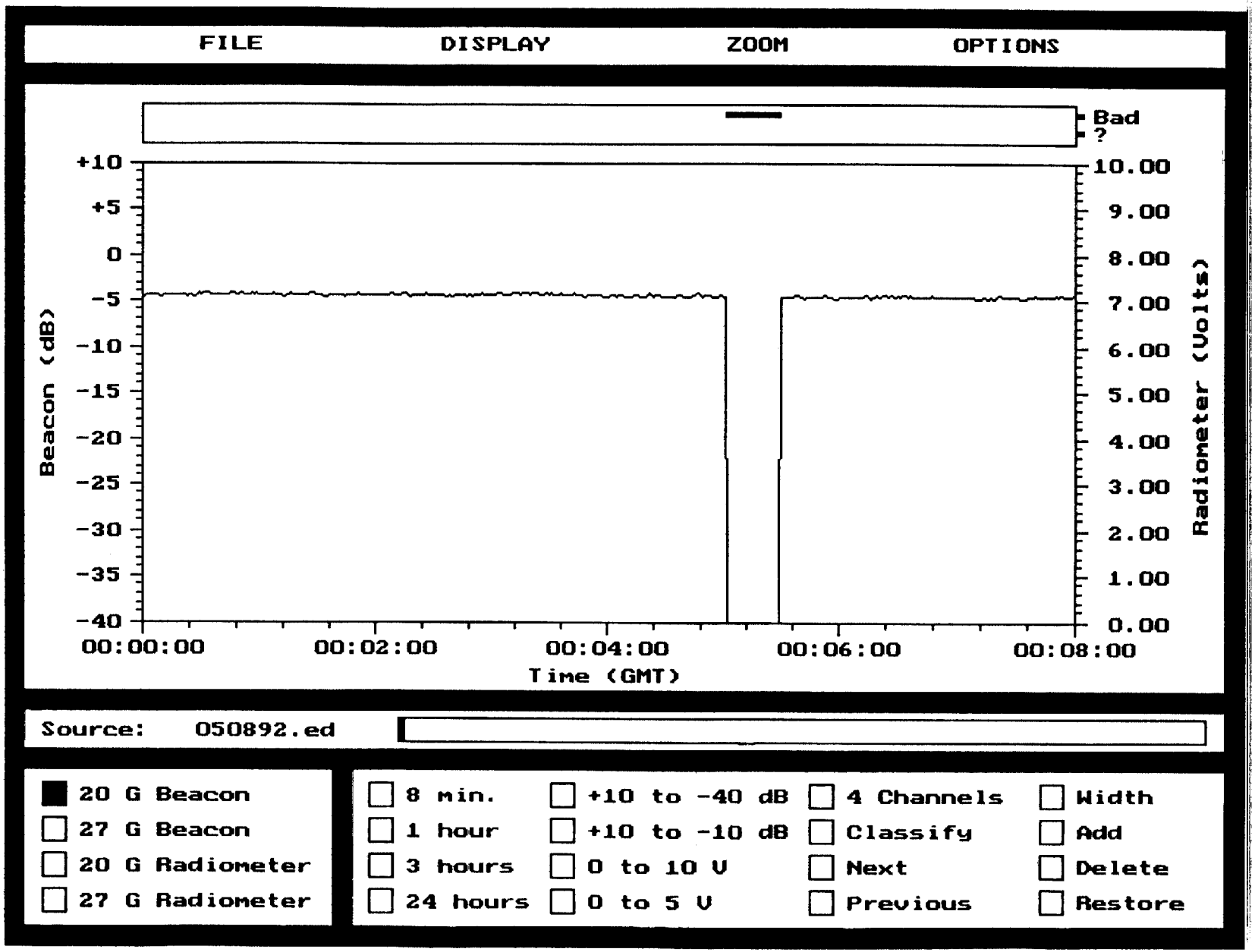
FILE
DISPLAY
ZOOM
OPTIONS
Bad
?
+10
+5
0
-5
-10
-15
-20
-25
-30
-35
-40
Beacon (dB)
10.00
9.00
8.00
7.00
6.00
5.00
4.00
3.00
2.00
1.00
0.00
Radiometer (Volts)
00:00:00
00:02:00
00:04:00
00:06:00
00:08:00
Time (GMT)
Source: 050892.ed
20 G Beacon
27 G Beacon
20 G Radiometer
27 G Radiometer
8 min.
1 hour
3 hours
24 hours
+10 to -40 dB
+10 to -10 dB
0 to 10 V
0 to 5 V
4 Channels
Classify
Next
Previous
Width
Add
Delete
Restore

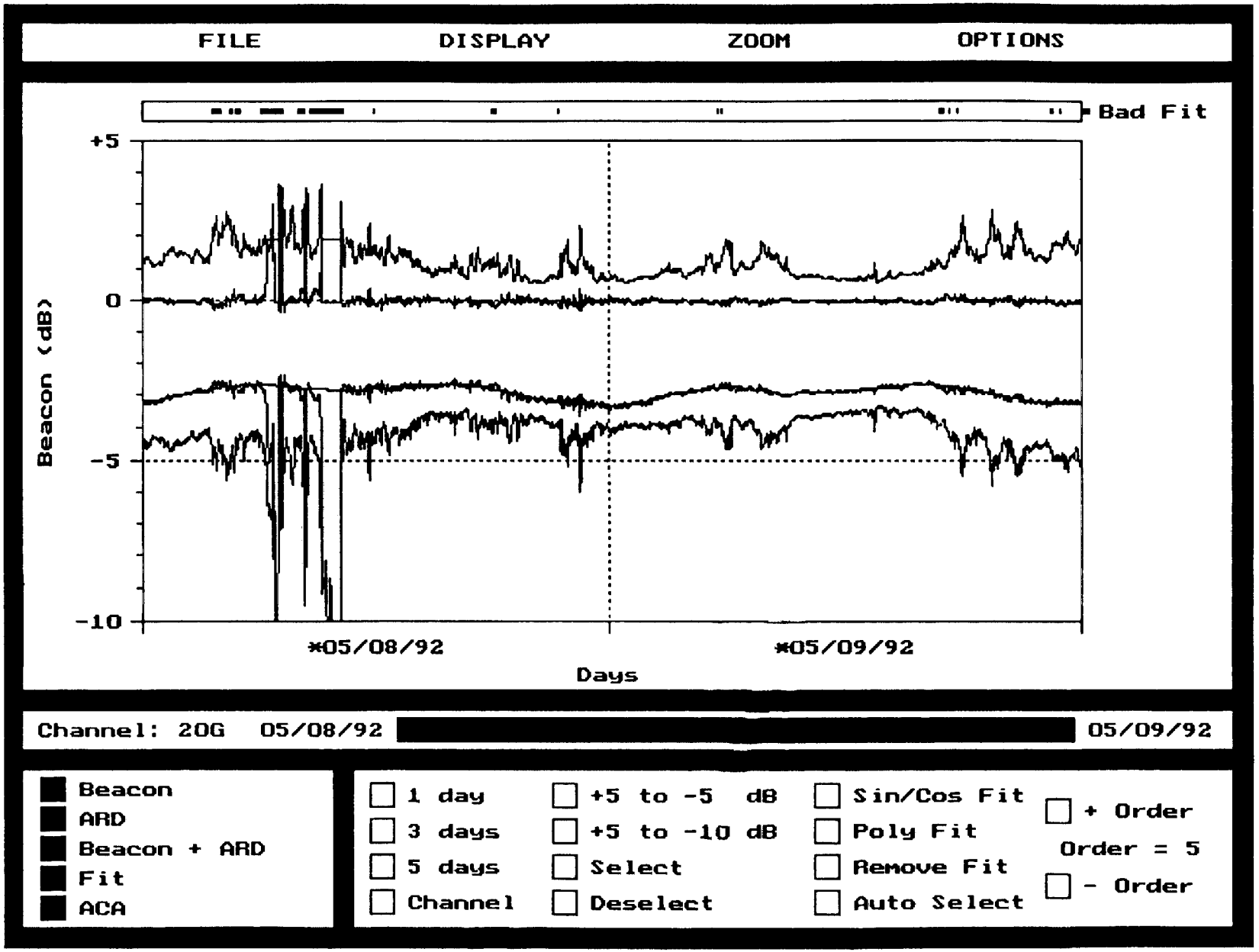
FILE
DISPLAY
ZOOM
OPTIONS
Bad Fit
+5
0
-5
-10
Beacon (dB)
*05/08/92
*05/09/92
Days
Channel: 20G 05/08/92
05/09/92
Beacon
ARD
Beacon + ARD
Fit
ACA
1 day
3 days
5 days
Channel
+5 to -5 dB
+5 to -10 dB
Select
Deselect
Sin/Cos Fit
Poly Fit
Remove Fit
Auto Select
+ Order
Order = 5
- Order

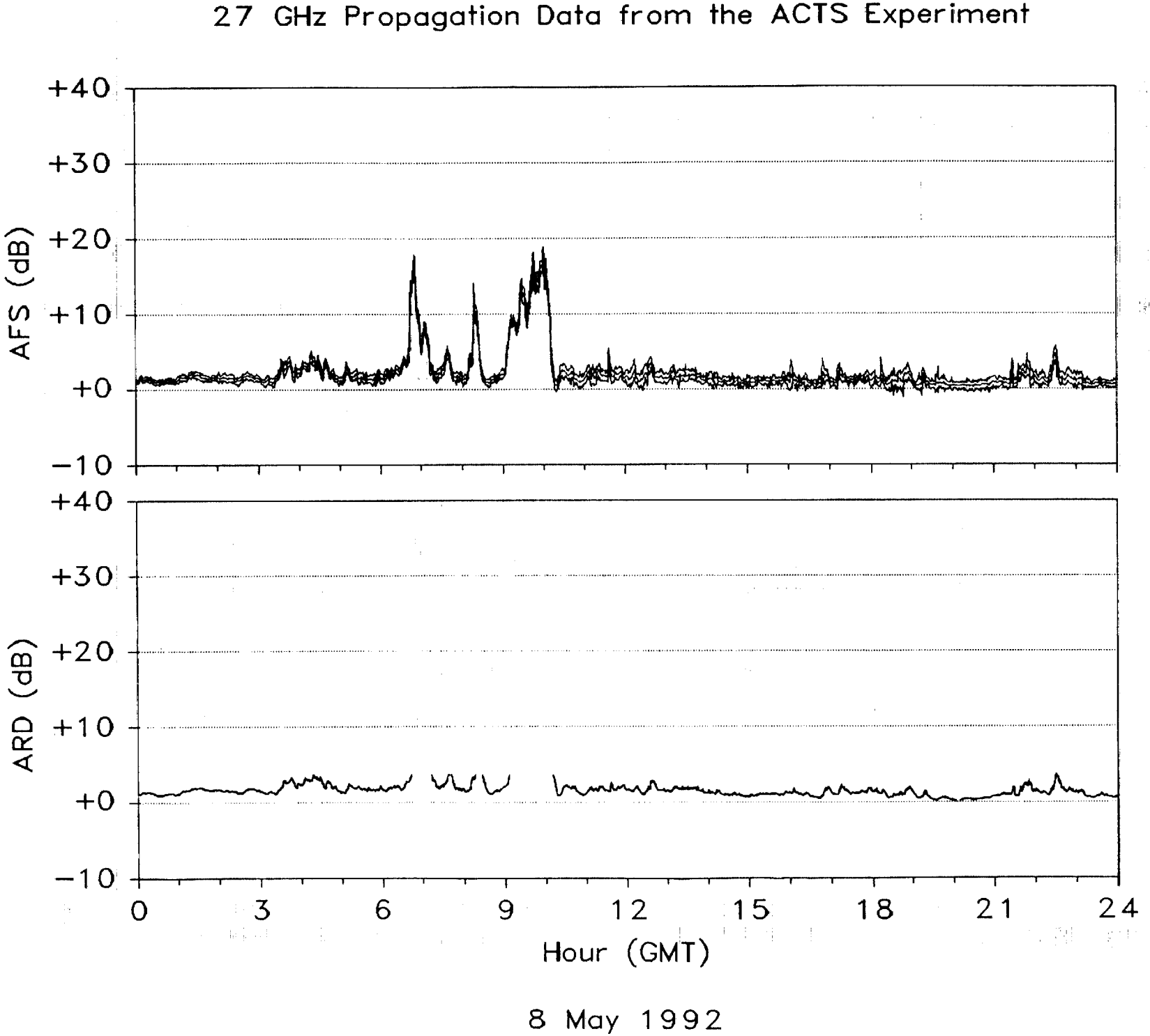
27 GHz Propagation Data from the ACTS Experiment
+40
+30
+20
+10
+0
−10
AFS (dB)
+40
+30
+20
+10
+0
−10
ARD (dB)
0
3
6
9
12
15
18
21
24
Hour (GMT)
8 May 1992

EERL / Univ. of Texas

ACTS DATA CENTER
STATUS REPORT

ALI SYED
WOLFHARD J. VOGEL
EERL / THE UNIVERSITY OF TEXAS AT AUSTIN

PRESENTED AT ACTS MINI-WORKSHOP
PASADENA, CA 14 JUNE 1993

EERL / Univ. of Texas

ACTS Data Center Functions

- Archive Raw and Pre-processed Data from Stations
- Audit Pre-processed Data
- Create and Maintain a Database
- Distribute Archived Data to Propagation Community
- Distribute Monthly Audit Reports to Stations

EERL / Univ. of Texas

D.C Development System

HARDWARE

- 486DX 66MHz
  16MB RAM
  1.7GB Hard Drive
- CD Writer/Reader
  340KB/sec Write rate
  ISO 9660 Compatible
- 120 MB Tape Drive

SOFTWARE

- Microsoft C++ 7.0
- Paradox for Windows
- PKZIP 2.04g

EERL / Univ. of Texas

Data Flow Overview

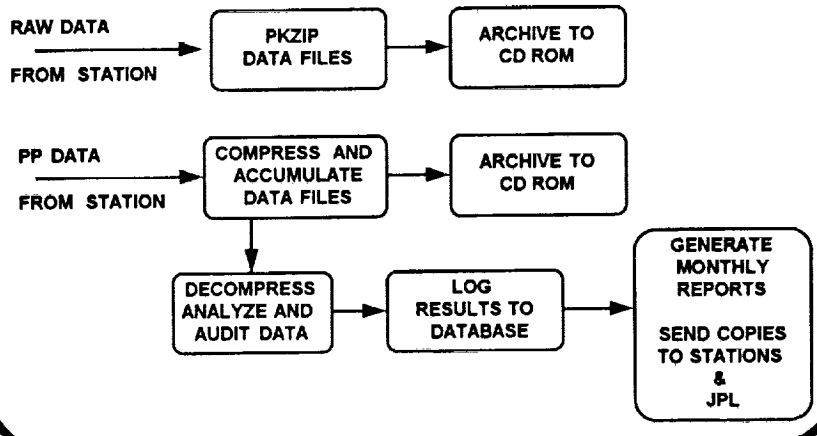

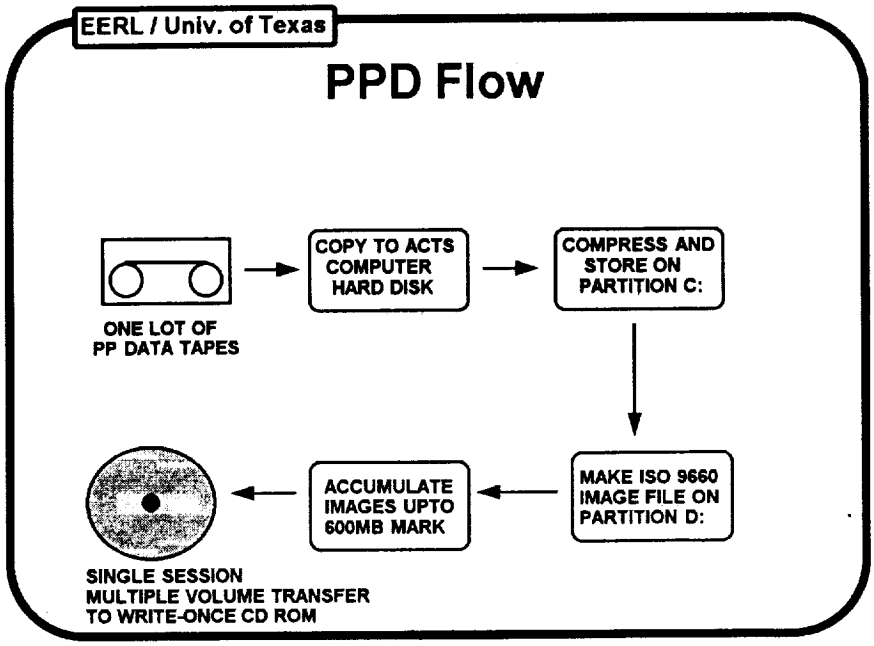
EERL / Univ. of Texas
PPD Flow
COPY TO ACTS COMPUTER HARD DISK
COMPRESS AND STORE ON PARTITION C:
ONE LOT OF PP DATA TAPES
MAKE ISO 9660 IMAGE FILE ON PARTITION D:
ACCUMULATE IMAGES UPTO 600MB MARK
SINGLE SESSION MULTIPLE VOLUME TRANSFER TO WRITE-ONCE CD ROM

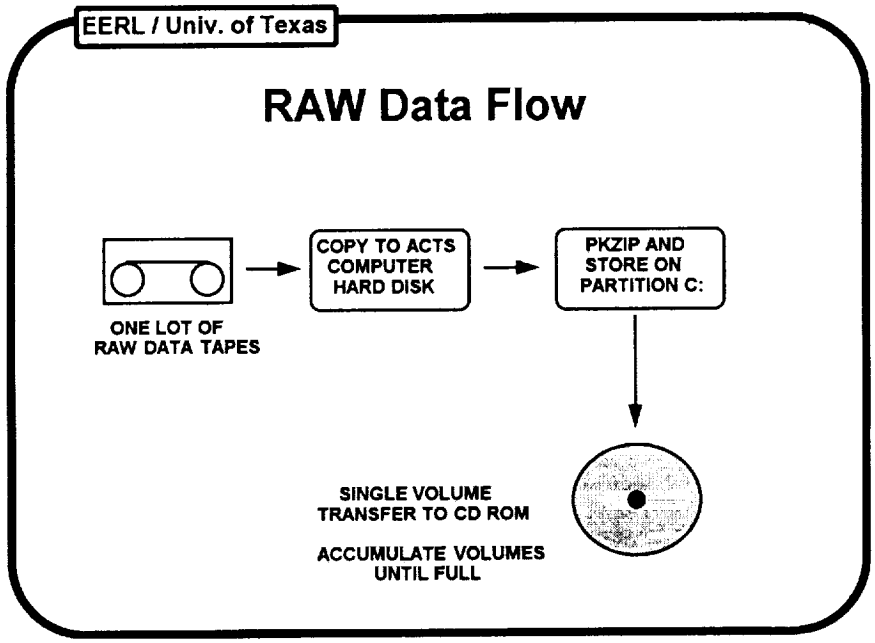
EERL / Univ. of Texas
RAW Data Flow
COPY TO ACTS COMPUTER HARD DISK
PKZIP AND STORE ON PARTITION C:
ONE LOT OF RAW DATA TAPES
SINGLE VOLUME TRANSFER TO CD ROM
ACCUMULATE VOLUMES UNTIL FULL

EERL / Univ. of Texas

Data Compression

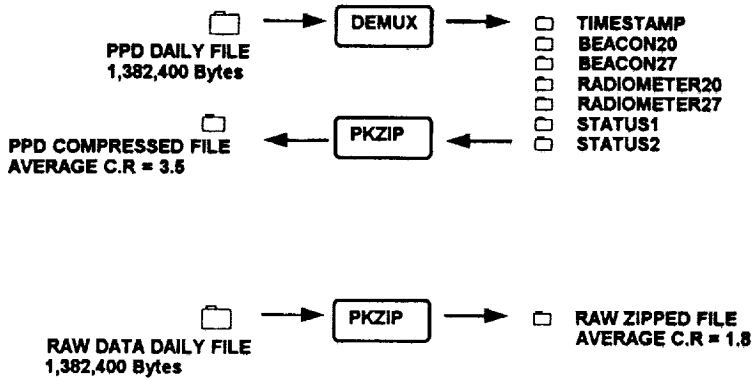

EERL / Univ. of Texas

PPD Distribution

PPD DATA VOLUME IN 6 MONTHS:
(44MB/Month/Station)(7Stations)(6 Months) ~ 1.8 GB

72 MINUTE CD ROM STORAGE CAPACITY:
(4320 Seconds)(75 Frames/Second)(2048 Bytes/Frame) ~ 630 MB

AVERAGE COMPRESSION RATIO:
C.R OF SIMULATED PPD ~ 3.5

COMPRESSED PPD ON CD ROM:
(1.8GB / 3.5) ~ 520MB

! BIANNUAL DISTRIBUTION OF PPD ON CD ROM IS POSSIBLE

EERL / Univ. of Texas

RAW Data Archival

RAW DATA VOLUME IN 3 MONTHS:
(44MB/Month/Station)(7Stations)(3 Months) ~ 924 MB

72 MINUTE CD ROM STORAGE CAPACITY:
(4320 Seconds)(75 Frames/Second)(2048 Bytes/Frame) ~ 630 MB

AVERAGE COMPRESSION RATIO:
C.R OF SAMPLE RAW DATA ~ 1.8

COMPRESSED RAW DATA ON CD ROM:
(924MB / 1.8) ~ 513MB

! QUARTERLY RAW DATA ARCHIVAL TO CD ROM IS POSSIBLE

EERL / Univ. of Texas

PPD Audit

- **? Scan Data Files from Station for BAD and MISSING Data**
- **Write Results to Text file**
- **Import Text file into PARADOX Table**
- **One Monthly Table for each Station**
- **Generate Reports on Table Data and Distribute**

EERL / Univ. of Texas

Table Structure

DAY	PARAMETER	STATE	START TIME	END TIME	DURATION
MM/DD/YY	FILE	GOOD	00:00:00	23:59:59	86400
	RECEIVER	BAD	01:00:50	11:00:49	36000
	METEORLG	UGLY	05:00:00	22:00:00	61201
	BEACON20	MISS	21:00:10	23:59:59	10790
	BEACON27				
	RADIOM20				
	RADIOM27				
	RAINRATE				
	AIRTEMP				
	RELHUMID				

BAD : MSB IN BEACON/RADIOMETER FIELD IS SET
UGLY : MSB IS NOT SET BUT DATA OUT OF RANGE
MISS : MISSING DATA

EERL / Univ. of Texas

Data Analysis

- *ANALYZE STATISTICALLY THE PARAMETERS:*
  BEACONS
  RADIOMETERS
  RAIN RATE
- *GENERATE HISTOGRAMS:*
  0.1 dB RESOLUTION FOR BEACON AND RADIOMETER
  1 mm/h RESOLUTION FOR RAIN RATE
- *DISTRIBUTE ANALYSIS PROGRAM WITH PPD*

EERL / Univ. of Texas

Development Status

- *DATA ARCHIVAL*
  90% COMPLETE
- *DATA AUDIT*
  80% COMPLETE
- *DATA ANALYSIS*
  40% COMPLETE

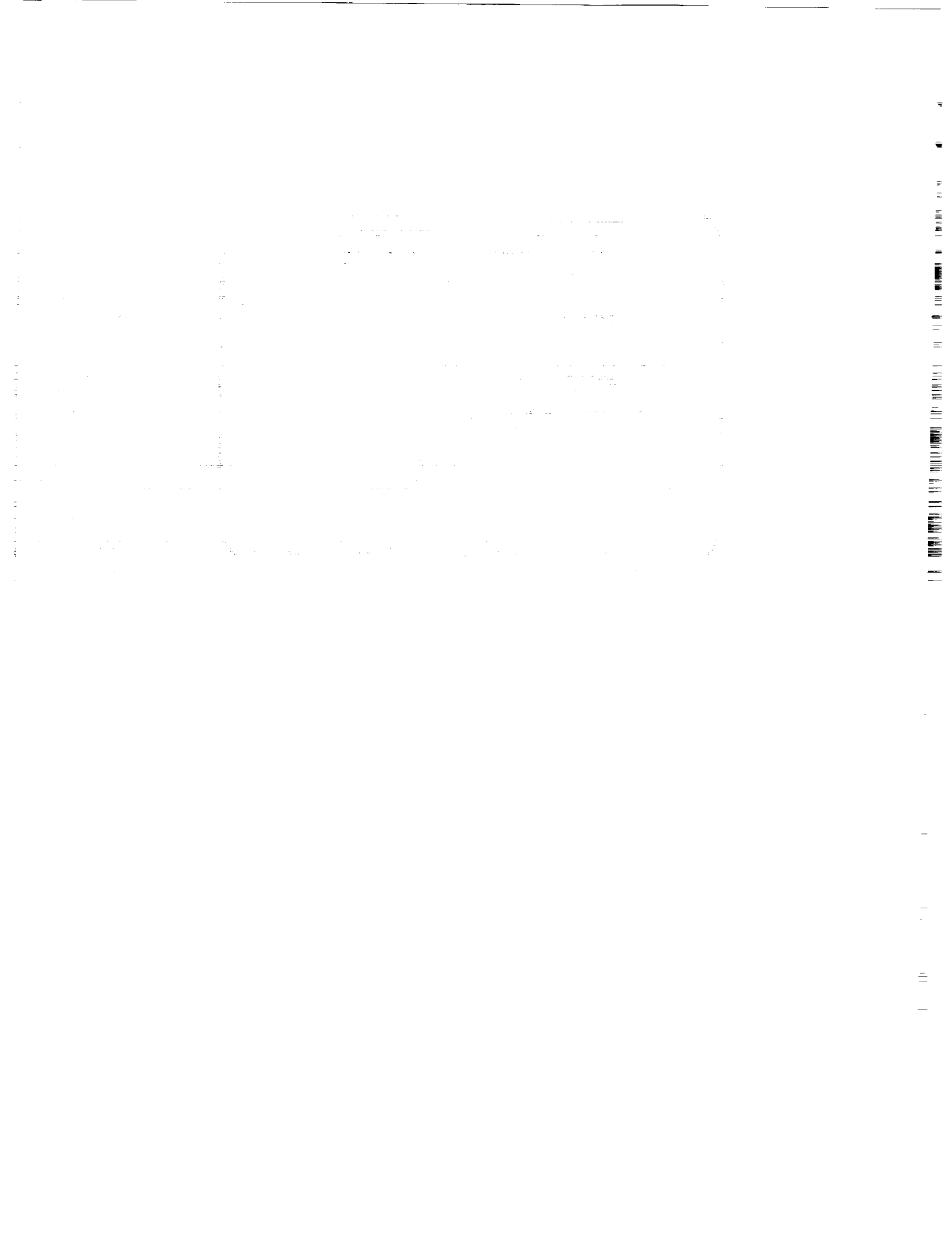

ACTS MINIWORKSHOP

Session 2

EXPERIMENTER REPORTS

Chairmen:

Robert K. Crane

University of Oklahoma

and

David V. Rogers

Communications Research Centre

Propagation Measurement Requirements Beyond the Needs of the CCIR

R. K. Crane, OU SOM

ACTS Propagation Mini-Workshop

Pasadena, CA

June 14, 1993

CCIR NEEDS:

- *ANNUAL EDFs* *('70s)*
- *WORST MONTH EDFs* *('80s)*
- *EVENT DURATION EDFs* *('80s)*
- *MONTHLY EDFs* *(New)*

NEEDS BEYOND THE CCIR:

- *VARIABILITY*
- *SEASONALITY*
- *SNOW*

SNOW EFFECTS:

- *MELTING LAYER*
- *RAIN HEIGHT*
- *EDFs FOR MIXED ICE / WATER CONDITIONS*
- *GRAUPEL / HAIL*

ACTS MEASUREMENTS:

- *OBSERVATION PROCEDURES*
- *COMPARISONS WITH PREDICTIONS*
- *SNOW EFFECTS*
- *FIELD SUPPORT*

OBSERVATION PROCEDURES:

- *ACCOUNT FOR ALL PERIODS OF TIME*
- *EDFs ARE SAMPLES FROM A RANDOM PROCESS*
- *"DOWN" TIME*
- *CONTRIBUTIONS TO TOTAL ATTENUATION*
  - > *RAIN*
  - > *CLOUDS*
  - > *SCINTILLATION*
  - > *WATER VAPOR*

COMPARE WITH PREDICTIONS:

- *RADIOMETER vs BEACON*
- *BEACON vs BEACON*
- *ATTENUATION vs RAIN RATE*
- *RAIN RATE vs CLIMATE PREDICTIONS*
- *RATE * TIME vs CLIMATE PREDICTIONS*
- *RATE * TIME vs ACCUMULATION MEASUREMENTS*

The ACTS propagation experiment discussion included participants from several companies and universities. As part of the discussion, the following two papers were presented and are included in these proceedings:

Ka-BAND PROPAGATION MEASUREMENTS USING THE ACTS PROPAGATION TERMINAL AND THE CSU-CHILL MULTIPARAMETER RADAR

V. N. Bringi
Colorado State University

SPACE COMMUNICATIONS TECHNOLOGY CENTER FLORIDA PROPAGATION PROGRAM

Henry Helmken
Florida Atlantic University

and

Rudy Henning
University of South Florida

Ka-band Propagation Measurements Using the ACTS Propagation Terminal and the CSU-CHILL Multiparameter Radar

Experimenters

Colorado State University
Department of Electrical Engineering
Ft. Collins, CO 80523

Principal Investigators

V.N. Bringi, Professor
V. Chandrasekar, Assistant Professor
Eugene A. Mueller, CSU-CHILL Radar

Joseph Turk, Research Associate
John Beaver, Ph.D. Candidate

ACTS Propagation Studies Mini-Workshop
June 14, 1993

UPDATE AND NEW DEVELOPMENTS

- Proposed rooftop site on the University of Northern Colorado Earth Sciences Building will be re-roofed in August. We may set up the terminal at the CHILL radar site (10 km north) for testing in the summer and then re-install the system on the rooftop site in late August to be ready for the measurements period.
- New reflector to be installed on the CSU-CHILL radar by end of December 1993. This will provide better cross-polar performance and lower sidelobe levels. Installation involves radome removal and some disassembly during October and November.
- NCAR-FAA Winter Icing and Storms Project (WISP-94) field program from January-March 1994. Instrumentation includes NOAA radiometers and Ka-band polarimetric radar, research aircraft. Good opportunity to study ACTS propagation through winter storms.

MICROWAVE RADIATIVE TRANSFER AND PROPAGATION MODELS

- We have completed development of a plane parallel, polarized radiative transfer model which employs different types of scatterers such as oblate raindrops, conically shaped graupel, ice needles, plates, and columns. The model outputs the up and down H and V T_B for any number of layers.
- We are working with colleagues at NCAR to complete the propagation model which will output the propagation parameters such as attenuation, depolarization, etc. for the same plane-parallel atmosphere as input to the radiative transfer model.
- These two models allow us to compare against the beacon attenuation and brightness temperature as measured by the ACTS station.
- With the CSU-CHILL polarimetric radar data, the vertical structure of the atmosphere can be inferred during rainy or snowy conditions, and this information will be used to initialize the propagation and radiative transfer models.

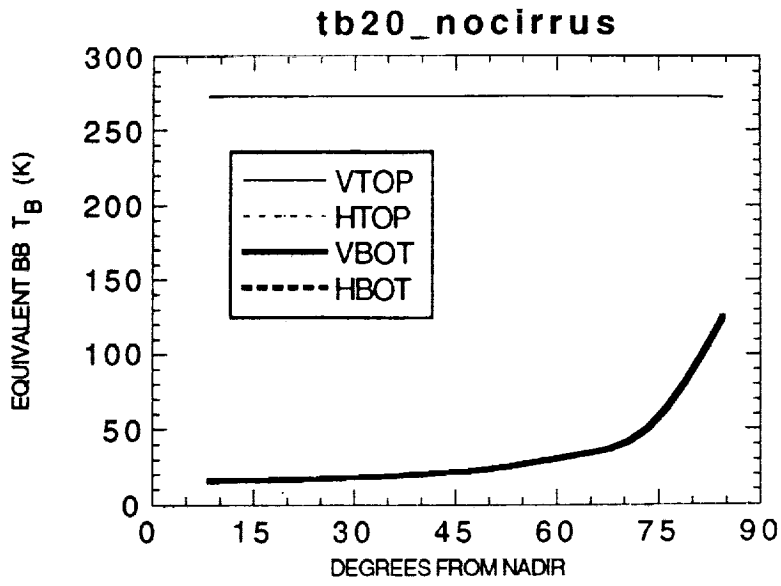

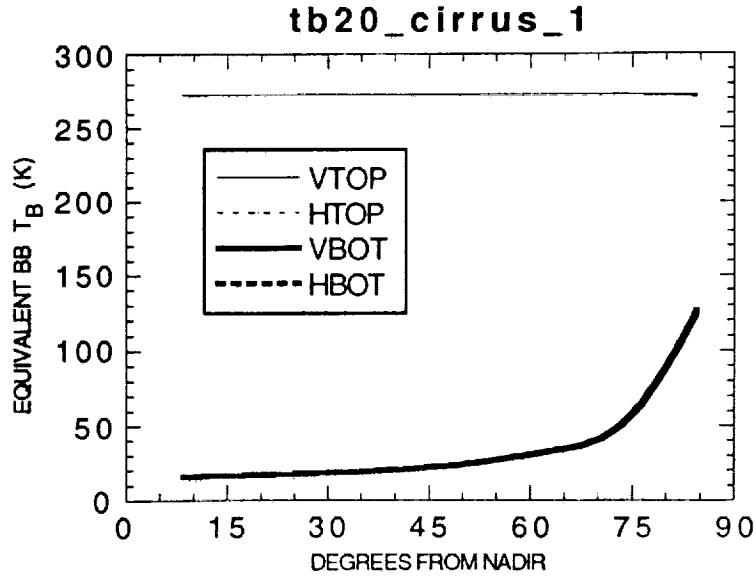

20 GHz up and down equivalent blackbody brightness temperatures T_B as a function of the angle from nadir. V and H refer to the vertical and horizontal T_B components. Top figure is for a standard atmosphere only. Bottom figure is for standard atmosphere + 2 km cirrus ice cloud with density 0.91 g/cm^3 placed between 10-12 km above a land surface. The cirrus cloud water content is fixed at 0.01 g/m^3, with an exponential size distribution of plate shaped particles.

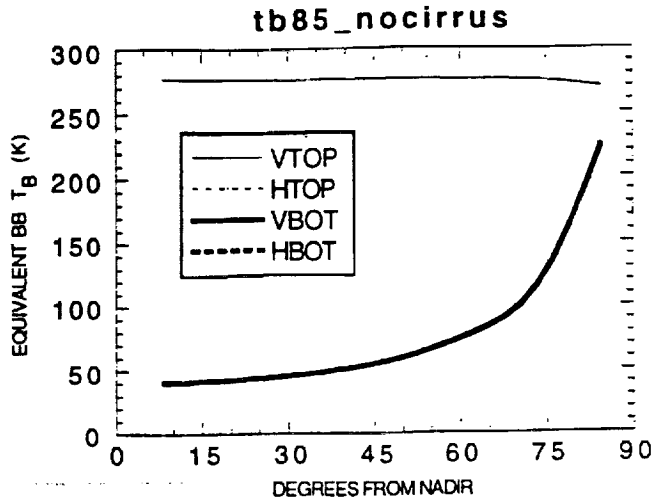

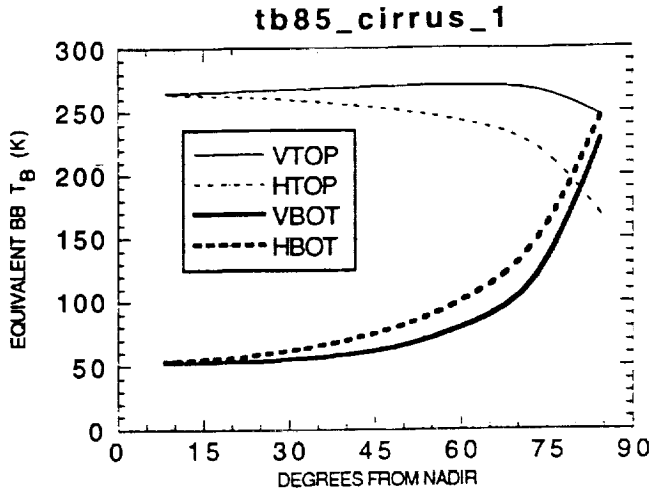

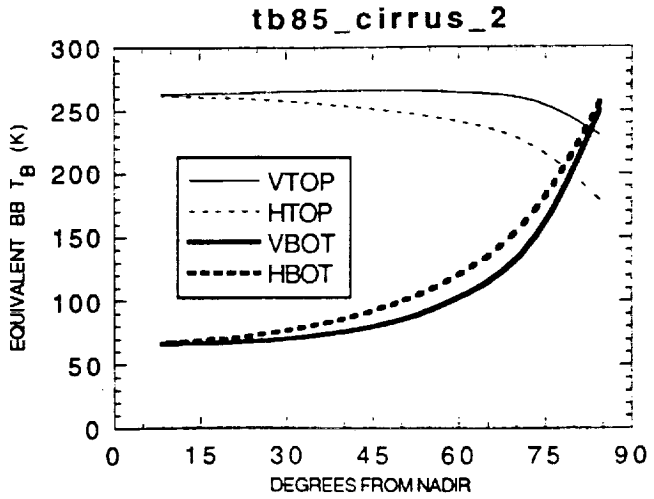

85 GHz up and down equivalent blackbody brightness temperature T_B as a function of the angle from nadir. V and H refer to the vertical and horizontal T_B components. Top figure is for a standard atmosphere only. Middle figure is for standard atmosphere + 2 km cirrus ice cloud with density 0.91 g/cm^3 placed between 10-12 km above a land surface. Bottom figure depicts the case where 0.05 g/m^3 cloud liquid water is included within the cirrus cloud. In all cases the cirrus cloud ice water content is fixed at 0.01 g/m^3, with an exponential size distribution of plate shaped particles.

SPACE COMMUNICATIONS TECHNOLOGY CENTER

(SCTC)

FLORIDA PROPAGATION PROGRAM

HENRY HELMKEN
FLORIDA ATLANTIC UNIVERSITY (FAU)

&

RUDY HENNING
UNIVERSITY OF SOUTH FLORIDA (USF)

June 14, 1993

NASA PROPAGATION TERMINAL STATUS

* UNIVERSITY OF SOUTH FLORIDA
  - Tampa, Florida (28° N, 82.5° W)
  - Severe Weather Area
  - In ACTS Fixed Beam
  - Site of GTE TRIAD Experiments
  - Tampa to have NEXT Radar in Summer 1994.

* SITE LOCATION
  - Roof, USF Engineering Building
  - Site Preparations 75% Complete
  - 5 KW UPS Auxiliary Power Source on Campus

* TERMINAL EQUIPMENT
  - Delivered as of 6/21/93
  - Undergoing Assembly

ACTS CHANNEL CHARACTERIZATION

* GOALS
  - Compare Beacon Signal to 19 - 20 GHz ACTS Channel
  - Channel Amplitude and Phase Characterization
  - Evaluate High Data Rate Transmission Performance

* SIGNALLING
  - Construct Transportable Receive-Only Terminal
  - Transmit from LET Facility at LeRC
  - Assume Constant EIRP Downlink
  - Single and Multi-tone Signals
  - Amplitude and Phase Measurements at Receive Site

* PREPARE FOR ACTS COMPRESSED VIDEO EXPERIMENTS
  - Fade Depths, Rates and Durations
  - Develop Modem Interface to LET and RO Terminals
  - Test 45 Mb/s Fujitsu and EF DATA Modems
  - BER Measurements

FAU RECEIVE ONLY TERMINAL

* SINGLE TONE MEASUREMENTS
  - MSM Linearity Measurements
  - MSM Intermodulation Products
  - Measure via Spectrum Analyzer at 1 Hz rate

* TWO TONE MEASUREMENTS
  - Transmit Two Phased Locked Tones from LET
  - Monitor ACTS Down-link Band vs. Time
  - Record Amplitudes via Spectrum Analyzer at 0.8 Hz rate
  - Record Relative Phase vs. Time

* BER MEASUREMENTS
  - Investigate Burst Error Rates via High Data Rate Modems
  - Develop Channel Characterization Models
  - Prepare for ACTS Compressed Video Experiments

FAU TERMINAL STATUS

* RECEIVE-ONLY TERMINAL
  - Prodelin 1.2 m Dish Ordered and Delivered
  - Front End Downconverter to 3.3 GHz under Assembly
  - Weatherproof Feed Enclosure on Order
  - Additional Rain Gauge on Order
  - Phase Measurement Hardware on Order

* SOFTWARE
  - Single and Two Tone Measuring Software Complete
  - COMDISCO SPW Channel Model under Development

* MODEMS
  - Fujitsu Burst Modem Interface under Development
  - EF Data Continuous Modem Hardware Ready

* PROPAGATION TEST BED

* PURPOSE
  - Test Bed For Link Evaluation
  - FEC Burst Error Algorithm Development
  - Test SCTC Video Compression and FEC prior to ACTS

* HARDWARE PROPAGATION TEST BED
  - Computer Controlled Signal and Noise Channel
  - Real Time Propagation Fading at IF Frequencies
  - Incorporate ACTS Channel Models
  - Evaluate High Data Rate Modem Performance

* DEVELOP COMDISCO SPW SOFTWARE
  - Incorporate ACTS Rain Models
  - Subject of Current M.S. Thesis

JPL

USING THE E-MAIL SYSTEM FOR INFORMATION EXCHANGE

Krisjani Suwitra
Jet Propulsion Laboratory

California Institute of Technology

JPL

E-mail is a quick way to ...

- Announce a meeting place and date
- Exchange experimental data
- Exchange results/analysis
- Ask questions and answer
- Announce software releases, bugs and improvements
-
-
-

JPL

ACTS ELECTRONIC MAILING LIST
acts@java.jpl.nasa.gov
June 15, 1993

Name	Telephone	FAX	E-mail
Robert Bauer	216-433-3431	216-433-6371	acbauer@lims01.lerc.nasa.gov
John Beaver	303-491-6758	303-491-2249	jb686028@longs.lance.colostate.edu
V.N. Bringi	303-491-2249	303-491-2249	bringi@longs.lance.colostate.edu
Alan Cha	818-354-0412	818-393-0096	cha@java.jpl.nasa.gov
Aimee Chan	604-293-6094	604-293-5787	achan@mprgate.mpr.ca
Robert Crane	405-325-4419	405-325-7689	bcrane@geohub.gcn.uoknor.edu
Faramaz Davarian	818-354-4820	818-393-0096	davarian@java.jpl.nasa.gov
Asoka Dissanayake	301-428-4411	301-428-3638	asoka_dissanayake@mr_mail.trans.comsat.com
Barry Fairbanks	216-433-3541	216-433-6371	acfair@lims01.lerc.nasa.gov
Julius Goldhirsh	301-953-5042	301-953-5548	julius@nansen.jhuapl.edu
Robert Gunderman	216-433-3544	216-433-6371	acgun@lims01.lerc.nasa.gov
Henry F. Helmken	407-367-3452	407-367-2336	helmkenh@acc.fau.edu
Rudolph Henning	813-974-4782	813-974-5250	henning@ec.usf.edu
Stephen Horan	505-646-5870	505-646-1435	shoran@nmsu.edu
Rafeh Hulays	604-822-2872		acts@ee.ubc.ca
Bradley Jaeger	907-474-7815	907-474-6087	fsbej1@aurora.alaska.edu
M.M.Z. Kharadly	604-822-2816	604-822-5949	acts@ee.ubc.ca
John Kiebler	202-646-9113	202-646-9109/8	jkiebler@mitre.org
Alexander Kukushkin	612-868-3724		akukushk@rp.csiro.au
Robert M. Manning	216-433-6750	216-433-6371	acmann@lims01.lerc.nasa.gov
Charlie Mayer	907-474-6091	907-474-6087	ffcem@aurora.alaska.edu
Timothy Pratt	703-231-6681	703-231-3355	satcom@vtvml.cc.vt.edu
Horst Salzwedel	415-378-7537	415-358-3601	horst@csi.com
Ed Satorius	818-354-5790	818-354-6825	satorius@voyager.jpl.nasa.gov
Ernest Smith	303-492-7123	303-492-2758	smithek@boulder.colorado.edu
Warren Stutzman	703-231-6834	703-231-3355	stutzman@vtvm1.cc.vt.edu
Krisjani Suwitra	818-354-9250	818-393-0096	suwitra@java.jpl.nasa.gov
Joseph Turk	303-491-7678	303-491-2249	turk@longs.lance.colostate.edu
Wolf Vogel	512-471-8608	512-471-8609	wjvogel@chpc.utexas.edu
Larry Ware	604-822-2816		acts@ee.ubc.ca
Mardy Wilkins	818-354-9250	818-393-0096	wilkins@java.jpl.nasa.gov

To be on the list, please contact the ACTS E-mail administrator:
Krisjani Suwitra Telephone: 818-354-9250 FAX: 818-393-0096 E-mail: suwitra@java.jpl.nasa.gov

JPL

A Sample e-mail message

Date: Wed, 17 Mar 1993 15:05:28 -0600
From: bcrane@geohub.gcn.uoknor.edu
To: suwitra@java.Jpl.Nasa.Gov
Subject: A Test

Kris,
This is a test.
Bob Crane

Date: Wed, 17 Mar 1993 15:05:28 -0600
From: suwitra@java.Jpl.Nasa.Gov
To: bcrane@geohub.gcn.uoknor.edu
Subject: Re: A Test

Bob,
I received your test message.
Kris Suwitra

JPL

Sending a message to the mailing list

Date: Mon, 14 June 1993 15:05:28 -0600
From: suwitra@java.jpl.nasa.gov
To: acts@java.jpl.nasa.gov
Subject: A Test

•
•
•

Receiving a message from the mailing list

Date: Mon, 14 June 1993 15:05:28 -0600
From: acts@java.jpl.nasa.gov
To: suwitra@java.jpl.nasa.gov
Subject: A Test

•
•
•

JPL

A reply message to an individual

Date: Mon, 14 June 1993 15:05:28 -0600
From: bcrane@geohub.gcn.uoknor.edu
To: ~~acts@java.jpl.nasa.gov~~ suwitra@java.jpl.nasa.gov
Subject: Re: A Test

-
-
-

VPI & SU ACTS Mobile Terminal Experiment Plan

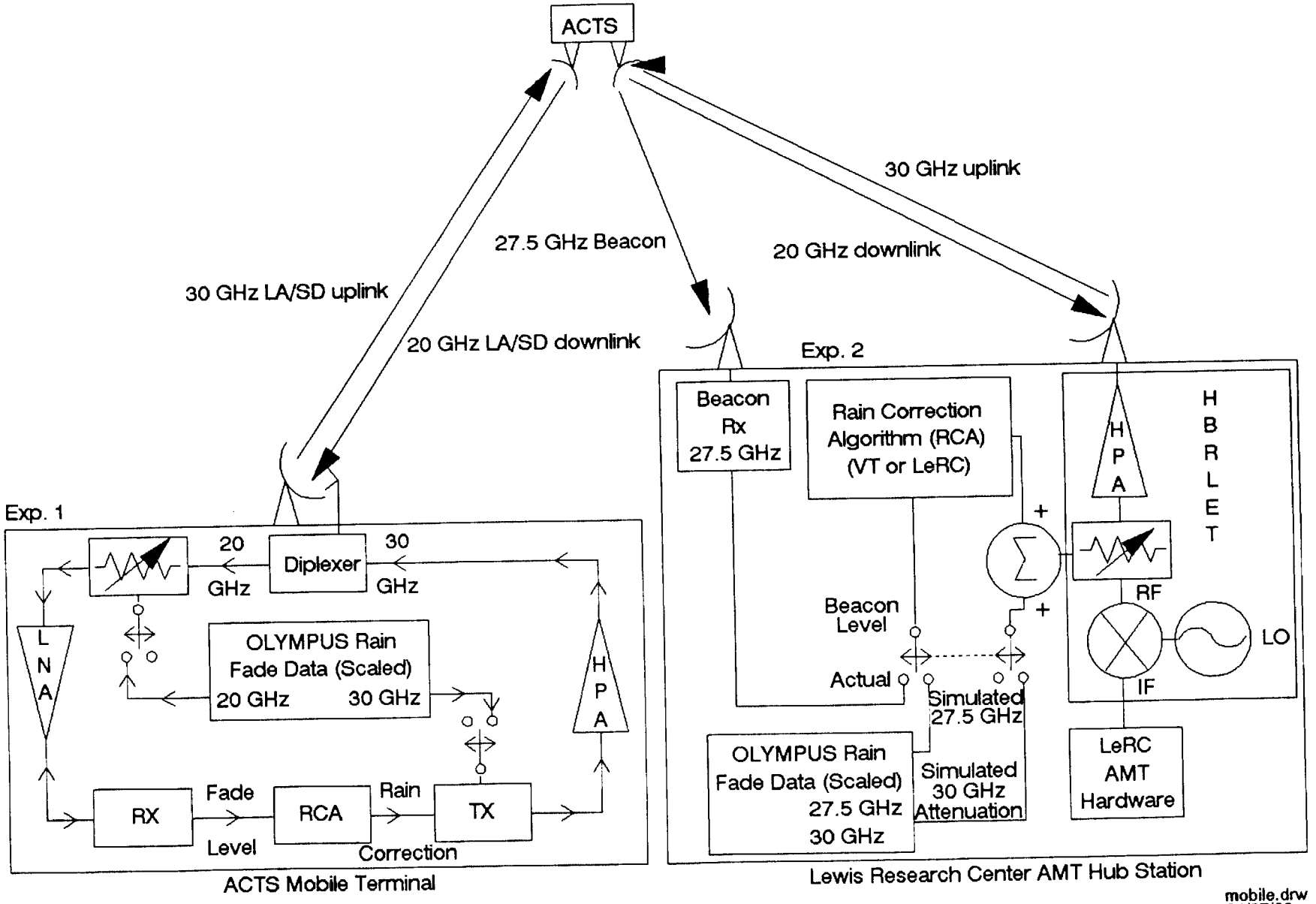

mobile.drw
04/07/93

(An absorptive attenuator at ~ T_{Rain} will accurately simulate rain attenuation including sky noise effects.)

Warren Stutzman, Virginia Polytechnic Institute & State University

JPL

A PLAN FOR ACQUIRING PROPAGATION DATA FROM ACTS COMMUNICATIONS EXPERIMENTS

A.G.Cha

Jet Propulsion Laboratory
Pasadena, CA

California Institute of Technology

Plan to Use EOA Data

THE STEPS

- Determine what data is available
- Determine what data to collect
- Present the plan at ACTS Propagation Workshop for discussions
- Promote plan at ACTS communications experimenters meeting
  - obtain cooperation of principal investigators
- Work out funding, management, technical, contracting and scheduling liaison details

JPL

Plan to Use EOA Data

DATA CHARACTERISTICS

NRA Class I	EOA
time stamp	time stamp
rain and other climatic data	climatic data usually not available
fade (attenuation) data	fade data
continuous measurement over two years	not continuous; duration can be from weeks to two years

JPL

Plan to Use EOA Data

SOME PROMISING CANDIDATES

1. NASA Ground Station and Master Control Station (NGS / MCS)

- 20 GHz telemetry beacon power level measured on a daily, quasi-continuous basis over the two-year ACTS experiment period
- Data stored at MCS
- Weather data may be available from nearby airport

Assessment : This looks like a Class I experiment for the Cleveland area.

2. VSAT's

- Fade data is deposited and stored at MCS
- Individual terminals : Look closely at terminals which will be at the same location for one year or longer and which will be used frequently and fairly uniformly over the year.
- The ensemble of all VSAT's :
  The data is deposited at MCS. The data aggregate represents the average fade statistics of the lower 48 states over two years.

3. Mobile terminals

- Data in mobile environment is valuable and should be deposited at APDC.

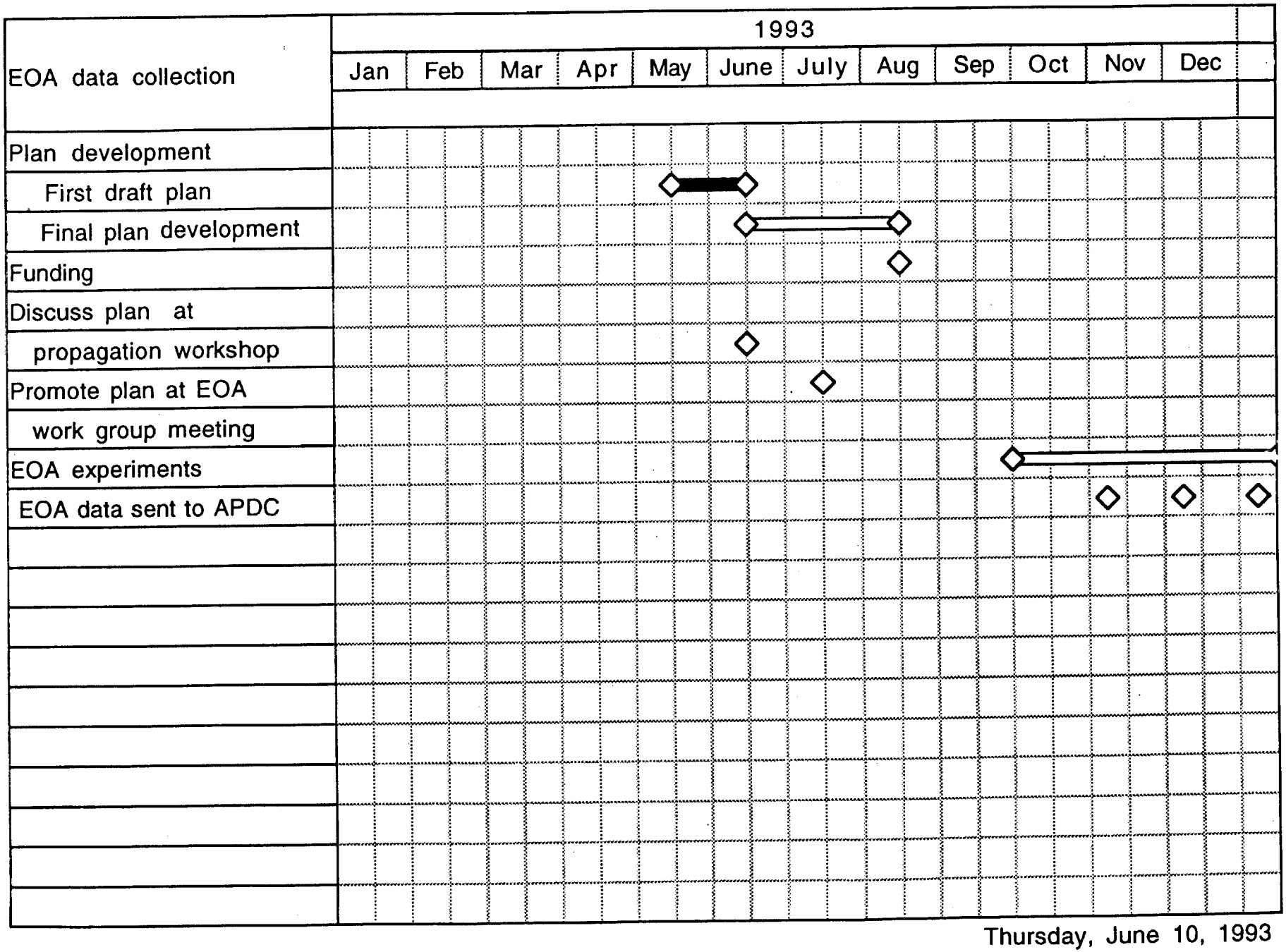
EOA data collection
1993
Jan
Feb
Mar
Apr
May
June
July
Aug
Sep
Oct
Nov
Dec
Plan development
First draft plan
Final plan development
Funding
Discuss plan at
propagation workshop
Promote plan at EOA
work group meeting
EOA experiments
EOA data sent to APDC
Thursday, June 10, 1993

Report of the Working Groups Joint Meeting

D. V. Rogers and R. K. Crane

In Session II of the ACTS Miniworkshop held on June 14, 1993, the Science and Systems Working Groups met jointly to conduct deliberations per the agenda listed in the Table of Contents of this publication. A brief report on this meeting and on the status of Action Items from the previous ACTS Propagation Studies Workshop (APSW IV) is provided here.

Action Items

The following Action Items, with responsible individual(s) noted, resulted from discussions at APSW IV. The status of each is briefly summarized.

1. E-Mail Status Reports/Computer Bulletin Board - Bob Bauer

   Krisjani Suwitra, the ACTS E-mail Administrator, described the benefits of the E-mail system for the ACTS propagation program, which is already operational. A list of E-mail addresses of the ACTS propagation experimenters is in preparation. Addresses for this list should be supplied to Krisjani Suwitra (suwitra@java.jpl.nasa.gov).

   An ACTS computer bulletin board is in preparation by NASA Lewis Research Center, and is expected to be operational by early August. Satellite ephemeris data will be supplied to experimenters for antenna pointing calculations. As ACTS is intended to be station-kept in a small (± 0.05∞) box, effects of pointing errors should be small for the ACTS propagation terminals.

2. Rain-Gauge Siting/Maintenance/Operation - Julius Goldhirsh

   J. Goldhirsh delivered two technical reports for dissemination. The first is titled "Operation, Calibration and Data Acquisition for Capacitive and Tipping Bucket Rain Gauges", by N. E. Gebo and J. Goldhirsh, and the second is "Comparative Assessment of R.M. Young and Tipping Bucket Rain Gauges", by J. Goldhirsh and N. E. Gebo. A 3.5 inch floppy disk of data acquisition and processing software for tipping bucket and capacitive rain gauges was also provided. The information is to be disseminated by VPI & SU.

3. Sample OPEX E-Mail Reports/Sample Data Set - Tim Pratt

   Samples of OPEX E-mail status reports were supplied by T. Pratt to R. Bauer for consideration in instituting a similar system for the ACTS program.

   A sample data set for use during experimenter training was prepared and applied for this purpose.

4. Experimenter Guide/Data Processing Outline - R. Crane and D. Rogers

   R. Crane discussed requirements for sophisticated data processing in the presentation, "Measurement Needs Beyond CCIR", which addressed CCIR needs, interannual and seasonal variability in statistics, measurement procedures, and comparisons of measurements with model predictions and among different

observations (e.g., comparison of beacon and radiometric data). Important for the assurance of propagation data quality is the identification of the cause of each observed outage or attenuation event (e.g., attenuation caused by rain or cloud, signal-level reduction caused by scintillation, loss of signal due to equipment malfunction, loss caused by antenna misalignment, wet snow on the antenna, graduate student in front of the antenna feed, etc.). During discussions generated by this presentation the need for specific systems information (diurnal distributions of fading, rates of fading, fade durations, etc.) was also noted.

An outline of a "strawman" guide for experimenters is planned for the next ACTS Propagation Studies Workshop. Per intentions stated during APSW IV, the guide would be prepared after experimenters have collected several months of ACTS propagation data. In preparation for discussions at the next ACTS workshop, experimenters are encouraged to: compare the monthly cumulative distributions of attenuation observed at one frequency with those predicted from observations at the other frequency using one or more models for frequency scaling; compare attenuation observations with predictions from radiometer observations using one or more models for medium temperature; and compare attenuation observations with predicted attenuations based on the rain rate distribution for the month (using all data, not just observations simultaneous with beacon measurements) and one or more models for attenuation prediction given the rain rate distribution. In addition, comparisons should be made between rain accumulation estimates tallied from the rain rate observations, accumulations estimated from nearby NWS and other cooperative observer reports, and climatologically-expected monthly accumulations.

Other Issues

Several other important issues were discussed during the Joint WG Meeting. The main issues were the following:

1. ACTS Field Support

   The degree of field support to be provided by NASA for ACTS Class I propagation experimenters was unclear and the cause of some concern. The NASA representative stated that some form of site support was still intended, but that it remained to be seen who would provide it.

   Several experimenters commented on this issue, noting that the satellite launch was imminent, and that there are bound to be hardware and software bugs discovered after installation of the propagation terminals. Some means to quickly and reliably diagnose problems confronted in the field and to supply remedies was deemed essential by the experimenters.

2. System-Application Requirements

   Several system designers and users participated in the ACTS Miniworkshop and expressed some systems concerns and requirements during the meeting.

   Cloud losses, snow (whether on the propagation path or the antenna), light rain, and other usually-small propagation effects were recognized as important for small-margin telecommunication systems and possibly for propagation impairment-mitigation technologies. Designers of satellite systems are

furthermore concerned with net impairments confronted by the system (e.g., snow on an earth-terminal antenna may be even more important that snow on the path), and would prefer prediction models that can account for all such weather-related effects.

However, propagation experimenters have difficulty in identifying and treating nonpath effects, which are often unique to local parameters (such as antenna type) and difficult to classify for modeling applications. If categorization is incomplete (e.g., if the prediction methods are purely empirical), there is little prospect for developing site-specific prediction capabilities. This problem is deserving of more attention and additional discussion at future meetings, particularly as to how the system needs can be addressed during the ACTS propagation experiments.

Interest was also expressed regarding "integration" of the results from the ACTS propagation experiments into suitable formats for system needs. The answer offered was that this process would occur collectively within the propagation community in collaboration with systems experts. A mechanism to ensure that those system needs that can be addressed via the ACTS propagation results are accommodated in the studies may be necessary.

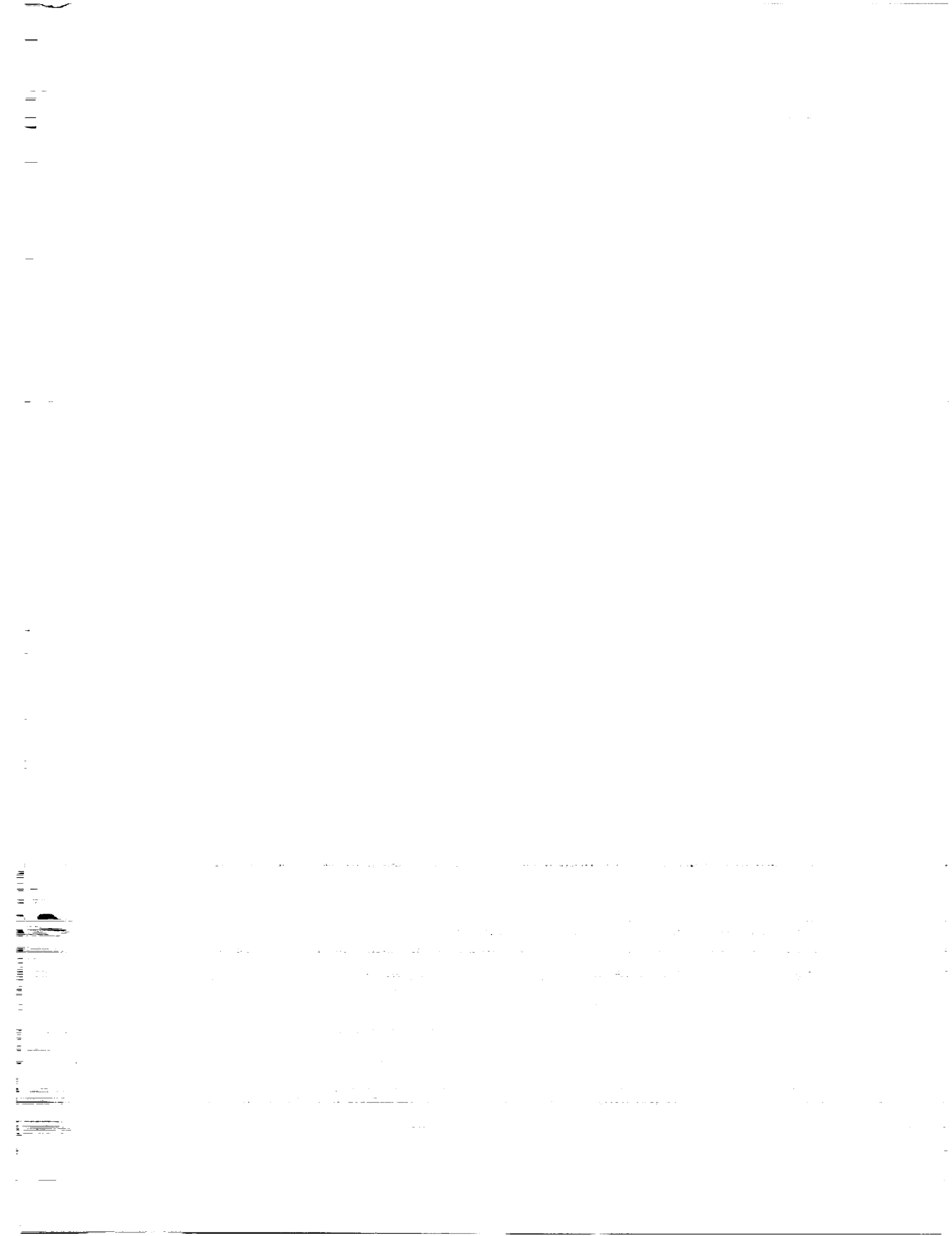

TECHNICAL REPORT STANDARD TITLE PAGE

1. Report No. 93-21	2. Government Accession No.	3. Recipient's Catalog No.
4. Title and Subtitle Proceedings of the Seventeenth NASA Propagation Experimenters Meeting (NAPEX XVII) and the Advanced Communications Technology Satellite (ACTS) ~~Propagation Studies Miniworkshop~~		5. Report Date August 1, 1993 6. Performing Organization Code
7. Author(s) Faramaz Davarian (editor)		8. Performing Organization Report No.
9. Performing Organization Name and Address JET PROPULSION LABORATORY California Institute of Technology 4800 Oak Grove Drive Pasadena, California 91109		10. Work Unit No. 11. Contract or Grant No. NAS7-918 13. Type of Report and Period Covered
12. Sponsoring Agency Name and Address NATIONAL AERONAUTICS AND SPACE ADMINISTRATION Washington, D.C. 20546		14. Sponsoring Agency Code BJ-144-10-20-00-00

15. Supplementary Notes

16. Abstract

The NASA Propagation Experimenters Meeting (NAPEX), supported by the NASA Propagation Program, is convened annually to discuss studies made on radio wave propagation by investigators from domestic and international organizations. NAPEX XVII was held on June 15, 1993, in Pasadena, California. Participants included representatives from Canada, Japan, Germany, the Netherlands, Portugal, England, Switzerland, Italy, and the United States, including researchers from universities, government agencies, and private industry. The meeting was organized into two technical sessions. The first session was dedicated to slant path propagation studies and experiments. The second session focused on propagation studies for mobile and personal communications. In total, nineteen technical papers and some informal contributions were presented.

Preceding NAPEX XVII, the Advanced Communications Technology Satellite (ACTS) Propagation Studies Miniworkshop was held on June 14, 1993, to review ACTS propagation activities with emphasis on ACTS experiments status and data collection, processing, and exchange. Ten technical papers were presented by contributors from government agencies, private industry, and university research establishments.

17. Key Words (Selected by Author(s))	18. Distribution Statement
Communications Electronics and Electrical Engineering Wave Propagation	Unclassified --Unlimited

19. Security Classif. (of this report)	20. Security Classif. (of this page)	21. No. of Pages	22. Price
Unclassified	Unclassified	350	